THE HONG KONG POLYTECHNIC UNIVERSITY
INSTITUTE OF TEXTILES AND CLOTHING

DISORDER BEHAVIOR IN NANO- AND SUBMICRON-STRUCTURED POLYMERIC COMPOSITE SYSTEMS WITH PASSIVE AND ACTIVE DIELECTRIC MEDIA

KAI-CHEONG KWAN

A THESIS SUBMITTED IN PARTIAL FULFILLMENT OF THE REQUIREMENTS
FOR THE DEGREE OF DOCTOR OF PHILOSOPHY

NOVEMBER 2006

CERTIFICATE OF ORIGINALITY

I hereby declare that this thesis is my own work and that, to the best of my knowledge and belief, it reproduces no material previously published or written, nor material that has been accepted for the award of any other degree or diploma, except where due acknowledgement has been made in the text.

_____ (Signed)

KWAN KAI CHEONG (Name of student)

ABSTRACT

This project aims to investigate the influence of disorder on the optical properties of passive and active disordered dielectric media. Submicron/nano-scaled disordered dielectric structures can be integrated into polymeric fibers/films to form a base for flexible fabric display, which is capable of scattering photons and self-amplification.

The theoretical investigation has been carried on the effect of position and size disorders on two-dimensional (2D) passive and active disordered dielectric systems with circular inclusions based on the time-dependent theory, which combines the time-dependent Maxwell's equations with the semi-classical laser theory. The numerical framework has been developed and used for finite-difference time-domain simulation. In the numerical experiments, the disordered dielectric systems are generated from ordered systems. The ordered systems are equivalent to photonic crystals which consist of a square array of infinitely long, parallel dielectric cylinders with lattice constant a. The electromagnetic (EM) waves are assumed to propagate in a plane perpendicular to the cylinders. In the 2D case, the dielectric cylinders are used to mimic the circular scattering particles. For the case of position disorder, the positions of each particle are randomized within a certain range from its lattice point. To create a random configuration, the position of each particle is randomly decided within a range giving a position disorder parameter of d_p. Size disorder is related to the uniformity in the radius of the cylinder. The position of each particle is fixed in its lattice position but the radius of particles can be random.

The radius of each particle is randomly changed within a distance d_r .

Numerically, the influence of the density of scattering particles on the mode distribution of passive ordered and disordered systems is examined. In a densely packed ordered system (particle density = $2\text{x}10^{13}\text{m}^{-2}$), two photonic band gaps (PBGs) are found at f = 4.51 $\text{x}10^{14}$ to 5.41x 10^{14}Hz and 7.90 $\text{x}10^{14}$ to $9.0\text{x}10^{14}$Hz. After a long time evolution, only long-lived modes, which locate close to the edge of the band gaps, survive in the passive disordered system. The lifetime of mode increases as the localization length of mode reduces. Since the modes close to the edge of PBGs have shorter localization length, the survived modes tend to lie on the edge of band gaps. It is demonstrated that the evolution of the mode energy is an exponential function of time. Furthermore, the competition of modes is revealed in the field distribution patterns at different time frames

PBGs formed in the most densely packed ordered systems (particle density = $2\text{x}10^{13}\text{m}^{-2}$) are destroyed when a moderate degree of disorder is introduced into the medium. The first band gap vanishes when the position disorder $d_p \geq 0.3a$ and $d_r \geq 0.1a$, respectively. The second band gap is fully destroyed when the amount of disorder reaches $d_p \geq 0.2a$ and $d_r \geq 0.05a$, respectively. It shows that a size disorder breaks down a gap more rapidly than position disorder does, which is consistent with previous published results by others. As the band gap is destroyed, the longest-lived modes emerge toward the band gap as the amount of disorder increases. From the field distribution patterns of the disordered medium, the field

patterns of the longest-lived modes become more localized when the amount of disorder intensifies.

The amplification process of active disordered systems is also investigated. The amplification curve is following an exponential relation. The exponential growth of total field energy and the dramatic drop of population difference density are the evidences of laser emission. It is found that the laser emissions are suppressed by the photonic band gap. The strength of amplification of EM wave can be enhanced by increasing the amounts of disorder. The laser emission can also be modified by alternating the relative spectral position of the band gap and the gain profile. The results implicate that the laser emission can be actively controlled by varying the amount of the disorder and the central wavelength of gain profile.

Experimentally, the stimulate emission of polymeric colloid liquid and solid random laser systems are investigated. The liquid random laser system is the ethanol solution which consists of Coumarin 480 dye and TiO_2 submicron-particles. The solid random laser system is the PMMA films which consist of Rhodamine 590 and TiO_2 submicron-particles. Coherent and incoherent laser emissions were observed in the systems. The influences of particle concentration on light emission were explored and optimum particle concentration was obtained. Optics microscopy and Scanning Probe Microscopy were used to investigate the film structure and the principle of incoherent and coherent laser was analyzed.

In the photoluminescence experiments, it was found that the slope of the peak

emission intensity curve of the colloid solution and PMMA films changed as the pump energy increased. These results indicate the lasing threshold and saturation behavior of the random laser system. The emission peaks of the colloid solution and PMMA films become narrower when pumping energy is above certain value. Several discrete peaks occurred in the emission spectra when the pump energy was further increased. This significant reduction of line-width and increase of the intensity of the emission peak confirm the existent of lasing threshold.

PUBLICATIONS ARISING FROM THE THESIS

Referred Journals Publications

1 X.H. Sun, X.M. Tao, X. Pu, K.C. Kwan, J.G Deng, *Low-Threshold Random Laser with One Mirror and Feedbacks in PMMA Nano-Composite Films*, Chinese Physics Letters, 22(10), P2568 (2005)

2 X.H. Sun, X.M. Tao, X. Pu, K.C. Kwan, J.G Deng, *Laser emission in PMMA nano-composite films,* Solid State Phenomena, 121-123, P1233 (2007)

2 K.C. Kwan, X.M. Tao, G.D. Peng, X.H. Sun, *Effect due to disorder on amplifying ordered media*, to be submitted to Applied Physics Letters

3 K.C. Kwan, X.M. Tao, G.D. Peng, X.H. Sun, J.G Deng, *Effect of disorder on the optical properties of two-dimensional photonic crystal with optical gain*, to be submitted to Journal of Applied Physics

4 K.C. Kwan, X.M. Tao, G.D. Peng, X.H. Sun, *Light localization from position and size disorder in amplifying random media with circular inclusions*, to be submitted to Physical Review B

Patent Application

1. X.M. Tao, X.H. Sun, J.G Deng, K.C. Kwan, *Laser emitting, method for making the same and use thereof*, US patent application 11/244,399, 2004.

2. X.M. Tao, J.G Deng, X.H. Sun, K.C. Kwan, *Large Area Colloidal Photonic Bandgap Structure, Equipment and Manufacturing Methods*, US patent application, pending.

Conference Publications

1. K.C. Kwan, X.M. Tao, *The Influence of Structural Parameters on the Reflection Band of One-Dimensional Photonic Band Gap*, *The Fiber Society 2004 Conference* The Fiber Society Fall Meeting, 2004 October 11-13, 2004, Ithaca, New York, USA

2. K.C. Kwan, X.H. Sun, X.M. Tao, J.G Deng, *The Lasing Action in Two-Dimensional Disordered System*, *The Fiber Society's Spring 2005 Conference*, May 25-27, 2005, St. Gallen, Switzerland.

ACKNOWLEDGEMENTS

First, I would like to express my sincerest thanks to my chief-supervisor, Prof. Xiao-Ming Tao, who always provides me with valuable guidance on my research works. This work would not be possible without her encouragement and patience.

I would also like to express my sincerest thanks to my co-supervisor, Prof. Gang-Ding Peng. He provided me with valuable professional knowledge. His advice and constant support always help me to solve the problem in my research work.

I also wish to express my thanks to my colleague Dr. Xiao-Hong Sun for her help and suggestions of the experimental works.

To my parents, the most patient and uncomplaining of all, I express my deep gratitude and deeper love. Finally, I would like to thank the most important one, the holy good God and our Savior Jesus Christ.

TABLE OF CONTENTS

LIST OF FIGURES

LIST OF TABLES

ABBREVIATION

1D	One dimension
2D	Two dimension
3D	Three dimension
ASE	Amplified spontaneous emission
BCHA-PPV	Poly(2,5-bis(cholestanoxy)-1,4-phenylenevinylene)
BDOO-PF	Poly(9,9-bis(3,6-dioxaoctyl)fluorene-2,7-diyl)
BEH-PPV	1,4-bis(2-ethylhexyloxy)phenylenevinylene
BuEH-MEH	Copolymers synthesized from varying ratios of BuEHPPV and MEH-PPV monomers.
BuEH-PPV	2-butyl-5-(2'-ethyl-hexyl)-1,4-phenylenevinylene
CN-PPP	Poly(2-(6'-cyano-6'-methyl-heptyloxy)-. 1,4-phenylene)
DCM/PS	4-(Dicyanomethylene)-2-methylene)-2-methyl-6-(4-(dimethylamino)styryl)-4*H*-pyran
DOO-PPV	2,5-dioctyloxy poly(*p*-phenylene-vinylene)
DOS	Density of states
EM	Electromagnetic
FDTD	Finite-difference time-domain
HEH-PF	Poly(9,9-bis(3,6-dioxaoctyl)fluorene-2,7-diyl)
GaAs	Gallium arsenide
GaN	Gallium nitride
MEH-PPV	(2-methoxy-5-(2’-ethylhexyloxy)-1,4-phenylenevinylene)
MMA	Methyl methacrylate
MOCVD	Metal Organic Chemical Vapor Deposition

$NdAl_3(BO_3)_4$	Neodymium aluminium borate
Nd:YAG	Neodymium-doped yttrium aluminium garnet
$Nd:YVO_4$	Neodymium-doped yttrium orthovanadate
PBG	Photonic band gap
PFO	Poly(9,9-dioctylfluorene)
PMMA	Poly(methyl 2-methylpropenoate)
PMT	Photomultiplier tube
PPE-PPV	Poly(phenylene-ethynylene) / poly(phenylene-vinylene)
SPM	Scanning Probe Microscopy
T5OCx	Quinquethienyl S,S-dioxide
TiO_2	Titanium dioxide
TE	Transverse electric
TM	Transverse magnetic
UV	Ultraviolet
ZnO	Zinc oxide

SYMBOL AND NOMENCLATURE

Symbol	Definitions
l_s	Scattering mean free path
l_t	Transport mean free path
$< \cos\theta >$	Average cosine of the scattering angle
l_g	Gain length
l_{amp}	Amplification length
S	Length of disordered medium
λ	Wavelength of electromagnetic wave
f	Frequency of electromagnetic wave
k	Wave vector of electromagnetic wave
τ	Dwell time of light
F_{photon}	Function of photon density
v	Transport speed of light in medium
D	Diffusion coefficient
$I(r)$	Light intensity distribution function
I_0	Constant amplitude of light intensity
ξ	Localization length
d_{beam}	Beam diameter
$I_{threshold}$	Threshold of pumping intensity
t_{pulse}	Laser pulse duration
$W_G(\vec{r},t)$	Energy density of pump light
$W_R(\vec{r},t)$	Energy density of probe light

$W_A(\vec{r},t)$	Energy density of amplified spontaneous emission
$A_1(\vec{r},t)$	Concentration of excited atomic particles
A_{total}	Total concentration of atomic particles
l_G	Mean free paths of pump light
l_R	Mean free paths of probe light
σ_{abs}	Absorption cross section of scattering particle
σ_{em}	Emission cross section of scattering particle
τ_e	Life time of the excited state
V1	Gain volume
V2	Scattering medium
γ_{th}	Threshold gain
R_1	Probabilities of photon returning in the gain volume
R_2	Probabilities of escaping in the gain volume
l_{path}	Average total path length
$I_{laser}(\lambda,t)$	Laser intensity
$p_2(t)$	Excited population density function
γ_0	Constant gain
B_p	Einstein coefficients for the pump
B_l	Einstein coefficients for the laser emissions
I_p	Pump intensities,
$I_{laser}(\lambda,t)$	Laser intensities

$\eta(\lambda)$	Spontaneous emission coefficient
C_{con}	Proportion constant
Γ	Spontaneous emission rate;
$\vec{E}$	Electric field
$\vec{H}$	Magnetic field
$\vec{D}$	Electric flux density
$\vec{B}$	Magnetic flux density
ρ	Free charge density
$\vec{J}$	Electric conduction current density
$\vec{M}$	Magnetic conduction current density
μ	Magnetic permeability
μ_r	Relative permeability
μ_0	Free space permeability
ε	Dielectric permittivity
ε_r	Relative permittivity
ε_0	Free space dielectric permittivity
σ	Electric conductivity
σ^*	Equivalent magnetic loss
$\vec{J}_{source}$	External electric current density
$\vec{M}_{source}$	External equivalent magnetic current density
$\sigma(\omega)$	Frequency-dependent conductivity function
σ_0	Constant amplitude of conductivity

ω_t	Transition frequency
T_2	Dipole relaxation time
ζ	Damping coefficient.
$\chi(\omega)$	Frequency-dependent susceptibility function
χ_0	Constant amplitude of susceptibility
ζ	Damping coefficient
P	Polarization density
$\vec{P}$ (t)	Time depend electric polarization density
λ_t	Lasing transition wavelength
$\Delta\omega$	Linewidth of the atomic transition
$T_{collision}$	Collision time of the atom
Q	Pumping rate
κ	Classical rate
c	Speed of light in vacuum
ε_0	Free-space permittivity
h	Planck's constant
$\Delta N(t)$	Population difference density of lasing energy levels
$N1$	Population density of ground energy state
$N2$	Population density of lower lasing level
$N3$	Population density of upper lasing level
$N4$	Population density of highest energy state
L_1	Ground energy level
L_2	Lower lasing level

L_3	Upper lasing level
L_4	Highest energy level
τ_{43}	Lifetime of highest energy state
τ_{32}	Lifetime of upper lasing level
τ_{21}	Lifetime of lower lasing level
$\hat{z}$	Unit vector of z-direction
H_x	Magnetic field component along the x-direction
H_y	Magnetic field component along the y-direction
E_z	Electric field component along the z-direction
Δx	Lattice spatial increment along x coordinates
Δy	Lattice spatial increment along y coordinates
Δt	Discretized time increment
n	Index for the time step
i	Index for the space step
R	Radius of scattering particle
ε_1	Dielectric constant of scattering particle
ε_2	Dielectric constant of host matrix
n_1	Reflective index of scattering particle
n_2	Reflective index of host matrix
$\gamma_x, \gamma_y, \gamma$	Probability density function
a	Lattice constant
d_p	Position disorder
d_r	Size disorder

U_E	Total electric field energy
ξ_{amp}	Amplification rate
T_t	Trigger time

CHAPTER 1
INTRODUCTION

1.1 Background

Fibers consisting periodically ordered structures, such as fiber Bragg grating (Hill and Fujii, 1978, Kersey, 1996, Du, Tao and Tam, 1999, Bass, 2002), which have functions of transmitting and modulating photons, can be used as sensors and transmitting media in smart textile structural composites (Tao, 2001). Films made of polymer dispersed or encapsulated liquid crystals can be used as electrically reflective displays.

On the other hand, disordered dielectric media integrating into polymeric fibers/films may be used as an element for flexible fabric display, which is capable of scattering and self-amplification of light. Disordered dielectric media are random structures that dielectric inclusions are random distributed. The disordered materials such as laser crystal powder, ceramic powder and suspensions of semiconductor particles form strongly scattering media. Light waves propagating in disordered dielectric media experiences random multiple scattering attributed to the fluctuations of random spatial and size distributions dispersion of the refractive index of the scattering elements.

By introducing optical gain materials such as laser dyes and conjugated polymer into disordered dielectric structures, optical amplification via stimulated emission can be achieved in the active disordered dielectric media. Active disordered dielectric media consists three basic components, i.e., the gain media, the scattering elements and the host. Light wave propagating in active disordered dielectric media is reinforced and scattered by the optical gain and scattering elements, respectively. Under certain conditions, laser-like emission (random laser) occurs in an active disordered medium as a result of combined actions of multiple scattering and stimulated emission amplification. In a random laser, the mode of laser is formed by a self-formed cavity rather than a regular cavity structure. Unlike a conventional laser, the feedback mechanism of random laser is due to multiple scattering of light in disordered dielectric structures. Random laser was predicted theoretically by Letokhov (Letokhov, 1967, 1968) and then observed experimentally in various types of active disordered systems such as semiconductor powders (Cao, Zhao, Ho, Seelig, Wang and Chang, 1999), laser dyer solution containing TiO_2 particles (Lawandy, Belachandran, Gomes and Sauvin, 1994) and conjugated polymer films (Polson, Huang and Vardeny, 2001).

Random laser systems have applications in the information technology and optoelectronic industry. Since random laser emissions can be generated in irregular cavities, random laser systems are easily fabricated down to micron-scale, they can be used to construct low-cost microsize sources of coherent light and minutial laser. The other applications such as lasing textiles (Lawandy, Belachandran, Gomes and Sauvin, 1994) and photonic paints (Balachandran and Lawandy, 1995) have been proposed. Furthermore, random laser systems open up the possibility of light self-amplification in polymeric composite fiber/film, which is a potential candidate of developing textile displays.

Recently, great deals of experimental and theoretical studies have been devoted to the origin of the laser action in active disordered media. These studies included emission spectra, dynamics of stimulated emission and optimization of lasing threshold. Only limited research (Chang, Cao and Ho, 2003, Yamilov and Cao, 2004) has explored the relationship between the random laser and the degree of disorder of the active disordered media.

1.2 Objectives

The present research is concerned with a study of nano- and submicron structured polymeric composite systems with passive and active disordered dielectric media in order to achieve light self-amplification. This project aims to investigate the influence of disorder on the optical properties of passive and active disordered dielectric media. The spatial and radial perturbations of scattering elements in the disordered dielectric media are selected as disorder parameters. The key issues to be addressed are:

1. To compare various theoretical approaches and select a time-dependent theoretical framework for the simulation of passive and active disordered media consisting scattering dielectric particles. The framework should have abilities to predict the optical response and stimulated emission of active materials by taking consideration of the optical gain profile of active materials and the structural parameters.

2. To implement numeric simulations based on the theoretical models to study the influences of disorder on the emission properties of both passive and active disordered dielectric systems.

3. To explore the emission properties of passive disordered dielectric systems in term of emission spectra, mode distribution and field distribution pattern in order to establish the relationship between the disorder and the localization properties of the passive disordered dielectric systems.

4. To examine the amplification process, the lasing dynamics and the light confinement in active disordered dielectric systems and study the effect of disorder on random lasing modes in active disordered dielectric systems.

5. To construct polymer composite disordered systems comprising gain medium and scattering particles, such as colloid solutions and polymeric films, and to achieve random laser emission in the polymer composite disordered systems and characterize the spontaneous and stimulated emission of the polymer composite disordered systems.

1.3 Methodology

The research methodology adopted in this study includes the following details:

1.3.1 Theoretical analysis and numeric simulation

Several theoretical modelling of active disordered dielectric systems have been developed previously by others such as the diffusion model, Monte Carlo simulation and finite-difference time-domain (FDTD) method. Based on the existing models, the initial work is to select and verify a theoretical framework for the simulation of passive and active disordered dielectric systems, in which the light coherent, scattering and amplification properties of disordered systems are taken into account. Furthermore, the model should be able to predict the lasing and atomic dynamic in the active disordered dielectric systems.

The time-dependent theory of random laser which combines the time-dependent Maxwell's equations with the semi-classical laser theory is adopted to investigate the laser emission of two-dimensional (2D) active disordered dielectric systems. According to the time-dependent theory, the optical gain is described by the rate equations of an atomic system. The numeric simulation is implemented based on the finite-difference time-domain (FDTD) method and experimental

considerations such as dye properties, refractive index of dielectric materials and the structure parameters of scattering particles. Verification of FDTD simulations will be conducted by using published examples: materials and structural parameters as well as results of the passive and active systems.

Various parameters of disordered dielectric system, i.e. the scattering particle concentration and the amount of disorder and the optical gain profile, are investigated in order to determine the significant light amplification and wave localization. In order to examine the amplification process, light localization and mode competition, the emission spectra, the population inversion and the field distribution of active disordered dielectric systems will be analyzed as functions of the degree of position and size disorder.

1.3.2 Fabrication of polymeric disordered systems

In the current works, liquid and solid-state polymeric active disordered systems will be constructed, i.e., dye colloid solution and dye-doped polymethylmethacrylate (PMMA) composite film. The amplification behavior and optical properties of the disordered systems are experimentally investigated. Organic dyes such as Coumarine and Rhodamine and TiO_2 particles will be used

as gain media and scattering material, respectively.

1.3.3 Characterization of polymeric disordered systems

Characterization of the PMMA composite films will be carried out by using a range of analytical instruments. The structures and morphology of the films will be investigated by using optical microscopy and scanning probe microscopy. The emission spectrum will be measured by using photomultiplier detection system. The emission spectra of the dye colloid solution and PMMA films, and the relationship between the emission peak intensity, the scattering concentration and the pumping energy density will be examined.

1.4 Thesis outline

This thesis consists of seven chapters. Structure of this thesis is outlined as follows:

Chapter 1 provides a brief introduction to the development and applications of random laser systems. The objectives of the current study also are stated. Finally, research methodology adopted in this thesis and the structures of the dissertation are summarized.

An overall review regarding to the fundamentals of random laser is presented in Chapter 2. The chapter begins with a description of basic characteristic length scales and diffusion theory. The features of random laser emission also are discussed. Various types of active disordered media and experimental research are reviewed.

In Chapter 3, various theoretical treatments of passive and active random media are briefly introduced. Then the time dependent theory of random laser and finite-difference time-domain method, which is adopted in the current study, are discussed in details including the formalisms, algorithm and implementation of the numerical simulation. The verification of the numerical model and the algorithm are also provided in this chapter.

Chapter 4 focuses on a theoretical investigation of the influence of disorder on passive disordered dielectric media. Definitions of position and size disorders are firstly provided. Then analysis of mode distribution of ordered and disordered media, effect of disorder on photonic band gap, mode distribution and competition of the passive disordered dielectric media are presented.

In Chapter 5, experimental studies of the random laser in dye-doped colloid polymeric solutions and PMMA films are described. Experimental setup and results are discussed.

In Chapter 6, influence of disorder on the active disordered media consisting of dielectric scattering particles will be examined by using the time-dependent theory. Investigations of amplification of electromagnetic wave and effect of particles density on laser emission are firstly presented. Then effect of disorder on laser emission at different transition frequency is discussed.

Chapter 7 summarizes the major findings of the study and draws conclusions. The future work is also suggested.

CHAPTER 2
LITERATURE REVIEW

2.1 Introduction

An overall literature review is presented in this chapter regarding to the fundamentals of the related topics covered in this dissertation. It starts with an introduction to disordered systems, diffusion theory and the basic characteristic length scales, then followed by the development of random lasers (active disordered media).

2.2 Disordered media

Disordered dielectric structures are random systems that the length scale of the refraction index variation is comparable to the light wavelength (John, 1987, Yablonovitch, 1987). In the visible frequency range, the wavelength is between 400nm-760nm. In a disordered medium without optical gain (passive disordered medium), light wave is multiply scattered due to the spatial fluctuation of the refraction index. If an optical gain is introduced into the disordered medium (active disordered medium), light will be amplified as well as scattered. Under certain conditions, interesting phenomena such as backscattering of light (Gu, Lu, Martinez, Mendez and Maradudin, 1994, Peng and Gu, 1999, Gu and Peng, 2000, Peng and Gu, 2000, Gu and Peng, 2001) and laserlike emission (Cao, Zhao, Ho,

Seelig, Wang and Chang, 1999, Cao, Xu, Ling, Burin, Seeling, Liu and Chang, 2003, Liu, Yamilov, Ling, Xu and Cao, 2003) would be exhibited in active disordered media due to the combined actions of multiple scattering and stimulated emission amplification. This phenomenon is unexpected to occur in a pure homogeneous gain medium.

Submicron/nano-scaled disordered structures with optical gain have many potential applications in information technology and optoelectronic industry. Furthermore, active disordered systems open up the possibility of light self-amplification in polymeric composite photonic fiber, which is a potential candidate of developing textile displays.

2.2.1 Basic characteristic length scales

In order to understand the light transport properties in both passive and active disordered media, it is necessary to define the basic length scales for light scattering problems. The first important length scale is the scattering mean free path l_s. It is the average distance between two consecutive scattering events when light travels in a disordered medium. It is obvious that l_s tends to infinity long when light travels in any vacuum as scattering element is missing. Another

important length scale is the transport mean free path l_t. It is an average distance a photon travels before its propagation direction is totally changed. The scattering mean free path l_s and the transport mean free path l_t are related by the equation:

$$l_t = \frac{l_s}{1 - < \cos\theta >}, \qquad \textbf{(2.1)}$$

where $< \cos\theta >$ is the average cosine of the scattering angle.

Furthermore, there are two relevant length scales, i.e., the gain length l_g and amplification length l_{amp}, to characterize the amplification process. The gain length l_g and the amplification length l_{amp} are defined as the path length and the root-mean-square average net distance of the light trajectory over which the light intensity is increased by a factor e, respectively. In a homogeneous gain medium without scattering elements, the light trajectory is a straight line. Thus, one can easily show that the gain length is equal to the amplification length.

According to the scattering properties of light, disordered media can be separated into three regimes (John, 1991): ballistic regime ($S \sim l_t$), diffusive regime ($S >> l_t >> \lambda$) and strongly scattering regime ($kl_t \sim 1$). S represents the length of the disordered medium. λ and k denote the wavelength and the wave vector of light,

respectively.

2.2.2 Diffusion theory

In the ballistic regime, the transport mean free path is comparable to the system length of disordered medium, i.e., $S \sim l_t$. The scattering strength is weak and the scattering events infrequently occur in ballistic disordered media. In general, the trajectories of light are almost straight-line paths. The residence time (dwell time τ) of the light in the ballistic disordered medium is very short and thus the amplification of light is insignificant when the optical gain is present.

In the diffusive regime, the transport mean free path is much smaller than the length of the disordered medium but larger than the wavelength of photon, i.e., $S >> l_t >> \lambda$. The transport of light is treated as a diffusion process and described by the diffusion equation. The scalar diffusion equation governing the diffusion process is expressed as

$$\frac{\partial F_{photon}}{\partial t} = D\nabla^2 F_{photon} + \frac{\nu}{l_g} F_{photon}, \qquad \textbf{(2.2)}$$

where F_{photon} is the function of photon density, ν is the transport speed of light

inside the medium, and *D* is the diffusion coefficient. The diffusion coefficient is related to the size of the system and the dwell time of light in the medium, i.e., $D = S^2 / \tau$. The dwell time of photon in diffusive media is relatively longer than that in ballistic media as photons are multiply scattered. Since the photons are frequently scattered in the active disordered media, the longer light path length and dwell time facilitate the amplification of light. If the mean path length of light is long enough, the light intensity will be reinforced substantially and the amplified spontaneous emission (ASE) may arise. Under certain circumstances, active diffusive disordered media exhibit laser-like emission. The laser spikes are randomly distributed over the gain volume. This phenomenon is called as incoherent random laser.

2.2.3 Localization of light

In strongly scattering regime, the transport mean free path is in the same order of the photon wavelength, i.e., $kl_t \sim 1$. The scattering strength is very strong and thereby the photons are scattered very frequently. The diffusion mechanism alone is no longer appropriate to describe the light transport behavior. Instead of the diffusive transport, localization of light dominates in the strongly scattering regime. Photons are trapped inside the strongly scattering medium as a result of

the multiple scattering. Under the Ioffe-Regel condition (Mott, 1974), i.e., $kl_t \leq 1$, the scattering strength becomes very strong and recurrent scattering events probably arise. The recurrent scattering events lead to the formation of closed loop light paths. It means that the light returns to the starting point of the light path. A closed loop light path is depicted in Figure 2.1.

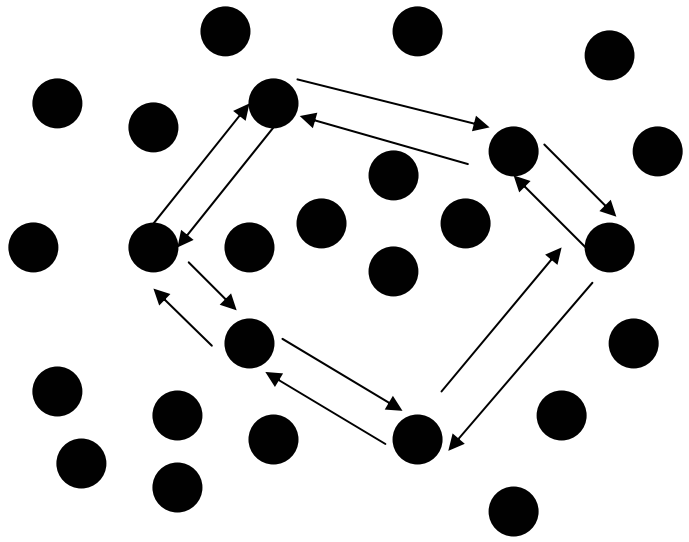

Figure 2.1 A closed loop light path

In other words, if the scattering strength is large enough, localized states will be formed randomly in the strongly disordered media. Light is tightly confined around the localization centers due to the multiple scatterings and the wave interferences. Away from the localization centers, light decays exponentially as described by the following equation:

$$I(r) = I_0 e^{-r/\xi} \quad \textbf{(2.3)}$$

where *I(r)* is the light intensity distribution function and I_0 is the constant amplitude of light intensity. ξ is the localization length. If the gain is introduced to the strongly scattering medium, one can expect that the light will be amplified nonlinearly because of the presence of localized state that serves as a resonator. The nonlinear light emissions due to the randomly formed localized state are named as coherent random lasers.

2.3 Random Lasers

In this section, detailed reviews of random laser systems will be presented. Random laser system is an active disordered medium that exhibits laser-like emission crossing a certain threshold. This laser action results from the mode of laser formed by a self-formed cavity rather than a regular cavity. Unlike a conventional laser, the feedback mechanism of random laser is due to the multiple scattering of light in a disordered medium. The random lasers are separated into two categories depending on the optical feedback.

There are two types: incoherent random lasers and coherent random lasers. The

optical feedback of incoherent random laser is intensity feedback whereas the optical feedback of coherent random laser is field feedback. The field feedback leads to the interference effect, which is a distinctive feature of coherent random laser. In fact, the extreme low lasing threshold and the super-narrow spectral peaks of the coherent random laser result from the interplay of the interference effect and optical gain. The incoherent random laser can be realized in a diffusive random medium such as laser crystal powders (Gouedard, Husson, Sauteret, Auzel and Migus, 1993) and dilute colloidal laser dye solution (Lawandy, Belachandran, Gomes and Sauvin, 1994). On the other hand, the coherent random laser is realized in highly disordered system like dye-doped cholesteric liquid crystals (Kopp, Genack and Zhang, 2001, Schmidtke, Stille and Finkelmann, 2003) and dye-doped gel films (Sobel, Gindre, Nunzi, Denis, Dumarcher, Fiorini-Debuisschert, Kretsch and Rocha, 2004).

Experimentally, it is reported that random lasers consist some common features such as threshold behavior of laser action(Cao, Zhao, Ho, Seelig, Wang and Chang, 1999), and dramatic narrowing of the emission band above the threshold (Cao, Xu, Chang and Ho, 2000), and nonisotropic multipeak properties (Cao, Zhao, Ong and Chang, 1999) in the emission spectra.

2.3.1 Spectral narrowing

Spectral narrowing is a typical feature of a random laser, which has been unambiguously demonstrated in various random laser systems. For instance, the collapse of emission band was observed in the photoluminescence experiments of zinc oxide (ZnO) film (Cao, Zhao, Ong, Ho, Dai, Wu and Chang, 1998). In this experiment, a oxide ZnO film (300 to 350nm thickness) composed of 50 to 150nm ZnO particles deposited on amorphous fused silica substrates was excited with 30ps pulses of a frequency-tripled Nd:YAG laser (λ =355nm). Figure 2.2 shows the evolution of the emission spectra with different pump intensities. When the film was pumped at a low pump intensity, a single broad amplified spontaneous emission peak (ASE peak) first appeared in the emission spectrum. As the pump intensity increases, the amplification was enhanced near the central frequency of the gain spectrum and thus the linewidth of emission peak was collapsed. When the pump power exceeded the lasing threshold, discrete narrow peaks emerged in the spontaneous emission spectrum. The linewidth of discrete peaks is less than 1nm. The frequencies of the discrete spectral peaks depended on the pumping spot position. It was also found that the number of emission peaks is depended on the dye concentration and pump intensity in laser paint

systems (Sha, Liu and Alfano, 1994).

In this strongly scattering system, the occurrence of the discrete emission peaks was originated from the closed loop light paths. Figure 2.3 shows that the laser resonance established in the close loop of light paths. It is believed that the constructive interference of the recurrent light in the closed loop light paths at certain frequencies is due to the inter-particle strong scattering rather than the total internal reflection inside the ZnO particles. It is because the nano-sized ZnO particles are too small to be the laser cavities.

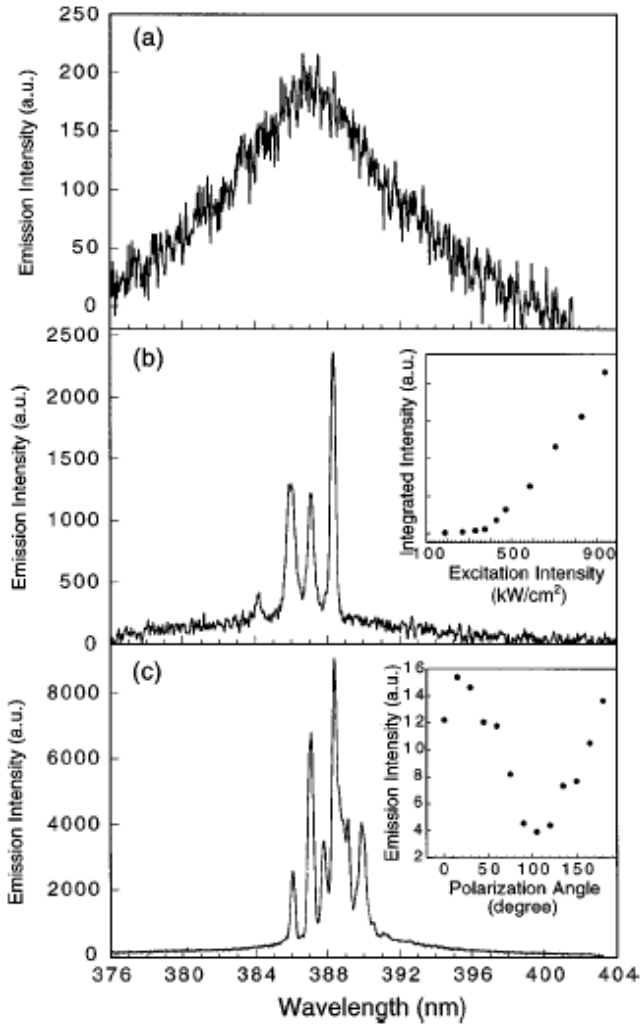

Figure 2.2 Spectra of emission from ZnO film. *Source*: (Cao, Zhao, Ong, Ho, Dai, Wu and Chang, 1998)

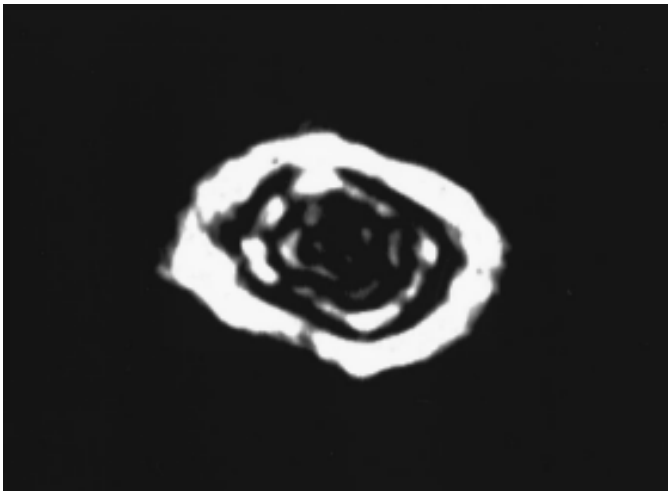

Figure 2.3 Amplified images of the excitation area above the lasing threshold on the film. *Source*: (Cao, Zhao, Ong, Ho, Dai, Wu and Chang, 1998)

Recently, the discrete emission peaks were also demonstrated in the diffusive disordered media with optical gain (Mujumdar, Ricci, Torre and Wiersma, 2004). In the diffusive regime, the interference effect is absence and the localized states do not exist. It is corroborated that the narrow peaks are associated with the amplification along rare long light paths in diffusive disordered media rather than self-formed resonators.

2.3.2 Lasing threshold

Lasing threshold is one of the important characteristics for laser systems. In a regular cavity, it is known that the loss of cavity mode would suppress the laser emission. When the pump intensity exceeds a critical value, the gain compensates the loss of the cavity mode. Simultaneously, population inversion builds up and stimulated emission dominates. Similarly, the threshold behaviors are revealed in the random laser systems. Figure 2.4 shows the peak intensity for the emitted light from a random laser as a function of the pump intensity. It is obvious that there exists a well-defined threshold at which the slope of the input-output curve changes.

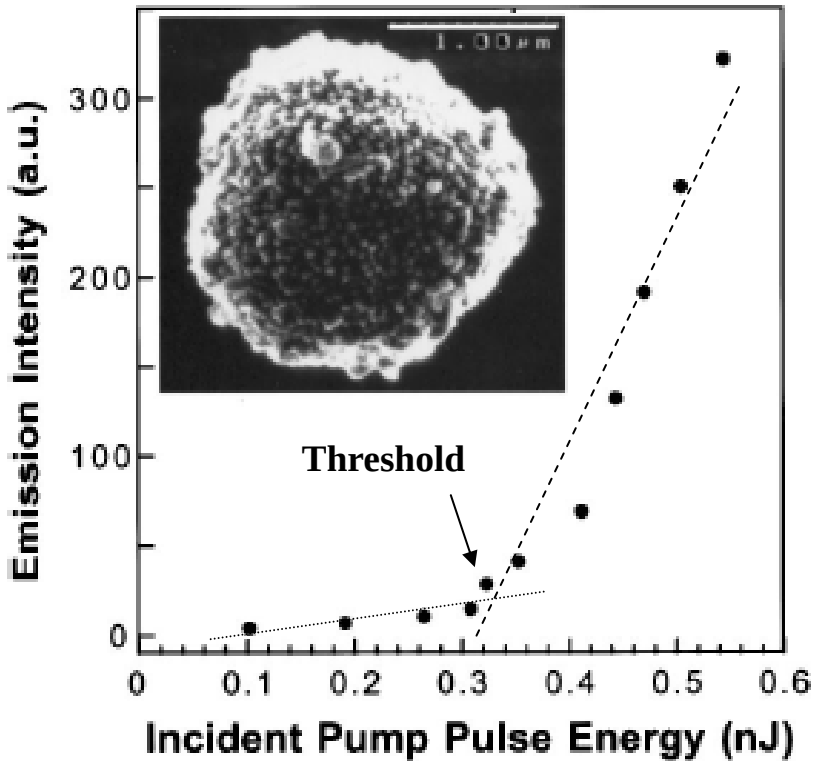

Figure 2.4 The input-output curves of the ZnO cluster random laser. The inset is the SEM image of the ZnO cluster *Source*: (Cao, Xu, Chang, Ho, Seelig, Liu and Chang, 2000)

In the localized regime, the lasing threshold is critically dependent on the quality factor of random cavities in a random laser. The modes with the highest quality factor have the smallest decay rates which determine the value of lasing threshold. In the modes with smallest decay rate, photons are rapidly cumulated by amplification and emitted out. Based on this idea, the influence of disorder strength on the lasing threshold was studied (Yamilov and Cao, 2004a). Furthermore, Patra calculated the distribution of the decay rates of the eigenstates of a disordered medium and found a simple analytical formula to predict the

lasing threshold of the active disordered media, which is applicable in both diffusive and in the localized regimes (Patra, 2003). Another study of one-dimensional random laser showed that the lasing threshold decreased exponentially with the system size by using an analytical approach (Burin, Ratner, Cao and Chang, 2002).

Several experimental and theoretical studies have been carried out to investigate the dependence of lasing threshold on the transport mean free path l_t and beam diameter d_{beam} in amplifying random media. In a photoluminescence experiment of PMMA film doped with dye and titanium dioxide (TiO_2) particles, it was found that the lasing threshold intensity varies with l_t as $I_{threshold} \propto l_t^{1/2}$ and with d_{deam} as $I_{threshold} \propto {d_{beam}}^{-a}, 1 \le a \le 2$ (Ling, Cao, Burin, Ratner, Liu, Seelig and Chang, 2001, Cao, Ling, Xu, Burin and Chang, 2003). The analytical proofs have been reported by Burin et al (Burin, Cao and Ratner, 2003). Pinheiro and Sampaio also predicted that the lasing threshold of three-dimensional diffusive random lasers follows the power law $I_{threshold} \propto l_t^{1/2}$ (Pinheiro and Sampaio, 2006). In this work, the lasing threshold was determined by using dipole model (Rusek and Orłowski, 1995).

Another attempt was to examine the dependence of threshold on the pump beam spot size (Soest, Tomita and Lagendijk, 1999). In a photoluminescence experiment of a solution containing sulforhodamine B dye and TiO_2 particles, the results indicated that the threshold was increased by a factor of 70 when the spot diameter was reduced to a scale comparable to the mean free path. The similar results were recaptured and explained in a numerical simulation based on a diffusion model (Florescu and John, 2004).

2.3.3 Various types of active disordered media

In 1968, the first prediction of the laser-like emission from active disordered media was proposed. Letokhov (Letokhov, 1968) investigated theoretically the possibility of lasing in multiple light scattering media with gain by solving the diffusion equation in an amplifying media with strong randomness. After two decades, the experimental observations of the laser-like emission in dye-doped solution with TiO_2 nanoparticles were reported (Lawandy, Belachandran, Gomes and Sauvin, 1994). The unusual behavior of stimulated emission in active disordered system stimulated the interest of the random laser both in theoretical and experimental studies. Up to now, the development of random lasers can be divided into two main catalogues: inorganic disordered system and organic

disordered system.

Inorganic disordered system

In the past twenty years, intense stimulated radiations were observed in a wide variety of laser crystal powder such as titanium-doped sapphire powder, semiconductor cluster and ceramic powder. Random laser action has been investigated in different forms of inorganic materials, such as powder, cluster and thin film. The inorganic particles are served as both the active medium and the light scattering element that light waves are multiply scattered and amplified. The studies of the inorganic disordered system are interesting because of the potential applications of compact, low-cost, simply designed amplification devices, which are easy to fabricate.

Laser crystal powder random laser

In 1986, Markushev et al. observed that the emission spectrum of a laser crystal $Na_5La_{1-x}\ Nd_x(MoO_4)_4$ narrowed to a sharp peak and nanosecond output pulse appeared under the excitation of 30-ns pumping pulse (Markushev, Zolin and Briskina, 1986). Following this work, many novel laser crystal materials have been explored such as $NdAl_3(BO_3)_4$, $NdSc_3(BO_3)_4$ (Noginov, Zhu, Frantz, Novak,

Williams and Fowlkes, 2004), Nd:$Sr_5(PO_4)_3F$ (Noginov, Noginova, Caulfield, Venkateswarlu, Thompson, Mahdi and Ostroumov, 1996), Nd^{3+}:$Y_3Al_5O_{12}$ (Feng, Bisson, Lu, Huang, Takaichi, Shirakawa, Musha and Ueda, 2004), and $Nd_{0.5}La_{0.5}Al_3(BO_3)_4$ (Bahoura, Morris and Noginov, 2002, Bahoura, Morris, Zhu and Noginov, 2005). It has been demonstrated that stimulated emission could be radiated without regular resonator. For example, Noginov et al. (Noginov, Noginova, Caulfield, Venkateswarlu, Thompson, Mahdi and Ostroumov, 1996) reported that the observation of shot pulses (>300-ps) stimulated emission in $NdAl_3(BO_3)_4$, $NdSc_3(BO_3)_4$ and Nd:$Sr_5(PO_4)_3F$ laser crystal powder during 532 and 805nm excitation. The average particles size of the crystal powder were 600nm to 24.8 μm. It was found that the threshold pump intensity was inversely proportional to the small-signal amplification along the photon trajectory in the pumped volume.

Semiconductor random laser

Another type of active disordered medium is semiconductor material laser system. Random lasing has been demonstrated in ZnO (Thareja and Mitra, 2000, Mitra and Thareja, 2001) which is an efficient light emitter with a wide electronic band gap (3.37eV). The corresponding emission wavelength is near

the ultraviolet range (λ ~385nm). Because of the high refractive index (n~2.2) of ZnO, it is feasible to construct strong scattering structures.

Recently, extensive studies have been focus on the potential applications in ZnO random laser for ultraviolet emission (Cao, Zhao, Ong, Ho, Dai, Wu and Chang, 1998). As early as 1981, the observation of stimulated emission in ZnO powder was reported (Nikitenko, Tereschenko, Kuz'mina and Lobachev, 1981) but the underlying mechanism was not investigated. Until the photoluminescence experiments of ZnO powders was performed by Cao's group (Cao, Zhao, Ong, Ho, Dai, Wu and Chang, 1998, Cao, Zhao, Ho, Seelig, Wang and Chang, 1999, Cao, Xu, Chang, Ho, Seelig, Liu and Chang, 2000, Cao, Xu, Seelig and Chang, 2000), it was confirmed that the strong light amplification and laser action in the highly disordered gain media are attributed to the self-formed cavities and the coherent feedback mechanism. In the experiments, the random laser actions were demonstrated in the micron-sized ZnO clusters (Cao, Xu, Seelig and Chang, 2000). The micro-sized clusters (diameter ~ 1 μm) were constructed by nano-sized powders synthesized by using the precipitation reaction method (Jézéquel, Guenot, Jouini and Fiévet, 1995). The scanning electronic microscope (SEM) image of the ZnO cluster is shown in the inset of Figure 2.4. The optical

experiment was conducted on a single cluster by using the fourth harmonic of a pulsed Nd:YAG laser (λ =266nm, t_{pulse}=25 μ s). The input-output curves and the evolution of the emission are shown in Figure 2.4 and Figure 2.5 a, c, e, respectively. The results are qualitatively similar to that of previous studies (Cao, Zhao, Ong, Ho, Dai, Wu and Chang, 1998, Cao, Zhao, Ho, Seelig, Wang and Chang, 1999). Bright spots appear in the ZnO cluster above the lasing threshold, as shown in Figure 2.5f. Nevertheless, there is no bright spot below the lasing threshold, as shown in2.5b. It was concluded that the emission of bright spots were originated to the confinement of light in micron-sized ZnO clusters. The observation of localization of emission seems to be the evidence of Anderson localization of light in micrometer scale disordered structures (Anderson, 1958, John, 1984, 1991)

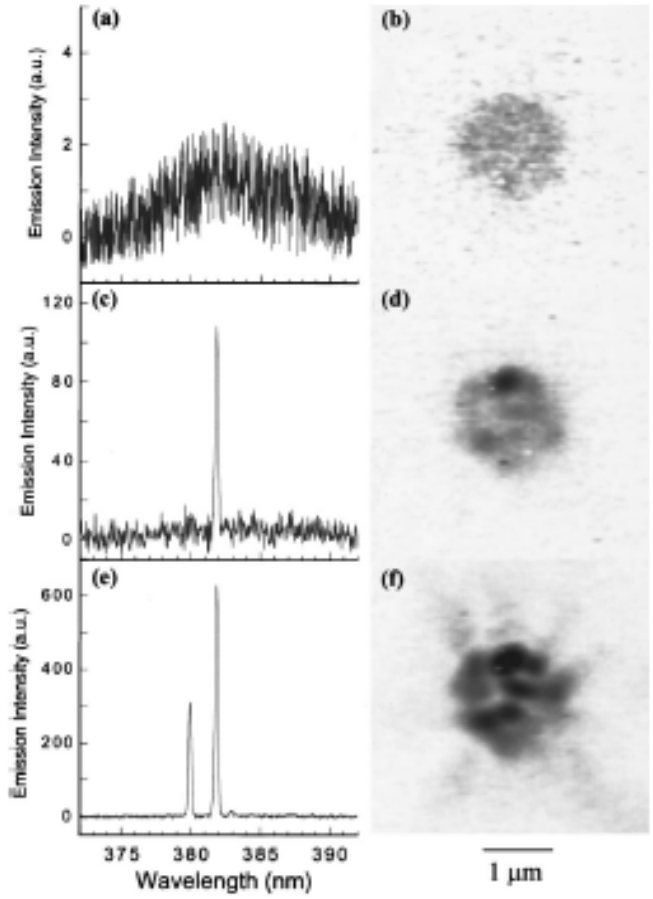

Figure 2.5 (a), (c), and (e) are the spectra of emission from the ZnO clusters. (b), (d), and (f) are the corresponding spatial distributions of emission intensity in the cluster. The incident pump pulse energy is 0.26 nJ for (a) and (b), 0.35 nJ for (c) and (d), and 0.50 nJ for (e) and (f). (*Source*: Cao 2000)

A number of attempts have been undertaken to achieve the random laser action in ZnO thin films (Zhang, 1995, Cao, Zhao, Ong, Ho, Dai, Wu and Chang, 1998, Cao, Zhao, Ong and Chang, 1999, Mitra and Thareja, 2001, Yu and Leong, 2004, Yu, Yuen, Lau and Lee, 2004, Lai, An and Ong, 2005, Stassinopoulos, Das, Giannelis, Anastasiadis and Anglos, 2005, Yuen, Yu, Leong, Yang, Lau and Hng, 2005). The polycrystalline ZnO thin films were fabricated by using different

synthesis techniques including spin coating method (Stassinopoulos, Das, Giannelis, Anastasiadis and Anglos, 2005), the filtered cathodic vacuum arc technique (Zhang, Chua, Yong, Li, Yu and Lau, 2006), laser ablation method (Cao, Zhao, Ong, Ho, Dai, Wu and Chang, 1998). For example, Yu et al. demonstrated room-temperature ultraviolet lasing in the waveguides composed of ZnO, which were growth on silicon substrate (Yu, Yuen, Lau and Lee, 2004). By using filtered cathodic vacuum arc technique and the post-growth annealing, ZnO thin films with a high crystal quality formed light resonators. The resonances were related to the light scattering of the inhomogeneities of zinc oxide grains.

Intense stimulated emission and threshold behavior were also observed in ZnO single-crystalline under optical excitation (Lv, Li, Guo, Wang, Wang, Xu, Yang, AI and Zhang, 2005). ZnO single-crystal star-shaped microcrystals were fabricated by electrochemical deposition method. This ZnO structure revealed the random laser actions with longer emission wavelength, 403.9nm, which was different from the known ZnO random laser, 380-390nm.

On the other hand, a great deal of experimental work has been devoted to ZnO

nano-sized structures such as nanowires (Hsu, Wu and Hsieh, 2005, Lau, Yang, Yu, Li, Tanemura, Okita, Hatano and Hng, 2005), nanorod (Liu, Yamilov, Wu, Zheng, Cao and Chang, 2004, Qiu, Wong, Wu, Lin and Xu, 2004, Yu, Yuen, Lau, Park and Yi, 2004, Han, Wang, Wang, Cao, Liu, Zou and Hou, 2005), nanosaws (Wu, Hsu, Cheng, Yanga and Hsieh, 2006) due to their unique properties. One of the examples is ZnO nanorod arrays grown on sapphire by using a metalorganic vapor-phase epitaxy system (Park, Kim, Jung and Yi, 2002). The nanorods with good vertical alignment were randomly embedded in ZnO epilayers. MgO was first deposited on the sample as a buffer layer and a layer of ZnO thin film covering the buffer layer to form the epilayer. The investigation of the formation conditions of random laser cavities inside ZnO epilayers showed that the triggering of coherent and incoherent random laser actions of ZnO epilayers was controlled by the selection of crystalline orientation.

GaAs and GaN are known to be the high gain semiconductor laser materials. Several active disordered systems based on the GaAs and GaN have been reported (Sun, Gal, Gao, Tan, Jagadish, Puzzer, Ouyang and Zou, 2003, Noginov, Zhu, Fowlkes and Bahoura, 2004, Gradečak, Qian, Li, Park and Lieber, 2005, Sun and Jiang, 2006). Demonstration of laser emission in GaAsN disordered

system was presented by Sun's group (Sun, Gal, Gao, Tan, Jagadish, Puzzer, Ouyang and Zou, 2003). The samples of GaAsN alloys containing 0.6, 1.77, and 2.8% nitrogen were grown on GaAs (100) substrates by metalorganic chemical vapor deposition (MOCVD). By pumping the samples with a frequency-doubled Nd:YAG laser (λ =532nm, t_{pulse}=1μs), several high intensity discrete peaks appeared in the emission spectrum above the lasing threshold. The lasing behaviors exhibited in the GaAsN films were similar to that of ZnO random lasers. It is believed that the structural irregularities at the interface between GaAsN film and GaAs substrate are the scattering sources of the stimulated feedback.

Recently, nano-sized GaN random laser system has been developed (Gradečak, Qian, Li, Park and Lieber, 2005). One example is GaN nanowire. GaN nanowires grown on sapphire substrates by MOCVD medthod. The samples were optically pumped by Nd:YVO_4 laser (λ =266nm, t_{pulse}=7ns). Since the GaN nanowires had single-crystal structures and triangular cross section, the GaN nanowires acted as laser cavity as well as gain medium. These optical excited studies also showed that the laser mode space is inversely proportional to the length of the nanowires. Furthermore, it was indicated that the lasing threshold was effectively reduced by

the excellent structural cavity property, crystalline growth direction and n-type doping. Tables 2.1(a)-(d) summarize the development of the inorganic random lasers including laser crystal powder random laser and semiconductor random laser.

Table 2.1a Parameters of different laser crystal powder and semiconductor random lasers

Laser crystal powder and semiconductor random media	Pumping Wavelength/ Pulse Duration	Particle Size	Sample Thickness	Pumped Area	Threshold Energy Density	Threshold Power Density/ Emission Lifetime	Emission frequency	Fabrication method
ZnO nanowire (Hsu, Wu and Hsieh, 2005)	325nm/500ps	diameter ~ 60 - 200nm length ~ 3 μm,		diameter ~100μm			3.2 - 3.25eV	Vapor transport method mediated by vapor-liquid-solid growth
ZnO whiskers (Qiu, Wong, Wu, Lin and Xu, 2004)	325nm/250fs	diameter ~150-1000nm, length ~20μm			70μJcm^{-2}	/30ps	378 nm	Hydrothermal oxidation technique
ZnO polycrystalline thin film (Zhang, Chua, Yong, Li, Yu and Lau, 2006)	320nm/150fs		0.36μm	diameter ~ 300μm	150μJcm^{-2}	/30ps	3.181 - 3.27eV	Filtered cathodic vacuum arc technique
ZnO nanorod arrays (Han, Wang, Wang, Cao, Liu, Zou and Hou, 2005)	325nm/150fs	diameter ~150-300nm length ~5.5μm			130μJcm^{-2}		377 nm	Metal-catalyst-free method and Pulsed laser deposition method
ZnO nanoneedles (Lau, Yang, Yu, Li, Tanemura, Okita, Hatano and Hng, 2005)		diameter ~100nm length ~ 200-400nm				0.34 MWcm^{-2}	390nm - 400nm	Ion-beam technique
Colloidal CdS/CdSe/CdS quantum wells (Xu and Xiao, 2005)	400nm/1ps		200nm	area ~ 2mm x 50μm		3 Wcm^{-2}	510nm - 550nm	Successive ion layer adsorption and reaction technique
ZnO rib waveguide (Leong, Yu, Abiyasa and Lau, 2006)	355nm/6ns		180nm			0.28 MWcm^{-2}	385nm	Filtered cathodic vacuum arc technique

Table 2.1b Parameters of different laser crystal powder and semiconductor random lasers

Laser crystal powder and semiconductor random media	Pumping Wavelength/ Pulse Duration	Particle Size	Sample Thickness	Pumped Area	Threshold Energy Density	Threshold Power Density/ Emission Lifetime	Emission frequency	Fabrication method
Nanostructured stars of ZnO microcrystals (Lv, Li, Guo, Wang, Wang, Xu, Yang, AI and Zhang, 2005)	266nm/5ns	Arc length 0.5-2μm				318 $kWcm^{-2}$	388.4nm	Simple solution method
ZnO nanostructures (Liu, Yamilov, Wu, Zheng, Cao and Chang, 2004)	355nm/20ps		600-750 nm	diameter ~ 20μm	6nJ		386 nm - 393nm	Plasma-enhanced chemical vapor deposition method
ZnO polycrystalline thin film (Ong, Dai, Li, Du, Chang and Ho, 2001)	410nm/2ns		400nm				3.2eV	Pulsed laser deposition method
ZnO nanosaws (Wu, Hsu, Cheng, Yanga and Hsieh, 2006)	355nm/500ps	diameter ~50-100nm length ~1μm				0.96 $MWcm^{-2}$	3.2eV	Simple vapor transport method
ZnO nanoparticles (Stassinopoulos, Das, Giannelis, Anastasiadis and Anglos, 2005)	308nm/30ns	diameter ~ 250-300nm	3μm	area ~ 4mm x 4mm	2μJcm^{-2}		385nm	Spin coating method
ZnO nanorod arrays embedded in ZnO epilayers (Yu, Yuen, Lau, Park and Yi, 2004)	355nm/6ns	diameter ~70nm length ~2μm, Density ~$1.7x10^{11}$ $rodcm^{-2}$		area ~ 5mm x 60μm		TE mode ~ 800 $kWcm^{-2}$ TM mode ~ 1.6 $MWcm^{-2}$	380nm	Filtered cathodic vacuum arc technique

Table 2.1c Parameters of different laser crystal powder and semiconductor random lasers

Laser crystal powder and semiconductor random media	Pumping Wavelength/ Pulse Duration	Particle Size	Sample Thickness	Pumped Area	Threshold Energy Density	Threshold Power Density/ Emission Lifetime	Emission frequency	Fabrication method
ZnO film (Lau, Yang, Yu, Yuen, Leong, Li and Hng, 2005)			200nm	area ~ 0.003 cm^2		0.8MWcm^{-2}	390nm	Filtered cathodic vacuum arc technique
para-sexiphenul nanofibers (Quochi, Cordella, Orru`, Communal, Verzeroli, Mura and Bongiovanni, 2004)	380nm/ 150fs	length = 220nm, height =110nm	0.3μm	diameter ~120μm	0.5 μJcm^{-2}		425nm	
GaAsN (Sun, Gal, Gao, Tan, Jagadish, Puzzer, Ouyang and Zou, 2003)	532nm/ 1μs		200nm	area ~ 2500μm^2		0.1-10k Wcm^{-2}	1080nm-1088nm	Metalorganic chemical vapor deposition method
GaN nabowires (Gradečak, Qian, Li, Park and Lieber, 2005)	266nm/ 7ns	diameter ~100-300nm length 10-30μm				22k Wcm^{-2}	365nm	Metalorganic chemical vapor deposition method
$Nd_{0.5}La_{0.5}Al_3(BO_3)_4$ (Bahoura, Morris, Zhu and Noginov, 2005)	532nm/ 10ns		1cm				1064nm	
$NdAl_3(BO_3)_4$, (Noginov, Noginova, Caulfield, Venkateswarlu, Thompson, Mahdi and Ostroumov, 1996)	532nm/10ns	diameter ~ 0.6-24.8μm	0.35μm	diameter ~ 20μm	200mJcm^{-2}	200 mJcm^{-2} for powder form; 600m mJcm^{-2} for single crystal form	1063 nm	

Table 2.1d Parameters of different laser crystal powder and semiconductor random lasers

Laser crystal powder and semiconductor random media	Pumping Wavelength/ Pulse Duration	Particle Size	Sample Thickness	Pumped Area	Threshold Energy Density	Threshold Power Density/ Emission Lifetime	Emission frequency	Fabrication method
$NdSc_3(BO_3)_4$ (Noginov, Noginova, Caulfield, Venkateswarlu, Thompson, Mahdi and Ostroumov, 1996)	532nm/10ns	diameter ~ 0.6-24.8μm			560mJcm^{-2}	560 mJcm^{-2} for powder form;	1061.5nm	
Nd:$Sr_5(PO_4)_3F$ (Noginov, Noginova, Caulfield, Venkateswarlu, Thompson, Mahdi and Ostroumov, 1996)	805nm/20ns	diameter ~ 0.6-24.8μm			170mJcm^{-2}	170 mJcm^{-2} for powder form; 625 mJcm^{-2} for 8-mm polished plate of single crystal; 920 mJcm^{-2} for 1.5-mm polished plate of single crystal; 1080 mJcm^{-2} for 0.8-mm unpolished plate of single crystal	1059nm	
$NdSc_3(BO_3)_4$ (Noginov, Zhu, Frantz, Novak, Williams and Fowlkes, 2004)	532nm/10ns	diameter ~ 3.55μm		diameter ~ 0.3-0.7mm		/1-2ns		Czochralaski technique

Organic disordered system

In this section, organic active disordered systems are discussed such as liquid dye and solid-state polymer random lasers. Nearly all organic active disordered systems consist of scattering element and gain medium. Generally, conjugated polymer and dye-doped polymer are utilized to provide the optical gain while dielectric particles are served as scattering centers. Since the gain medium and the scattering elements are separated, the scattering strength and the randomness of the disordered systems can be varied independently.

Dye-doped polymer random laser

Recently, random lasing has been reported in a variety of organic active disordered systems such as colloidal dye solutions (Ahmed, Zang, Yoo, Ali and Alfano, 1994, Lawandy, Belachandran, Gomes and Sauvin, 1994, Sha, Liu and Alfano, 1994, Balachandran and Lawandy, 1995, Noginov, Noginova, Caulfield, Venkateswarlu and Mahdi, 1995, Sha, Liu, Liu and Alfano, 1996, Siddique, Alfano, Berger, Kempe and Genack, 1996, Prasad, Ramachandran, Sood, Subramanian and Kumar, 1997, Sfez and Kotler, 1997, Eradat, Shkunov, Frolov, Gellermann, Vardeny, Zakhidov, Baughma and Yoshino, 1999, Cao, Xu, Chang and Ho, 2000, Soest, Poelwijk and Lagendijk, 2002, Zacharakis, Papadogiannis and Papazoglou, 2002), films of dye-doped polymer consisting of dielectric particles (Cao, Ling, Xu, Burin and Chang, 2003, Watanabe, Oki, Maeda and Omatsu, 2005), biological tissues (Zhang, Cue and Yoo, 1995, Polson and Vardeny, 2004, Polson and Vardeny, 2005). The first demonstration of the narrowing of the spontaneous emission spectrum from a dye-doped methanol solution was presented by Lawandy et al. (Lawandy, Belachandran, Gomes and

Sauvin, 1994). A Rhodamine 640 dye solution consisting of TiO_2 sub-micron particles was optically excited. When the pumping density exceeded some threshold value, strong spectral narrowing and nonlinear emission enhancement were observed. Following Lawandy's investigation, active disordered media consisting of colloidal suspension of scatterers in a dye-doped solution attracted much attention. It was shown that the lasing threshold for simulated emission was dependent on the concentration of laser dye and scattering particles (Sha, Liu and Alfano, 1994, Noginov, Noginova, Caulfield, Venkateswarlu and Mahdi, 1995, Zhang, Cue and Yoo, 1995, Siddique, Alfano, Berger, Kempe and Genack, 1996, Sfez and Kotler, 1997). Furthermore, Zhang et al. (Zhang, Cue and Yoo, 1995) experimentally examined the effect of the gain length on the emission bandwidth in order to study the spectral properties of the diffusive random laser. It was found that the spectral shift of the stimulated emission peak was dependent on the concentration of scattering particles and the pumping density. These results were explained by using with an amplified spontaneous emission (ASE) model (Noginov, Noginova, Caulfield, Venkateswarlu and Mahdi, 1995).

Furthermore, coherent random laser also was realized in colloidal dye solution. Cao's group successfully observed the transition between the incoherent random laser to coherent random laser by increasing the amount of scattering particles in the dye solutions, the gain medium (Cao, Xu, Chang and Ho, 2000). In the Rhodamine 640 dye solutions containing ZnO nanoparticles, a drastic spectral narrowing which was identical to the finding of Lawandy's experiments appeared when the pump intensity surpassed the threshold. The emission linewidth collapsed to ~5nm. This phenomenon is due to the incoherent feedback.

By increasing the ZnO particle density, an unexpected spectral narrowing phenomenon was observed. Several discrete spectral peaks (linewidth ~ 0.2nm) appeared before the collapse of the emission linewidth. The lasing with coherent feedback is attributed to the resonant feedback caused by recurrent light scattering in strong scattering regime.

Conjugated polymer random laser

Conjugated polymers do not undergo concentration quenching, which is different from the laser dyes (Diaz-Garcia, Hide, Schwartz and Andersson, 1997). The gains of undiluted conjugated polymers are much higher than that of liquid dyes. In some π - conjugated polymers, high optical gain and stimulated emission have been noted (Diaz-Garcia, Hide, Schwartz and Andersson, 1997, Polson, Huang and Vardeny, 2001b, Polson and Vardeny, 2003). Experimentally, the low threshold light amplification was demonstrated in blue, green and red spectral ranges via amplified spontaneous emission in optically pumped planar waveguides based on fluorine polymer gain media (Xia, Heliotis and Bradley, 2003). Another study revealed that the stimulated emission of different semiconducting polymer films covered almost the full range of visible light (Hide, Diaz-Garcia, Schwartz and Andersson, 1996, Diaz-Garcia, Hide, Schwartz and Andersson, 1997). The detailed studies on the chemical structures, absorption and emission spectra of conjugated polymers have been conducted (Diaz-Garcia, Hide, Schwartz and Andersson, 1997). The absorption and photoluminescence spectra of 12 neat polymer thin films are shown in Figure 2.6.

In the past, several random lasers based on conjugated polymers have been reported such as 2,5-dioctyloxy poly(*p*-phenylene-vinylene) [DOO-PPV] film (Eradat, Shkunov, Frolov, Gellermann, Vardeny, Zakhidov, Baughma and Yoshino, 1999, Polson, Huang and Vardeny, 2001b, Polson, Raikh and Vardeny, 2002), quinquethienyl S,S-dioxide [T5OCx] film (Anni, Lattante, Cingolani, Gigli, Barbarella and Favaretto, 2003, 2004, Anni, Lattante, Stomeo, Cingolani and Gigli, 2004), poly(9,9-dioctylfluorene) and poly(phenylene-ethynylene) / poly(phenylene-vinylene) [PPE-PPV] film (Tong, Sheng, Yang, Vardeny and Pang, 2004). Various types of dye and conjugated polymers random laser systems are summarized in Tables 2.2a-

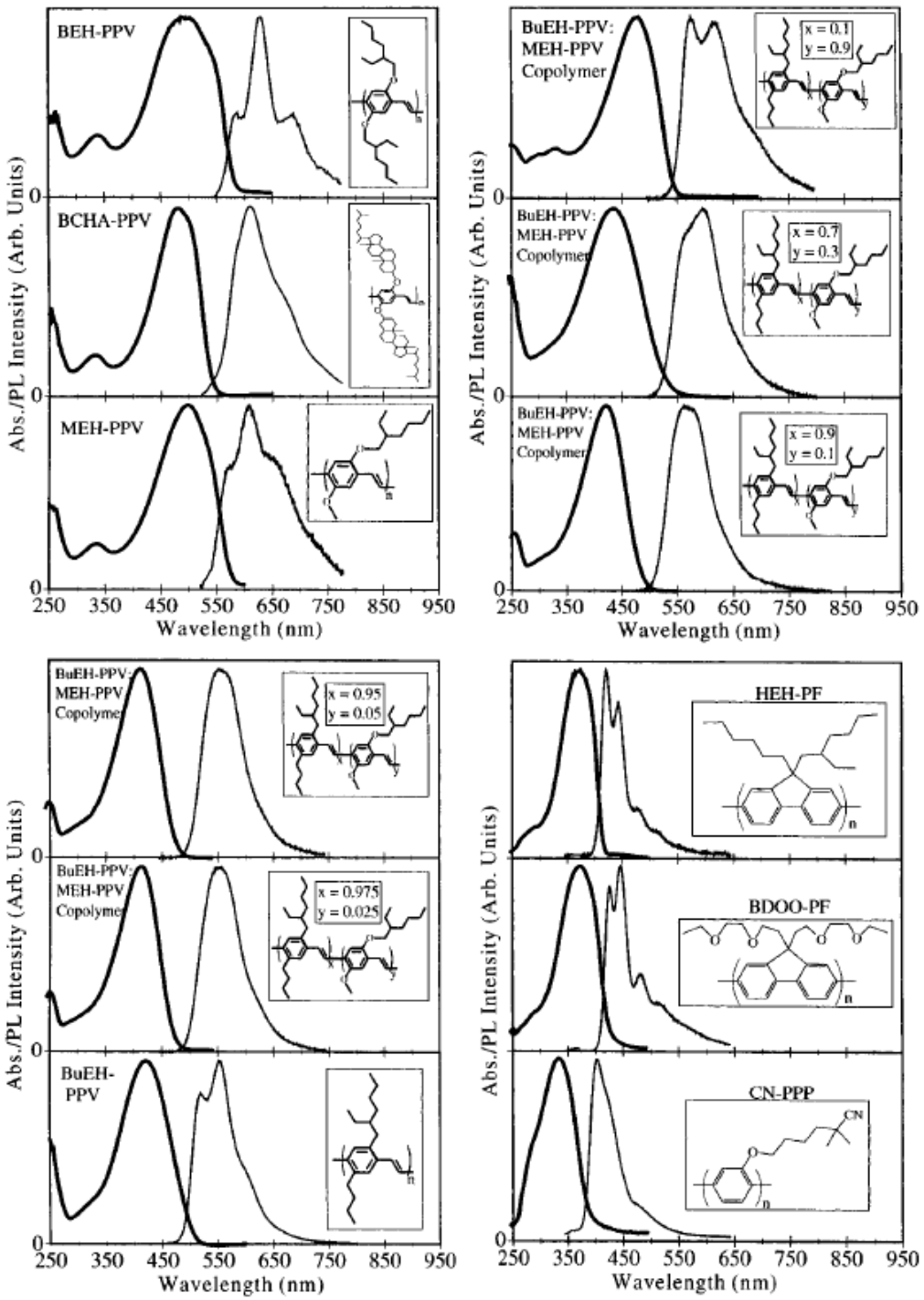

Figure 2.6 Absorption (heavy smooth curves) and photoluminescence (thin, slightly noisy curves) spectra of neat thin films of BuEH-PPV, BCHA-PPV, MEH-PPV, BEH-PPV, BuEH-PPV/MEH-PPV copolymers at different monomer ratios, HEH-PF. BDOO-PF, and CN-PPP. Insets: molecular structures. (Source: Hide 1997)

Table 2.2a Parameters of different dye random lasers

Dye and polymer random media	Pumping Source	Particle Size / concentration	Dye concentration	Sample Thickness	Pumped Area	Threshold Energy	Emission frequency
ZnO PMMA hybrid (Vutha, Tiwari and Thareja, 2006)	Third harmonic (355nm) of Nd: YAG laser (5ns pulse width FWHM)	diameter ~1-4μm			Spot diameter ~400μm	7MW/cm^2	380-385nm
Waveguide dye laser including active random scattering layer with Rhodamine-6G and SiO_2 nanoparticles (Watanabe, Oki, Maeda and Omatsu, 2005)	Frequency-doubled Q-switched Nd: YAG laser (pulse duration ~0.5ns)	diameter ~50nm	30mM		area ~ 1.5cm x 250μm	0.34μJ	594.2nm
DCM doped polycarbonate film with silica spheres (Zhang, Chua, Yong, Li, Yu and Lau, 2006)	Frequency-doubled Q-switched Nd: YAG laser (10Hz repetition rate, 35ps pulse width)	diameter ~ 75nm		Thickness of PC waveguide laser = 340nm	area ~ 20mm x 150μm	70μJ/cm^2	600-610nm
Rhodamine 640 perchlorate suspension containing TiO_2 nanoparticles (Sha, Liu and Alfano, 1994)	Frequency-doubled (532nm) Nd: YAG laser (20Hz repetition rate)	diameter ~0.26μm / $2.5x10^{12}$ cm^{-3}	$5x10^{-4}$ – $2.5x10^{-2}$M		Spot diameter ~1cm	0.07mJ	620nm and 650nm
Neat film of substituted quinquethienyl S,S-oxide (Anni, Lattante, Cingolani, Gigli, Barbarella and Favaretto, 2004)	Third harmonic (355nm) of Nd: YAG laser (10Hz repetition rate, 3ns pulse width)				area ~ 7mm x 100μm	0.75mJ/cm^2	625nm
Methanol solutions of Rhodamine 6G dye containing Al_2O_3 particles (Noginov, Noginova, Caulfield, Venkateswarlu and Mahdi, 1995)	Frequency-doubled (532nm) Nd: YAG laser (80ns pulse width)	diameter ~ 1μm	$3.5x10^{16}$ – $3.6x10^{18}$ cm^{-3}	Thickness of cuvette = 1mm			565nm

Table 2.2b Parameters of different dye random lasers

Dye and polymer random media	Pumping Source	Particle Size/ concentration	Dye concentration	Sample Thickness	Pumped Area	Threshold Energy	Emission frequency
Nylon-6 fibers containing Rhodamine 640 perchlorate and TiO_2 nanoparticles (Balachandran, Pacheco and Lawandy, 1996)	Frequency-doubled Q-switched (355nm) of Nd: YAG laser (7ns pulse width)	diameter =250nm	$2x10^{-3}M$	Fiber diameter =200μm	Spot diameter ~400μm	$8mJ/cm^2$	608nm
Solution of Rhodamine 640 perchlorate and TiO_2 nanoparticles (Lawandy, Belachandran, Gomes and Sauvin, 1994)	Frequency-doubled Q-switched Nd: YAG laser (pulse duration ~7ns)	diameter =250nm / $10^{11}cm^{-3}$	$2.5x10^{-3}M$				
Methanol Solution of Rhodamine 640 perchlorate and alumina-coated titanic particles (Siddique, Alfano, Berger, Kempe and Genack, 1996)	Frequency-doubled (527nm)single-shot Nd: glass laser (10ps pulse width)	diameter ~ 0.25μm/ $5x10^{11}cm^{-3}$	50mol/L	Solution contained within 1cm x 1cm x3cm glass cvette	Spot diameter ~0.5mm	13μJ	
Methanol solution containing Sulforhodamine 640 and TiO_2 nanoparticles (Sha, Liu, Liu and Alfano, 1996)	Frequency-doubled (532nm) Nd: YAG laser (20Hz repetition rate, 3ns pulse width)	diameter ~210nm / 10^{11} cm^{-3}	$2.5x10^{-2}M$		Spot diameter ~0.5cm	0.2mJ for 610-620nm band, 8.8mJ for 645-650nm band	610-620nm, 645-650nm
Methanol solution of Rhodamine 640 perchlorate and TiO_2 nanoparticles (Balachandran and Lawandy, 1995)	Frequency-doubled Q-switched (532nm) Nd: YAG laser (pulse duration ~100ns)	diameter ~250nm / $2x10^{11}$ cm^{-3}	$2.5x10^{-3}M$		Spot diameter ~300μm	$16mJ/cm^2$	610nm
Rhodamine 610 solutions containing TiO_2 particles (Sfez and Kotler, 1997)	Q-switched (532nm) Nd: YAG laser (10Hz repetition rate, 7ns pulse width)	diameter ~32nm / $3x10^{13}$ cm^{-3}	$1.4x\ 10^{-4}$ M		Spot diameter ~2.5mm	$0.8mJ/cm^2$	590nm

Table 2.2c Parameters of different dye random lasers

Dye and polymer random media	Pumping Source	Particle Size/ concentration	Dye concentration	Sample Thickness	Pumped Area	Threshold Energy	Emission frequency
Methanol solution of Sulforhodamine B and TiO_2 particles (Soest, Tomita and Lagendijk, 1999)	Frequency-doubled Q-switched of Nd: YAG laser (20Hz repetition rate, 6ns pulse width)	diameter =220 ± 20μm	0.1mM	Sample thickness = 1cm	Spot diameter ~80μm - 2mm	~0.03mJ/mm^2	590nm
Coumarin 307 dye-infiltrated random gain media containing TiO_2 particles (Zacharakis, Papadogiannis and Papazoglou, 2002)	Mode-locked (800nm) Ti: Sapphire laser (82Hz repetition rate, pulse duration =200fs)	diameter =400nm / $1.33x10^{-3}$M	$4x10^{-3}$M	Sample size = 1x1x1 cm	Spot area ~0.15mm^2	60μJ	480nm
Methanol solution of Rhodamine 640 perchlorate and ZnO particles (Cao, Xu, Chang and Ho, 2000)	Frequency-doubled (532nm)single-shot Nd: glass laser (10Hz repetition rate, 25ps pulse width)	diameter ~ 100nm/ $1x10^{12}cm^{-3}$	$5x10^{-3}$M	Solution contained within 1cm x 1cm x3cm cvette	Spot diameter ~0.5mm	1μJ	605-610nm
PMMA polymer film containing Rhodamine 640 and TiO_2 particles (Ling, Cao, Burin, Ratner, Liu, Seelig and Chang, 2001)	Frequency-doubled (532nm) Nd: YAG laser (10Hz repetition rate, 25ns pulse width)	diameter ~400nm/ $8x10^{10}$ -$6x10^{12}$ cm^{-3}	$1 x10^{-2}$-$5x10^{-2}$M	Sample thickness = 150-400μm	Spot diameter ~50μm	$3.6x10^3$ μJ/cm^2	382-386nm
Methanol solution of Rhodamine 640 perchlorate and TiO_2 nanoparticles (Balachandran, Lawandy and Moon, 1997)	Frequency-doubled, Q-switched, mode-locked (532nm) Nd: YAG laser	diameter ~250nm /20-50mg/mL	$5x10^{-4}$M		Spot diameter ~500μm	1.2μJ	
Methanol solution of Rhodamine 6G and Al_2O_3 nanopowder (Dice, Mujumdar and Elezzabi, 2005)	Frequency-doubled (532nm) Nd: YAG laser (10Hz repetition rate, 10ns pulse width)	diameter ~100nm /$2.3 x10^{13}$ -$4.2x10^9$ cm^{-3}	10^{-3}mol/L			~4.9mJ/cm^2	564nm

Table 2.2d Parameters of different dye random lasers

Dye and polymer random media	Pumping Source	Particle Size/ concentration	Dye concentration	Sample Thickness	Pumped Area	Threshold Energy	Emission frequency
Rhodamine 6G doped gel film with SiO_2 balls (Frolov, Vardeny, Yoshino, Zakhidov and Baughman, 1999)	Frequency-doubled (532nm) Nd: YAG laser (100Hz repetition rate, 100ps pulse width)	diameter = 300nm/ $2x10^{10}$ cm^{-3}		30000nm	area ~ 3mm x 30μm	250 mJ/cm^2	555-565nm
Solution of Rhodamine 590 infiltrated in opal of SiO_2 balls (Eradat, Shkunov, Frolov, Gellermann, Vardeny, Zakhidov, Baughma and Yoshino, 1999)	Frequency-doubled (532nm) Nd: YAG laser (100Hz repetition rate, 100ps pulse width)	Silica balls close-packed in a fcc lattice	10^{-3}M	crystallite sizes = 20-100μm		~3μJ/pulse	580nm
Solution of DOO-PPV infiltrated in opal of SiO_2 balls (Eradat, Shkunov, Frolov, Gellermann, Vardeny, Zakhidov, Baughma and Yoshino, 1999)	Frequency-doubled (532nm) Nd: YAG laser (100Hz repetition rate, 100ps pulse width)	Silica balls close-packed in a fcc lattice		crystallite sizes = 20-100μm		0.05mJ/pulse	598nm
PMMA hybrid with ZnO powder (Vutha, Tiwari and Thareja, 2006)	Third harmonic (355nm) Nd: YAG laser (10Hz repetition rate, 5ns pulse width)	diameter ~1-4μm/			Spot diameter = 400μm	6MW/cm^2	~384nm
MEH-PPV/glass waveguide with TiO_2 particles (Liu, Liu, Zhang and Dou, 2005)	Ti:Sapphire laser (544nm, 1kHz repetition rate, 150fs pulse width)	Diameter =20nm				45μJ/ cm^2	~612nm

Table 2.3a Parameters of different polymer random lasers

Material	Emission frequency	Pumping wavelength/pulse width	Sample Thickness	Threshold Energy	Reference
BuEH-PPV	520,560nm	435nm/10ns	126-252nm	0.4 ± 0.2μJ/pulse	(Hide, Diaz-Garcia, Schwartz and Heeger, 1997)
BuEH-PPV	520,560nm	435nm/10ns	87-208nm	0.2 ± 0.1μJ/pulse	
BCHA-PPV	540,630nm	532nm/10ns	277-650nm	1.0 ± 0.4μJ/pulse	
MEH-PPV	585,625nm	532nm/10ns	87-405nm	1.1 ± 0.4μJ/pulse	
MEH-PPV	585,625nm	532nm/10ns	355nm	3μJ/pulse	
MEH-PPV	585,625nm	532nm/10ns	325nm	4μJ/pulse	
BEH-PPV	580,650nm	532nm/10ns	300nm	0.5μJ/pulse	
BuEH-MEH copolymers 10:90	580,625nm	532nm/10ns	330nm	3.2μJ/pulse	
BuEH-MEH copolymers 70:30	565,600nm	532nm/10ns	420nm	1.0μJ/pulse	
BuEH-MEH copolymers 90:10	550,580nm	435nm/10ns	370nm	1.0μJ/pulse	
BuEH-MEH copolymers 95:5	545,580nm	435nm/10ns	450nm	1.6μJ/pulse	
BuEH-MEH copolymers 97.5:2.5	540,570nm	435nm/10ns	500nm	1.0μJ/pulse	
HEH-PF	425,445nm	355nm/10ns	120nm	4.2μJ/pulse	
BDOO-PF	430,450,540nm	355nm/10ns		2.3μJ/pulse	
CN-PPP	420nm	355nm/10ns	100nm	4.0μJ/pulse	
DCM/PS (2.6%w/v)	640nm	532nm/10ns	390-4800nm	400 ± 150μJ/pulse	
BuEH-PPV	555-570nm	435nm/10ns	210nm	~0.6μJ/pulse	(Hide, Schwartz, Diaz-Garcia and Heeger, 1997)
CN-PPP	~420nm	355nm/10ns	100nm	~9μJ/pulse	
BCHA-PPV	~600nm	532nm/10ns	580nm	~2μJ/pulse	

Table 2.3b Parameters of different polymer random lasers

Material	Emission frequency	Pumping wavelength/pulse width	Sample Thickness	Threshold Energy	Reference
DOO-PPV	~630nm	540nm/150ps	30-2000nm	~60μ J/cm^2	(Frolov, Ozaki, Gellermann, Vardeny and Yoshino, 1996)
DOO-PPV	~630nm	400nm/150fs	200nm	<50 μJ/cm^2	(Lee, Wong, Huang, Frolov and Vardeny, 1999)
DOO-PPV	625-635nm	532nm/100ps	~1000nm	0.05μJ/pulse	(Frolov, Shkunov, Fujii, Yoshino and Vardeny, 2000)
DOO-PPV	625-640nm	532nm/100ps	1000nm	1μJ/pulse	(Polson, Huang and Vardeny, 2001b)
DOO-PPV	630-640nm	532nm/100ps	~1000nm	<2μJ/pulse	(Polson, Huang and Vardeny, 2001a)
DOO-PPV	625-640nm	532nm/100ps	500-000nm	0.03μJ/pulse	(Frolov, Vardeny, Yoshino, Zakhidov and Baughman, 1999)
T5OCx	~615-625nm	355nm/3ns	450nm	300μJ/cm^2	(Anni, Lattante, Cingolani, Gigli, Barbarella and Favaretto, 2003, Anni, Lattante, Stomeo, Cingolani and Gigli, 2004)
PPE-PPV	~446nm	375nm/100fs		7μJ/cm^2	(Tong, Sheng, Yang, Vardeny and Pang, 2004)

2.4 Summary

In the development of random lasers, a lot of effort has been devoted to study the underlying mechanism of the random laser. The investigations of random laser always link to the localization theory and diffusion theory. On the other hand, much work has been attempted to optimize and control the laser-like emission of disordered system. One important aspect is to reduce the lasing threshold by controlling the scattering strength in the disordered medium. It is believed that the randomness of the scattering structure is one of the key factors to control the scattering strength. Up to now, only limited research (Chang, Cao and Ho, 2003, Yamilov and Cao, 2004b) has been reported on the studies of the influence of disorder on the random laser. It is valuable to explore the disorder effect on the random laser systems.

CHAPTER 3
THEORETICAL ANALYSIS AND NUMERIC SIMULATION

3.1 Introduction

Theoretically, several models have been established to study the temporal and spectral properties of active disordered media, such as the diffusion model with gain (Letokhov, 1967, 1968, John and Pang, 1996, Wiersma and Lagendijk, 1996, Burin, Cao and Ratner, 2003, Florescu and John, 2004), the Monte Carlo simulation (Balachandran, Lawandy and Moon, 1997, Berger, Kempe and Genack, 1997, Soest, Tomita and Lagendijk, 1999, Noginov, Novak, Grigsby, Zhu and Bahoura, 2005), and finite-difference time-domain (FDTD) simulation (Jiang and Soukoulis, 2000, Vanneste and Sebbah, 2001, Jiang and Soukoulis, 2002, Sebbah and Vanneste, 2002, Soukoulis, Jiang, Xu and Cao, 2002, Liu, Yamilov, Ling, Xu and Cao, 2003, Yamilov and Cao, 2004, Wang, Liu and Yuan, 2005, Wang and Liu, 2006). Those models successfully explained the experimental results such as ASE peak narrowing, lasing threshold behavior and nonlinear input-output characteristics.

In this chapter, it begins with a description of the existing models of random lasers such as Monte Carlo simulation and finite-difference time-domain (FDTD)

modeling. Followed the review of existing modeling, the work principle and formulism of the time dependent theory will be presented. The time-dependent theory (Jiang and Soukoulis, 2000) which combines the time-dependent Maxwell's equations with the semi-classical laser theory (Siegman, 1986) is selected for investigation in the current study. The modeling and analysis specific for the present research are clarified in the latter section.

3.2 Existing theoretical models of random laser

3.2.1 Diffusion model

John and Pang speculated the random laser system by solving the coupling diffusion equations and the electron rate equations with nonlinear gain and loss, but without the saturation effect (John and Pang, 1996). Similarly, Wiersma et al. (Wiersma and Lagendijk, 1996) proposed a diffusion model to investigate the powdered lasing crystal powder. A slab of powder was considered as a disorder medium and the amplification mechanism was proposed as four-level atomic systems. In the numerically experiments, pump pulse and probe pulse were injected into the powder slab. The energy density of pump light, probe light, and amplified spontaneous emission (ASE) were described by three diffusion equations, which coupled with the rate equation. The four equations can be

written as

$$\frac{\partial W_G(\vec{r},t)}{\partial t} = D\nabla^2 W_G(\vec{r},t) - \sigma_{abs}\upsilon[A_{total} - A_1(\vec{r},t)]W_G(\vec{r},t) + \frac{I_G(\vec{r},t)}{l_G} \quad \textbf{(3.1)}$$

$$\frac{\partial W_R(\vec{r},t)}{\partial t} = D\nabla^2 W_R(\vec{r},t) - \sigma_{em}\upsilon A_1(\vec{r},t)W_R(\vec{r},t) + \frac{I_R(\vec{r},t)}{l_R} \quad \textbf{(3.2)}$$

$$\frac{\partial W_A(\vec{r},t)}{\partial t} = D\nabla^2 W_A(\vec{r},t) - \sigma_{em}\upsilon A_1(\vec{r},t)W_A(\vec{r},t) + \frac{A_1(\vec{r},t)}{\tau_e} \quad \textbf{(3.3)}$$

$$\frac{\partial A_1(\vec{r},t)}{\partial t} = \sigma_{abs}\upsilon[A_{total} - A_1(\vec{r},t)]W_G(\vec{r},t) + \sigma_{em}\upsilon N_1(\vec{r},t)[W_R(\vec{r},t) + W_A(\vec{r},t)] - \frac{A_1(\vec{r},t)}{\tau_e} \quad \textbf{(3.4)}$$

where $W_G(\vec{r},t), W_R(\vec{r},t)$ and $W_A(\vec{r},t)$ represent the energy density of pump light, probe light, and amplified spontaneous emission, respectively. $A_1(\vec{r},t)$ is the concentration of the excited atomic particles. A_{total} is the total concentration of atomic particles, υ is the velocity of light in the medium. l_G and l_R are the mean free paths of pump light and probe light, respectively. σ_{abs} and σ_{em} are the absorption and emission cross section, D is the diffusion coefficient, τ_e is the life time of the excited state. v is the transport speed of light in the medium Numerically, these coupled differential equations were solved and a time

dependent solution can be obtained.

3.2.2 Monte Carlo simulation

In the past ten years, Monte Carlo simulation of the random walk of photons has been employed to study the properties of emission from optically pumped diffusive active disordered media. Balachandran developed a laser model to explain the results of dye solution experiments (Balachandran1997). The laser model is schematically shown in Figure 3.1

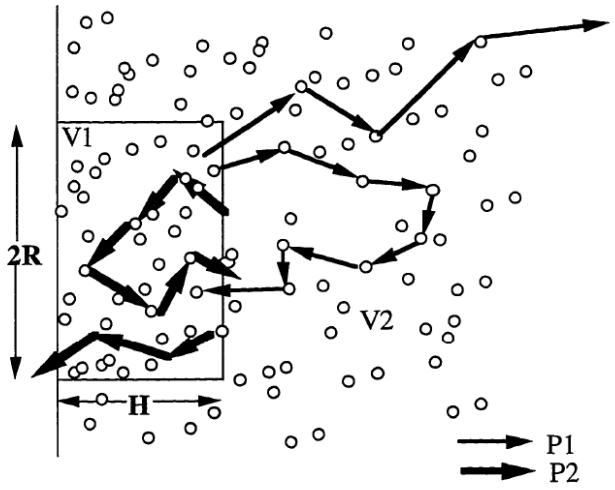

Figure 3.1 Schematic diagram of the laser model. Source: (Balachandran1997)

It was assumed that photon performs a random walk in the scattering medium. Photons P2 experience optical gain though the spontaneous emission process due to the excited dye molecules in gain volume V1. When the photons reach the boundaries of V1, photons travel to either V2 or out of the scattering medium.

The photons P1 are probably scattered back to the V1. The threshold gain (γ_{th}) for the diffusive random laser was determined by using the Monte Carlo simulation. Equation 3.5 defines the threshold condition for the random laser.

$$\gamma_{th} = \frac{-\ln(R_1 R_2)}{l_{path}}, \qquad \textbf{(3.5)}$$

where l_{path} is average total path length; R_1 and R_2 are the probabilities of photon returning and escaping in the gain volume, respectively.

The emission linewidth and peak intensity of the random laser can be evaluated by integrating the laser intensity over time. The laser intensity $I_{laser}(\lambda, t)$ can be obtained from the following two equations:

$$\frac{dn_2(t)}{dt} = \frac{[1-n_2(t)]B_p I_{pump}(t)}{\upsilon} - n_2(t)\int d\lambda B_l(\lambda) I_{pump}(\lambda, t) - n_2(t)\Gamma \qquad \textbf{(3.6)}$$

$$\frac{dI_{laser}(\lambda, t)}{dt} = C_{con}[\gamma_0(\lambda) n_2(t) - \gamma_{th}]\, I_{laser}(\lambda, t) + \eta(\lambda) n_2(t), \qquad \textbf{(3.7)}$$

where n_2 is the excited population density function, γ_{th} is the threshold gain, γ_0 is the constant gain. B_p and B_l are the Einstein coefficients for the pump and

the laser emissions, respectively. I_{punp} and I_{laser} are the pump and the laser intensities, respectively, Γ is the spontaneous emission rate, η is the spontaneous emission coefficient that initiates the laser action. C_{con} is the proportion constant. The emission spectra, the input-output characteristics, the evolution of population inversion of dye molecules can be obtained in the simulation.

3.2.3 Finite-difference time-domain (FDTD) modeling

The previous models established for the random laser with incoherent feedback are inadequate to describe the random laser with coherent feedback because of the phase of the optical field is neglected. The models only take account of light intensity rather than the electromagnetic field in the calculation. Thus the interference effect, which is essential to coherent feedback, is excluded.

To explain the optical properties and the phenomena exhibiting in the disordered media, a model should be based on Maxwell's time-dependent equations that can be adapted to different random configuration of dielectric structures. For the active disordered system, the model has to include a realistic amplifying mechanism. Accordingly, Taflove (Taflove and Brodwin, 1975, Taflove, 1995)

proposed a finite-difference time-domain (FDTD) method to deal with electromagnetic scattering problem in amplifying media. FDTD technique is a computationally efficient method of directly solving Maxwell's time-dependent curl equations or their equivalent integral equations using the finite-difference technique. It can fully describe the behavior of classical electromagnetic properties in both passive and active disordered media. The time-dependent Maxwell's equations are expressed as follows:

$$\nabla \times \vec{E} + \frac{\partial \vec{B}}{\partial t} = -\vec{M} \quad \textbf{(3.8)}$$

$$\nabla \times \vec{H} - \frac{\partial \vec{D}}{\partial t} = \vec{J} \quad \textbf{(3.9)}$$

$$\nabla \cdot \vec{D} = \rho \quad \textbf{(3.10)}$$

$$\nabla \cdot \vec{B} = 0 \quad \textbf{(3.11)}$$

where $\vec{E}$ is the electric field, $\vec{H}$ is the magnetic field, $\vec{D}$ is the electric flux density, $\vec{B}$ is the magnetic flux density, ρ is the free charge density. $\vec{J}$ and $\vec{M}$ are the electric conduction current density and the magnetization, respectively. In linear and nondispersive materials, $\vec{D}$ and $\vec{B}$ can be related to $\vec{E}$ and $\vec{H}$, respectively, by using simple proportions.

$$\vec{D} = \varepsilon \vec{E} = \varepsilon_r \varepsilon_0 \vec{E} \quad \textbf{(3.12)}$$

$$\vec{B} = \mu \vec{H} = \mu_r \mu_0 \vec{H} \quad \textbf{(3.13)}$$

where ε_r is the relative permittivity, ε_0 is the free space dielectric permittivity, μ_r and μ_0 are the relative permeability and the free space permeability. To consider the conductive property of material, the external current and conductivity terms should be included. This yields :

$$\vec{M} = \vec{M}_{source} + \sigma^* \vec{H} \quad \textbf{(3.15)}$$

$$\vec{J} = \vec{J}_{source} + \frac{\partial \vec{P}}{\partial t} + \sigma \vec{E} \quad \textbf{(3.16)}$$

where σ is the electric conductivity. σ* is equivalent magnetic loss. $\vec{J}_{source}$ and $\vec{M}_{source}$ are the external electric and equivalent magnetic current density, respectively, which are the independent sources of electric and magnetic field energy. $\vec{P}$ is electric polarization density. By using standard FDTD method (Taflove, 1995), the electrodynamics of random media can be fully described.

Negative conductance

Recently, a variety of FDTD approaches has been proposed to combine the

amplification mechanism with the Maxwell's equations in order to investigate the optical amplification in active random media.

The first approach introduces optical gain into the Maxwell's equations by negative conductance (Taflove and Haginess, 2000). The spectral gain linesharp of the dye solution is described by

$$\sigma(\omega) = \frac{\sigma_0 / 2}{1 + i(\omega - \omega_t)T_2 + 1 + i(\omega + \omega_t)T_2}, \qquad \textbf{(3.17)}$$

where $\sigma(\omega)$ is the frequency-dependent conductivity function, σ_0 represents the constant amplitude of conductivity which is maximum value of the gain magnitude, ω_t represents the transition frequency which is the central frequency of the gain profile and T_2 is the dipole relaxation time, which is inversely proportional to the width of the spectral gain. In this model, it is assumed that the gain and absorption are dependent on the frequency of electromagnetic wave. By using this model, the transition from ASE to laser oscillation in a two dimensional active random medium was reported (Cao, Xu, Chang and Ho, 2000). Lately, the influence of absorption in the diffusive random medium was also examined (Yamilov, Wu, Cao and Burin, 2005).

Electric susceptibility of the material

The second approach is to embed a electric susceptibility of the material $\chi(\omega)$ into Maxwell's equations in order to describe the amplifying effect of the gain medium (Hawkins and Kallman, 1993, Wang, Liu and Yuan, 2005). The frequency-dependent electric susceptibility $\chi(\omega)$ is expressed as

$$\chi(\omega) = \frac{\chi_0 \omega_t^2}{\omega_t^2 + i\zeta\omega - \omega^2} \qquad \textbf{(3.18)}$$

where ω_t is the resonant frequency, ζ is a damping coefficient, χ_0 is the constant amplitude of electric susceptibility. The optical gain profile of the gain medium is derived from the imagine part of $\chi(\omega)$. The gain can be expressed as the following:

$$\gamma(\omega) = -\frac{\zeta}{2} \frac{\chi_0 \omega_0^2}{(\omega_0 - \omega)^2 + (\zeta/2)^2}, \qquad \textbf{(3.19)}$$

where χ_0 and ζ determine the peak value and spectral width of the gain, respectively. By using the polarization equation $P = \varepsilon_0 \chi(\omega) E$, where P is polarization density and ε_0 is free space dielectric permittivity, and the classical

electron oscillator model (Siegman, 1986), a second-order different equation can be obtained:

$$\frac{\partial^2 P}{\partial t^2} + \zeta \frac{\partial P}{\partial t} + \omega_t^2 P = \varepsilon_0 \chi_0 \omega_t^2 E \,. \qquad \textbf{(3.20)}$$

This equation is directly coupled to the Maxwell's equation and numerically solved by using the FDTD method. The advantage of this model is that the gain lineshape can be arbitrarily modified by varying χ_0, ω_0 and ζ. Accordingly, the effect of gain lineshape on the localized modes in active disordered media has been reported (Wang, Liu and Yuan, 2005).

3.3 Time-dependent theory

Time-dependent theory for random laser was firstly proposed by Jiang and Soukoulis (Jiang and Soukoulis, 2000). It demonstrated that the time-dependent theory has the ability to count for the nonlinear effect in the disordered lasing material. By using this theory, one can follow the evolution of the electromagnetic (EM) field and the population inversion. In the time-dependent theory, Maxwell's equations combining with the rate equations of a four-level atomic system are used to deal with active disordered media in order to describe the key characteristics of the random lasers. The equations can be solved numerically via the finite-difference time-domain (FDTD) method (Taflove, 1995).

Maxwell's equations coupling with the rate equations of electronic material was firstly reported in the study of wave propagation in nonlinear absorbing and gain media (Nagra and York, 1998). Following the development of the time dependent theory for random laser, many research works were presented on the localized mode in one-dimensional (Jiang and Soukoulis, 2000) and two-dimensional active random media (Vanneste and Sebbah, 2001, Sebbah and Vanneste, 2002), the polarization dependence of lasing modes (Wang and Liu, 2006). By using the

time-dependent theory and FDTD method, the emission spectra and the field intensity distribution of localized lasing modes inside the random laser system were obtained (Jiang and Soukoulis, 2000, 2002) random media. Lately, this model was extended to include a partial quantum mechanic effect in which the Pauli Exclusion Principle was taken into account. This model is more suitable to analyze the dynamic response in random lasers because one can follow the evolution of energy level population and field strength simultaneously. The FDTD simulations are valid both for ballistic, diffusive and strongly scattering regime.

3.3.1 Formalisms of the time-dependent theory

The time-dependent theory can be used to describe dynamics of the electromagnetic (EM) field in random media with gain. This theory is adequate to study the active disordered medium that the gain medium and the scattering elements are separated. The typical examples are colloidal dye solutions (Lawandy, Belachandran, Gomes and Sauvin, 1994, Sha, Liu and Alfano, 1994) and films of dye-doped polymer consisting of scattering particles (Cao, Xu, Ling, Burin, Seeling, Liu and Chang, 2003). In the model, it is assumed that electromagnetic waves propagate in an active matrix material comprising

complex disordered structure. In the amplifying random medium, light waves are both multiply scattered and amplified. Electromagnetic waves are scattered by the complex disordered structure without gain and amplified in the active matrix material background. The time-dependent theory, which bases on the Maxwell's equations, is capable of describing the optical properties of different materials. Thus, it is valid over a various type of disordered structures such as semiconductor, dielectric and metallic material. In order to mimic real experiments (Cao, Xu, Ling, Burin, Seeling, Liu and Chang, 2003), a disordered system consisting of dielectric particles randomly distributed in an active matrix material is under consideration. The particles have a relatively higher dielectric constant. The active matrix material is a homogenous non-magnetic and dispersive dielectric medium which has a lower dielectric constant. The average distance between the particles is in the order of light wavelength. In the numerical treatment, continuity of the tangential electric and magnetic field is naturally maintained across an interface of dissimilar materials. Hence, there is no need to specifically enforce field boundary conditions at the interface between the scattering particles and the active matrix material.

In the classical electrodynamics theory, Maxwell's equations govern the

propagation of electromagnetic wave. As mentioned in the section 3.2.3, the Maxwell's equations 3.8 and 3.9 can fully describe the transport behavior of electromagnetic wave in both dielectric and metallic material. It is assumed that $\vec{M}_{source} = \vec{J}_{source} = 0$ and $\sigma = \sigma^* = 0$ in the Equation 3.14 and 3.15. If the scattering particles and the active matrix medium are made of non-metallic material. Maxwell's equations 3.8 and 3.9 are read as

$$\nabla \times \vec{E} + \mu \frac{\partial \vec{H}}{\partial t} = 0 \qquad \textbf{(3.21)}$$

$$\nabla \times \vec{H} - \varepsilon \frac{\partial \vec{E}}{\partial t} - \frac{\partial \vec{P}}{\partial t} = 0 \qquad \textbf{(3.22)}$$

Equation 3.21 and 3.22 can only describe the transport and scattering behavior of electromagnetic wave but they are not adequate to describe the behavior of light amplification of an active matrix material. In order to simulate the gain of amplifying material, the electric polarization density term $\vec{P}$ should be linked the gain properties of laser dye. Using the classical electron oscillator model (Siegman, 1986) and the quantum theory, the electric polarization density $\vec{P}(t)$ is described by the quantum polarization equation of motion (Siegman, 1986). The modified Maxwell's equations and the polarization equation are given as

$$\nabla \times \vec{E} + \mu \frac{\partial \vec{H}}{\partial t} = 0 \qquad \textbf{(3.23)}$$

$$\nabla \times \vec{H} - \varepsilon \frac{\partial \vec{E}}{\partial t} - \frac{\partial \vec{P}}{\partial t} = 0 \qquad \textbf{(3.24)}$$

$$\frac{d^2 \vec{P}(t)}{dt^2} + \Delta\omega \frac{d\vec{P}(t)}{dt} + \omega_t^2 \vec{P}(t) = \kappa \Delta N(t) \vec{E}(t) \qquad \textbf{(3.25)}$$

where ω_t is the transition frequency, $\Delta\omega = 1/\tau_{32} + 1/T_{collision}$ is the linewidth of the atomic transition. τ_{32} is the lifetime of lasing level. $T_{collision}$ is the collision time of the atom. $\kappa = 6\pi\varepsilon_0 c^3 / \tau_{32}\omega_t^2$ is the classical rate (Jiang and Soukoulis, 2000). c is the speed of light. ε_0 is the free-space permittivity. $\Delta N(t) = N2(t) - N3(t)$ is the population difference density of lasing energy levels, which can be determined by using the atomic rate equations.

For active disordered systems, the gain medium can be considered as a four-level electronic material. The four-level atomic system is normally used to fully describe the properties of laser dyes. The energy level structure of the atomic system is shown in Figure 3.2. The lifetimes of atomic level L_2, L_3 and L_4 are denoted by τ_{21}, τ_{32} and τ_{43}, respectively.

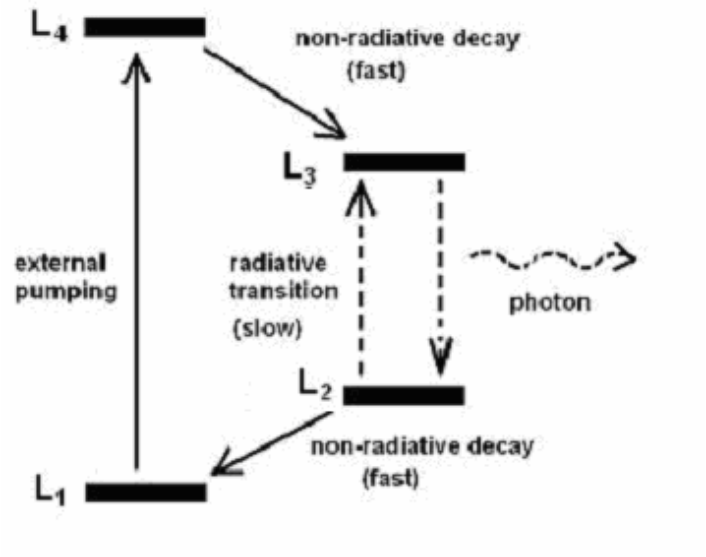

Figure 3.2 Energy levels of a four-level atomic system

Initially, the electrons at the ground energy state L_1 are pumped to the highest energy state L_4 at a certain pumping rate Q. The excited electrons can nonradiatively decay to the next lower state L_3 with a lifetime of τ_{43}. The energy state L_3 and L_2 are the upper lasing level and the lower lasing level. After the radiative transition from energy state 3 to 2, the electrons nonradiative transfer back to the ground state. The non-radiative transitions of $L_4 \rightarrow L_3$ and $L_2 \rightarrow L_1$ are proportional to the decay rates $1/\tau_{43}$ and $1/\tau_{21}$, respectively. The rate equations are used to describe the atomic transition of atomic systems and the population of energy levels. The rate equations of a four-level atomic system are given as (Jiang and Soukoulis, 2000)

$$dN1/dt = N2/\tau_{21} - QN1 \quad \textbf{(3.26)}$$

$$dN2/dt = N3/\tau_{32} - N2/\tau_{21} - (2\pi E/h\omega_t)dP/dt \quad \textbf{(3.27)}$$

$$dN3/dt = N4/\tau_{43} - N3/\tau_{32} + (2\pi E/h\omega_t)dP/dt \quad \textbf{(3.28)}$$

$$dN4/dt = -N4/\tau_{43} + QN_1, \quad \textbf{(3.29)}$$

where *N1*, *N2*, *N3* and *N4* are the population density of atomic level L_1, L_2, L_3 and L_4, respectively. *h* is Planck's constant. *Q* is the pumping rate which is proportional to the pump energy intensity in the real experiment (Jiang and Soukoulis, 2001). The lasing transition with transition wavelength ω_t is contributed by the spontaneous emission and stimulated emission. The stimulated emission rate is proportional to the term $(2\pi E/h\omega_t)dP/dt$. The Maxwell's equations coupled to the nonlinear polarization equation can be solved numerically together with the four rate equations for the time variation of $\Delta N(t)$. The algorithm of the Finite-Difference Time-Domain (FDTD) method, the initial and boundary conditions of numerical simulations will be discussed in the next section.

3.3.2 Algorithm of FDTD method

The set of Equations 3.23-3.29 can be solved simultaneously by the

Finite-Difference Time-Domain (FDTD) method (Taflove, 1995, Taflove and Haginess, 2000). FDTD is a computationally efficient method of directly solving Maxwell's time-dependent curl equations or their equivalent integral equations using the finite-difference technique. By using the FDTD method, a full-vector solution of Maxwell's equations can be obtained. Thus, the phase information of the wave electromagnetic wave can be retained.

The FDTD approach was first proposed in a paper by Yee (Yee, 1966a). In FDTD scheme, the Maxwell's equations are discretized and adapted to a discrete space mesh. Both the electric field and magnetic field, which are discretized on numerical grids, can be calculated at successive discrete time step series. According to Yee's algorithm, the electric and magnetic field components in three-dimensional space centered in a cube are depicted in the Figure 3.3. Every electric field $\vec{E}$ component is surrounded by four magnetic field $\vec{H}$ components, and every $\vec{H}$ component is also enclosed by four $\vec{E}$ components. The algorithm centers its $\vec{E}$ and $\vec{H}$ components in time in a leapfrog arrangement. The leapfrog time-stepping is illustrated in Figure 3.4. All of the $\vec{E}$ components in the current time step are computed by using the $\vec{H}$ components obtained in the previous time step according to the discretized

Maxwell's equations. The cycle can be completed by recomputation of the $\vec{H}$ components based on the newly obtained $\vec{E}$.

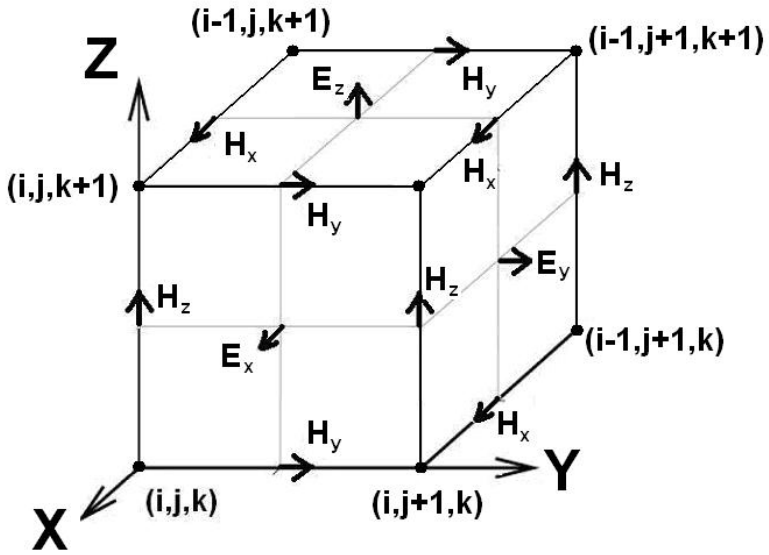

Figure 3.3 E and H components are placed into a cubic unit cell of the Yee Cube. Source: (Yee, 1966a)

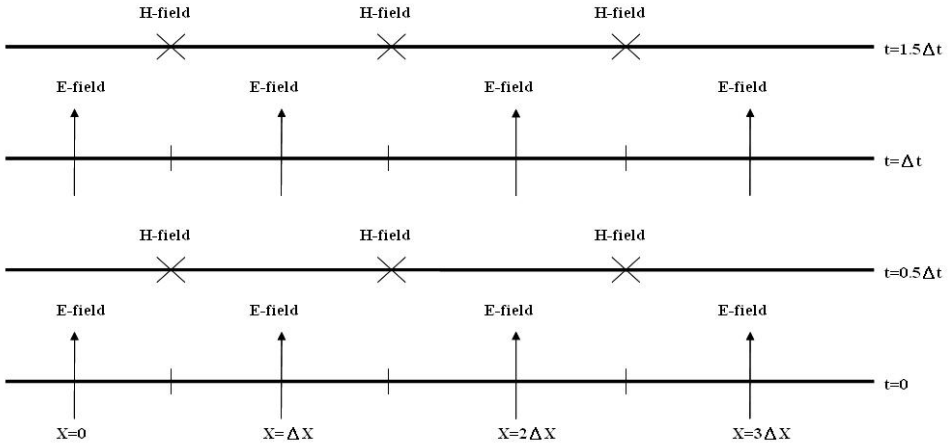

Figure 3.4 Space-time chart of the Yee algorithm for a one-dimensional wave propagation example showing the use of central differences for the space derivatives and leapfrog for the time derivatives. Source: (Taflove and Haginess, 2000)

Reduction to the two-dimensional (2D) transverse-magnetic (TM) mode

In the real experiment, the lasing actions were generated in three-dimensional (3D) random laser systems such as colloidal dye solution (Zacharakis, Papadogiannis and Papazoglou, 2002). Despite FDTD method is adequate to simulate 3D disordered system, 3D FDTD simulation requires huge computer memory and is very time consuming. Instead of the 3D disordered system, 2D disordered system is considered in the numerical experiments. Hence, the computation time and computer memory are significantly reduced for 2D computer simulations.

The 3D Yee's algorithm can be reduced to the proper algorithms for the 2D transverse-magnetic mode case. In a 2D system, it assumes that the structure being modeled extends to infinity in a direction, i.e., z-direction, perpendicular to the transverse x-y plane with no change in the shape or position of its transverse cross section. If the incident wave is also uniform in the z-direction, then all partial derivatives of the fields with respect to the z-direction must be equal to zero. Under these conditions, the electromagnetic wave can be classified into two distinct polarizations. Transverse-electric (TE) modes have $\vec{E}$ perpendicular to the z-direction, $\vec{E}(r)\cdot\hat{z}=0$ and $\vec{H}$ parallel to the z-direction, $\vec{H}=H(r)\hat{z}$.

Transverse-magnetic (TM) modes have just the reverse: $\vec{E} = E(r)\hat{z}$ and $\vec{H}(r) \cdot \hat{z} = 0$.

A 2D problem of a TM wave propagating in the z direction is considered as follows. The vector components of the curl operator in Equation 3.23, 3.24 and 3.25 to yield the following three scalar equations are given as:

$$\frac{\partial E_z}{\partial t} = \frac{1}{\varepsilon}\left[\frac{\partial H_y}{\partial x} - \frac{\partial H_x}{\partial y} - \frac{\partial P_z}{\partial t}\right] \quad \textbf{(3.30)}$$

$$\frac{\partial H_x}{\partial t} = -\frac{1}{\mu}\frac{\partial E_z}{\partial y} \quad \textbf{(3.31)}$$

$$\frac{\partial H_y}{\partial t} = \frac{1}{\mu}\frac{\partial E_z}{\partial x} \quad \textbf{(3.32)}$$

where H_x and H_y are the magnetic field component along the x-direction and y-direction, respectively. E_z is the z-direction component of electric field. P_z is electric polarization density along the z-direction.

Discretized equations for 2D TM wave propagation

In FDTD manner, the field equations, the polarization equation and the rate equations can be discretized by using central differencing scheme and Yee's grid technique (Yee, 1966b). According to the Yee algorithm, the central differencing

approximations of the spatial and temporal partial derivatives are second–order accuracy. In order to discretize the Maxwell's equations and the rate equations, it should firstly specify the space and time notation. Since the coupled scalar equations are valid for all values of *x*, *y* and *t*, it is assumed that the components of the electric and magnetic fields are continuous or at least piecewise continuous with respect to the *x*, y and *t* variables. Let Δx and Δy represent the lattice spatial increment along *x* and *y* coordinates, respectively, and Δt represent the discretized time increment. It can denote a space point in a uniform, rectangular lattice as

$$(i, j) = (i\Delta x, j\Delta y) \qquad \textbf{(3.33)}$$

Furthermore, any function *u* of space and time evaluated at a discrete point in the grid and at a discrete point in time is

$$u(i\Delta x, j\Delta y, n\Delta t) \qquad \textbf{(3.34)}$$

where Δt is the time increment, assumed uniform over the observation interval, and *n* is an integer. The spatial and temporal partial derivatives of the field

components are given by

$$\frac{\partial u(i\Delta x,\, j\Delta y, k\Delta z, n\Delta t)}{\partial x} = \frac{u_x^n(i+1/2,\, j, k) - u_x^n(i-1/2,\, j, k)}{\Delta x} + O[(\Delta x)^2] \tag{3.35}$$

$$\frac{\partial u(i\Delta x,\, j\Delta y, k\Delta z, n\Delta t)}{\partial y} = \frac{u_x^n(i,\, j+1/2, k) - u_x^n(i,\, j-1/2, k)}{\Delta y} + O[(\Delta y)^2] \tag{3.36}$$

$$\frac{\partial u(i\Delta x,\, j\Delta y, k\Delta z, n\Delta t)}{\partial t} = \frac{u^{n+1/2}(i, j, k) - u^{n-1/2}(i, j, k)}{\Delta t} + O[(\Delta t)^2] \tag{3.37}$$

$$\frac{\partial^2 u(i\Delta x,\, j\Delta y, k\Delta z, n\Delta t)}{\partial t^2} = \frac{u^{n+1}(i, j, k) - 2u^n(i, j, k) + u^{n-1}(i, j, k)}{(\Delta t)^2} + O[(\Delta t)^2] \tag{3.38}$$

In Equations 3.35-3.38, the second-order terms of spatial and temporal increment, i.e., $O[(\Delta x)^2]$, $O[(\Delta y)^2]$ and $O[(\Delta t)^2]$, can be neglected. By applying the notation and the central differencing approximation, the discretized equations are obtained and expressed as

$$P_z^{n+1}(i,j)=\frac{2-\omega_t^{\,2}\Delta t^2}{1+\Delta\omega\Delta t/2}P_z^{n}(i,j)+\frac{\Delta\omega\Delta t/2-1}{1+\Delta\omega\Delta t/2}P_z^{n-1}(i,j)+\frac{\Delta t^2}{1+\Delta\omega\Delta t/2}\kappa\Delta N^{n}(i,j)E_z^{n}(i,j) \tag{3.39}$$

$$E_z^{n+1}(i,j)=E_z^{n}(i,j)+\frac{\Delta t}{\varepsilon(i,j)}\{[H_y^{n+1/2}(i+1,j)-H_y^{n-1/2}(i,j)]/\Delta x-[H_x^{n+1/2}(i,j+1)-H_x^{n-1/2}(i,j)]/\Delta y\}-\frac{\Delta t}{\varepsilon(i)}[P_z^{n+1}(i,j)-P_z^{n}(i,j)] \tag{3.40}$$

$$H_x^{n+1/2}(i,j)=H_x^{n-1/2}(i,j)-\frac{\Delta t}{\mu_0\Delta y}[E_z^{n}(i,j+1)-E_z^{n}(i,j)] \tag{3.41}$$

$$H_y^{n+1/2}(i,j)=H_y^{n-1/2}(i,j)+\frac{\Delta t}{\mu_0\Delta x}[E_z^{n}(i+1,j)-E_z^{n}(i,j)] \tag{3.42}$$

$$N1^{n+1}(i,j)=[1-Q(i,j)\Delta t]N1^{n}(i,j)+\frac{\Delta t}{2\tau_{21}}[N2^{n+1}(i,j)+N2^{n}(i,j)] \tag{3.43}$$

$$N2^{n+1}(i,j)=\frac{2\tau_{21}-\Delta t}{2\tau_{21}+\Delta t}N2^{n}(i,j)+\frac{\tau_{21}\Delta t[N3^{n+1}(i,j)+N3^{n}(i,j)]}{\tau_{32}(2\tau_{21}+\Delta t)}-\frac{\tau_{21}[E_z^{n+1}(i,j)-E_z^{n}(i,j)][P_z^{n+1}(i,j)-P_z^{n}(i,j)]}{(2\tau_{21}+\Delta t)(h/2\pi)\omega_t} \tag{3.44}$$

$$N3^{n+1}(i,j)=\frac{2\tau_{32}-\Delta t}{2\tau_{32}+\Delta t}N3^{n}(i,j)+\frac{\tau_{32}\Delta t[N4^{n+1}(i,j)+N4^{n}(i,j)]}{\tau_{43}(2\tau_{32}+\Delta t)}+\frac{\tau_{32}[E_z^{n+1}(i,j)-E_z^{n}(i,j)][P_z^{n+1}(i,j)-P_z^{n}(i,j)]}{(2\tau_{32}+\Delta t)(h/2\pi)\omega_t} \tag{3.45}$$

$$N4^{n+1}(i,j)=\frac{2\tau_{43}\Delta t}{2\tau_{43}+\Delta t}QN1^{n}(i,j)+\frac{2\tau_{43}-\Delta t}{2\tau_{43}+\Delta t}N4^{n}(i,j) \tag{3.46}$$

where Δt, Δx *and* Δy represent the time increment, the x-direction and the y-direction space increment, respectively. The index *n* and *i* denote the time step and the space step, respectively. For given initial and boundary conditions, the polarization density, the electric field, the magnetic field and the electronic numbers at each energy level in the time step *n+1* can be calculated and updated according to Equations 3.39 to 3.46, respectively, which are based on the data in the previous time step *n*.

3.4 Numerical implementation

In the previous section, the full set of discretized equation is presented. The next step is to adapt random configurations to the computational domain. Figure 3.5 shows one of random configuration of active disordered medium.

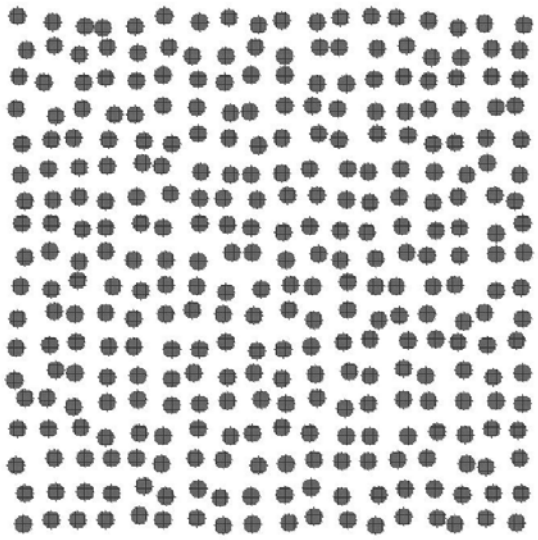

Figure 3.5 Schematic diagram of 2D disordered dielectric system

The size of the 2D disordered medium is *S*x*S*, where S is the length of the medium. The medium consists of relatively high dielectric circular particles (black color area) with a radius of *R* and refractive index of n_2. The circular particles act as scattering particles distributed randomly in a background medium (white color area) with a lower refractive index n_1. The scattering of EM waves is

due to the difference of dielectric constant between the background medium and the particles. The background medium can be considered as a homogenous active material, which is modeled as a four-level atomic systems. The population density of electrons is uniformly distributed across the whole system.

3.4.1 Boundary conditions

Special boundary conditions are employed in the simulation, which models an open system. In others words, the system is bounded by a perfectly matched layer (PML) (Berenger, 1995) which is unphysical absorption layer. All outgoing EM wave is absorbed without reflection in PML. The boundary conditions for the field at the interfaces between the disordered system and PML are self-satisfied numerically because of the continuity of EM field.

3.4.2 Initial conditions

In the present FDTD algorithm, it is necessary to assign the initial values of the polarization density, the electric field, the magnetic field and the electronic numbers at each level for all the meshes in the computation domain. At *t = 0,* it assumes that $P_z^0 = 0$, $E_z^0 = 0$, $H_x^0 = H_z^0 = 0$ and $N2^0 = N3^0 = N4^0 = 0$ everywhere in grid. The electron number of the ground state $N1^0$ is equal to the total

number of the atomic system at $t = 0$. It means that all the atomic systems lie in the ground state. When $t>0$, the electrons in the ground state L_1 are pumped to the highest energy state L_4 with a pumping rate Q, which model as the external optical pumping. After certain time steps, a Gaussian excitation electric pulse is introduced in the computation domain in order to trigger the stimulated emission. The evolution of field, the population density of lasing levels and the spatial field distribution of the system are recorded. By using Fourier transformation, the emission spectra of the system can be calculated.

3.4.3 Numerical stability

In the FDTD algorithm, the selection of the space increment Δx and time step Δt can affect the numerical stability and the numerical error. To ensure the stability and accuracy of the algorithm, the value Δx = 10nm and Δt = 2.4x10^{-17}s are used in all the simulations. The space increment is sufficiently small as compared with the optical wavelength, i.e., $\Delta x < \lambda / 20$. The selection of time step Δt fulfills the stability criterion (Taflove and Brodwin, 1975), i.e., $\Delta t \le \Delta x / c\sqrt{2}$.

In the current work, the computational codes of the FDTD algorithm were written in FORTRAN 90 language. The codes were compiled and run on the UNIX

environment in a mainframe Sun Microsystems Sun-Fire E6900. The program codes of the FDTD modeling of the active disordered systems are shown in Appendix.

3.4.4 Validation of the FDTD program

After the set-up of the algorithm of FDTD method, verification of the FDTD program was carried out. In order to verify the program, simulations of passive and active system based on the time dependent theory and FDTD method were conducted to duplicate published results (Villeneuve, Fan and Joannopoulos, 1996, Qiu and He, 2000, Sebbah and Vanneste, 2002, Guo and Albin, 2003).

Passive System

The first numerical experiment was conducted to determine defect states of TM mode in 2D photonic crystals with dielectric inclusions. Since the photonic crystal is a passive system (without optical gain), the polarization equation (Equation 3.39), the rate equations (Equations 3.43 -3.46) and the polarization terms (P_z^{n+1}, P_z^n) in Equation 3.40 can be neglected in the modeling. The structure of the 2D photonic crystals is depicted in Figure 3.6, which is the same as the system described in the reference (Qiu and He, 2000). The photonic crystal consists of

infinity long dielectric cylinders arranged in a square array. A defect is introduced into the photonic crystal by modifying the size of the central cylinder. The computational domain is enclosed by perfectly matched layers (PML). The simulation parameters are listed in Table 3.1.

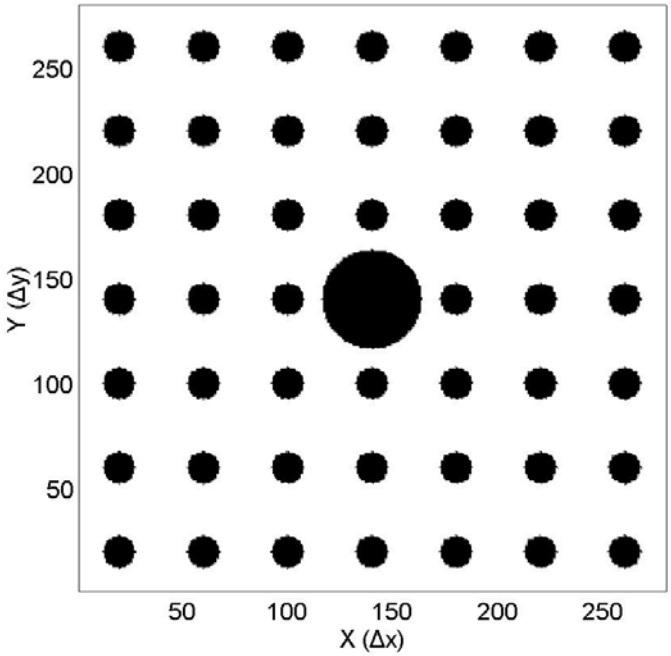

Figure 3.6 Schematic diagram of 2D photonic crystal. Black spots denote dielectric cylinders.

Table 3.1 Parameters of the photonic crystal and the FDTD simulation

Spatial increment	$\Delta x = \Delta y$ =100nm
Time increment	Δt = 2.33 x10^{-16}s
Total number of time step	*30000*
Size of system	SxS = 280Δx x 280Δx
Lattice constant of photonic crystal	$a=40\Delta x$
Radius of cylinder	$8\Delta x$
Radius of central defect cylinder	$0.6a=24\Delta x$
Dielectric constant of background medium	*1*
Dielectric constant of cylinder and defect	*11.56*

In order to determine the defects modes of the photonic crystal, the simulation procedures exactly followed what Qiu did (Qiu and He, 2000). Qiu's results were obtained by using standard FDTD method of TM mode. The photonic crystal was initially excited by a magnetic field pattern. The initial conditions are given as:

$$H_y(x,y,t=0) = -e^{\left[-(\frac{5x}{a}+1)^2-(\frac{5y}{a})^2\right]}/3 + 3(1-\frac{5x}{a})^2 e^{\left[-(\frac{5x}{a})^2-(\frac{5y}{a}+1)^2\right]} \\ -10[\frac{x}{a}-(\frac{5x}{a})^3-(\frac{5y}{a})^5]e^{\left[-(\frac{5x}{a})^2-(\frac{5y}{a})^2\right]},$$

$$H_x(x,y,t=0) = 0,$$

$$E_z(x,y,t=0) = 0,$$

where a is lattice constant.

Electric field is recorded in 10 observation points assigned randomly in the computational domain. The power spectrum is calculated by using Fourier transform of the recorded electric field signal. Figure 3.7 shows the power spectra of the photonic crystal including present calculation and Qin's results. Four peaks are found in the power spectrum, which associate with the four defect modes. Table 3.2 summarizes the frequency of the four defect modes. Compared to Qin's and the present results, the maximum percentage difference is 0.51%. Figure 3.8 shows the electric field distribution of the four defect modes. The electric field distribution is consistent with the published results obtaining by FDTD and

plane-wave explanation methods (Villeneuve, Fan and Joannopoulos, 1996, Qiu and He, 2000, Guo and Albin, 2003). The agreements of the published results confirm the validation of the FDTD theoretical framework and numerical implementation for the simulation of passive dielectric system.

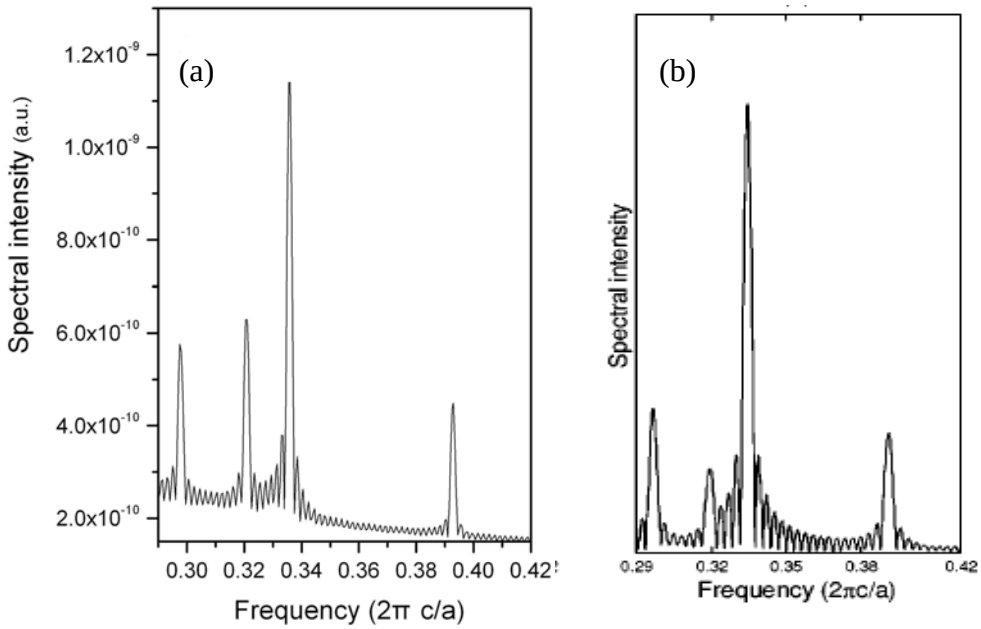

Figures 3.7 Power spectra of photonic crystal. (a) Results of current calculation and (b) Results of Qin's calculation. Source: (Qiu and He, 2000)

Table 3.2 Frequency of defect mode in the photonic crystal.

	Defect mode frequency calculated by the present simulation, ($2\pi c/a$)	Defect mode frequency listed in reference (Qiu and He, 2000), ($2\pi c/a$)	Percentage difference
First defect mode	0.2975	0.297	0.17%
Second defect mode	0.320	0.319	0.31%
Third defect mode	0.336	0.335	0.30%
Forth defect mode	0.393	0.391	0.51%

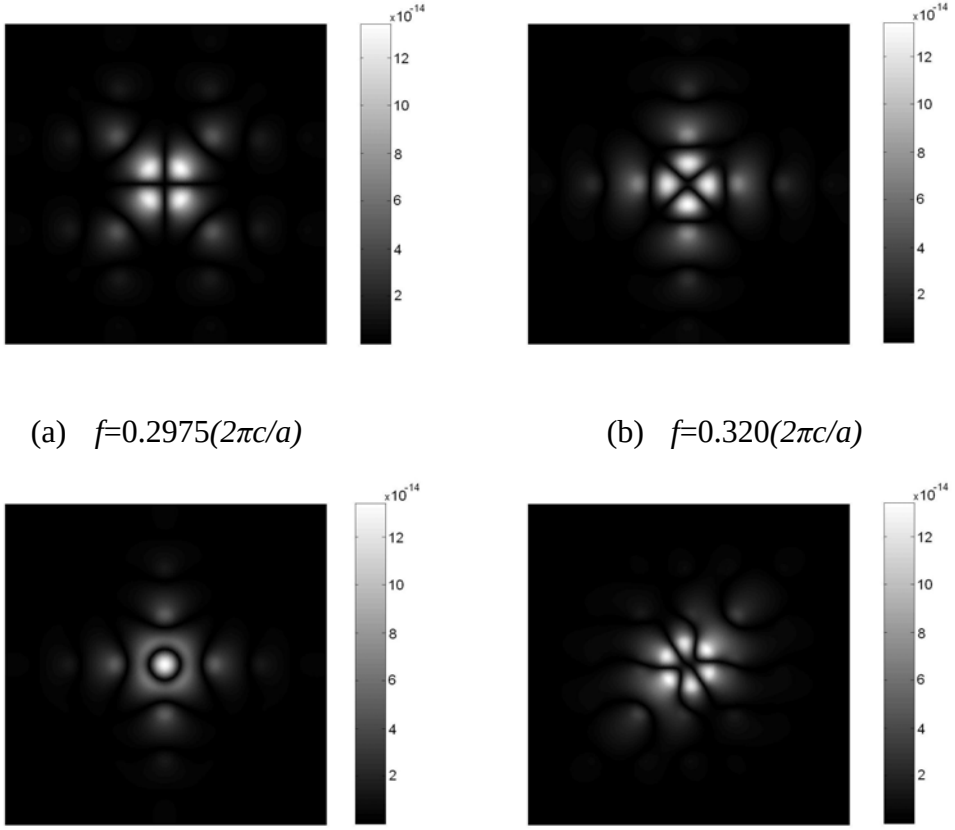

(a) f=0.2975$(2\pi c/a)$ (b) f=0.320$(2\pi c/a)$

(c) f=0.336$(2\pi c/a)$ (d) f=0.393$2(2\pi c/a)$

Figures 3.8 Electric field distribution of defect modes with frequency of (a) 0.2975, (b) 0.320, (c) 0.336 and (d) 0.393$2(2\pi c/a)$

Active system

Verification of FDTD modeling on active systems was carried out on a 2D active disordered dielectric system described in reference (Sebbah and Vanneste, 2002). An attempt was undertaken to compute the multi-mode emission spectra and the time evolution of electric field of the 2D active disordered dielectric system. The configuration of the 2D active disordered dielectric system is depicted in Figure 3.9. The simulation parameters are listed in Table 3.3. The values of parameters of the system are the same as the parameters listed in the reference (Sebbah and Vanneste, 2002).

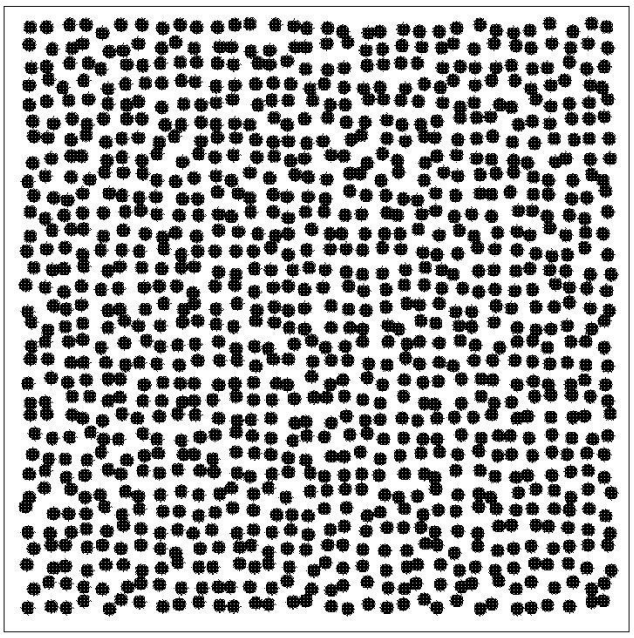

Figures 3.9 Configuration of 2D active disordered dielectric system

Table 3.3 Parameters of the four-level atomic structure and the FDTD simulation

Wavelength of the lasing transition	λ_t= 446.9nm
Frequency of the lasing transition	$\omega_t = 2\pi c/\lambda_t = 6.71 \times 10^{14}$ Hz
Collision time	$T_{collision} = 2 \times 10^{-14}$s
Life time of energy state L_2	$\tau_{21} = 5 \times 10^{-12}$s
Life time of energy state L_3	$\tau_{32} = 1 \times 10^{-10}$s
Life time of energy state L_4	$\tau_{43} = 1 \times 10^{-13}$s
Total atomic density	3.313×10^{24}m^{-3}
Pumping rate	$Q = 1 \times 10^{14}$s^{-1}
Size of system	SxS = 5500nm x5500nm
Radius of scattering particle	R = 60nm
Volume fraction of scattering particles	*40%*
Refractive index of scattering particles	$n_2 = 2$
Refractive index of background medium	$n_1 = 1$
Spatial increment	$\Delta x = \Delta y$ =10nm
Time increment	$\Delta t = 2.36 \times 10^{-17}$s
Total number of time step	250000Δt (=5.9 x10^{-12}s)

Initially, all the field components were set to be zero and the atomic systems stayed in the ground level, i.e., $E_x(x,y,t=0) = H_x(x,y,t=0) = H_y(x,y,t=0) = 0$, $N4(x,y,t=0) = N3(x,y,t=0) = N2(x,y,t=0) = 0$ and $N1(x,y,t=0) = 3.313 \times 10^{24}$m^{-3}. Then a Gaussian pulse of duration 10^{-16}s was injected inside the system. The impulse response was recorded during a time window [0, 250000Δt] at several observation points. Power spectrum was calculated by using Fourier transform of electric fields in a time window [1250000Δt, 250000Δt].

Figures 3.10 and 3.11 show the power spectra and the time evolution of electric field, respectively. The main features of multimode laser emission such as discrete multi-peaks and great amplification of electric field amplitude are captured in the present simulation, which qualitatively agrees with the results of Sebbah. Since the pumping rate and amplitude of excite pulse are not mentioned in the reference, different values may be used in the present simulation and therefore spectral peak intensity and emission profile (Figure 3.10) of our system

are different from Sebbah's results. The discrepancies are also attributed to the difference of system configuration. In the current numerical experiments, it cannot exactly mimic the configuration of the system described in Sebbah's work because the configuration of the active disordered system is randomly generated.

The FDTD simulation results of passive and active systems are consistent with the published results. It suggests that the algorithm of FDTD method is valid and feasible for studying both passive and active dielectric system.

3.5 Summary

Various existing theoretical treatments for random laser emission in amplifying random media have been reviewed. Among the existing methods, the time-dependent theory, which combines the time-dependent Maxwell's equations with the semi-classical laser theory, is employed for studying the random laser with coherent feedback. This theory is applicable in the investigation of the optical properties of passive and active disordered media with dielectric inclusions as well as metallic inclusions. It is adequate to explore the stimulated emission of active random media with arbitrary scatting structures.

A numerical framework has been set up based on the time-dependent theory. Maxwell's equations coupling with the rate equations of electronic population are solved with a finite-difference time-domain (FDTD) method. The optical gain of active material is described by the rate equations of electronic population of the four-level electronic system. Arbitrary disordered structures can be adopted in the simulation if the structure and material information are given. The temporal and

spatial distribution of EM field in the computational domain can be obtained and the emission spectra are determined by using Fourier transform of EM field.

After the set-up of the algorithm of FDTD method, verification of the FDTD program was conducted to duplicate the published results of defect modes of two-dimensional (2D) photonic crystal and lasing spectrum of a 2D active random medium. It is unambiguously shown that the numerical simulation is feasible to study the emission properties of both passive and active disordered media with dielectric inclusions.

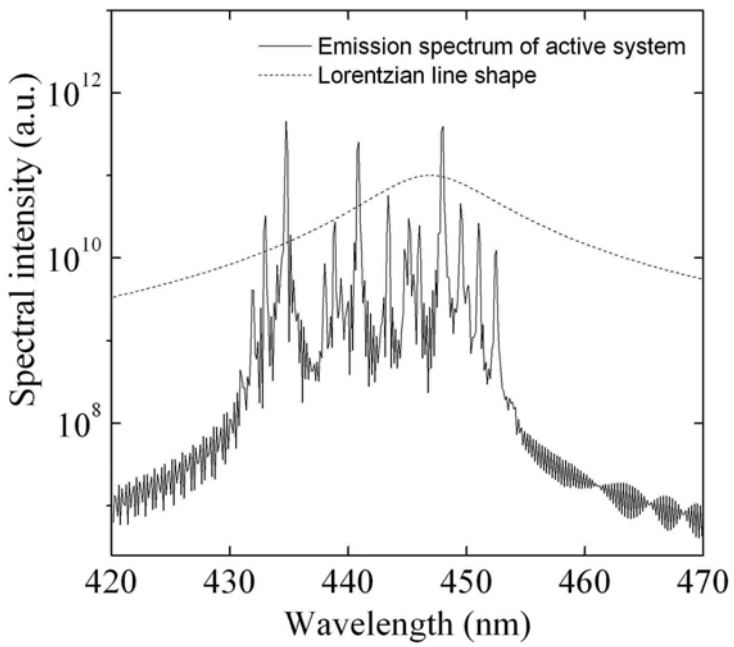

(a)

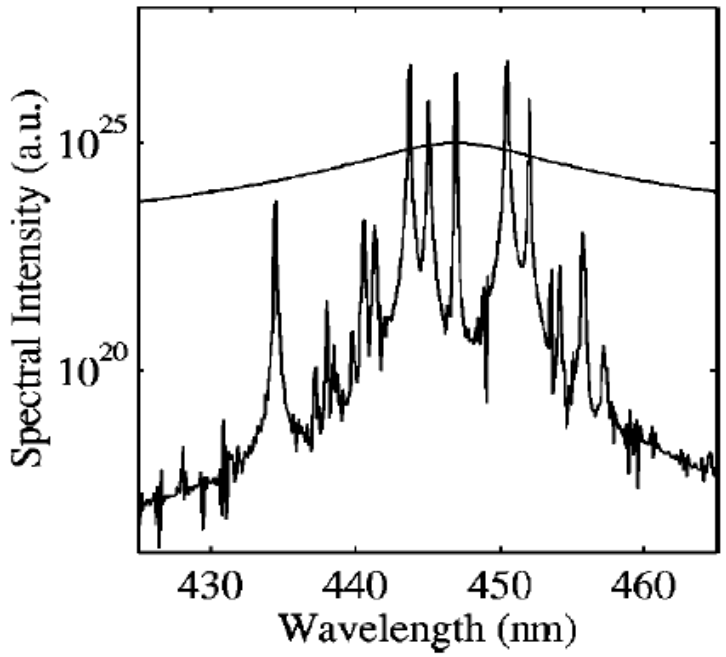

(b)

Figures 3.10 Power spectrum of (a) present method and (b) Sebbah's simulation. Source: (Sebbah and Vanneste, 2002)

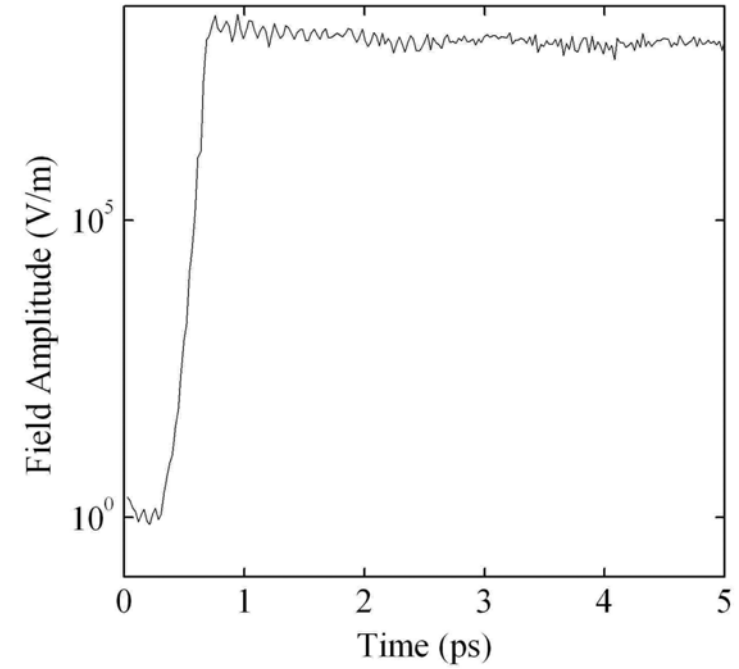

(a)

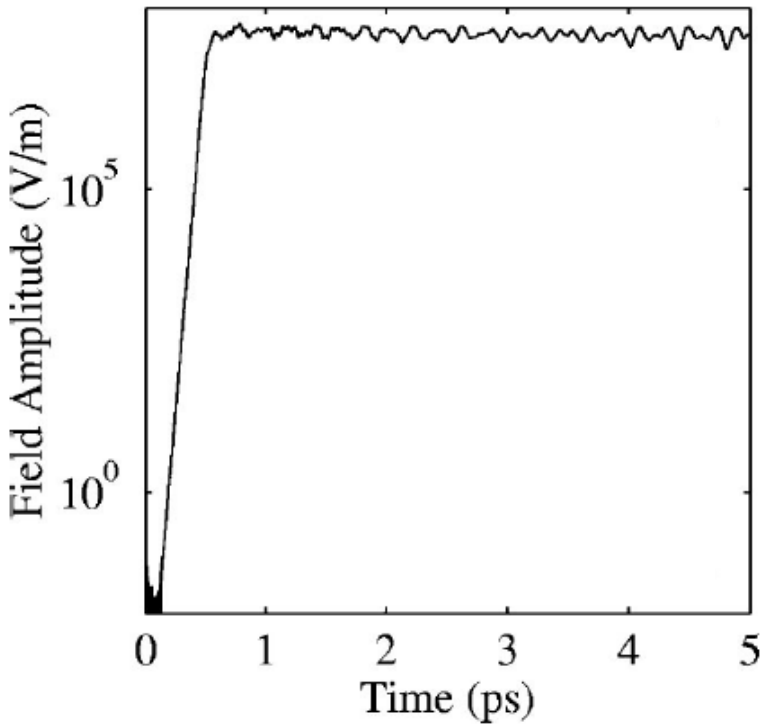

(b)

Figures 3.11 Time evolution of electric field amplitude of (a) present method and (b) Sebbah's simulation. Source: (Sebbah and Vanneste, 2002)

CHAPTER 4
INFLUENCE OF DISORDER ON PASSIVE DISORDERED MEDIA WITH DIELECTRIC SCATTERING PARTICLES

4.1 Introduction

In Chapter 3, the time-dependent theory and the numerical framework of finite-difference time-domain (FDTD) simulation were discussed. The FDTD method is adequate to describe the propagation of electromagnetic wave in both active and passive disordered media. In this chapter, the transport properties of electromagnetic wave in a two-dimensional (2D) passive disordered dielectric system with circular scattering particles are investigated with a numerical approach. Since the scale of the dielectric structure of the disordered system is comparable to the scale of visible wavelength, the system may exhibit interest phenomena in the optical frequency range such as photonic band gaps (PBGs) and localized states. It is valuable to study the influence of the disorder on the wave localization of passive disordered systems. Furthermore, the study of the disorder effects on the mode distribution of disordered systems can facilitate to understand the nature of random lasing in active disordered media.

4.2 Two-dimensional passive disordered system

By using FDTD numerical method, numerical experiments are preformed in order to study the effects of disorder on the mode distribution disordered systems. Our disordered dielectric system is a disordered medium without optical gain. The amplification of electromagnetic wave is neglected in the numerical simulations. In the numerical experiments, the disordered media are generated from ordered systems. The ordered systems are equivalent to photonic crystals which consist of a square array of infinitely long, parallel dielectric cylinders, each with a circular cross section of radius R and characterized by a dielectric constant ε_2. The array of cylinders is embedded in a background dielectric material with a dielectric constant ε_1. The intersections of these cylinders with a perpendicular plane form a square lattice. The lattice constant is a. The electromagnetic waves are assumed to propagate in a plane perpendicular to the cylinders. In the 2D case, the dielectric cylinders are used to mimic the circular scattering particles. The schematic diagram of the ordered system is shown in Figure 4.1.

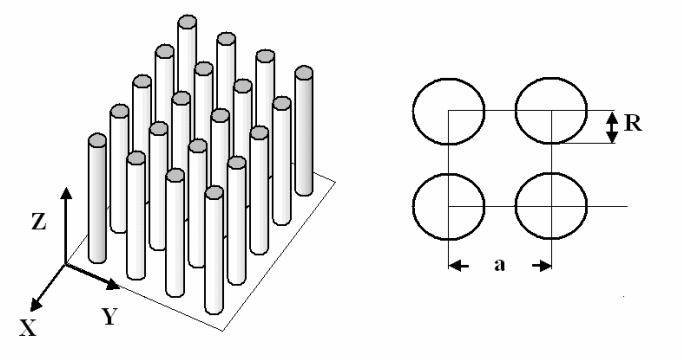

Figure 4.1 Two-dimensional (2D) ordered photonic crystal (square lattice)

By including certain randomness into the ordered system, we can create a random media with varying disorder. Hence, the degree of disorder can be quantified by using randomness. In the following, the definition of the random disorder is given. In this study, two kinds of disorder, i.e., position and size disorders are considered. In order to manifest their individual effects, the position and size disorders are investigated independently in the numerical simulations. Hence, the cases with both position and size disorders are not studied here.

4.2.1 Definition of position disorder

For the case of position disorder, the positions of each particle are randomized within a certain range from its lattice point. To create a random configuration, the position of each particle is randomly decided within a range giving a position disorder parameter of d_p. Figures 4.2a and 4.2b show a position disorder

configuration of 2D medium and the range (the square of the dashed line) of a particle position (*x*,*y*) allowed by a given d_p. The spatial position (*x*,*y*) of the particles is a random that $x = x_0 + \gamma_x d_p$, $y = y_0 + \gamma_y d_p$, where γ_x and γ_y are random variables. We assume that the probability density function γ_x and γ_y are uniform density functions between -1 and 1, i.e. $\gamma_x, \gamma_y \in [-1,1]$. In order to standardize the quantity of position disorder, the position disorder d_p is expressed in unit of lattice constant *a*. For example, if the lattice constant is 200nm and the amplitude of position disorder is 50nm, the position disorder can be expressed as $d_p = 0.25a$.

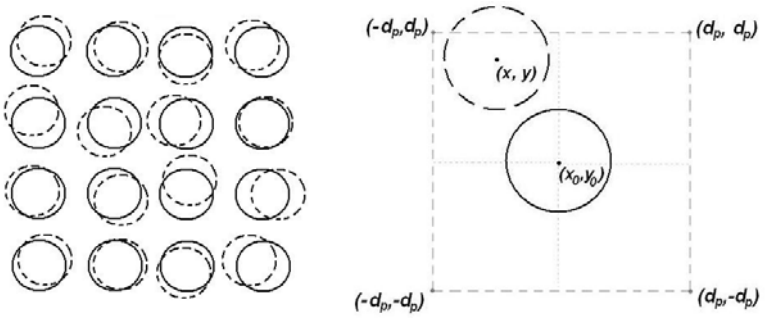

(a) (b)

Figure 4.2 (a) The position disorder of 2D disordered medium. (b) The definition of position disorder d_p.

4.2.2 Definition of size disorder

Size disorder is related to the uniformity in the radius of the cylinder. The position of each particle is fixed in its lattice position but the radius of particles

can be random. The radius of each particle is randomly changed within a distance d_r . The radius (R) of the circular particles is a random value $r = R + \gamma d_r$, where γ is a uniform density function between -1 and 1, i.e. $\gamma \in [-1,1]$. The probability density function γ is a uniform density function. Similarly, the size disorder d_r is standardized the same as the position disorder does, i.e., $d_r = 50nm = 0.25a$ where a = 200nm.

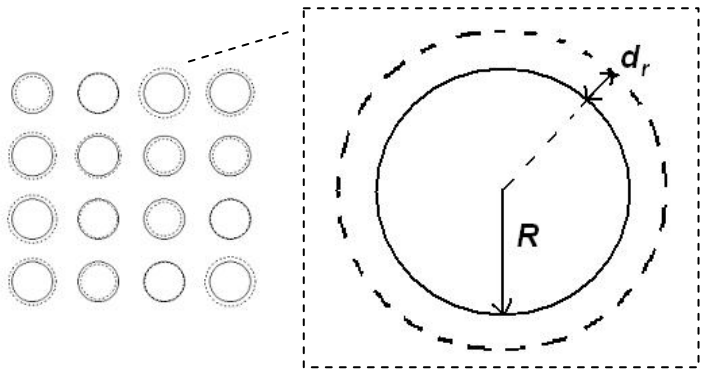

(a) (b)

Figure 4.3 (a) The size disorder of 2D disordered medium. (b) The definition of size disorder d_r.

4.3 Mode distribution of ordered and disordered media

In the first serial of numerical experiments, the mode distributions of disordered medium are first analyzed. By controlling the filling fraction of scattering particles, the influence of the density of scattering particles on the mode distribution of disordered medium is examined.

4.3.1 Ordered media

We start with the ordered system of size 4μm x 4μm, which consists of circular particles. The radius is 60nm. The dielectric constant of the particles and the host matrix medium are chosen as 7 and 1, respectively, because the larger dielectric contract can produce a significant scattering effect.

To determine the mode distribution of the ordered system over a wide frequency range, a short Gaussian pulse (pulse duration = 7 x10^{-16}s) is utilized to excite the system, which launches at the center of the medium. The bandwidth of the pulse covers the whole visible to near ultraviolet region. The temporal and spectral profiles of the Gaussian pulse are shown in Figure 4.4.

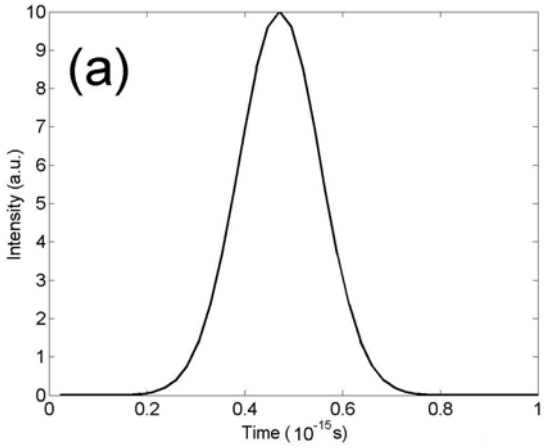

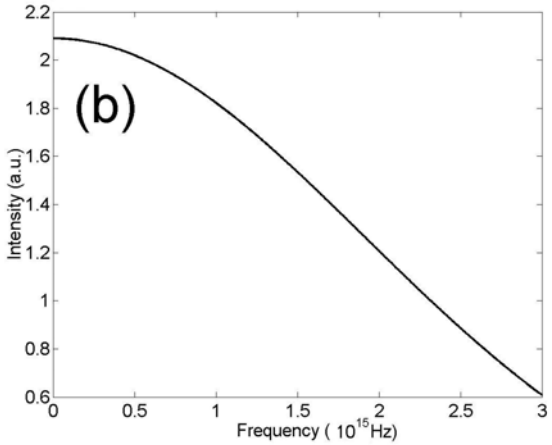

Figure 4.4 (a) Temporal and (b) spectral profiles of the Gaussian pulse

The transverse magnetic (TM) fields are calculated by using FDTD method within a time window (duration = 11.79 $x10^{-12}$s). Since the value of the electric and magnetic fields are calculated at every mesh of the computational domain, the field distribution pattern can be easily obtained. To observe the pulse response, the evolution of electromagnetic wave is recorded at several observation points which are evenly distributed cross the whole computational domain. By using Fourier transformation, the recorded time domain signals are converted to the frequency domain in order to obtain the spectral information.

Figure 4.5 shows the configurations of ordered media with various filling fractions. In order to control the filling fraction of the ordered medium, the density of particles is varied from $1x10^{12}m^{-2}$ to $2x10^{13}m^{-2}$ while the radius of

particles is kept as a constant. Figure 4.6 shows the particular configurations of the disordered system, in which the position disorder is applied. The parameters of the numerical simulation and the FDTD calculation are listed in table 4.1.

Table 4.1 Parameters of the numerical simulation and the FDTD calculation

Refractive index of matrix medium	$n_1 = 1$, $\varepsilon_1 = n_1^2 = 1$
Refractive index of scattering particle	$n_2 = 2.646$, $\varepsilon_2 = n_2^2 = 7$
The radius of scattering particle	$R = 60$nm
Spatial increment	$\Delta x = \Delta y = 10$nm
Time increment	$\Delta t = 2.36 \times 10^{-17}$s
Total number of time step	$500000\Delta t$ $(=11.79 \times 10^{-12}$s)
Size of system	$SxS = 4000$nm x4000nm
Perfectly matched layer thickness	100nm

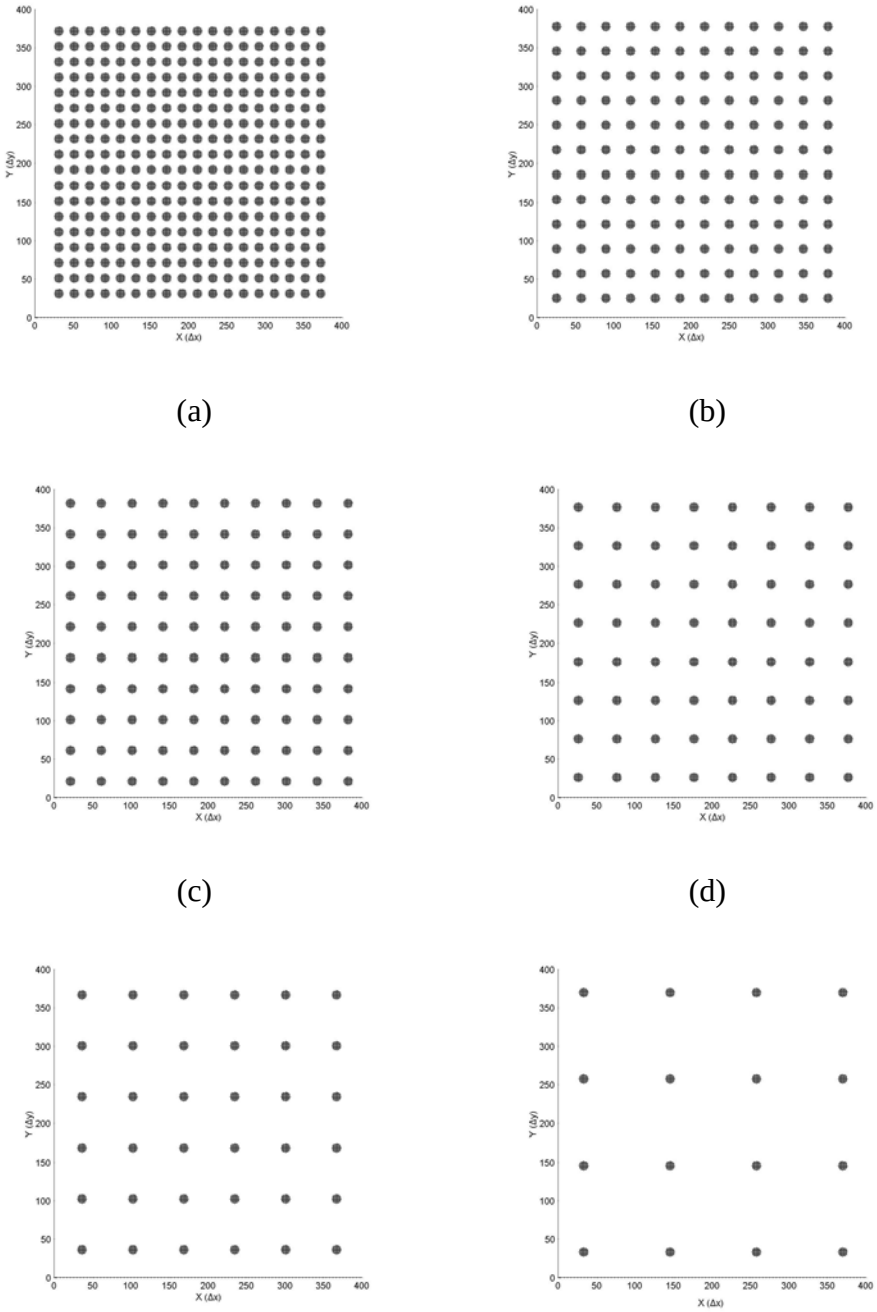

Figure 4.5 Schematic diagrams of 2D passive ordered media with various particle density: (a) $2x10^{13}m^{-2}$, (b) $9x10^{12}m^{-2}$, (c) $6.25x10^{12}m^{-2}$, (d) $4x10^{12}m^{-2}$, (e) $2.25x10^{12}m^{-2}$, (f) $1x10^{12}m^{-2}$. The lattice constant of the disorder systems is: (a) a = 200nm, (b) a = 320nm, (c) a = 400nm, (d) a = 500nm, (e) a = 660nm, (f) a = 1120nm

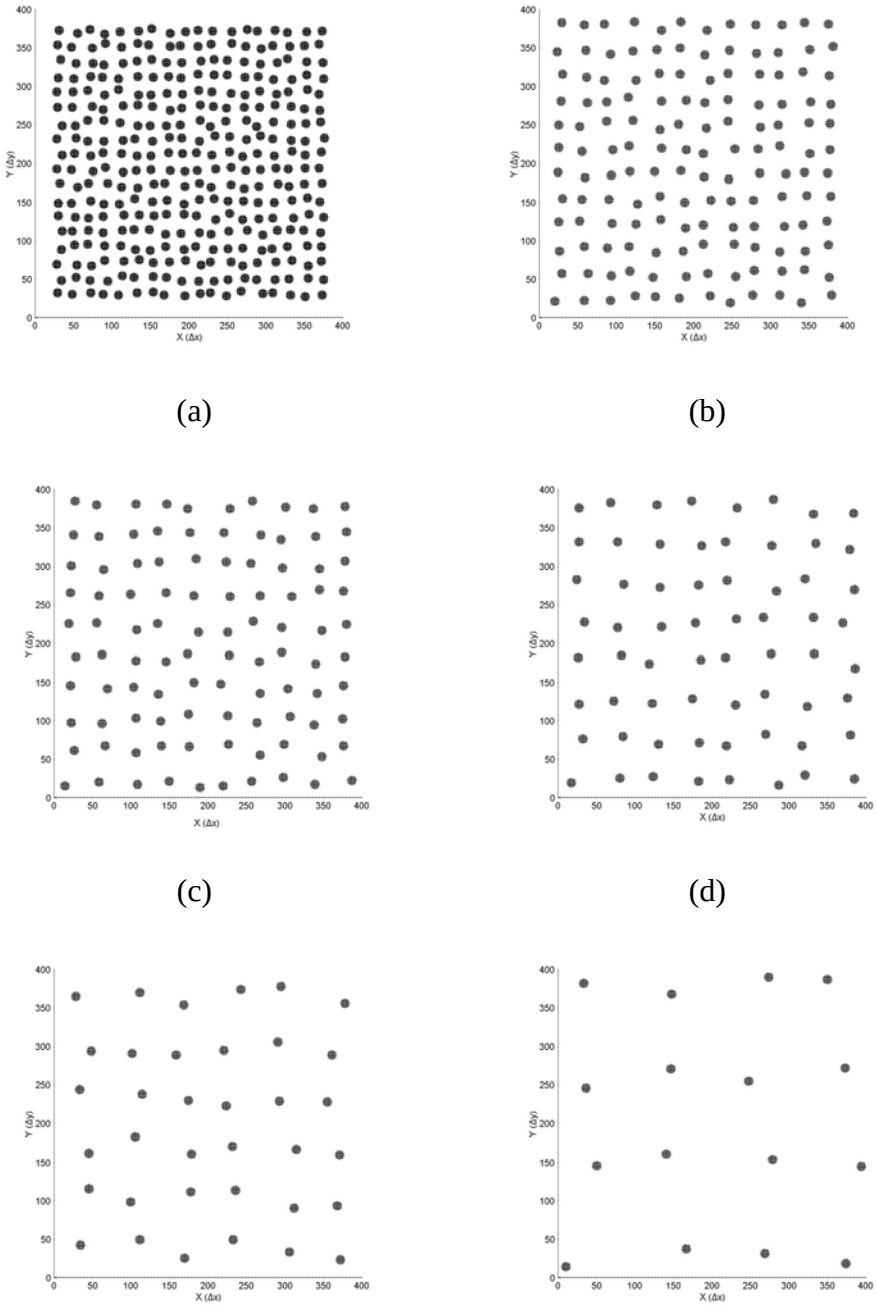

(a) (b)

(c) (d)

(e) (f)

Figure 4.6 Schematic diagrams of particular configurations of 2D passive disordered media generated from the ordered media of Figure 4.5(a)-(f), respectively. The position disorder d_p of the disordered systems is: (a) d_p = 0.2a, (b) d_p = 0.19a, (c) d_p = 0.2a, (d) d_p = 0.2a, (e) d_p = 0.21a, (f) d_p = 0.23a

4.3.2 Disordered media

Figure 4.7 shows the power spectra of the ordered and disordered systems with various particle densities. The dash line curves denote the power spectra of the disordered systems, which represent the averaged results of 10 random configurations of position disorder. The spectral information is determined from the averaged field signals recorded at observation points in a time window [0, 500000Δt]. It can be observed that many spectral peaks emerge in the spectra, which associate with the eigen-states of the systems. At a lower particle density, both disordered and ordered systems exhibit smoother spectral curves in which the intensities of the spectral peaks are relatively low. The results demonstrate that the intensity of the peaks is increased as the density of scattering particles increases. In the mean time, more high intensity peaks emerge in the system with a higher particle density, as shown in Figure 4.7a and Figure 4.7b. The peaks associated with eigen-states may be created when the particle density of the system is increased. It is believed that the strength of scattering and the number of scattering event of the electromagnetic wave are reinforced in the densely packed system.

Another finding is that some spectral dips emerge in the spectra of both ordered

and disordered system, as shown in Figure 4.7a. The corresponding system has a high particle density of $2x10^{13}m^{-2}$. The formation of spectral dips is a direct consequence of the photonic band gaps (PBGs), as shown in Figure 4.8. Inside the frequency range of the PBG, the propagation of electromagnetic wave is forbidden. The density of states (DOS), which represents the density of propagation mode, is equal to zero. Since there is no eigen-state inside in the PBG, the spectral intensity in the frequency range of PBG is extremely low and thereby the dips are developed.

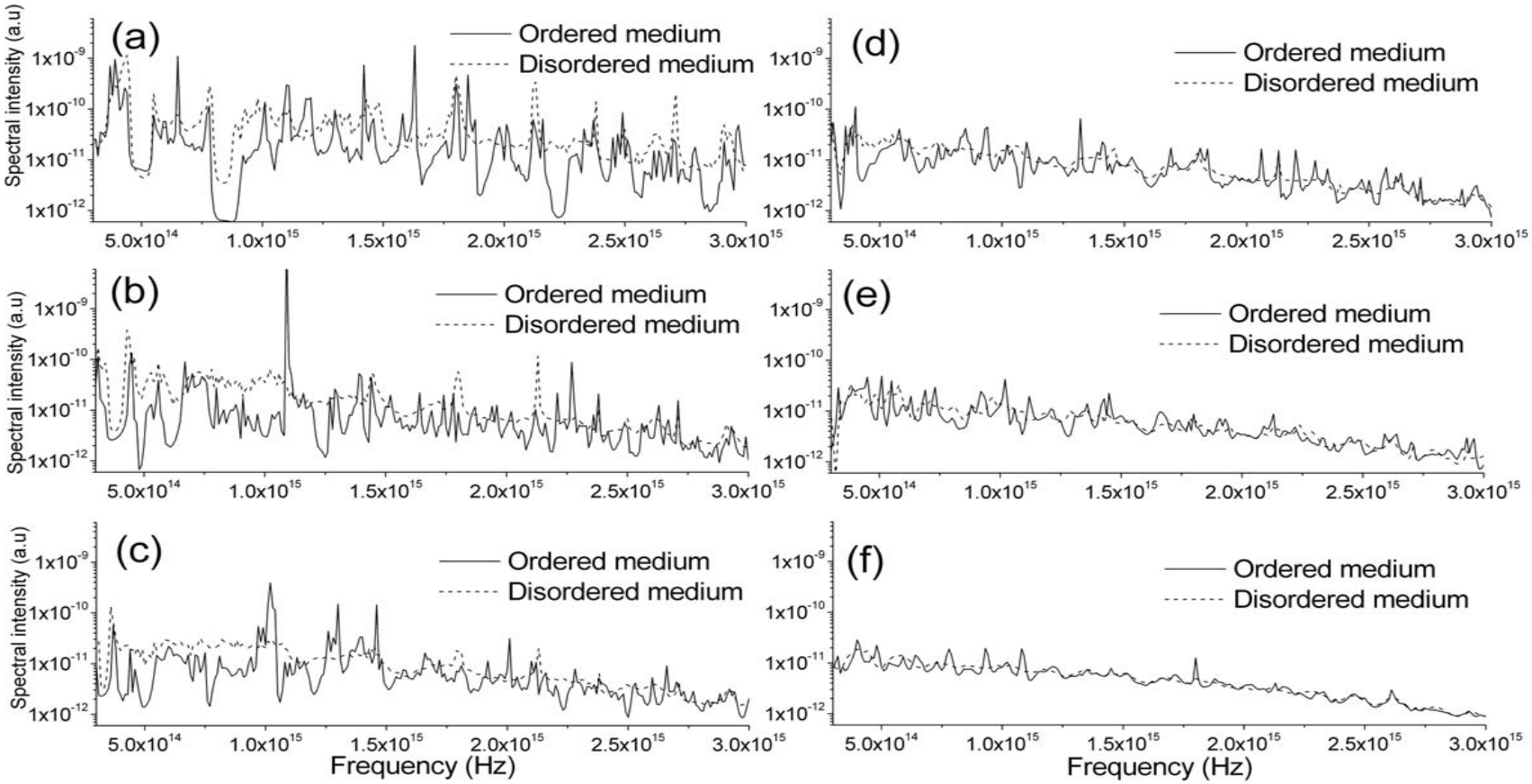

Figure 4.7 Intensity spectra for the 2D passive ordered and disordered systems with a particle density of (a) $2x10^{13}m^{-2}$, (b) $9x10^{12}m^{-2}$, (b) $6.25x10^{12}m^{-2}$, (d) $4x10^{12}m^{-2}$, (e) $2.25x10^{12}m^{-2}$, (f) $1x10^{12}m^{-2}$

Figure 4.8 illustrates the intensity spectra of the disordered system with a particle density of $2x10^{13}m^{-2}$. The frequency range is from the near infrared ($3x10^{14}$Hz) to near ultraviolet region ($1x10^{15}$Hz). The PBGs are denoted by the shade area. In the current simulation, the spectra are obtained from two consecutive time windows. The duration of the first and second time windows are [0, 250000Δt] and [250000Δt, 500000Δt], respectively. The configuration of the disordered system with position disorder (d_p = 0.1a) is shown in the inset of Figure 4.8. In the spectrum of the first time window (solid line), it is observed that several peaks appear over the whole frequency range except the frequency range of the PBGs. Compared to the spectrum captured from the first time window, only two main peaks remain in the that from the second time window (dot line). The two peaks are located in the band edge of PBGs. It is believed that the modes remaining in the spectrum of the second time window (dot line) are the longest-lived states of the system.

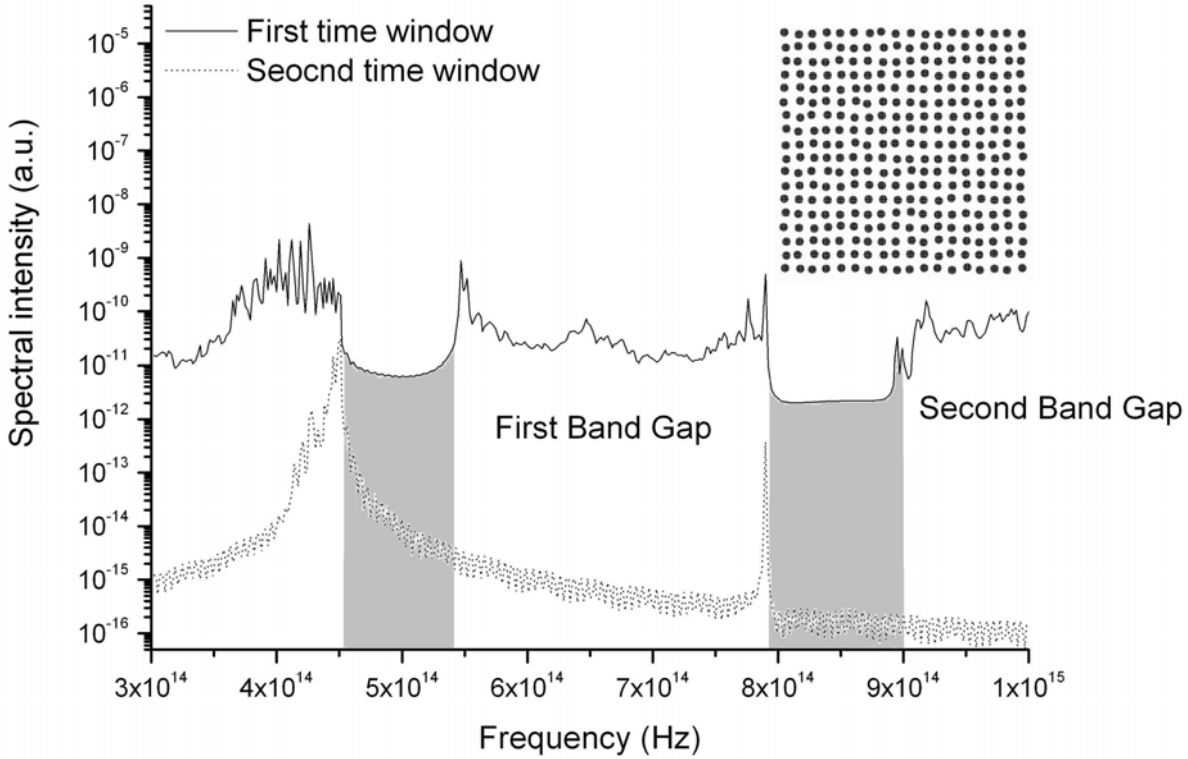

Figure 4.8 Intensity spectrum of the 2D passive disordered system with particle density of $2x10^{13}m^{-2}$. Inset: schematic diagram of the particular configuration of the 2D passive disordered medium ($d_p = 0.1a$). Lattice constant a is equal to 200nm.

These results may be understood in the following way. After the passive disordered medium is triggered by the Gaussian pulse, all the modes are excited and compete against each other. Therefore, several spectral peaks emerge in the spectrum. With the time evolution of the electromagnetic wave, the strength of the field reduces and the excited modes begin to decay. Since the excited modes have different lifetimes, the excited modes decay at different rates. The modes that have shorter lifetime decay more rapidly than that the modes that have longer lifetime. After a long time evolution, only few modes can survive while other modes are diminishing. Therefore, the spectral peaks illustrated in Figure 4.8 (dash line spectrum) are associated with the longer-lived modes.

Another interpretation of the results is related to the localization length of the eigen-state. As mentioned in Chapter 2, the energy stored in a mode decays exponentially away from the localization centers. Each mode has a different localization length. If the localization length is large, the energy of the mode may extend to the whole system. Since the disordered medium is an open system with a definite size, the field energy may leak out from the boundaries of the system to the surround environment. Hence, the loss of the field energy of the mode is depended on their localization length. A mode which has a large localization length will suffer a large high energy loss and diminish more quickly. With small localization lengths, light is well confined inside the modes and the energy loss is relatively low. To conclude, modes with shorter localization lengths have longer lifetimes and will survive after the long time evolution and mode competition. It also can explain why the survived modes tend to lie on the low frequency edge of PBGs, as the modes closed to the lower band edge of PBGs have shorter

localization lengths.

The full decay process of the modes can be illustrated in the evolution of the total energy of electric field U_E of the disordered medium, as shown in Figure 4.9. The configuration of the disordered medium (d_p = 0.2a) is depicted in the inset of Figure 4.8. The results are obtained by integrating the electric field intensity of all the meshes, i.e., $U_E \propto \frac{1}{2}\sum_{i,j} \varepsilon(i,j)E_z^{\,2}(i,j)$ at every time step. In the first stage of the evolution, the intensity of the energy drops dramatically because the extended modes begin to decay. The field energy of the extended modes radiates out from the boundaries of the passive system. In the second stage, the modes with longer lifetimes dominate the system. The evolution of the mode energy is following an exponential relation. The violent oscillation of the curve is caused by the interplay of the surviving modes. Figure 4.9b shows the exponential fitting curve which can well describe the time evolution of the total energy of electric field.

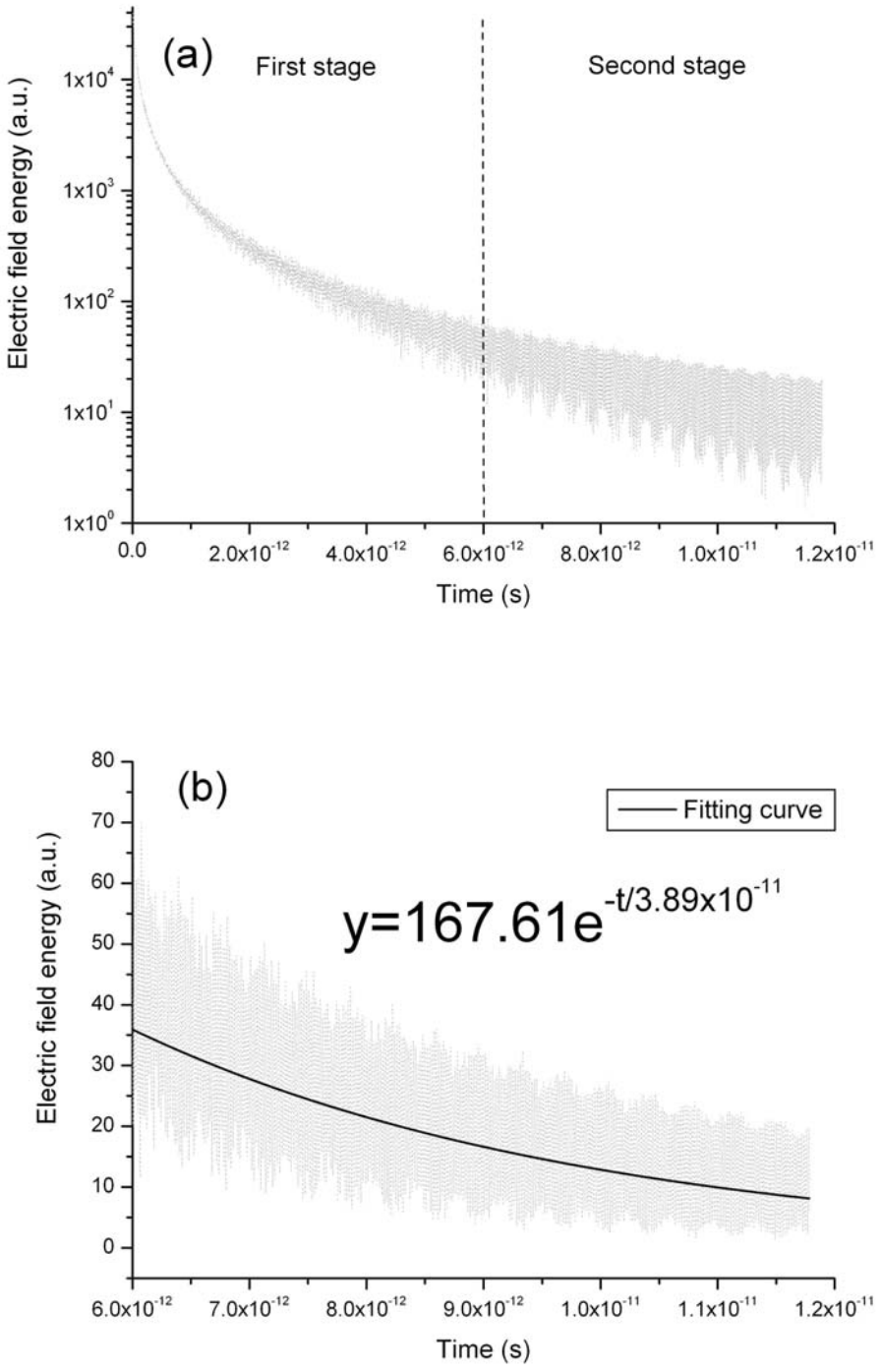

Figure 4.9 (a) Time evolution of total electric field energy of a 2D passive disordered medium with in a time window [0, 500000Δt]. The configuration of the disordered medium is depicted in the inset of Figure 4.8. (b) Time evolution of total electric field energy with in a time window [250000Δt, 500000Δt]

4.4 Effects of disorder on passive media

4.4.1 Effect of disorder on photonic band gap

In the previous numerical experiments, the mode distribution and the time evolution of electromagnetic wave of the disordered medium have been characterized. In the following sections, the effects of disorder on the mode distribution of the 2D passive disordered medium are examined. In the numerical experiments, the same disordered system described in section 4.3 is used but various amounts of random disorder are assigned. The information of the numerical simulation and the FDTD calculation are summarized in Table 4.2. The configurations of the disordered systems are illustrated in Figure 4.10.

Disordered media involved position disorder are considered. The simulations are performed at various amounts of random disorder which varies from d_p = 0 to 0.4a. Figure 4.11 shows the power spectra of the disordered media with various amount of disorder. The spectrum for each amount of d_p is obtained by averaging over 10 different configurations. The spectra are obtained from the recorded field signals within a time window [0, 250000Δt]. From the results, it is revealed that the quality and the size of band gap are depended on the amount of disorder. At d_p =0, the ordered medium exhibits two band gaps in the optical frequency range. The first and second band gaps locate at 4.51 x10^{14}Hz to 5.41 x10^{14}Hz and 7.90 x10^{14}Hz to 9.0x10^{14}Hz, respectively. As the amount of disorder increases, the bandwidth of PBGs is narrowed. When a larger amount of disorder is applied, more defects are created in the ordered medium. Consequently, more extra states are induced and the size of the band gaps becomes smaller. If the position disorder is further intensified, some states may be induced inside the band gaps

and destroy the band gaps.

Table 4.2 Parameters of the numerical simulation for the 2D passive disordered medium

Size of system	SxS = 4000nm x4000nm
Refractive index of matrix medium	n_1 = 1, $\varepsilon_1 = n_1^2 = 1$
Refractive index of scattering particle	n_2 = 2.646, $\varepsilon_2 = n_2^2 = 7$
Radius of scattering particle	R = 60nm
Number of scattering particle	324
Density of particle	$2x10^{13}m^{-2}$
Lattice constant	a = 200nm
Filling fraction	22.6%
Spatial increment	$\Delta x = \Delta y$ =10nm
Time increment	$\Delta t = 2.36 \times 10^{-17}$s
Total number of time step	$500000\Delta t$ (11.79×10^{-12}s)
Prefect match layer thickness	100nm

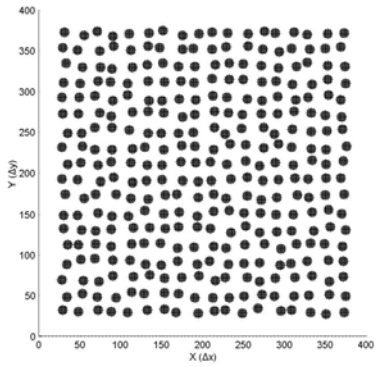

(a)

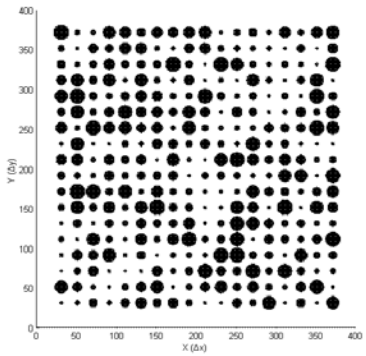

(b)

Figure 4.10 (a) configuration of disordered medium with position disorder, d_p =0.2a. (b) configuration of disordered medium with size disorder, d_r=0.2a

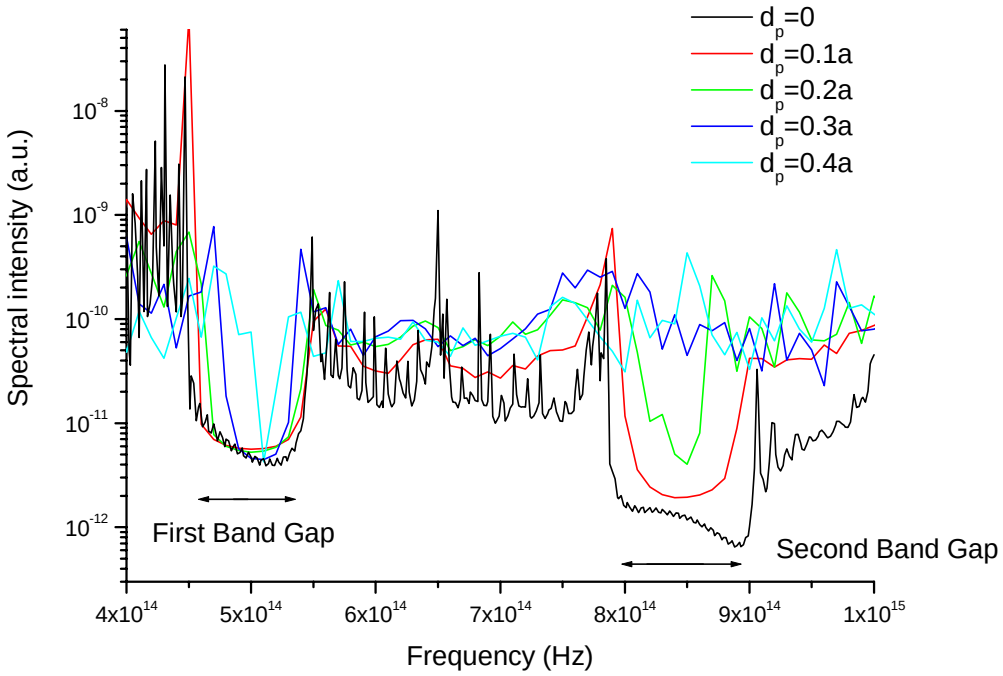

Figure 4.11 Intensity spectra of the 2D passive disordered systems with particle density of $2x10^{13}m^{-2}$ and various amounts of position disorder

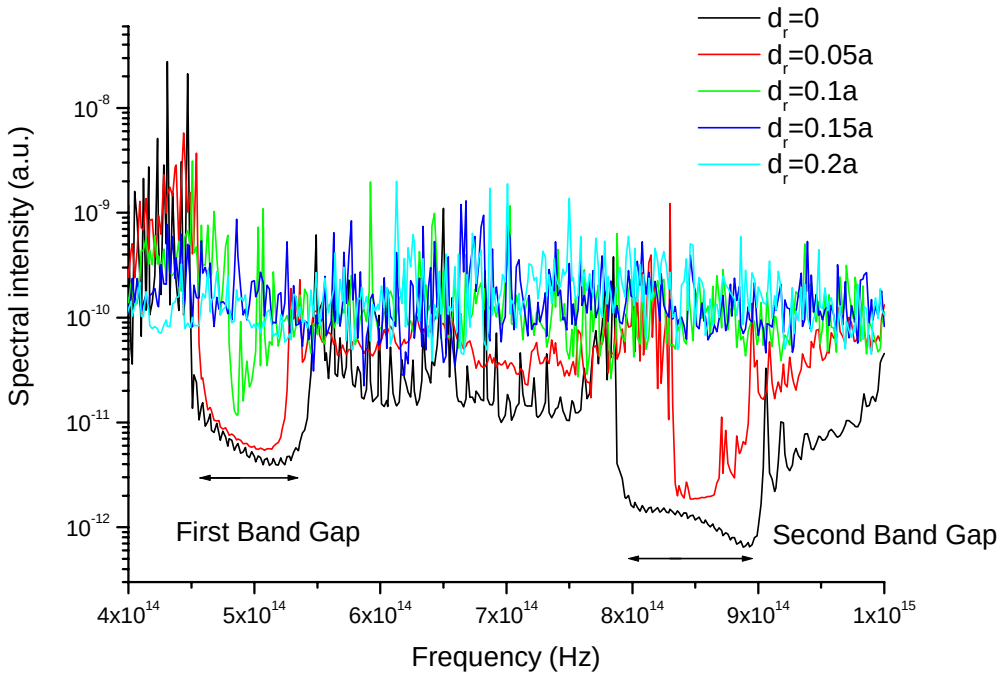

Figure 4.12 Intensity spectra of the 2D passive disordered systems with particle density of $2x10^{13}m^{-2}$ and various amounts of size disorder

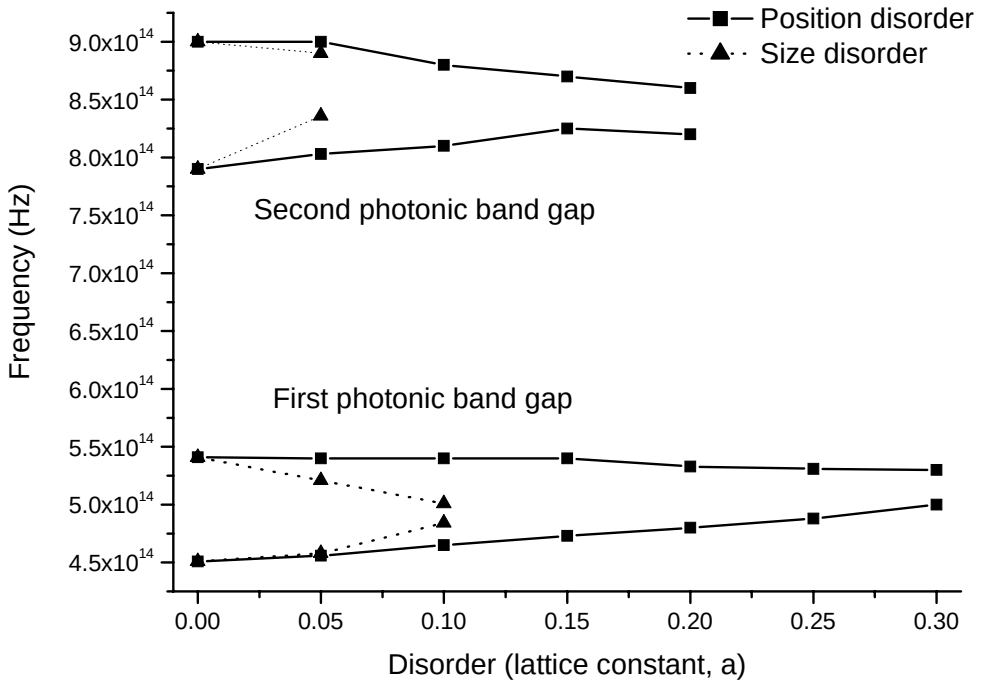

Figure 4.13 Photonic band gaps of the 2D passive disordered systems with a particle density of $2\text{x}10^{13}\text{m}^{-2}$

The influence of the disorder effect on the band gaps can be further clarified by plotting the upper and lower limits for the band gap as a function of the amount of disorder, as shown in Figure 4.13. It is observed that the first and second band gap vanish when $d_p \geq 0.3a$ and $d_p \geq 0.2a$, respectively. It is found that the band gaps at a higher frequency vanish firstly. One would expect that the high frequency band gap is more sensitive to the disorder because the equivalent wavelength of high frequency band gap is shorter. Therefore, the electromagnetic wave with short wavelength is more sensitive to the position fluctuations of scattering particles.

The effect of size disorder on the PBGs is also evident in Figure 4.13. In the numerical experiments, the parameters of the disordered media are the same as

the previous simulation cases of position disorder. The power spectra of the disordered media are calculated with various amounts of size disorder. d_r varies from 0 to 0.2a. The results are obtained by averaging over 10 configurations of disordered medium. Figure 4.12 shows the power spectra of the disordered media with various amount of size disorder. The results of the size disorder case are similar to those of position disorder case. However, the results of the size disorder demonstrate that the band gaps diminish at much smaller amount of the size disorder, as shown in Figure 4.13.

Comparing to the position disorder case, the effect of the size disorder on the band gap is more serious. The first and second band gap are fully destroyed when the amount of disorder reaches $d_r \geq 0.1a$ and $d_r \geq 0.05a$, respectively, while the band gap still remains with the same amount of position disorder. This is consistent with the results of previous studies that size disorder breaks down a gap more rapidly than position disorder does (Fan, Villeneuve and Joannopoulos, 1995, Sigalas, Soukoulis, Chan and Turner, 1996, Li, Zhang and Zhang, 2000).

4.4.2 Effect of disorder on mode distribution

The investigations of the disordered effect on the long-lived mode are also carried out. In order to trigger the eigen-states near and inside the first band gap, a modified Gaussian pulse with a narrower bandwidth is used. The frequency range of this pulse is from $4.2\text{x}10^{14}$Hz to $5.7\text{x}10^{14}$Hz and the central peak frequency is at $4.93\text{x}10^{14}$Hz. The wave form of the pulse can be expressed in the following equation,

$$E_z(t) = \sin(2\pi t \times 4.93\times 10^{14}\, Hz)\, e^{-(\frac{t-1.18\times 10^{-14}\, s}{8.25\times 10^{-15}\, s})^2}$$

Since the central peak of the modified Gaussian pulse is close to the central frequency of the first band, it facilitates to excite the modes inside the band gap of disordered systems. Furthermore, modes lying on the band edge of the gap can also be excited because the bandwidth of the modified Gaussian pulse covers the full range of the first band gap. The temporal and spectral profiles of the pulse are plotted in Figure 4.14.

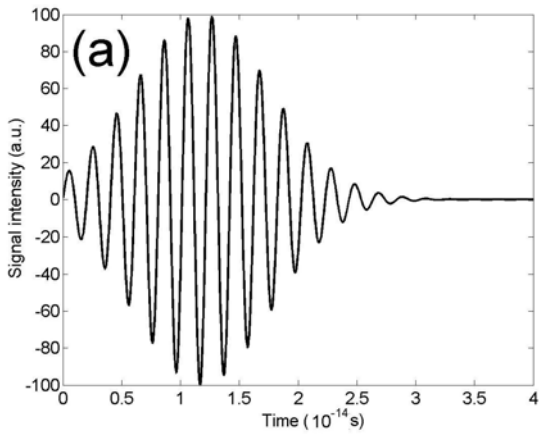

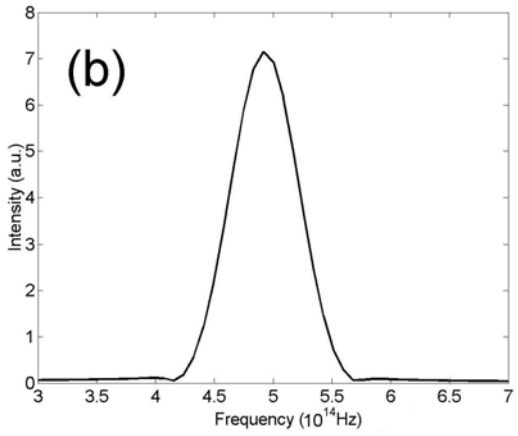

Figure 4.14 (a) Temporal and (b) spectral profiles of excitation pulse

Figure 4.15 shows the spectral locations of the highest intensity long-lived modes for various amounts of disorder. The spectral positions of the modes are determined in the time window [250000Δt, 500000Δt]. At each level of disorder, the longest-lived modes of 10 configurations are determined. The results of the position disorder cases are shown in Figure 4.15a. It is easy to observe that the longest-lived modes emerge toward the band gap as the disorder increases. When the amount of position disorder is small, i.e., d_p = 0.05a to 0.15a, the modes are mainly distributed at the lower edge of the band gap. At a larger amount of disorder d_p = 0.2a to 0.4a, the mode distribution spread toward the center of the band gap. Similar results are obtained for the size disorder cases, as shown in Figure 4.15b.

Compared to the case of position disorder, the size disorder is more influential on the quality of the band gap. For example, even the amount of size disorder is small, i.e., d_r = 0.1a, the modes are created inside the band gap. At d_r = 0.15a and d_r = 0.2a, it is obvious that the modes widely distribute in a high frequency region which is far away from the band gap range.

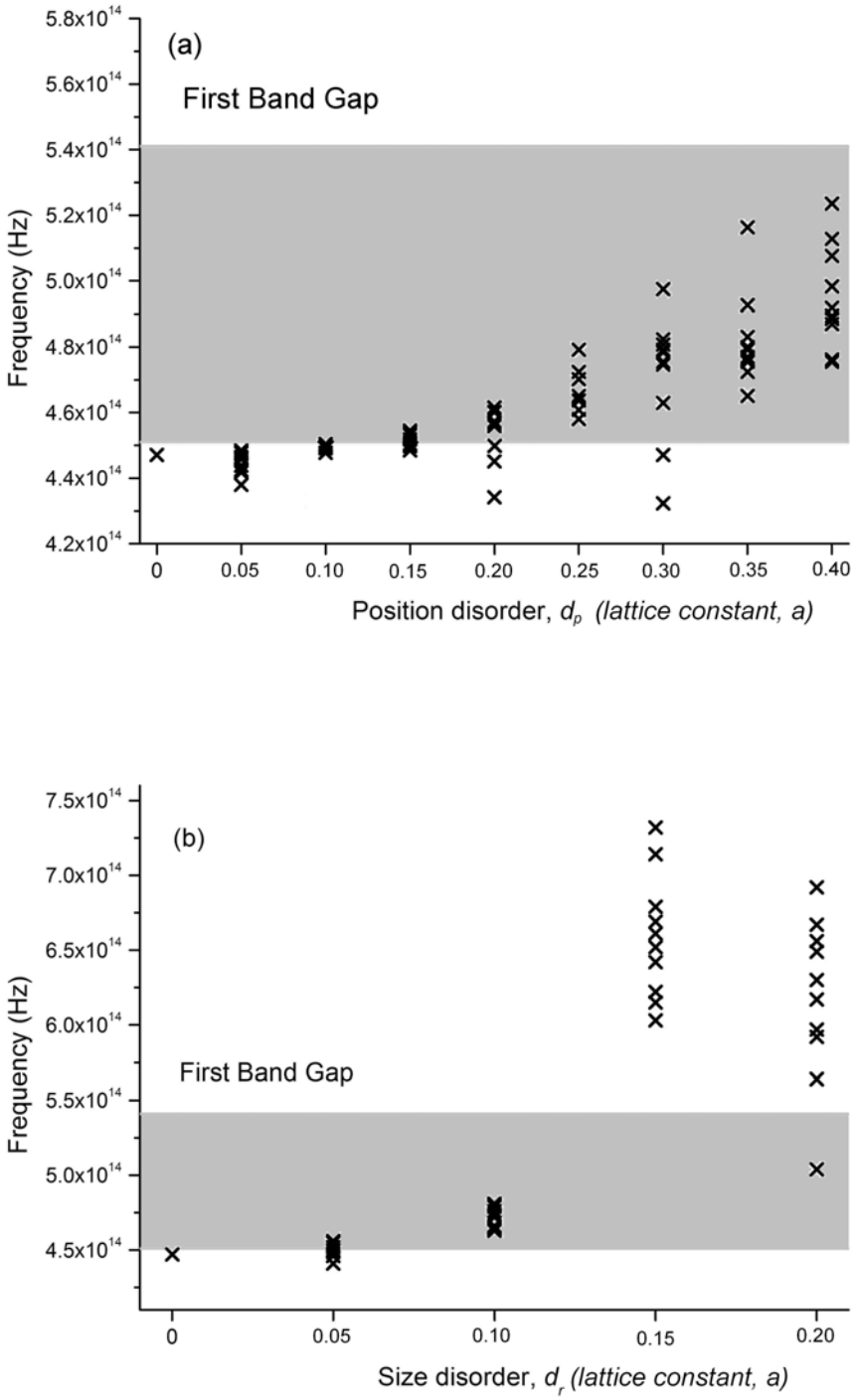

Figure 4.15 Counterplot of the long-lived modes for (a) position disorder and (b) size disorder. Frequency range of band gap is denoted by the gray area. Lattice constant *a* is 200nm

It is interesting to study the field distribution pattern of the disorder media with variation in the amount of disorder. Figure 4.16 and Figure 4.17 show the field distribution patterns for position and size disorder, respectively. The results are obtained after a long time evolution of electromagnetic wave with a duration of 11.79×10^{-12}s (total time steps = 500000). From Figure 4.16a, the field distribution pattern of the ordered medium (d_p =0) is regular and symmetrical around the centre. As the amount of disorder increases, the regular pattern is destroyed. Instead of the symmetry field pattern, some spots of high intensity are formed randomly (see Figures 4.16d and 4.17c), which correspond to the long-lived modes. At the highest amount of disorder, the electromagnetic field is more concentrated at a small spot area. As shown in Figures 4.16e and 4.17d, EM waves are confined in small areas rather that extended to the whole media. The high intensity spots are attributed to the localization of EM wave in the highly disordered media. It is believed that the field spots pertain to the localized modes of the disordered systems. Our results demonstrate that localized modes will be formed in both position and size disordered media.

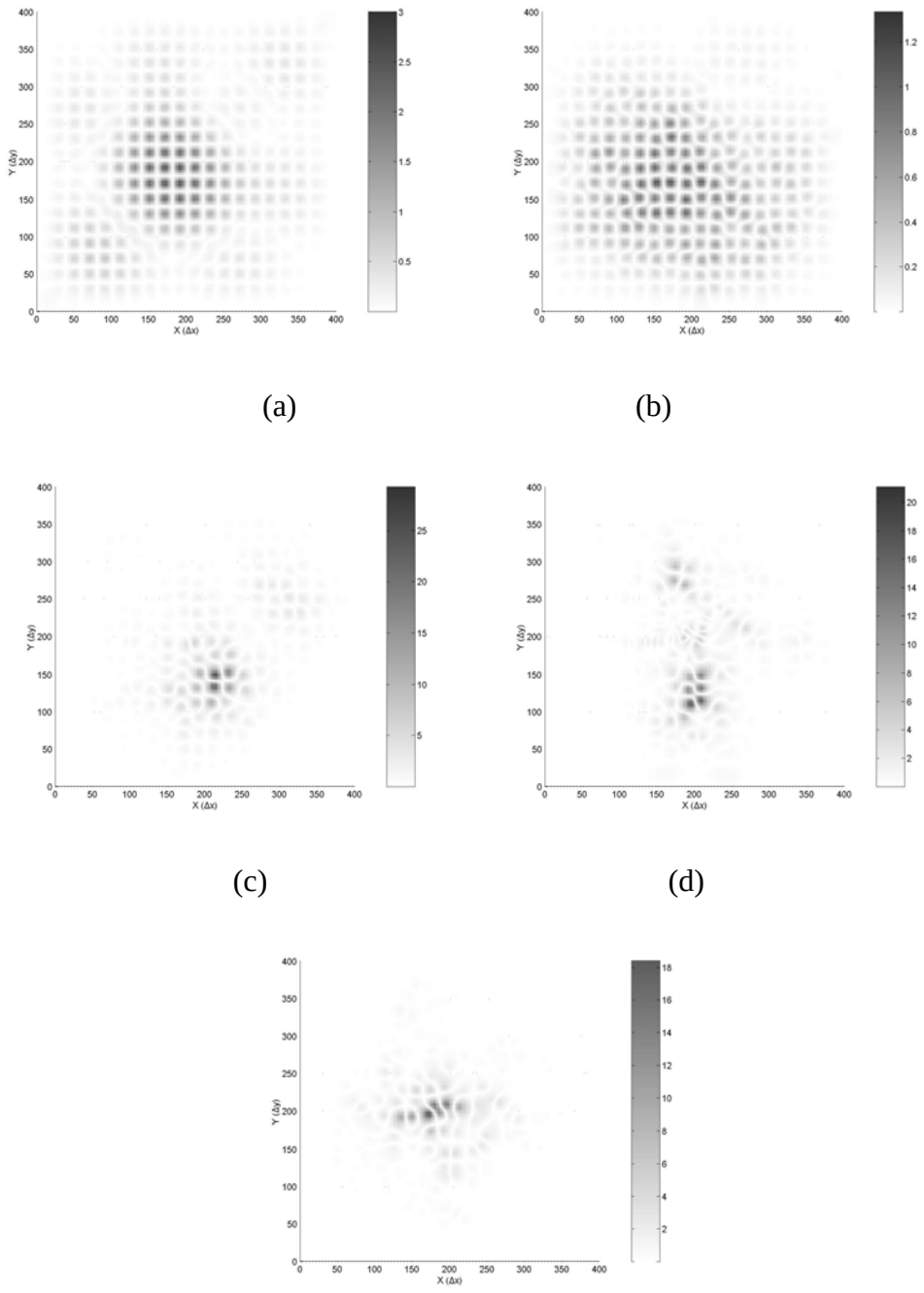

Figure 4.16 Field distribution patterns of 2D passive ordered media with various amounts of position disorder: (a) d_p = 0, (b) d_p = 0.1a, (c) d_p = 0.2a, (d) d_p = 0.3a, (e) d_p = 0.4a. Lattice constant a is 200nm

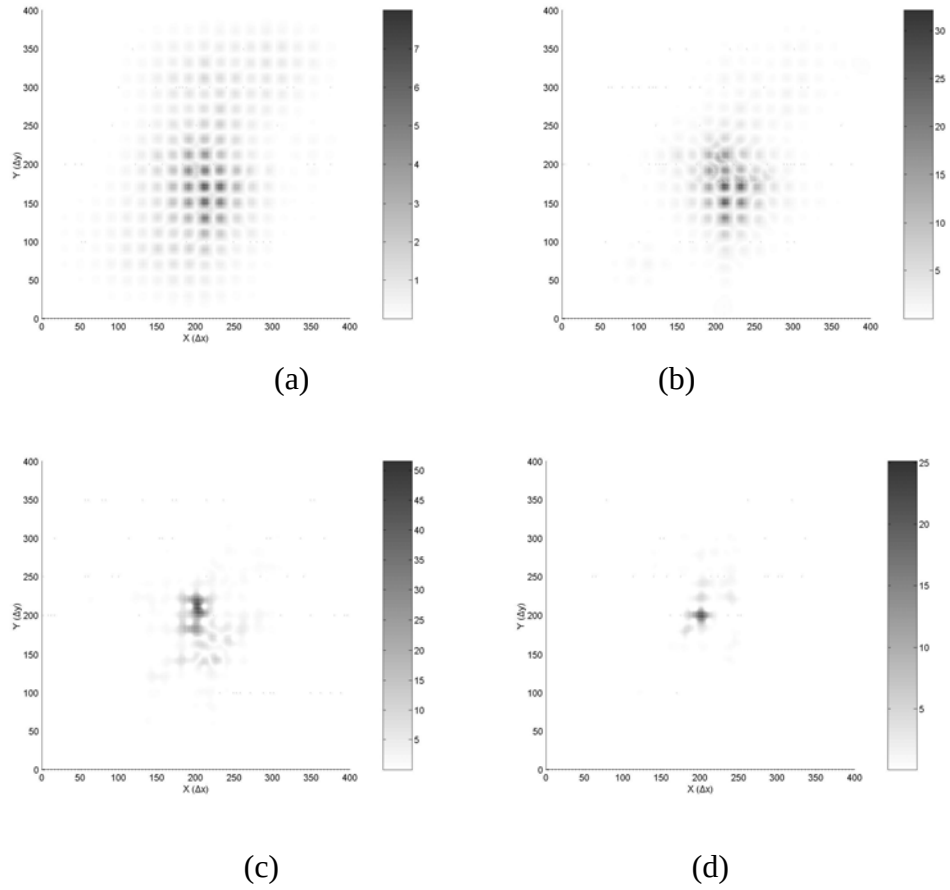

Figure 4.17 Field distribution patterns of 2D passive ordered media with various amounts of size disorder: (a) d_r = 0.05a, (b) d_r = 0.1a, (c) d_r = 0.15a, (d) d_r = 0.2a. Lattice constant a is 200nm

According to Figure 4.16e, the spots of high intensity are obtained after a long time evolution. In order to investigate the evolution of the localized modes, the field distribution patterns of the highly disordered system are recorded in different time frames, as shown in Figure 4.18. The amount of position disorder d_p in the system is equal to 0.4a. The configuration of the disordered medium is depicted in Figure 4.19. From t=3.54x10^{-14}s (=1500Δt) to t=5.89x10^{-13}s (=25000Δt), the excited modes are revealed gradually in the system. As time increases, the field energy becomes more concentrated because the localized modes retain in the system while the extended modes diminish. At t=2.36x10^{-13}s (=100000Δt), two clusters of field spots are substantially formed in the disordered medium. Cluster A and B are indicated by solid line circle and dash line circle (see Figure 4.18e), respectively. As is illustrated in Figure 4.18e to Figure 4.18i, the competition of the localized modes is exhibited in the time evolution process. Since the energy field is exchanged between the localized modes, the localized modes repeatedly dominate the system. Consequently, the intensities of the modes are changed at different time frames and thereby the total field energy of the disordered medium oscillated. It consists with the observation of the time evolution of the total energy field energy (see Figure 4.9).

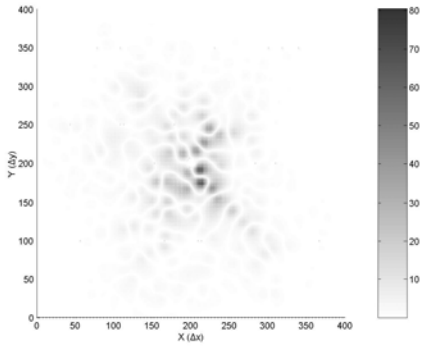

(a) t=3.54x10^{-14}s (=1500Δt)

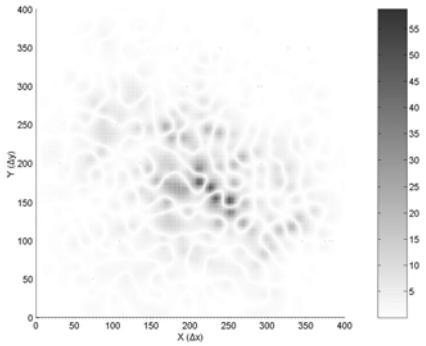

(b) 7.07x10^{-14}s (=3000Δt)

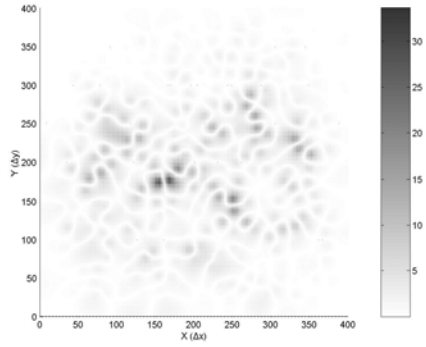

(c) t=2.36x10^{-13}s (=10000Δt)

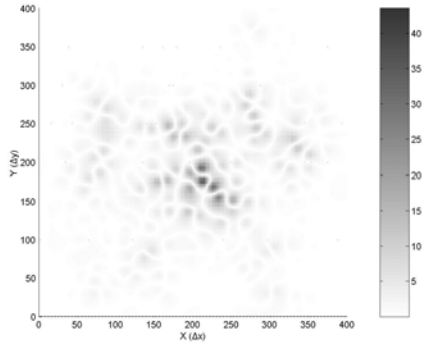

(d) 5.89x10^{-13}s (=25000Δt)

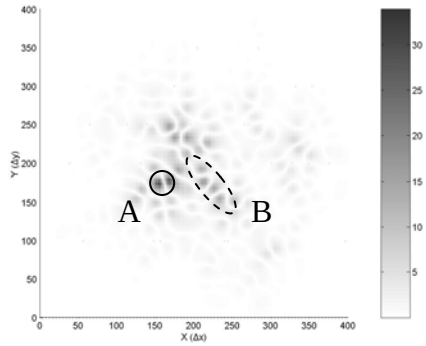

(e) t=2.36x10^{-12}s (=100000Δt)

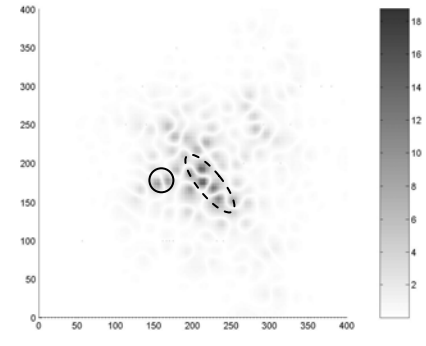

(f) t=4.71x10^{-12}s (=200000Δt)

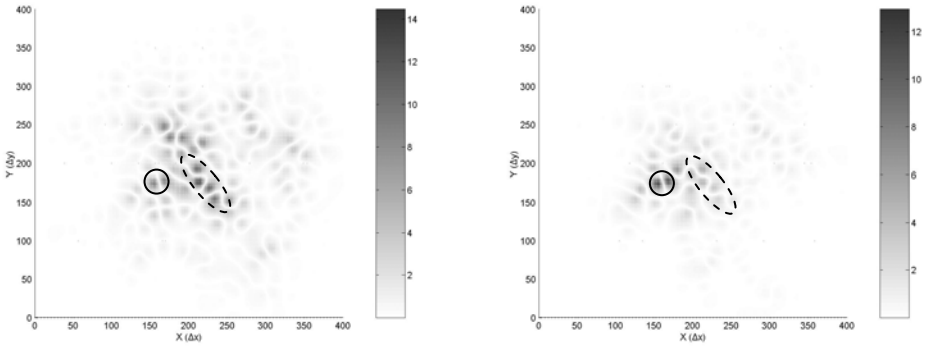

(g) t=7.07x10^{-12}s (=300000Δt) (h) t=9.43x10^{-12}s (=400000Δt)

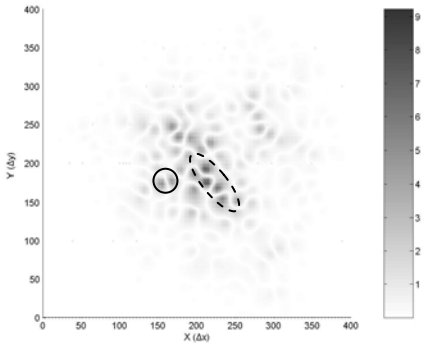

(i) t=11.79x10^{-12}s (=500000Δt)

Figure 4.18 Time evolution of the field distribution pattern

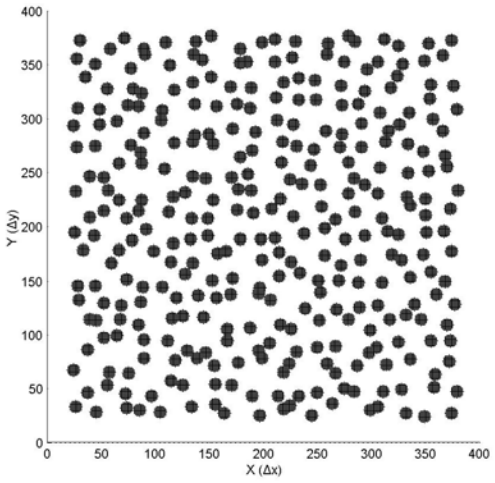

Figure 4.19 Configuration of the disordered medium with d_p = 0.4a. Lattice constant a is 200nm.

4.5 Summary

Using FDTD method, numerical experiments are performed to study of the effects of disorder on the field distribution and spectra of disordered systems. 2D passive disordered dielectric systems with position and size disorders (d_p and d_r) are considered in the simulations.

The influence of the density of scattering particles on the mode distribution of ordered and disordered systems is examined for the first time. In the most densely packed ordered system (particle density = $2x10^{13}m^{-2}$), two PBGs can be observed at f = 4.51 $x10^{14}$ to 5.41x 10^{14}Hz and 7.90 $x10^{14}$ to 9.0$x10^{14}$Hz. After a long time evolution, only long-lived modes, which locate close to the edge of the band gaps, survive in the disordered system. These results can be explained in term of localization length of the eigen-state. The lifetime of mode increases as the localization length of mode reduces. Since the modes close to the edge of PBGs have shorter localization length, the survived modes tend to lie on the edge of band gaps. The decay process and mode competition of the disordered media are also studied. It is found that the evolution of the mode energy is an exponential function of time. Furthermore, the competition of modes is revealed in the field distribution patterns in different time frames.

The effect of both position and size disorder on the disordered medium is investigated. The numerical results demonstrate that the PBGs formed in the most densely packed ordered systems (particle density = $2x10^{13}m^{-2}$) are destroyed when a moderate degree of disorder is introduced into the medium. Since the spatial and radial perturbations of scattering particles sitting on the

regular lattice points create defects in the ordered systems, more extra states may be induced in the band gap. The first band gap vanishes when $d_p \geq 0.3a$ and $d_r \geq 0.1a$, respectively. The second band gap is fully destroyed when the amount of disorder reaches $d_p \geq 0.2a$ and $d_r \geq 0.05a$, respectively. Our results show that a size disorder breaks down a gap more rapidly than position disorder does, which is consistent with previously published results by others.

As the band gap is destroyed, the longest-lived modes emerge toward the band gap as the amount of disorder increases. From the field distribution patterns of the disordered medium, the field patterns of the longest-lived modes become more localized when the amount of disorder intensifies. To conclude the results of numerical simulations of 2D passive disordered dielectric systems, the effect of disorder can enhance the confinement of EM waves in passive disordered dielectric media as the localized modes are more easily to be created in the highly disordered media.

CHAPTER 5

CHARACTERIZATION OF LASING IN ACTIVE DISORDERED MEDIA

5.1 Introduction

In 1994, Lawandy reported stimulated emission from laser dye solutions containing micro-particles (Lawandy, Belachandran, Gomes and Sauvin, 1994). This discovery triggered many experimental studies (Sha, Liu and Alfano, 1994, Noginov, Noginova, Caulfield, Venkateswarlu and Mahdi, 1995, Zhang, Cheng, Yang, Zhang, Hui and Li, 1995, Siddique, Alfano, Berger, Kempe and Genack, 1996, Cao, Zhao, Ong and Chang, 1999, Soest, Tomita and Lagendijk, 1999, Cao, Xu, Chang and Ho, 2000, Cao, Xu, Ling, Burin, Seeling, Liu and Chang, 2003). The studies focused on light amplification in diffusive media, that is, Amplified Spontaneous Emission (ASE) with incoherent feedback. Zacharakis used a femtosecond pulse laser at 800nm to two-photon excite a Coumarin 307 colloid solution and obtained 480nm blue emission (Zacharakis, Papadogiannis and Papazoglou, 2002). Yellow emission was achieved by using a frequency-doubled Nd:YAG laser to pump a colloid solution containing Rhodamine 590 perchlorate and polystyrene micro-spheres . Red emission in colloid solutions was reported by Lawandy and Cao et al (Cao, Xu, Chang and Ho, 2000, Cao, Ling, Xu, Burin and Chang, 2003).

Random lasers with coherent feedback stimulated emission were realized with disordered semiconductor and organic materials in the late 1990s (Cao, Zhao, Ong, Ho, Dai, Wu and Chang, 1998, Cao, Zhao, Ho, Seelig, Wang and Chang,

1999, Frolov, Vardeny, Yoshino, Zakhidov and Baughman, 1999). However, up to now, very few workable polymeric systems have been reported. Only red emission was realized in PMMA at a threshold of 15mJ/cm^2 by Balachandran et al (Balachandran, Pacheco and Lawandy, 1996b) and by Ling et al (Ling, Cao, Burin, Ratner, Liu, Seelig and Chang, 2001). Overall the published results, it is interesting to study the random laser based on polymeric systems such as composite PMMA film because the stimulated emission from polymeric solids is very attractive in terms of applications, stability and cost.

In the previous chapter, the passive disordered media were investigated in a numerical approach. To understand the origin of the laser emission phenomena in active disordered media, it is necessary to explore the active disordered media in both experimental and theoretical approaches. In this chapter, experimental studies of dye-doped nano-composite solutions and films will be carried out to gain understanding of the amplification behavior and optical properties of polymer random lasers. Effects of parameters of the material systems and pumping conditions are discussed. Optical microscopy and scanning probe microscopy are used to investigate the film structure, and the principle of incoherent and coherent laser is analyzed. The experimental work devoted to the random lasers phenomenon can act as a reference for the theoretical studies of active disordered media. Although the random laser systems investigated in the experiments are three-dimensional, most of their parameters are relevant to the 2D numerical simulation of the active disordered media.

5.2 Experimental

5.2.1 Materials

In the research, both liquid and solid-state random laser systems, i.e., dye colloid solution and dye-doped polymethylmethacrylate (PMMA) nano-composite film, were considered. The polymer random laser systems consisted of a scattering element, gain medium and host. Laser dye was utilized to be a gain medium. The laser dye was dissolved in an organic solvent, which was used as a host. Nano-scaled titanium dioxide TiO_2 particles acted as the scattering element, which were deposited in hosts. In the experiments, ethanol and PMMA were used as the hosts for the liquid-state and solid-state random laser, respectively. Since the gain medium and the scattering elements were separated, the scattering strength and the randomness of the disordered systems can be varied independently. The light propagated in the active disordered system is scattered due to the difference of refractive index between the scattering element and the active matrix material.

Laser dye

In the current study, two organic laser dyes, Rhodamine 590 ($C_{28}H_{31}N_2O_3$) and Coumarin 480 ($C_{16}H_{17}NO_2$), were used as the gain medium in the random laser systems. The laser dyes used in the experiments were provided by Exciton Inc. The molecule structures of Rhodamine 590 and Coumarin 480 are depicted in Figure 5.1. The absorption, emission and excitation spectra of Coumarin 480 and Rhodamine 590 are shown in Figures 5.2 and 5.3, respectively. The emission bands of Rhodamine 590 and Coumarin 480 locate at yellow (~590nm) and blue (~460nm) wavelength ranges, respectively. The laser dyes are soluble in a few

solvents such as methanol, ethanol and water. Because of their strong absorption of light in an organic solvent, common liquid lasers are based on laser dyes. The light absorption of dyes is rather difficult to be derived exactly from their molecular structure as the complex structure of the dye molecule consisting of a larger number of atoms. The basic mechanism responsible for light absorption of dye molecules in an organic solvent is the transitions of conjugate π electrons owning to the change in electronic densities over the bonds constituting the conjugated chain. The radiative emission of dye is dominated by the transition of singlet bands. Instead of isolated energy state, the singlet bands are formed as a result of the vibrational and rotational vibrations associated with the binding of the atoms of dye molecule.

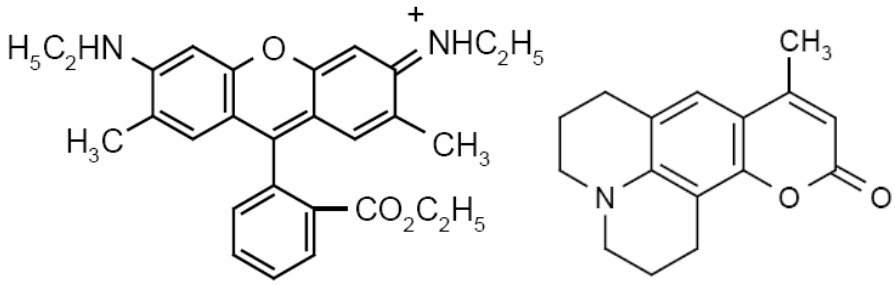

(a) (b)

Figure 5.1 Structure of dye molecule: (a) Rhodamine 590 and (b) Coumarin 480

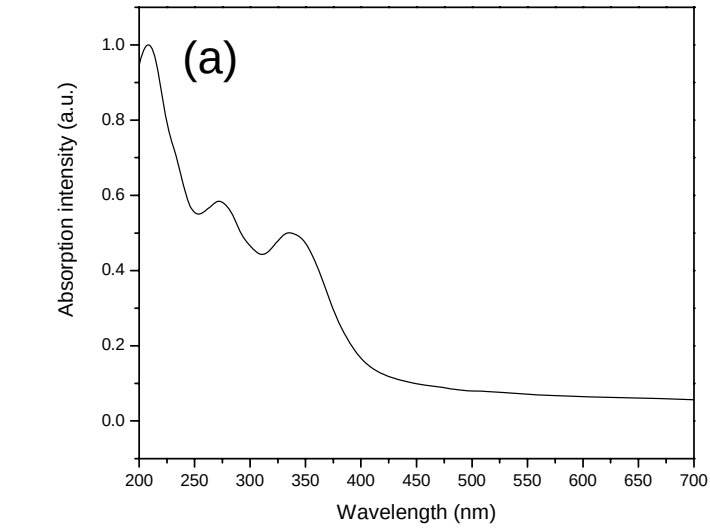

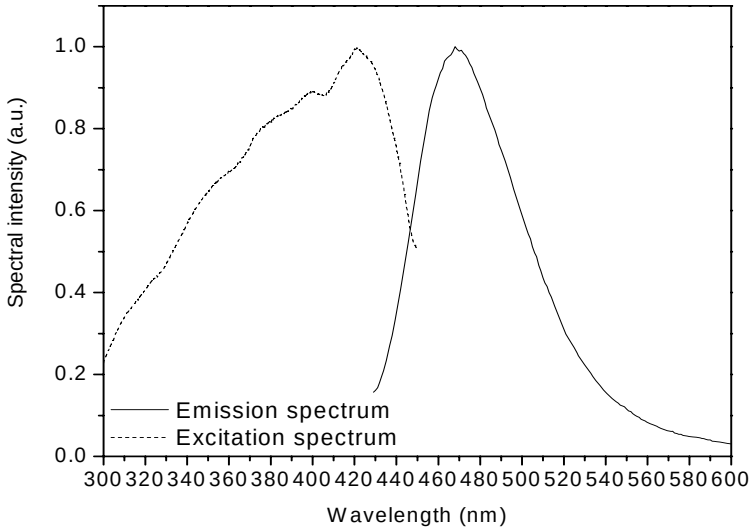

Figure 5.2 (a) Absorption and (b) emission and excitation spectra of Coumarin 480. The measurements are carried out on a dye ethanol solution with dye concentration of 10^{-3}M (1M=1mole/liter)

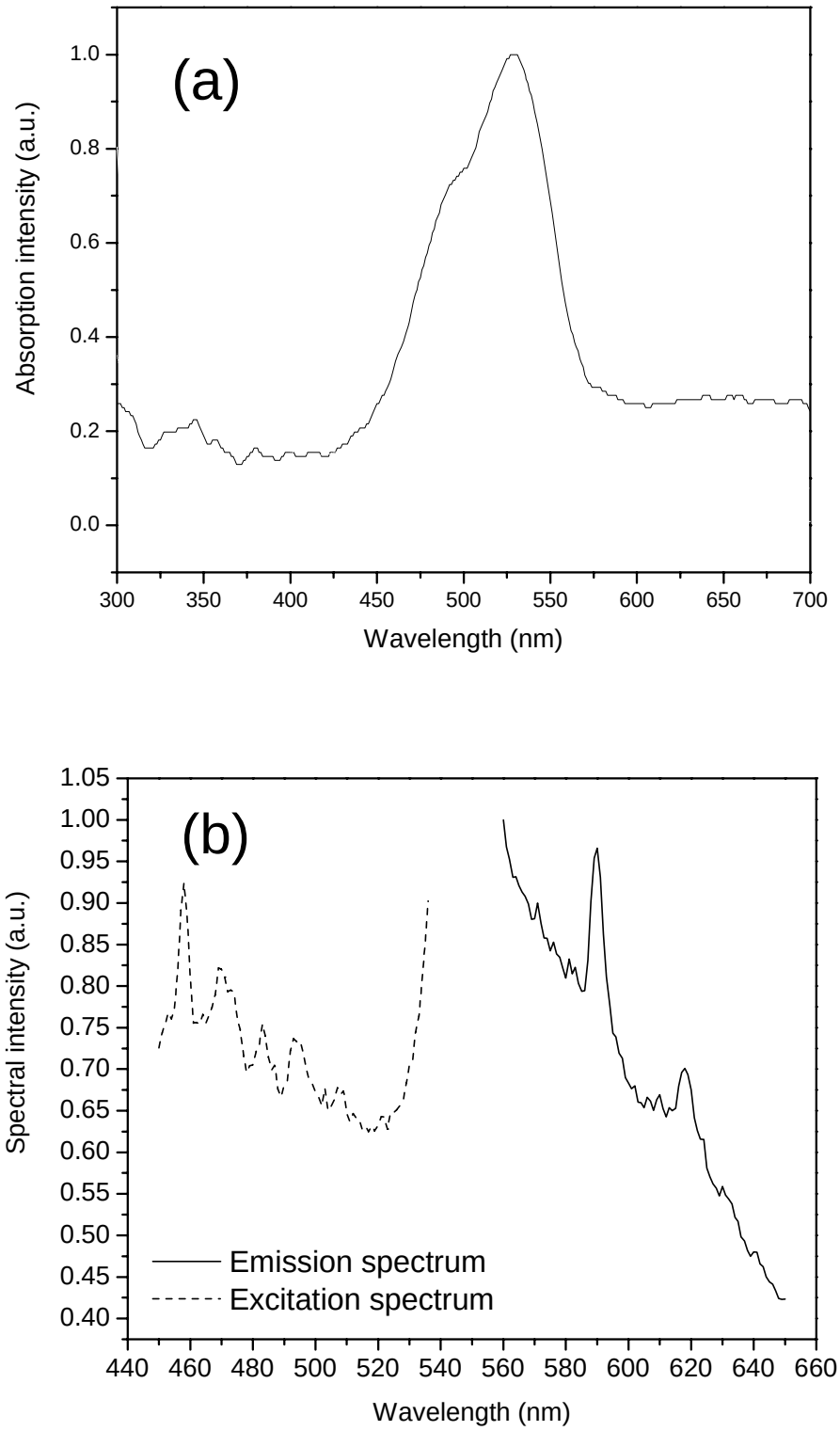

Figure 5.3 (a) Absorption and (b) emission and excitation spectra of Rhodamine 590. The spectra are measured on a PMMA film with Rhodamine 590. (dye concentration = 10^{-3}M)

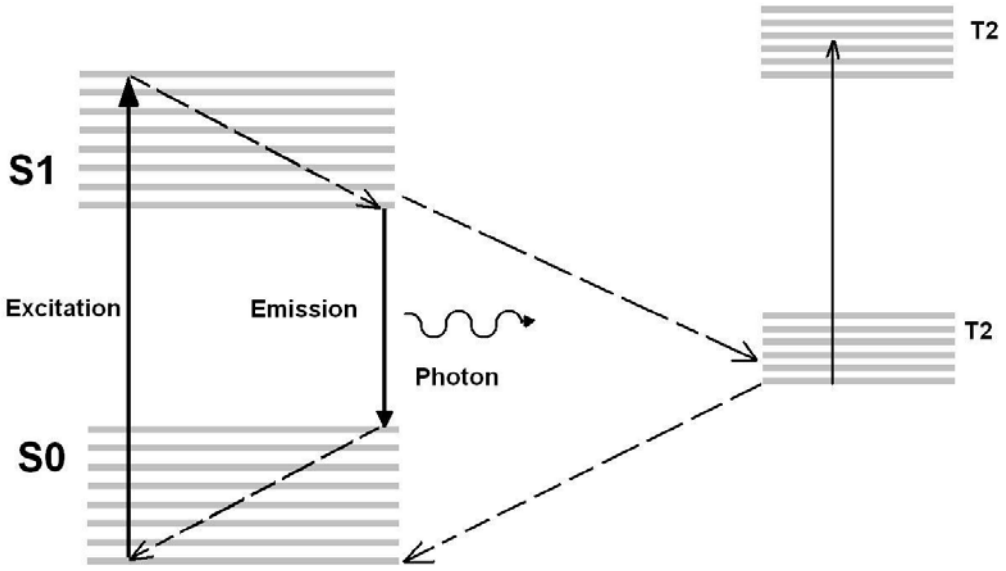

Figure 5.4 Energy level structure of laser dye molecule dissolved in a solvent

The typical energy diagram of dye molecule is depicted in Figure 5.4, which is suitable to describe the lasing transition of most organic laser dye including Coumarin 480 and Rhodamine 590 (Schafer, 1977, Weichel, 1991). The energy level structure of the dye molecule consists of two singlet states, i.e., the ground state singlet S0 and the excited state singlet S1. The two singlet states can be treated as two vibrational-rotational bands because each singlet state is constituted by a number of vibrational and rotational sub-levels. At room temperature, all the dye molecules are at the bottom of the ground state singlet S0. The molecules can be excited to the excited state singlet S1 at a high vibrational-rotational level under an external pumping. Within a very short lifetime (~ 0.1×10^{-12}s), the molecules will decay to a lower energy level, i.e., the bottom vibrational-rotational level of S1. This decay occurs by non-radiation transitions by transferring some energy to other dye molecules during collisions.

Then the excited dye molecules will transit back to the ground state singlet S0 and emit photons. Finally, the dye molecules decay non-radiationally from a high vibrational level to the initial position in the ground state singlet S0 during collisions. In fact, the laser dye molecule consists of other energy band such as triplet states T1 and T2. Since the transition between the singlet and triplet bands only occurs in very concentrated dye condition ($>10^{-2}$ mol/L) (Sha, Liu and Alfano, 1994, John and Pang, 1996), the triplet transition was be neglected in our low concentration dye systems. Instead the complicated energy level structure, a simplified four-level laser system is considered in the time dependent theory. The four-level model is simple but accurate analytical model for the dye laser systems (Siegman, 1986). In fact, dye models were developed based on this ideal four-level energy system and have been successfully explained experimental results (Jiang and Soukoulis, 2000, 2002). In the current research, the four-level models are utilized to simulation the gain of dye in the numerical simulations (see Chapter 3 and 6).

Scattering particle and host

Titanium dioxide TiO_2 particles of 168nm were used as a scattering element in the dye-doped solution and polymer composite film because of its high refractive index (~2.4). Unlike other high refractive materials such as ZnO and metallic materials, TiO_2 particle is a passive scatterer in which visible light is only scattered rather than absorbed and amplified.

Various materials such as organic solvent, polymer and gel media can be used as the host of laser dye and scattering particle. Ethanol and Polymethyl

methacrylate (PMMA) were selected in the experiments because they are transparent and easy to handle. For a liquid-state random laser, laser dye is necessarily dissolved in an organic solvent. Ethanol is a versatile solvent, which has a low refractive index of 1.36. Thus, it is suitable for acting as a liquid-state host medium. PMMA has been widely used as the host of polymer random lasers such as dye-doped thin film and fiber because it is chemically stable. The typical refractive index of PMMA is 1.42. The PMMA macromolecular chain is formed by repeating the methyl methacrylate (MMA) monomer units. The chemical structure of MMA and PMMA are depicted in Figure 5.5. In the experiments, PMMA chips were supplied from Mitsubishi Rayon Corporation (trade name VH-001) with a viscosity-average molecular weight (MW_V) of 12.3×10^4. Ethanol was supplied by BDH Laboratory Supplies, England. Anatase TiO_2 particles were purchased from Advanced Technology & Industrial Co. Ltd, Hong Kong.

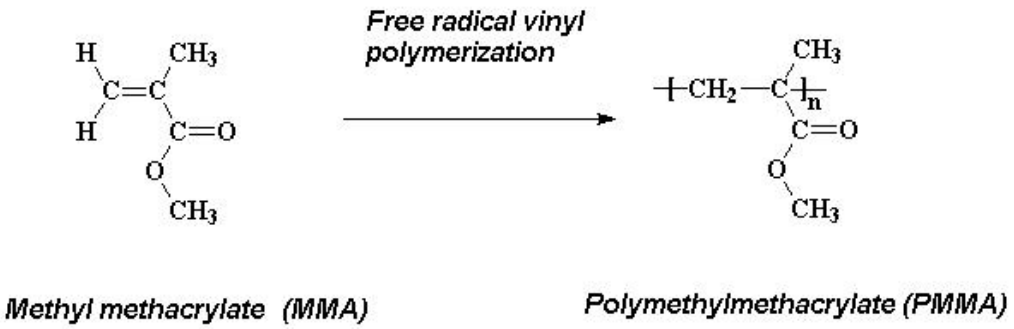

Figure 5.5 Chemical structures of ethanol, MMA monomer and PMMA

5.2.2 Sample preparation

In our experiments, two types of active disordered systems have been fabricated, i.e., PMMA nano-composite film and colloidal dye solution. PMMA nano-composite films were prepared by the cell casting method. We first prepared two dichloromethane (CH_2Cl_2) solutions. We took 2.2mg Rhodamine

590 and 2.4mg TiO_2 nano-particles and mixed in 2ml of dichloromethane (CH_2Cl_2) solution until the dye was dissolved completely. At the same time, PMMA was dissolved in another dichloromethane solution to form 2ml 13wt.% PMMA dichloromethane solution. Then this PMMA dichloromethane solution was added to the mixture solution of Rhodamine 590 and TiO_2. The final mixture was sonicated until a homogeneous solution was formed. A PMMA film containing Rhodamine 590 and TiO_2 particles was formed by cell-casting of 1ml of the solution. The fabrication process was carried out at room temperature. The high-reflectivity mould made of aluminum foil acted as a mirror. The films were left at room condition for nine hours before further experiments.

On the other hand, colloid solutions were prepared by dissolving Coumarin 480 dye (concentration = 10^{-3}M= 10^{-3}mole/liter) in ethanol and mixing with TiO_2 particles (concentration = $3.25x10^{11}cm^{-3}$). Because of large specific gravity the sedimentation of particle was rather serious, especially for those of large diameter. To eliminate the effect caused by sedimentation the colloid solution stored in cuvette was shaken for a long time by an ultrasonic unit before measurement.

5.2.3 Experimental setup

The PMMA composite films were pumped by linearly polarized 532nm radiation from a double-frequency Nd:YAG laser (Model LAB–170-10, Spectra Physics) operating at 1.064μm. Similarly, the colloid solutions were pumped by linearly polarized 355nm radiation from a triple frequency Nd:YAG laser. The excitation beam was incident at an angle of 45^o with respect to the sample surface. The

experiments were performed with a Q-switched laser which produced pulses of 8ns at a repetition rate of 10Hz. The beam spot on the film and solution cell surface had an area of 0.9 cm^2. The emission from the film surface was collected by using a lens and sent to a spectrometer equipped with a Model 810/814 Photomultiplier Detection System provided by Photon Technology International, Inc, whose resolution is 0.25nm. The schematic diagram of the experimental setup is shown in Figure 5.6.

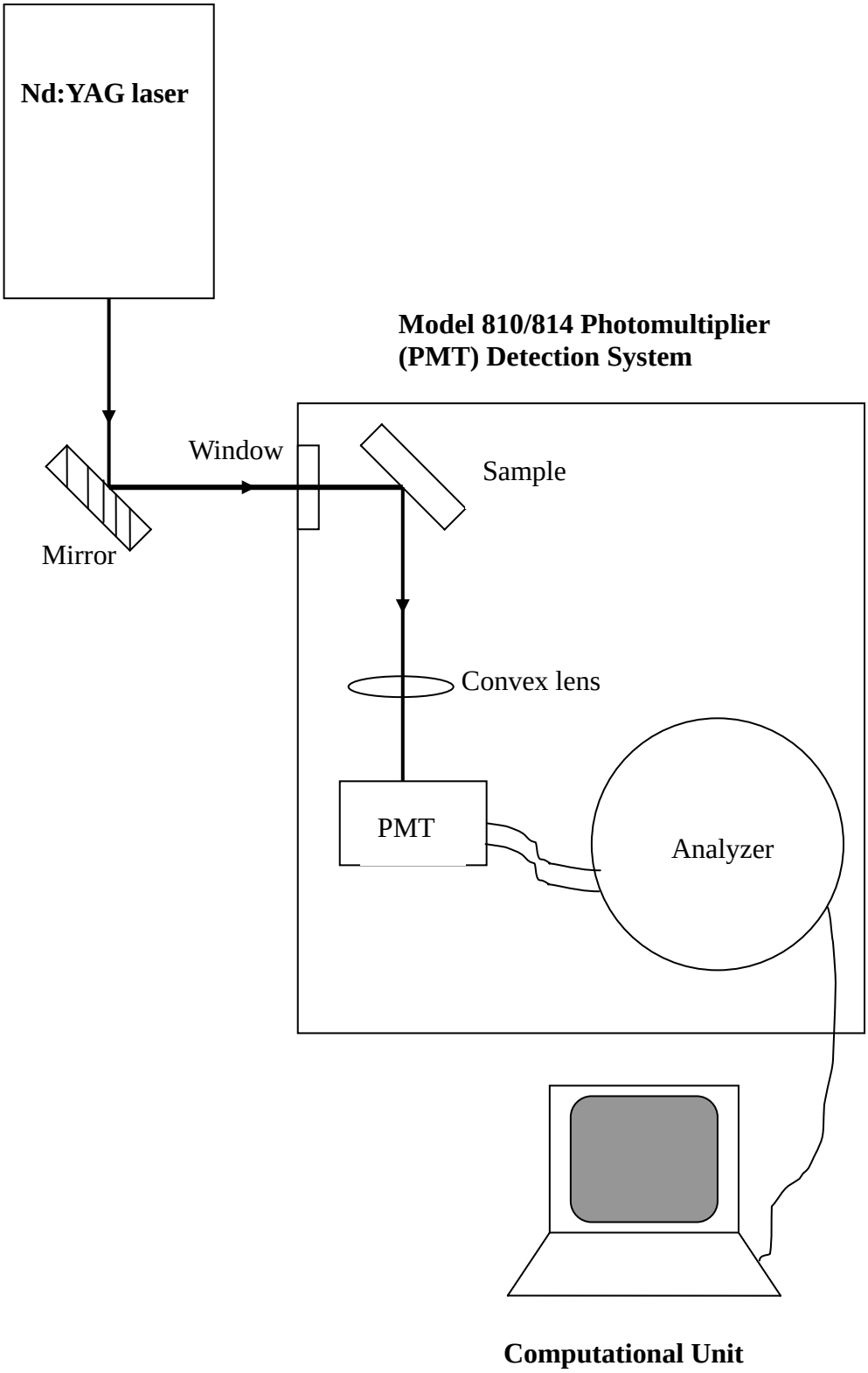

Figure 5.6 Schematic diagram of the experimental setup

5.3 Results and discussions

5.3.1 Structures of PMMA composite films

The structure of the PMMA composite films was investigated by using optic microscopy and Scanning Probe Microscopy (SPI4000 SERIES Scanning Probe Microscope System, Seiko Instruments Inc.). In the film sample, the concentration of Rhodamine 590 and TiO_2 particles was 10^{-3}M (=10^{-3} mol/L =1mol/m^3) and 1.25x$10^{11}$$cm^{-3}$, respectively. TiO_2 particles had a mean diameter of 168nm. Figure 5.7a shows the internal structure of PMMA film doped with Rhodamine 590 and TiO_2 particles with an amplification of 400 times. The particles are distributed very randomly. There exist single particles and clusters with multiple particles. Figure 5.7b is the external or surface photograph. These are some ordered structures. Figure 5.7c is the topography of Scanning Probe Microscopy (SPM) in a localized area. Disordered distribution of particles is seen. These particles scatter photons and increase the path length which the photons walk in the film.

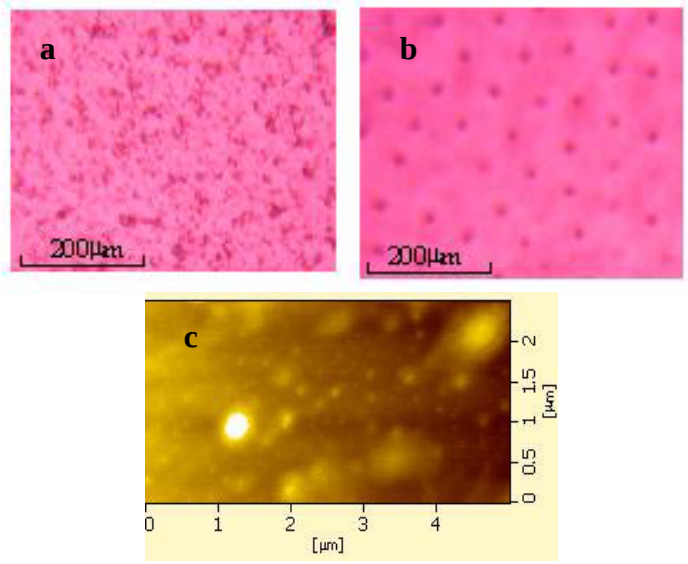

Figure 5.7 (a) Internal (b) Surface structure photograph of PMMA film doped with Rhodamine 590 and TiO_2 particles by using 400 times optic microscopy (c) topography of Scanning Probe Microscopy

5.3.2 Effect of particle concentration

The influence of the concentration of the scattering particle on the emission intensity of the PMMA composite film was investigated. The film samples consisting of TiO_2 particles of different concentration were excited at three different pumping energy intensities. The concentration of Rhodamine 590 in all the sample films was 10^{-3}M. Figure 5.8 shows the plot of emission peak intensity as functions of the scattering particle concentration. As the pumping energy intensity increases, the emission peak intensity arises and reaches a maximum level which is associated with an optimum concentration of TiO_2, i.e., concentration = 0.6mg/ml ($1.25x10^{11}cm^{-3}$). The particles concentration of PMMA composite film (($1.25x10^{11}cm^{-3})^{2/3}=2.5x10^{11}m^{-2}$) is lower than that of the least densely packed disordered system ($1x10^{12}m^{-2}$) described in Chapters 6. It is obvious that the film sample with this optimum particle concentration of 0.6mg/ml has the largest emission intensity under different pumping energy intensities. In order to enhance the emission strength of the PMMA composite film, the PMMA composite film which had an optimum particle concentration was used in the photoluminescence experiments in the next section.

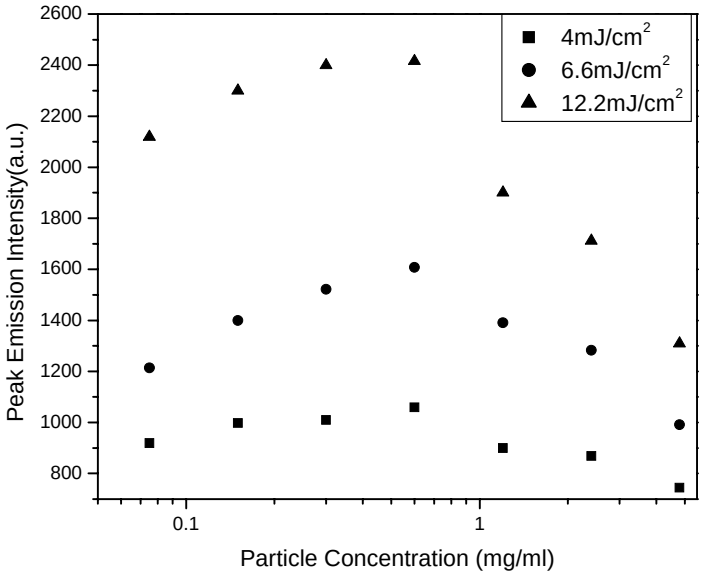

Figure 5.8 The influence of particle concentration on the light emission intensity of PMMA films

5.3.3 Lasing threshold

After the investigations of the structure of the PMMA composite films, photoluminescence experiments were conducted in order to study the incoherent and coherent lasing emission of the PMMA composite film and the colloid solution. The concentration of Rhodamine 590 and TiO_2 particles in the PMMA film sample were 10^{-3}M and $1.25x10^{11}cm^{-3}$, respectively. The concentration of Coumarin 480 and TiO_2 particles in the colloid solution were 10^{-3}M and $3.25x10^{11}cm^{-3}$, respectively. The peak intensity and line-width plotted against increasing pump energy density are shown in Figures 5.9 and 5.10, respectively.

The variations of the slope of the input-output curve indicate that the lasing threshold and saturation behavior of the random laser system. It is found that the saturation is above the pump energy density of $70mJ/cm^2$ in the PMMA composite film while the saturation effect is absent in the colloid solution within

the experimental range. The lasing threshold is observed in both the film and solution samples. The lasing threshold of the PMMA composite film and the colloid solution is below 13mJ/cm^2 and 18mJ/cm^2, respectively.

Furthermore, the significant reduction of line-width of the emission peak provides an experimental proof for the existent of lasing threshold, which is given in Figure 5.10. The lasing threshold is much lower than the previous reported value (Balachandran, Pacheco and Lawandy, 1996a). This may be because the reflective mould stops the photons escaping from the disordered media and decreases the loss.

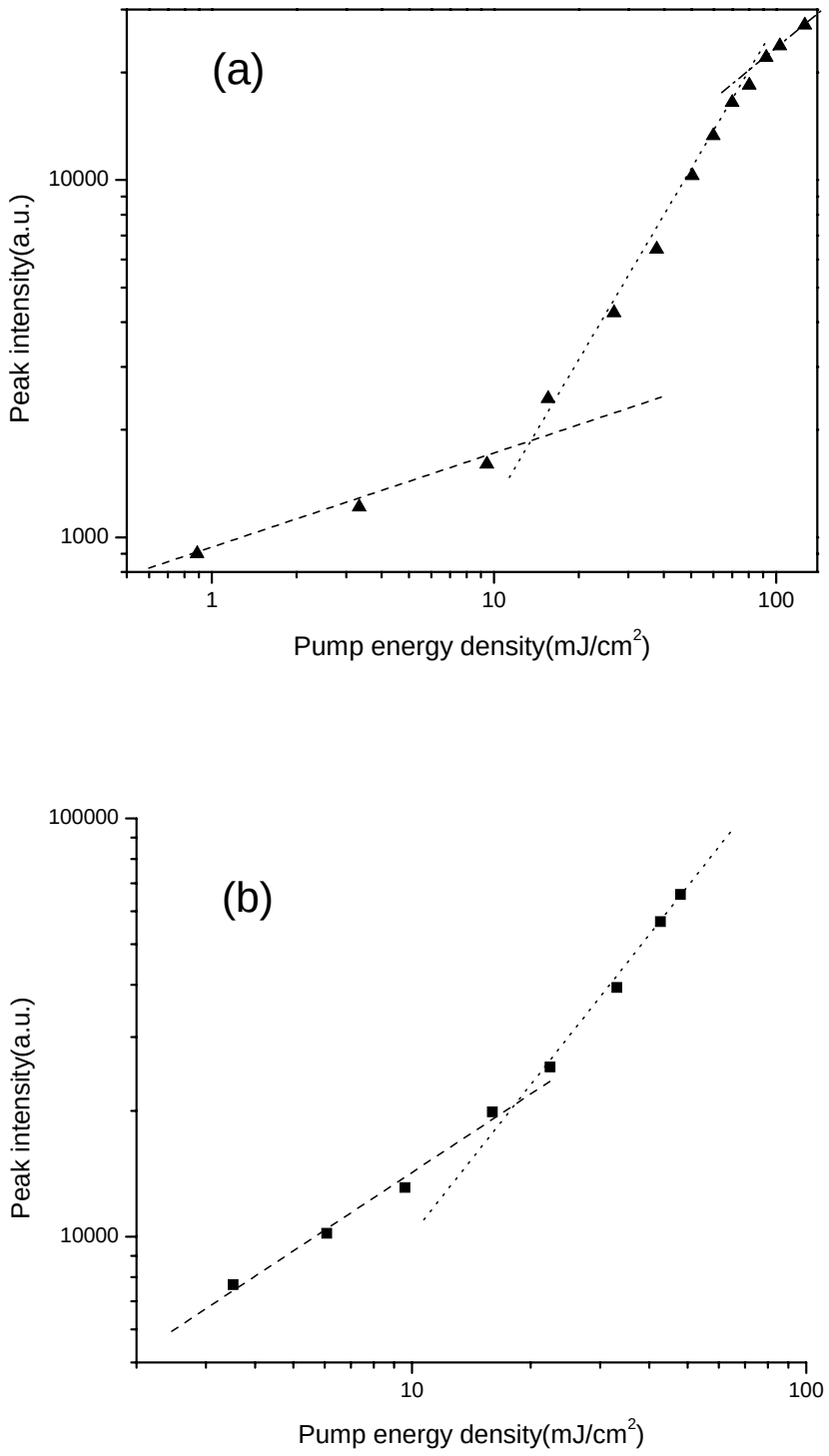

Figure 5.9 (a) Peak emission intensity of PMMA film plotted against pump energy density in logarithmic representation. (b) Peak emission intensity of colloid solution plotted against pump energy density in logarithmic representation.

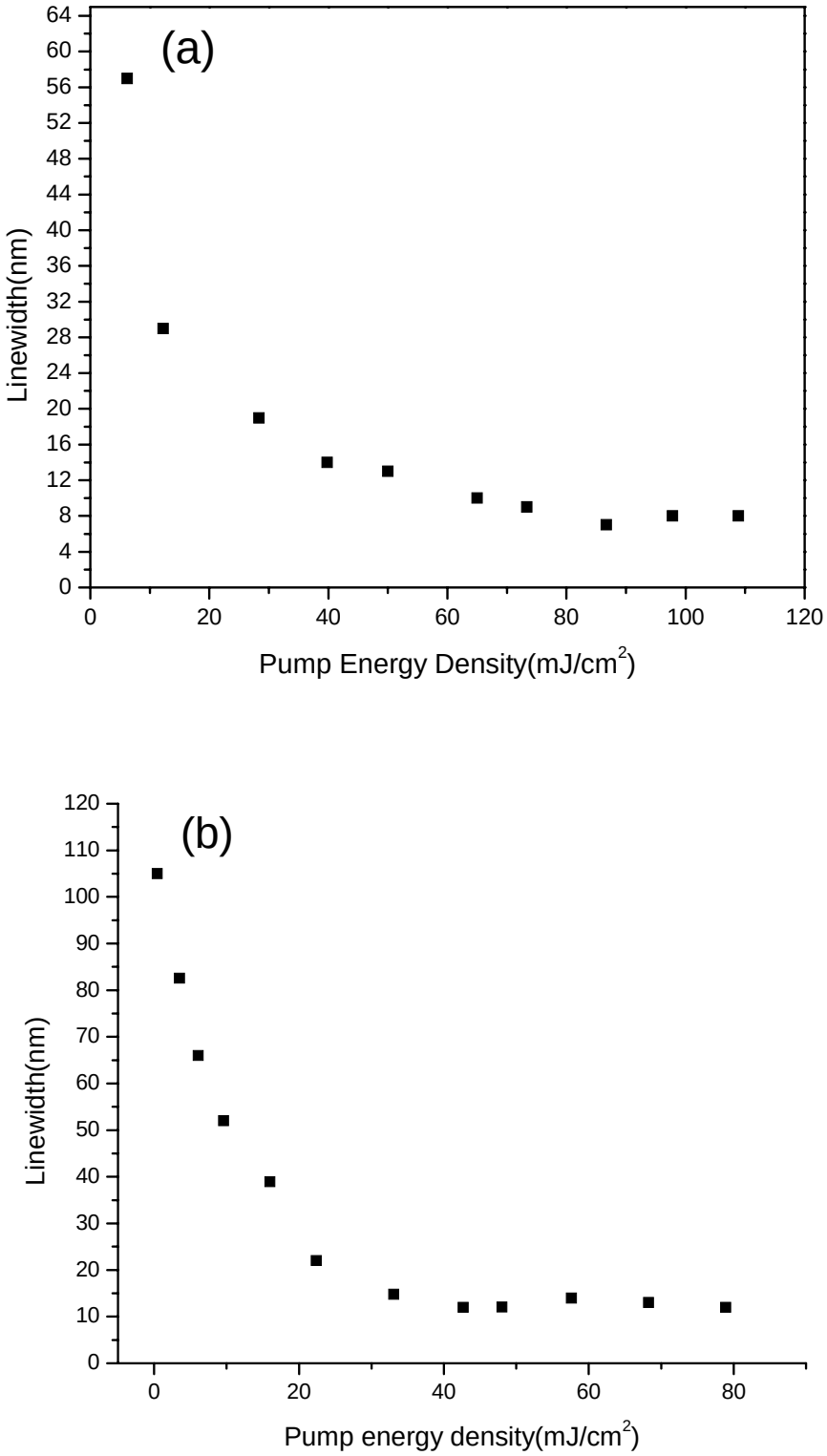

Figure 5.10 (a) Peak line-width of PMMA film plotted against pump energy density. (b) Peak line-width of colloid solution plotted against pump energy density

5.3.4 Amplified spontaneous emission

The emission spectra below and above the lasing threshold are shown in Figure 5.11. In Figure 5.11(a), solid and dash lines represent the emission spectra of the PMMA composite film at a pump energy density of 1.9mJ/cm^2 and 50mJ/cm^2, respectively. The solid line is scaled up by a factor of 5. In Figure 5.11(b), solid and dash line are denoted for the emission spectra of the colloid solution at a pump energy density of 0.4mJ/cm^2 and 79mJ/cm^2, respectively. The solid line is scaled up by a factor of 10. As shown in Figure 5.11, a board spontaneous emission band could be observed in the emission spectra at the pump energy density below the lasing threshold. When the pump energy density increases and exceeds the lasing threshold, a narrow emission peak appears at the central frequency close to the maximum gain of the laser dyes. The emission peak intensities are higher than that at the lower pump energy density by at least one order of magnitude. The full width at half maximum (FWHM) of the emission peak is about 13nm. It is known that the collapse of emission spectrum is due to the amplified spontaneous emission.

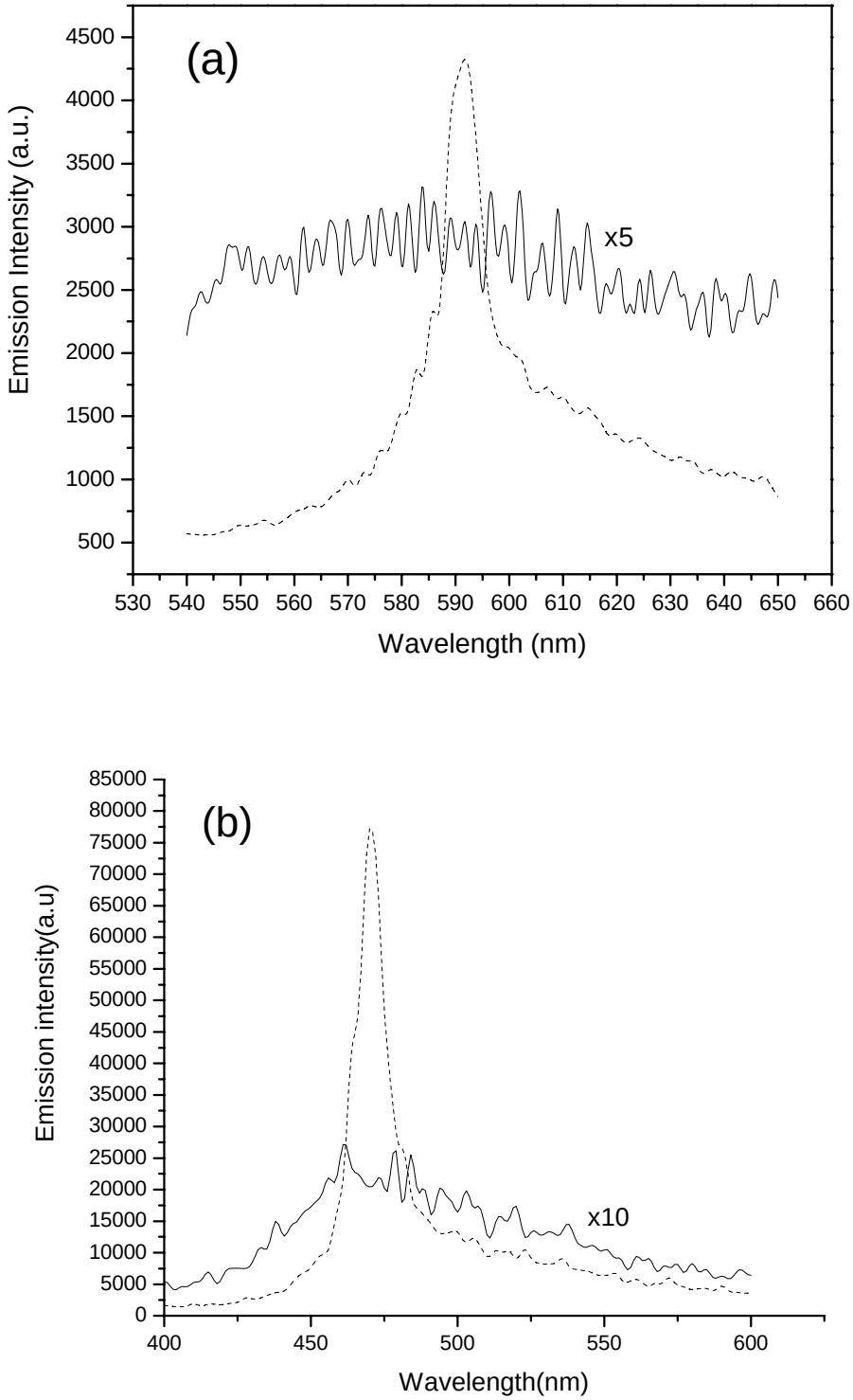

Figure 5.11 (a) Emission spectra of PMMA film with a pumping energy density (solid line) 1.9mJ/cm^2, (dash line) 50mJ/cm^2. Solid line is scaled up by a factor of 5. (b) Emission spectra of colloid solution with a pumping energy density (solid line) 0.4mJ/cm^2, (dash line) 79mJ/cm^2. Solid line is scaled up by a factor of 10.

5.3.5 Coherent laser emission

Figure 5.12 shows the random laser emission spectrum of the PMMA composite film. When the pump energy density increases, discrete emission peaks are observed. The linewidth of the discrete narrow peaks is less than 1nm, which is an evidence of random laser with coherent feedback. When a photon travels in the disorder active system, it may induce the stimulated emission of a second photon and the light intensity is amplified. The amplification of light can be reinforced by increasing the probability of stimulated emission which directly relates to the pumping energy intensity and the optical path of photons in the disordered dielectric media. At the low pumping energy intensity, the spontaneous transitions dominate the atomic transitions. The spontaneous emission mainly contributes to the gain of modes near the central wavelength of the gain profile of the active medium. When the pumping energy intensity is further increased and reaches the threshold value, the stimulated emission rate exceeds the spontaneous emission rate and the light amplification grows significantly along the scattering light paths. If the light paths are longer than the gain saturation length, gain saturation can be achieved. In the disordered dielectric systems, photons may be trapped in the localized modes due to the multiple scattering of photons. Thus, the scattering light path of photons and the gain in the localized modes can be significantly reinforced. Consequently, the discrete narrow peaks corresponding to the different frequencies of the localization modes emerge into the emission spectrum. In fact, the observation of the discrete narrow peaks unambiguously shows the random laser emission of PMMA composite film.

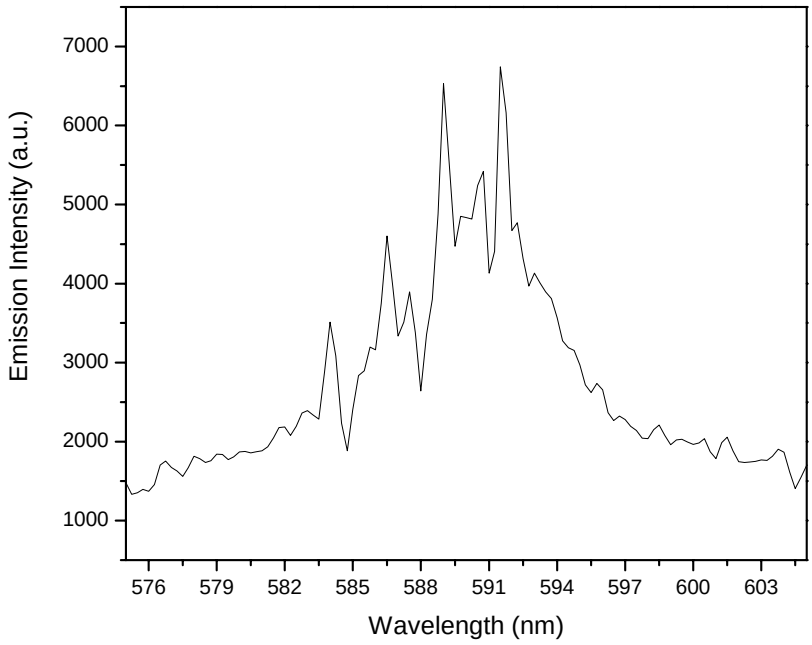

Figure 5.12 The multimode output well above the threshold in PMMA film containing Rhodamine 590 and TiO_2 nano-particles pumped at 60mJ/cm^2

5.4 Summary

The laser actions of polymeric colloid liquid and solid random laser systems were investigated experimentally. The liquid random laser system is the ethanol solution which consists of Coumarin 480 dye and TiO_2 nano-particles. The solid random laser system is the PMMA films which consist of Rhodamine 590 and TiO_2 nano-particles. The TiO_2 particles had a mean diameter of 168nm. Coherent and incoherent laser emission were observed in the systems. The influences of particle concentration on light emission were explored and optimum particle concentration was obtained. Optics microscopy and Scanning Probe Microscopy were used to investigate the film structure and the principle of incoherent and coherent laser was analyzed.

In the photoluminescence experiments, it was found that the slope of the peak emission intensity curve of the colloid solution and PMMA films changed as the pump energy increased. These results indicate the lasing threshold and saturation behavior of the random laser system. The emission peaks of the colloid solution and PMMA films become narrower when pumping energy is above certain value. Several discrete peaks emerge in the emission spectra when the pump energy was further increased. This is a direct consequence of random laser emission with coherent feedback. This significant reduction of line-width and increase of the intensity of the emission peak confirm the existent of lasing threshold.

CHAPTER 6

INFLUENCE OF DISORDER ON ACTIVE DISORDERED MEDIA WITH DIELECTRIC SCATTERING PARTICLES

6.1 Introduction

In Chapter 4, disorder effects on passive disordered media were investigated in a numerical approach. In Chapter 5, experimental studies of the random laser in dye-doped colloid polymeric solutions and PMMA films were described. In this chapter, the study is extended to the active disorder media based on the numeric simulations of passive disordered systems and the experimental investigation of the dye-doped PMMA composite films. The influence of disorder on the active disordered media consisting of dielectric scattering particles will be examined by using the time-dependent theory which has been described in Chapter 3.

6.2 Numeric simulation

6.2.1 Methods and material parameters

In this section, the amplification process of electromagnetic (EM) wave in an active disordered medium is considered. The numerical experiments are performed based on a two-dimensional (2D) active disordered dielectric system with circular dielectric scattering particles. An optical gain, which is absent in passive systems, is presented in the host matrix background. According to the model in Chapter 3, the optical gain is described by a four-level electronic structure. The parameters of the four-level atomic system are chosen based on the published results (Sebbah and Vanneste, 2002) and listed in Tables 6.1. The values of the parameters are close to the dye molecules of Rhodamine 590. τ_{21},

τ_{32} and τ_{43} represent the lifetimes of atomic level L_2, L_3 and L_4, respectively, which are inversely proportional to the decay rates of atomic levels, i.e., $1/\tau_{21}$, $1/\tau_{32}$ and $1/\tau_{43}$. $T_{collision}$ is the dephasing time which represents the mean collision time of dye molecules in the solvent solution. The collision time $T_{collision}$ and the lifetime of energy states L_4 and L_2 are much shorter than that of energy states of the lasing level L_3. In order to keep a good numerical accuracy, the time increment Δt is set to be shorter than the collision time $T_{collision}$ by three orders of magnitude. The parameters of the simulation and the active disordered system are summarized in 6.2.

Table 6.1 Parameters of the four-level electronic structure

Wavelength of the lasing transition	λ_t= 590nm
Frequency of the lasing transition	$\omega_t = 2\pi c/\lambda_t = 325 \times 10^{13}$ Hz
Collision time	$T_{collision} = 5\times10^{-14}$s
Life time of energy state L_2	$\tau_{21} = 5\times10^{-12}$s
Life time of energy state L_3	$\tau_{32} = 1\times10^{-10}$s
Life time of energy state L_4	$\tau_{43} = 1\times10^{-13}$s
Total atomic density (dye concentration)	10^{-3}M (=6.022×10^{23}m^{-3})
Pumping rate	$Q = 1\times10^{14}$s^{-1}

Table 6.2 Parameters of the active disordered system and the FDTD simulation

Size of system	SxS = 4000nm x4000nm
Refractive index of matrix medium	$n_1 = 1$, $\varepsilon_1 = n_1^2 = 1$
Refractive index of scattering particle	$n_2 = 2.646$, $\varepsilon_2 = n_2^2 = 7$
Radius of scattering particle	R = 60nm
Number of scattering particle	324
Density of particle	2×10^{13}m^{-2}
Lattice constant	a = 200nm
Filling fraction	22.9%
Position disorder	d_p=0.4a
Spatial increment	$\Delta x = \Delta y$ =10nm
Time increment	$\Delta t = 2.36\times10^{-17}$s
Total number of time step	500000Δt (11.79×10^{-12}s)
Perfectly matched layer thickness	100nm

6.2.2 Configuration of the disordered media

The schematic diagram of an active disordered system is shown in Figure 6.1. The amount of position disorder is 0.4*a*, where the lattice constant *a* is 200nm. Based on the experiment of PMMA composite film described in Chapter 5, the central wavelength of the lasing transition of the four-level electronic system is chosen as 590nm in order to mimic the laser dye Rhodamine 590. It is assume that the electronic systems are pumped uniformly over the entire active medium at a constant pumping rate *Q*.

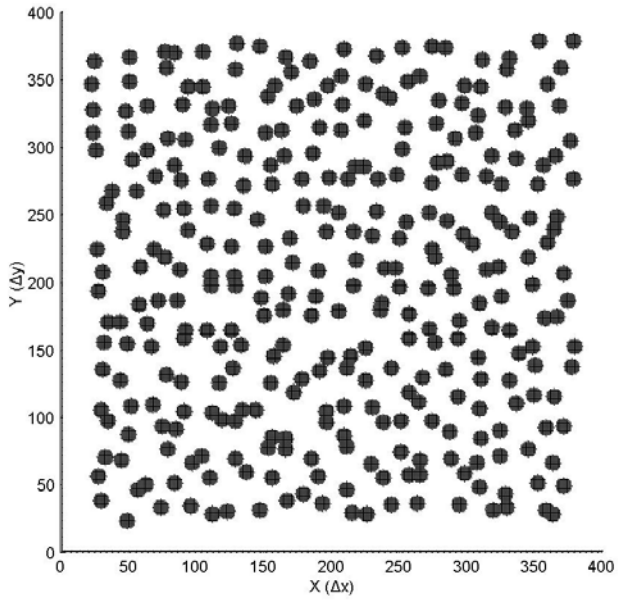

Figure 6.1 Configuration of the active disordered system with a position disorder of d_p = 0.4a. (a= 20Δx =200nm)

6.3 Results and discussions

6.3.1 Results of simulation

Figures 6.2 and 6.3 show the time evolution of the total electric field energy $U_E = \frac{1}{2}\int \varepsilon(x,y)\vec{E}^2(x,y)dxdy$ and the population difference density of electrons with lasing energy levels $\Delta N = |N3 - N2|$, respectively. In our computation, the total electric field energy is proportional to the summation of the electric field energy term over all the mesh points, i.e., $U_E \propto \frac{1}{2}\sum_{i,j} \varepsilon(i,j)E_z{}^2(i,j)$. At the initial time step (t = 0), a short Gaussian pulse (pulse duration = 7 x10^{-16}s) launches at the center of the system in order to trigger the evolution of the EM wave. As shown in Figure 6.2, the total field energy decreases slightly and then begins to increase after the first 100 femtoseconds (~1x10^{-13}s). The population difference density, however, shows a strong upward trend initially. The accumulation of the population difference density is due to a constant pumping rate Q (=1x10^{14}s^{-1}). In fact, the whole active medium is pumped homogenously at a constant rate within the time window. Since the active system is pumped continually, the atomic systems are excited to the highest energy state N4 and fast decay to the upper lasing state N3. As the population difference density increases, the total electric field energy exponentially increases and reaches a peak. The rising curve follows an exponential relation, i.e., $y(t) = 5.06\times10^{-4}e^{\xi_{amp}t}$, as shown in the inset of Figure 6.2. The exponential coefficient ξ_{amp} is defined as the amplification rate and equal to 1.37x10^{14}s^{-1}. At this stage, the amplification of EM wave is dominated by the spontaneous emission. In Figure 6.3, the initial monotonic increasing curve indicates that the rate of the spontaneous emission is lower than

the excitation rate of the atomic systems. The excited atomic systems are accumulated continually and the population inversion is built up finally. Transiently, a large number of excited electrons transits to lower energy level N2. In the meantime, the simulated emission induces a significant amplification of the EM wave. Therefore, a dramatic drop of the population difference density and a huge amplification of the total field energy can be observed simultaneously. As shown in Figure 6.3, the trigger time of the dramatic drop of the population difference density are denoted by T_t.

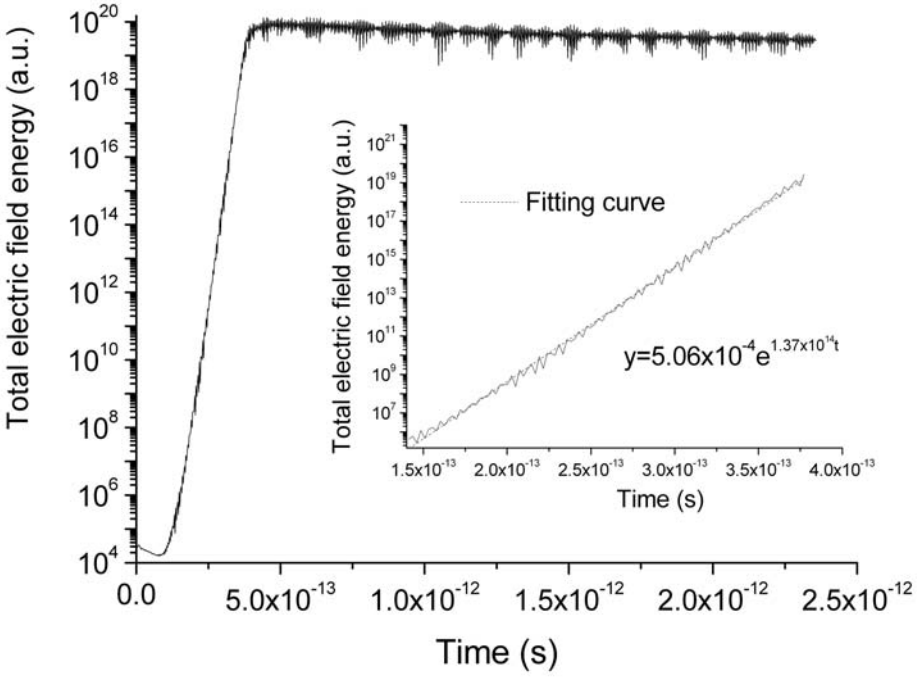

Figure 6.2 Time evolution of the total electric field energy. The total electric field energy expresses in arbitrary unit due to the summation of energy term at discrete grid points. Inset: Fitting curve for the amplification process from t = 1.5 x10^{-13}s to 4 x10^{-13}s.

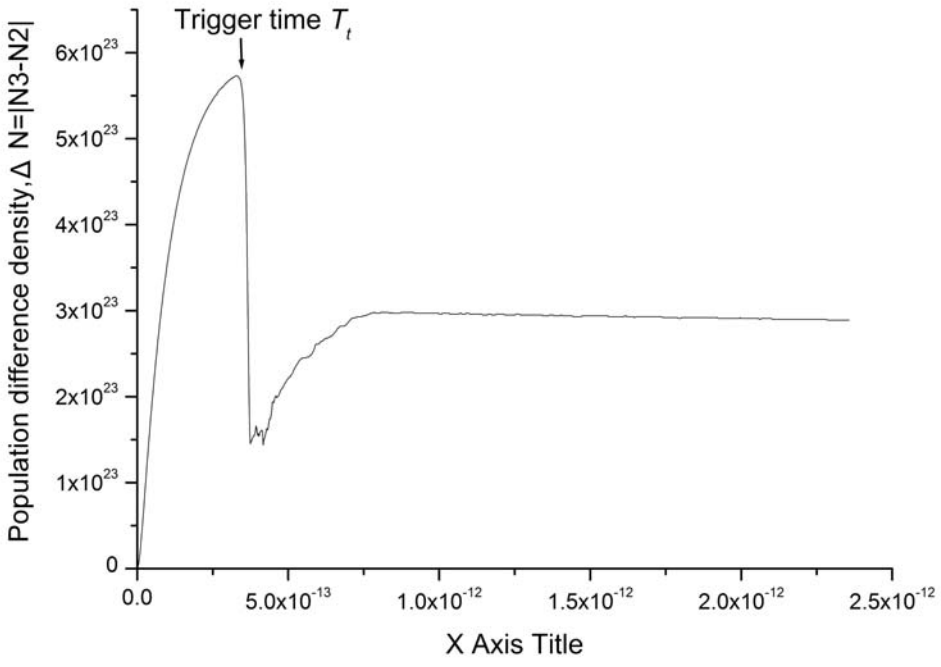

Figure 6.3 Population difference density of lasing energy levels $\Delta N = |N3 - N2|$

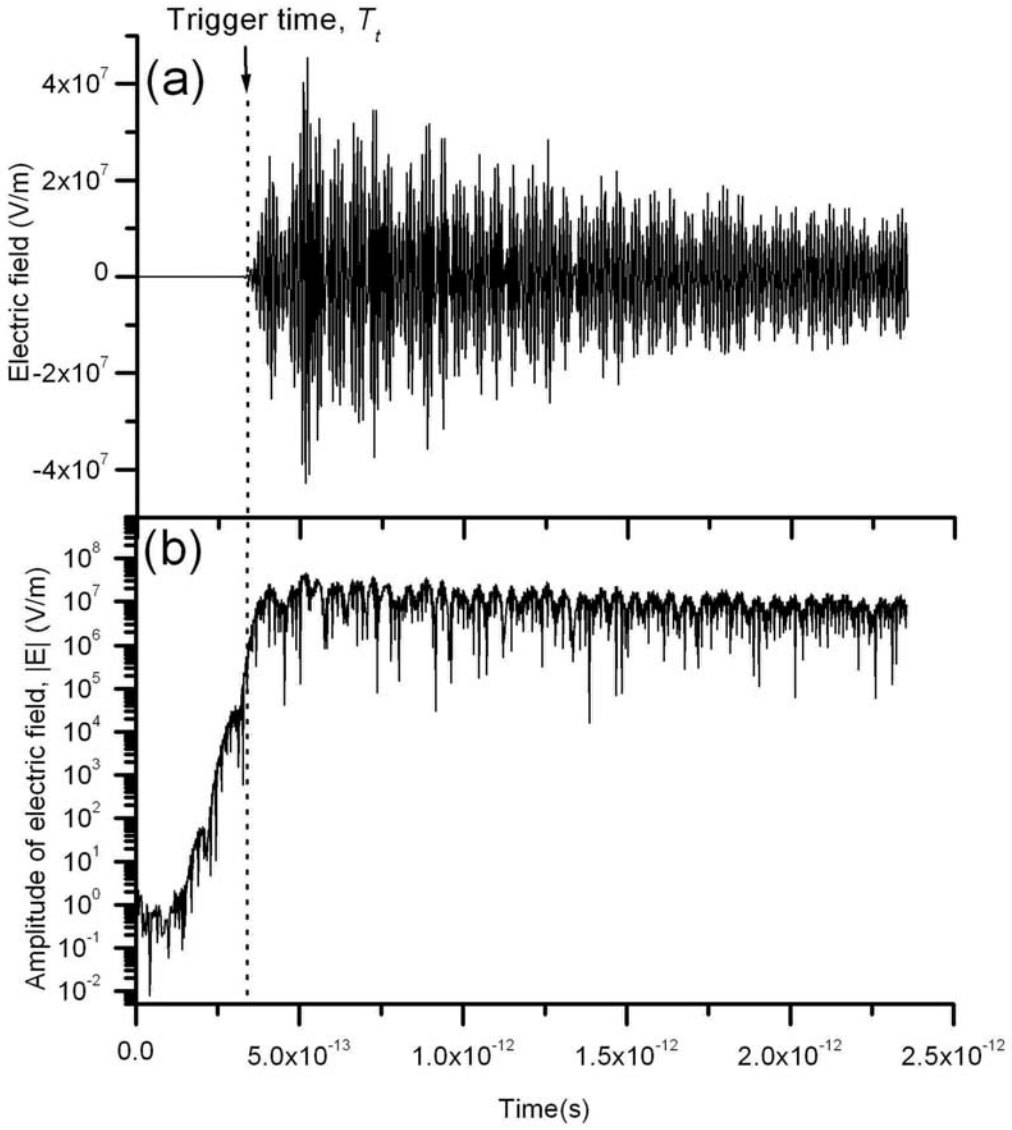

Figure 6.4 Time evolution of the electric field recorded in the central position of the disordered system: (a) electric field and (b) absolute amplitude of the electric field

Figure 6.4 illustrates the time evolution of the electric field recorded the central position of the active disorder system. The trigger time T_t also indicates that the EM wave is subjected to a great amplification that the amplitude of electric field is enlarged by six orders of magnitude (see Figure 6.4b). Initially, the amplitude of the electric field is very small. At T_t, a large amplitude vibration of the electric field is shown. Followed by the great amplification of the electric field, it is observed that several oscillation envelops are formed. The formation of the oscillation envelops of the electric field can be attributed to the interaction between the excited modes of the active disordered system. Similarly, the oscillations of the population difference density and the total electric field energy are associated with the random laser.

Beside the time evolution of the field energy and population difference density, it is valuable to study the change of the emission modes and the field distribution pattern in the amplification process. Figures 6.5 and 6.6 show the emission spectra and the field distribution pattern at different stages of the amplification process, respectively. In Figure 6.5, the spectra are calculated from five different time windows. In the first time window [0, $3000\Delta t$] (duration $=7.07\text{x}10^{-14}$s), there is no sharp peak emerging in the emission spectrum, as shown in Figure 6.6a. EM wave is evenly distributed over the active disordered medium. It is difficult to specify any clear field patterns for excited modes. The eigen-states are not well formed immediately after the injection of Gaussian excitation pulse. At t = $2.36\text{x}10^{-13}$s ($=10000\Delta t$), it can be seen from curve *b* in Figure 6.5 that a peak with a wide linewidth appears at 590nm. The shape of peak is similar to the gain profile of the four-level atomic structure. During the amplification process,

the gain profile dominates the emission spectrum and thereby a smooth peak is shown. From t = 5.89x10^{-13}s (=25000Δt) to 23.57 x10^{-13}s (=100000Δt), several spectral peaks are gradually revealed in the spectra. The typical linewidth of the peaks is approximately 1~2nm. The narrow peaks emerge as a result of the coherent random laser. The highest intensity peaks are formed around the central wavelength of the gain profile. It seems that the modes closed to the center position of the gain profile would experience a larger amplification.

In Figure 6.5, a large number of narrow peaks show in the emission spectrum determined in the spectral curve *e* (time window = [0, 100000Δt]). It is argued that only few peaks corresponding to the long-lived modes can survive in the mode competition. Some modes have diminished in the amplification process. In order to demonstrate the mode competition, two spectra are captured from two consecutive time windows and plotted in Figure 6.7. The dash and solid lines represented the spectra determined in two consecutive time windows [0, 50000Δt] and [50000Δt, 100000Δt], respectively. The duration of each time window is 11.78x10^{-13}s. Several spectral peaks are observed in the spectrum of the first time window. In the second time window, all peaks except a, b, c, d decay and diminish, as indicated in Figure 6.7. In active disordered system, eigen-modes are subject to the amplification caused by the stimulated emission. In the mean time, the mode energy may leak out. If the gain cannot compensate the loss rate of the mode, the mode will decay.

The evolution of the lasing mode may be revealed in the field distribution pattern. As shown in Figure 6.6b, several high intensity spots corresponding to the lasing

modes are clearly illustrated in the field distribution. In order to determine the decay process of the lasing mode, for instance, one mode denoted by dash circle in different frames is being traced. Initially, the intensity of the mode increases and then reaches to a high level at $t = 11.78 \times 10^{-13}$s. However, the intensity of the mode begins to decline and completely diminish at $t = 23.57 \times 10^{-13}$s. It is observed that the field distribution pattern at $t = 11.78 \times 10^{-13}$s is approximately the same as that at $t = 23.57 \times 10^{-13}$s. It may indicate that the mode competition trends to become steady. The results unambiguously show that some excited modes would decay even though the optical gain is introduced in the disordered systems.

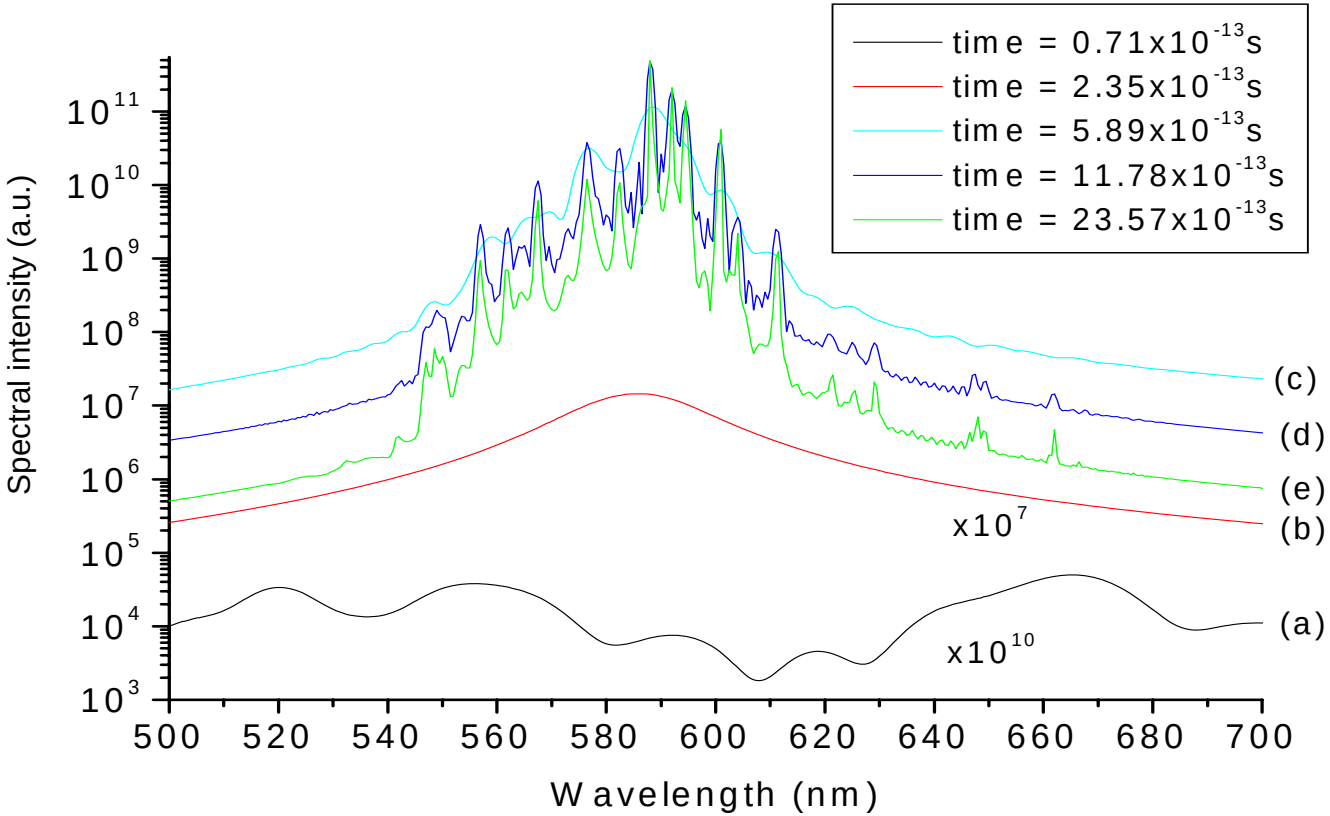

Figure 6.5 Spectra of the disorder system captured in different time windows: [0, 3000Δt], (b) [0, 10000Δt], (c) [0, 25000Δt], (d) [0, 50000Δt], (e) [0, 100000Δt]

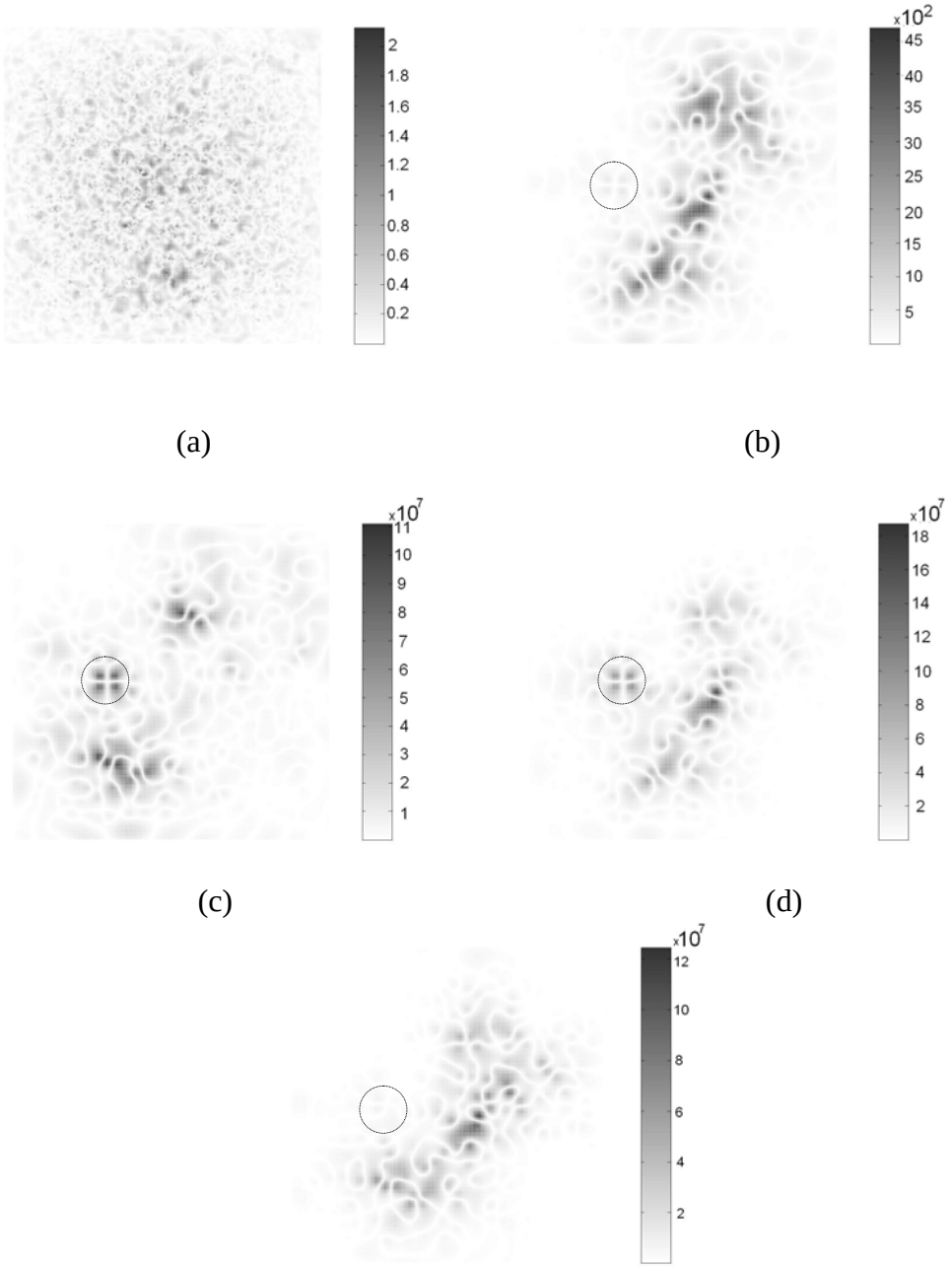

Figure 6.6 Field distribution pattern recorded at different times: (a) t =7.1x10^{-14}s (=3000Δt), (b) t = 2.35x10^{-13}s (=10000Δt), (c) t = 5.89x10^{-13}s (=25000Δt), (d) t = 11.78x10^{-13}s (=50000Δt), (e) t = 23.57 x10^{-13}s (=100000Δt)

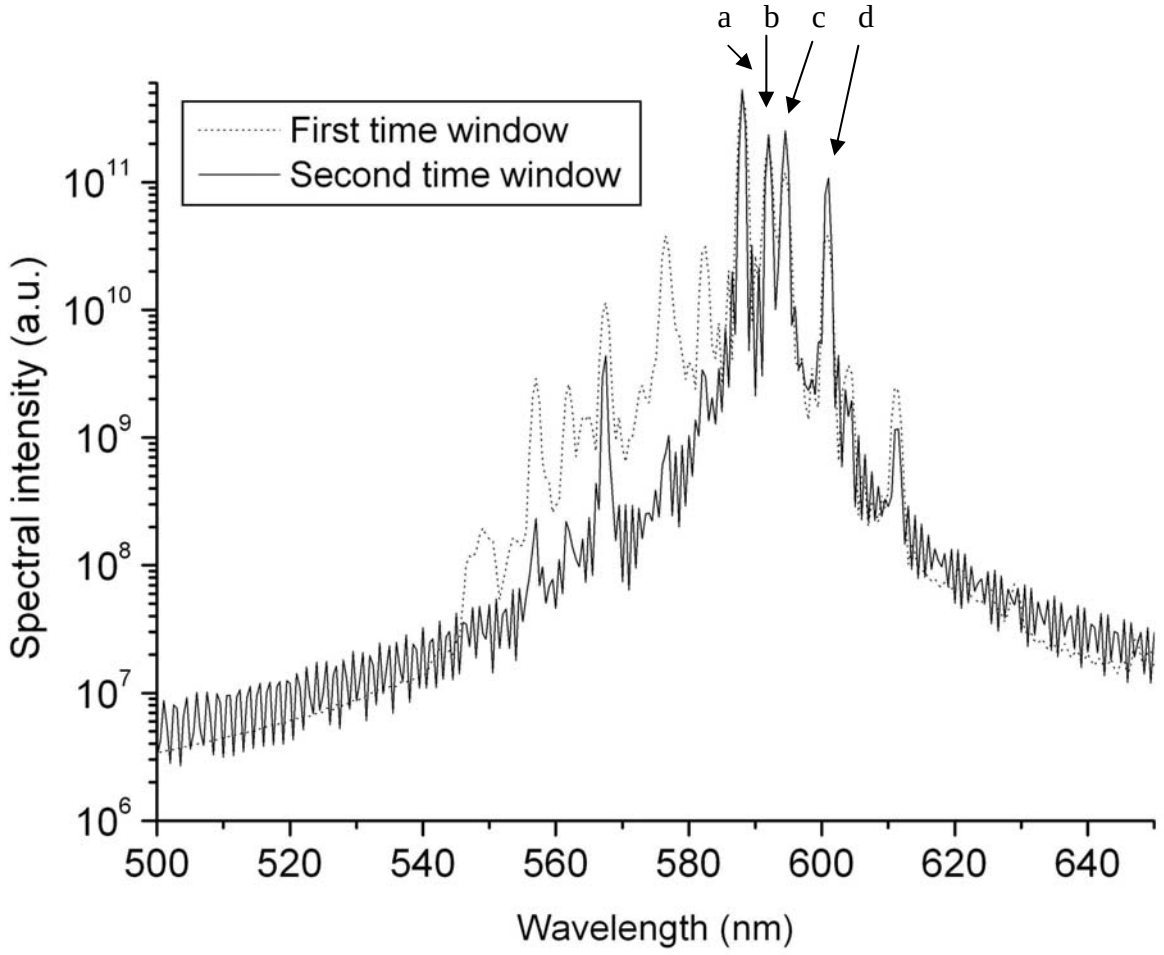

Figure 6.7 Spectra of the active disorder system in two consecutive time windows [0, 50000Δt] and [50000Δt, 100000Δt]

6.3.2 Effect of particle density on the laser emission

In the previous section, the amplification process and mode competition in active disordered systems have been investigated. In this section, the studies of the laser action in active disordered media with various particle densities are presented. In the numerical experiments, both active ordered and disordered systems are considered. The simulation parameters of the active systems are listed in Table 6.3.

Table 6.3 Parameters of the simulation and the system

Wavelength of the lasing transition	λ_t= 590nm
Frequency of the lasing transition	$\omega_t = 2\pi c/\lambda_t = 325 \times 10^{13}$ Hz
Collision time	$T_{collision} = 5\times10^{-14}$s
Life time of energy state L_2	$\tau_{21} = 5\times10^{-12}$s
Life time of energy state L_3	$\tau_{32} = 1\times10^{-10}$s
Life time of energy state L_4	$\tau_{43} = 1\times10^{-13}$s
Total atomic density (dye concentration)	10^{-3}M (=6.022×10^{23}m^{-3})
Pumping rate	$Q = 1\times10^{14}$s^{-1}
Size of system	SxS = 4000nm x4000nm
Refractive index of matrix medium	n_1 = 1, $\varepsilon_1 = n_1^2 = 1$
Refractive index of scattering particle	n_2 = 2.646, $\varepsilon_2 = n_2^2 = 7$
Radius of scattering particle	R = 60nm
Spatial increment	$\Delta x = \Delta y$ =10nm
Time increment	$\Delta t = 2.36\times10^{-17}$s
Total number of time step	500000Δt (11.79×10^{-12}s)
Prefect match layer thickness	100nm

The particle density of the active ordered systems varies from $1x10^{12}m^{-2}$ to $2x10^{13}m^{-2}$. The configurations of the active ordered systems are exactly the same as those described in Section 4.3, and shown in Figures 4.5. Figures 6.8 and 6.9 show the time evolution of the total electric field energy and the population difference density of the ordered systems respectively. Table 6.4 shows the amplification rate ξ_{amp} and the trigger time T_t of the ordered systems with various particle densities.

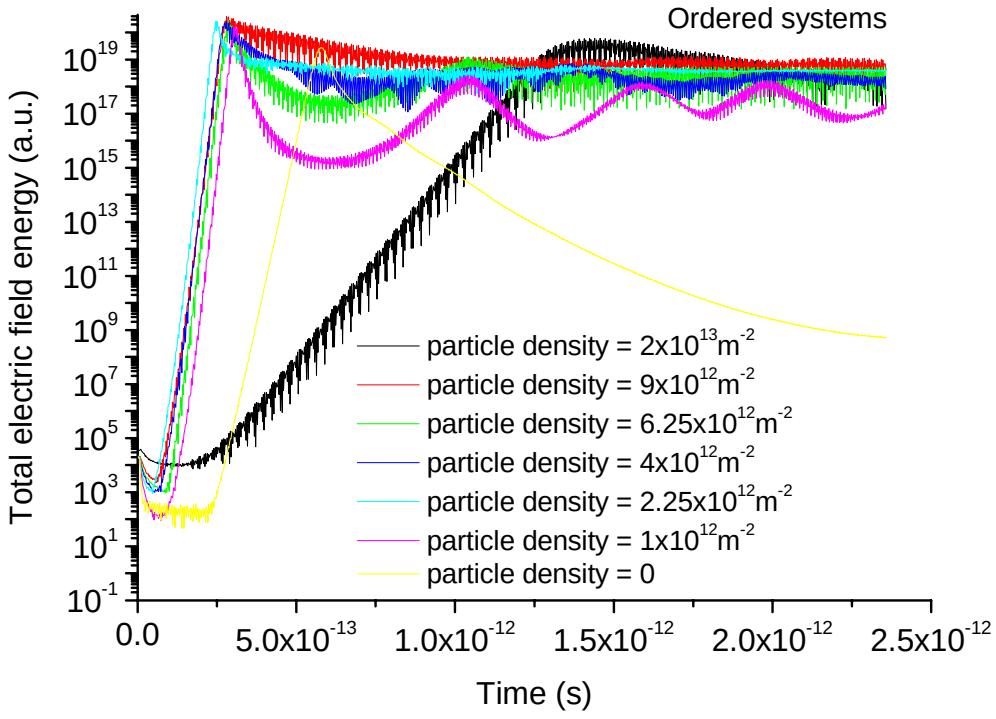

Figure 6.8 Time evolution of the total electric field energy of the ordered systems with various particle densities

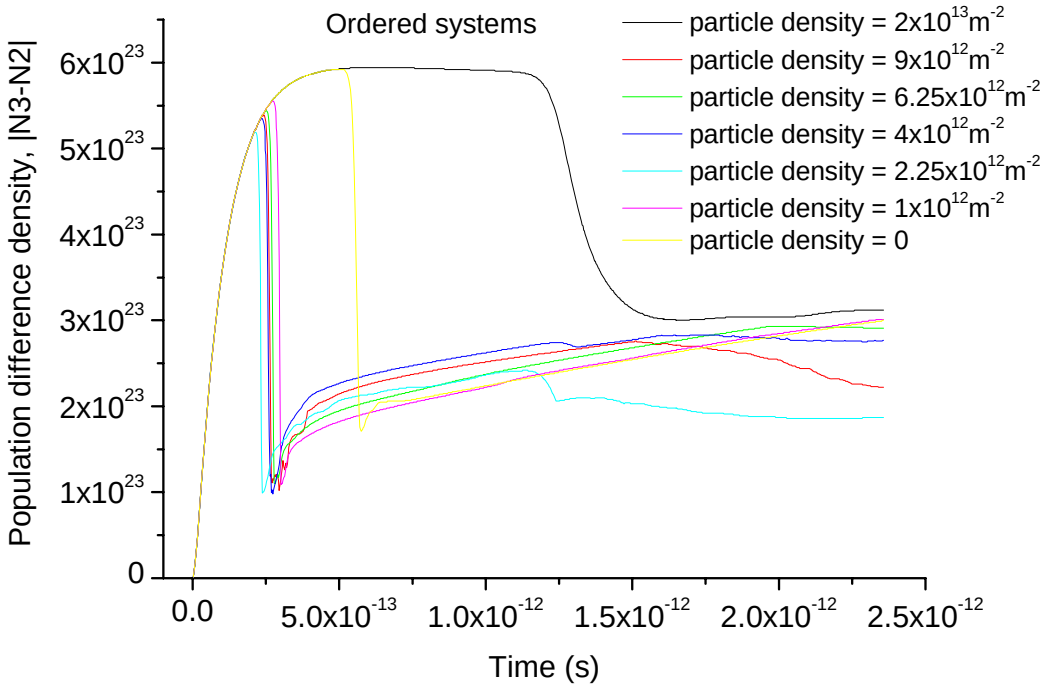

Figure 6.9 Time evolution of the population difference density of the ordered systems with various particle densities

Table 6.4 Amplification rates and trigger times of the ordered systems

Particle density	Amplification rate ξ_{amp}	Trigger time T_t
Pure dye medium	1.23 x10^{14}s^{-1}	5.26 x10^{-13}s (=22300Δt)
1x10^{12}m^{-2}	2.24 x10^{14}s^{-1}	2.82 x10^{-13}s (=11950Δt)
2.25x10^{12}m^{-2}	2.20 x10^{14}s^{-1}	2.14 x10^{-13}s (=9100Δt)
4x10^{12}m^{-2}	2.15 x10^{14}s^{-1}	2.45 x10^{-13}s (=10400Δt)
6.25x10^{12}m^{-2}	2.25 x10^{14}s^{-1}	2.56x10^{-13}s (=10850Δt)
9x10^{12}m^{-2}	2.20 x10^{14}s^{-1}	2.37x10^{-13}s (=10050Δt)
2x10^{13}m^{-2}	0.33 x10^{14}s^{-1}	1.17x10^{-12}s (=49800Δt)

Figure 6.8 reveals that the EM wave is subjected to a huge amplification in all the ordered systems within the time window [0, 100000Δt]. In the pure dye system (particle density = 0), there is a peak in the curve of the total electric field energy (see Figure 6.8) and a dramatic drop of population difference correspondingly (see Figure 6.9). This means that EM wave would be amplified in a pure dye medium. After the total field energy of the pure dye system reaches a maximum peak, the field energy curve declines steadily. Since the pure dye system does not contain any scattering particle, EM wave leak out from the computational domain in a short time. Therefore, the total field energy of the medium decreases continuously.

For the least densely packed system, i.e., particle density = $1x10^{12}m^{-2}$, the time evolution of the total field energy shows decrease then increase after the trigger times T_t. Whereas the total field energy of other ordered systems, i.e., particle density = $2.25x10^{12}m^{-2}$ to $9x10^{12}m^{-2}$, show a leveling off and relatively smaller amplitude oscillation at a high intensity level after the trigger times T_t. The results can be attributed to the multiple scattering of EM wave which facilitates effectively the amplification of EM wave. As the particle density increases, the scattering effect becomes more significant and thereby the total field energy can keep at a high level.

For the most densely packed system, i.e., particle density = $2x10^{13}m^{-2}$, however, unexpected results are obtained. It is found that the amplification rate of the system is much smaller than that of the less densely packed systems. Furthermore, a longer trigger time is shown in the most densely packed system. The trigger time is equal to $1.17x10^{-12}$s (=49800Δt) which is much longer than that of the less densely packed systems. The results indicate that the amplification of EM wave is suppressed in the

most densely packed system. The origin of the suppression may be related to the photonic band gap. Since the most densely packed system exhibits a band gap which overlaps the lasing transition wavelength (λ_t=590nm), the laser emission may be delayed under the circumstances. This interpretation is consistent with the results of the passive ordered media (see Figure 4.7). There is no photonic band gap which covers the lasing transition frequency ($f_t=c/\lambda_t=5.08\text{x}10^{14}$Hz) in the less densely packed systems, i.e., particle density = $1\text{x}10^{12}$ - $9\text{x}10^{12}\text{m}^{-2}$. Compared to the most densely packed system, relatively higher amplification rates can be observed in the less densely packed systems (see Figure 6.8 and Table 6.4).

The configurations of the disordered systems are shown in Figures 4.6 in Section 4.3. Table 6.5 show the amount of position disorder d_p and the lattice constant a of the disordered systems with various particle densities.

Table 6.5 Amount of position disorder in disordered systems

Particle density	Position disorder, d_p	Lattice constant, a
$1x10^{12}m^{-2}$	0.23a	1120nm
$2.25x10^{12}m^{-2}$	0.21a	660nm
$4x10^{12}m^{-2}$	0.2a	500nm
$6.25x10^{12}m^{-2}$	0.2a	400nm
$9x10^{12}m^{-2}$	0.19a	320nm
$2x10^{13}m^{-2}$	0.2a	200nm

Figures 6.10 and 6.11 show the time evolution of the total electric field energy and the population difference density of the disordered systems, respectively. For the disordered systems with a particles density ranging from $2.25x10^{12}m^{-2}$ to $9x10^{12}m^{-2}$, the amplification process are similar to that of the corresponding ordered systems. However, a different result is found for the most densely packed disordered system. Compared to the corresponding ordered system, the amplification rate of the most densely packed disordered system increases sharply, as shown in Figures 6.8 and 6.10. It is believed that the disorder can enhance the amplification rate under the influence of photonic band gap.

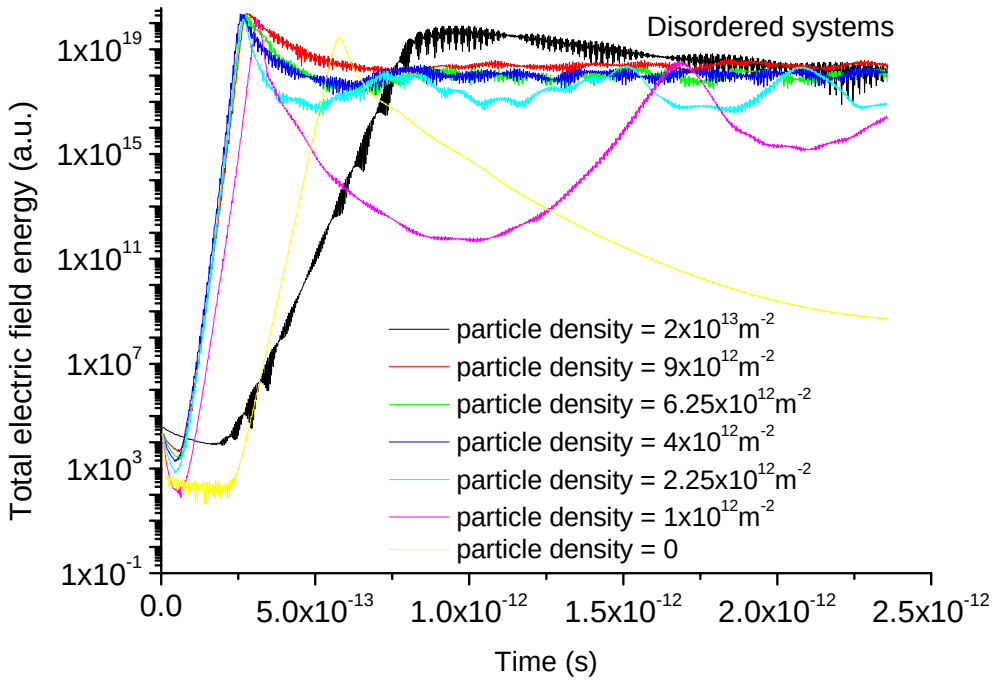

Figure 6.10 Time evolution of the total electric field energy of the disordered systems with various particle densities

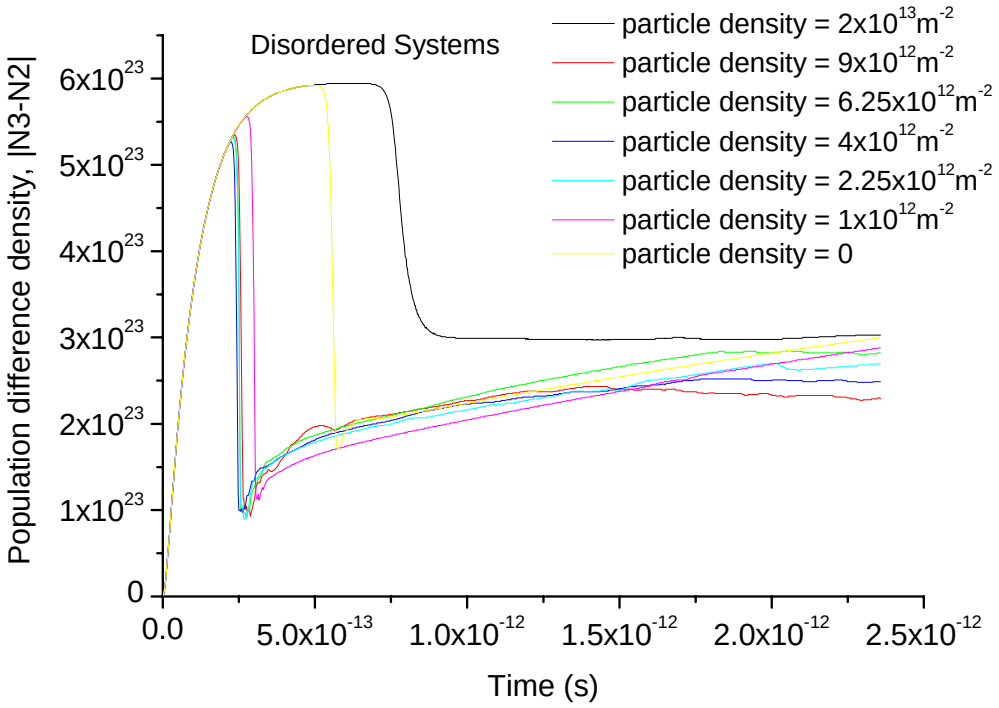

Figure 6.11 Time evolution of the population difference density of the disordered systems with various particle densities

Table 6.6 summarizes the amplification rate ξ_{amp} and the trigger time T_t of the disordered systems. It is found that the amplification rate of the most densely packed disordered system is increased by doubled and the trigger time is significantly reduced from those of the ordered systems (see Table 6.4). Hence, only a small deviation of the trigger time and amplification rate can be observed in the other disordered systems. It is clear that the disorder effect on the densely packed disordered system is serious while the effect of the disorder on the less densely packed disordered systems is insignificant.

Table 6.6 Amplification rates and trigger times of the disordered systems

Particle density	Amplification rate ξ_{amp}	Trigger time T_t
Pure dye medium	$1.23 \times 10^{14} s^{-1}$	5.26×10^{-13}s (=22300Δt)
$1 \times 10^{12} m^{-2}$	$1.98 \times 10^{14} s^{-1}$	2.66×10^{-13}s (=11300Δt)
$2.25 \times 10^{12} m^{-2}$	$2.14 \times 10^{14} s^{-1}$	2.43×10^{-13}s (=10300Δt)
$4 \times 10^{12} m^{-2}$	$2.17 \times 10^{14} s^{-1}$	2.18×10^{-13}s (=9250Δt)
$6.25 \times 10^{12} m^{-2}$	$2.06 \times 10^{14} s^{-1}$	2.25×10^{-13}s (=9550Δt)
$9 \times 10^{12} m^{-2}$	$1.97 \times 10^{14} s^{-1}$	2.35×10^{-13}s (=9950Δt)
$2 \times 10^{13} m^{-2}$	$0.64 \times 10^{14} s^{-1}$	6.51×10^{-13}s (=27600Δt)

Figure 6.12 shows the field distribution patterns of the ordered systems. The field patterns are recorded after a very long time evolution (t=650000Δt=1.532×10^{-11}s) in order to eliminate the short-lived modes. In the ordered systems, the field patterns are regular and symmetric. The dashed lines represent the symmetric axes which clarify the symmetric patterns. The formation of the symmetric field pattern is a consequence of the coherent diffraction of EM wave in the ordered system. When a random position disorder (the amount of position disorder is listed in Table 6.5) is introduced in the ordered system, the symmetric field patterns are broken down (see Figure 6.13) because the square lattice is disturbed.

As shown in Figures 6.13e and 6.13f, EM energy is evenly distributed in the less

densely packed disordered systems (particles density varied from $1x10^{12}m^{-2}$ to $2.25x10^{12}m^{-2}$). Since these two systems contain few scattering particles, the strength of scattering of EM wave is weak. Therefore, the eigen-modes of EM wave would leak out and extended to the whole medium. As localized modes are seldom found in the less densely disordered systems, the field energy can be evenly distributed in the media. When the number of the scattering particle increases, the scattering strength is reinforced and the localization of EM wave is more easily to be observed. As shown in Figure 6.13b, high intensity spots corresponding to a localized mode can be found in the densely packed disordered system with a particle density = $9x10^{12}m^{-2}$. However, as shown in Figure 6.13a, high intensity field clusters are found in the densely packed system. This field pattern of the disordered system pertains to the field pattern of the ordered system (see Figure 6.12a). A possible explanation is that the amount of disorder (d_p =0.2a) is not sufficient to destroy the coherent diffraction of EM wave of the ordered system.

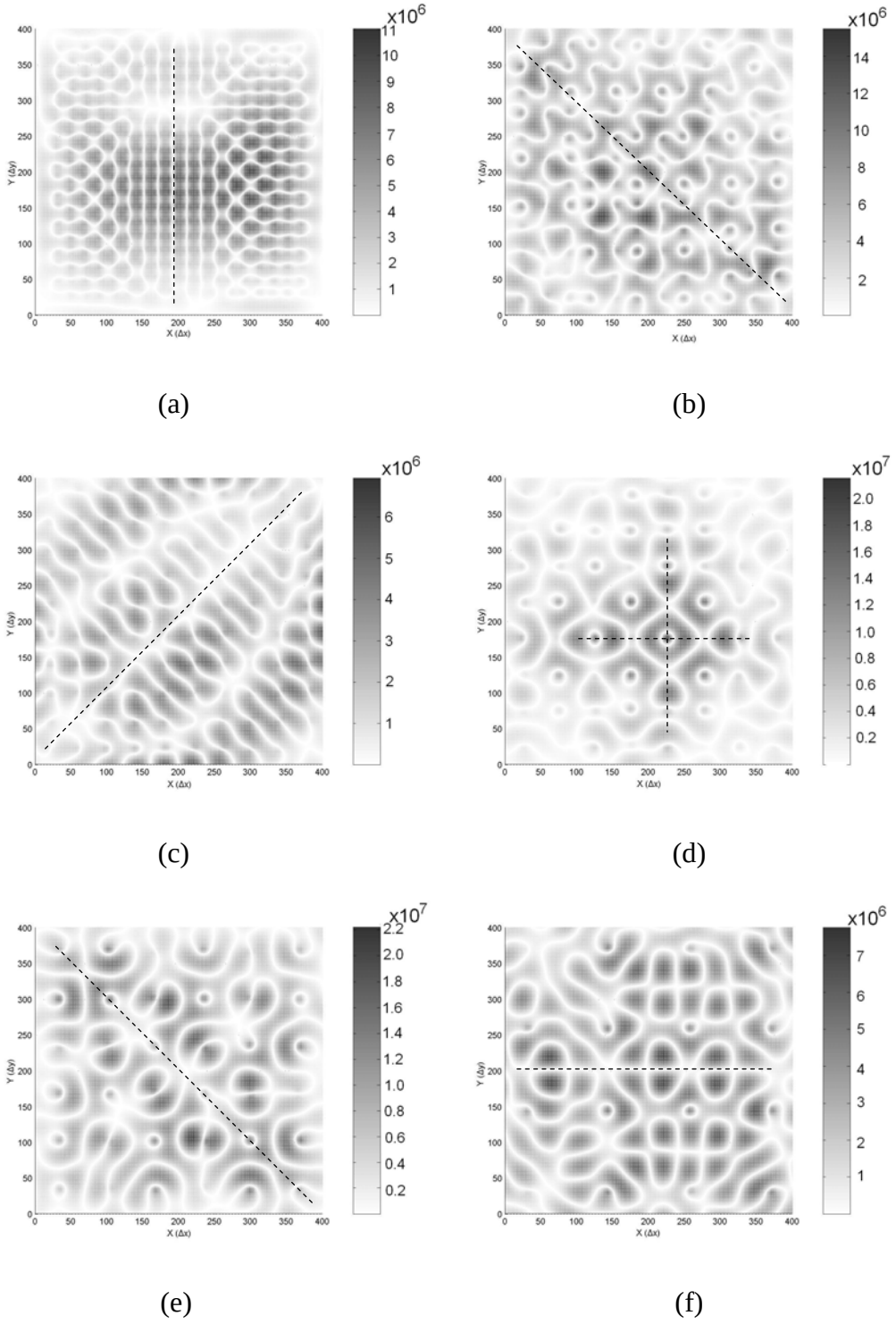

Figure 6.12 Field distribution pattern recorded in the ordered systems with various particle densities at t = 1.532x10^{-11}s (=650000Δt): (a) particle density = 2x10^{13}m^{-2}, (b) particle density = 9x10^{12}m^{-2}, (c) particle density = 6.25x10^{12}m^{-2}, (d) particle density = 4x10^{12}m^{-2}, (e) particle density = 2.25x10^{12}m^{-2}, (f) particle density = 1x10^{12}m^{-2}.

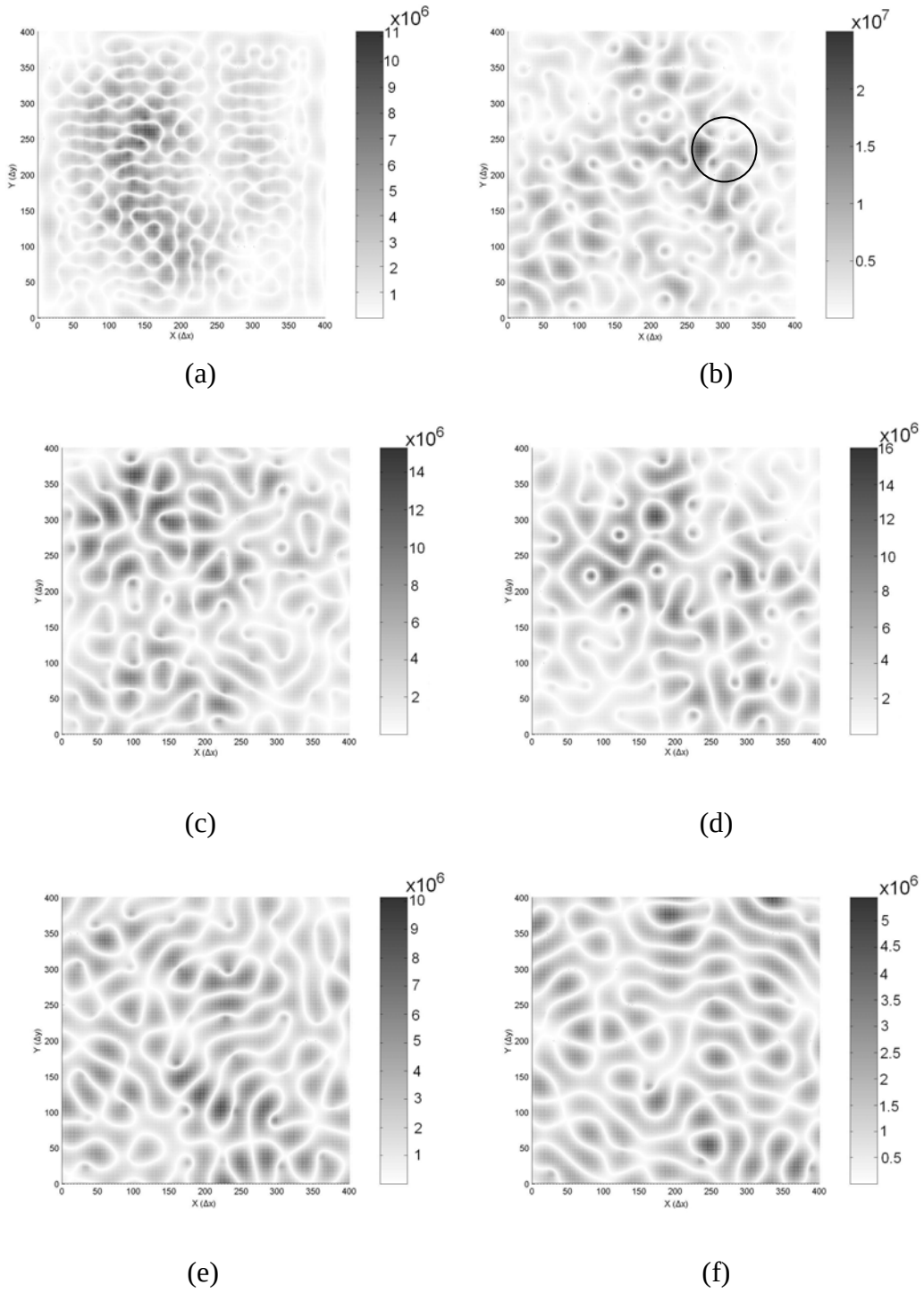

Figure 6.13 Field distribution pattern recorded in the disordered systems with various particle densities at t=1.532x10^{-11}s (=650000Δt): (a) particle density = 2x10^{13}m^{-2}, (b) particle density = 9x10^{12}m^{-2}, (c) particle density = 6.25x10^{12}m^{-2}, (d) particle density = 4x10^{12}m^{-2}, (e) particle density = 2.25x10^{12}m^{-2}, (f) particle density = 1x10^{12}m^{-2}.

Beside the investigation of the field pattern, the emission spectra of the active disordered systems are also considered. Figures 6.14 and 6.15 show the emission spectra of the ordered and disordered systems, respectively, which are determined in a time window of [487500Δt, 650000Δt] (duration =3.83x10^{-12}s). It is found that the spectra of the disordered systems are roughly the same as those of the ordered systems. For the ordered systems, most of the spectral peaks locate close to the central wavelength of the gain profile (λ_t= 590nm) except the emission peak of the most densely packed system. As shown in Figure 6.14, the peaks of the most densely packed ordered system emerge near wavelength of λ = 550nm (f =545x10^{14}Hz). In fact, this peak is very close to the edge of the first band gap.

For the disordered system, the emission peak of the most densely packed disordered system is again found at the edge of the band gap (see Figure 6.15). The wavelength of the peak is λ = 554nm (f =541x10^{14}Hz), which is approximately the same as the result of the ordered system. The emission peak of the most densely packed disordered system is higher than that of ordered system by one order of magnitude. It can see that the emission peaks of the most densely packed disordered system shift from the central wavelength of the gain profile to the edge of the band gap. Obviously, the shift of the wavelength of the emission peak of the most densely packed disordered system is caused by the band gap. Inside the photonic band gap, there is no eigen-mode and the amplification is suppressed significantly. Hence, the modes nearest the edge of band gap are firstly reinforced instead. Since the edge of band gap is far away from the central wavelength of the gain profile, the strength of the amplification is relatively weaker. As a result of the weak amplification, the most densely packed disordered system exhibits a lower amplification rate and long trigger

time.

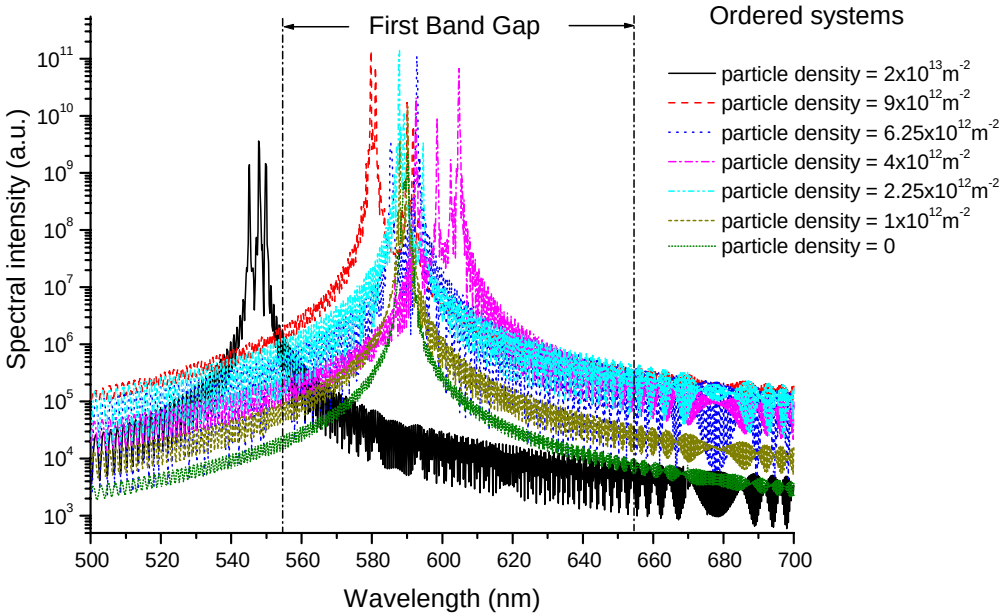

Figure 6.14 Emission spectra of the active ordered systems.

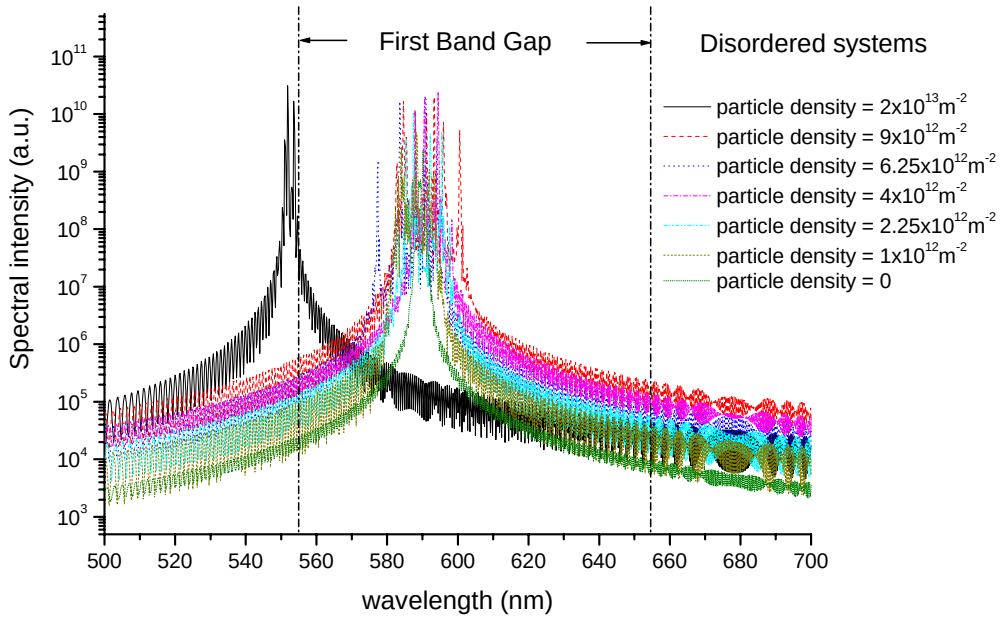

Figure 6.15 Emission spectra of the active disordered systems. The amounts of the position disorder are shown in Table 6.5.

6.3.3 Effect of disorder on the laser emission

In Section 6.3.2, it has been reported that the amplification of EM wave seems to be suppressed by the photonic band gap in the most densely packed disordered system. The reduction of the amplification rate, the time lag of the trigger time T_t and the shift of lasing frequency perhaps indicate that the photonic band gap is a detrimental factor for the random laser emission. According to the investigation of the passive disordered system in Chapter 4, photonic band gaps in the most densely packed ordered system are destroyed by the position ($d_p \geq 0.3a$) and size disorders ($d_r \geq 0.1a$), where a = 200nm. Therefore, it is expected that the suppression of the photonic band gap on the amplification process can be improved by controlling the amount of disorder in the active disordered media. Therefore, it is valuable to study, the interplay of band gap and disorder effect on the random laser emission.

In the numerical experiments, position and size disorders were assigned into the most densely packed ordered system. i.e., particle density = $2\text{x}10^{13}\text{m}^{-2}$, which was described in Section 6.3.2. In order to determine the disorder effect, the amounts of the position and size disorders were varied from d_p = 0.05a to d_p = 0.4a and d_r = 0.05a to d_r = 0.2a, respectively, where a = 200nm. The simulation results were obtained by averaging 10 different configurations of disordered systems with the same amount of disorder. Figures 6.16 and 6.17 plot the time evolution of the total electric field energy of the disordered systems with various amounts of position and size disorders, respectively. In Figure 6.16, it is easy to see that the slope of the rising curves gradually increases as the amount of the position disorder increases from d_p = 0.05a to 0.4a. However, for the size disorder, it is surprising to see from Figure 6.17 that there is a sudden rise of the slope of the rising curves even when d_r=0.05a. From d_r=0.05a

to 0.2a, however, the slopes of the rising curves are almost the same.

The amplification rates estimated from the slope of the rising curves are plotted as a function of the amount of the position and size disorders, as shown in Figure 6.18. It is obvious that the amplification rate slightly increases when a small amount of the position disorder is assigned. It is followed by a sharp upward trend. It seems that the change of amplification rate becomes steady and reaches a saturation level at d_p = 0.35a.

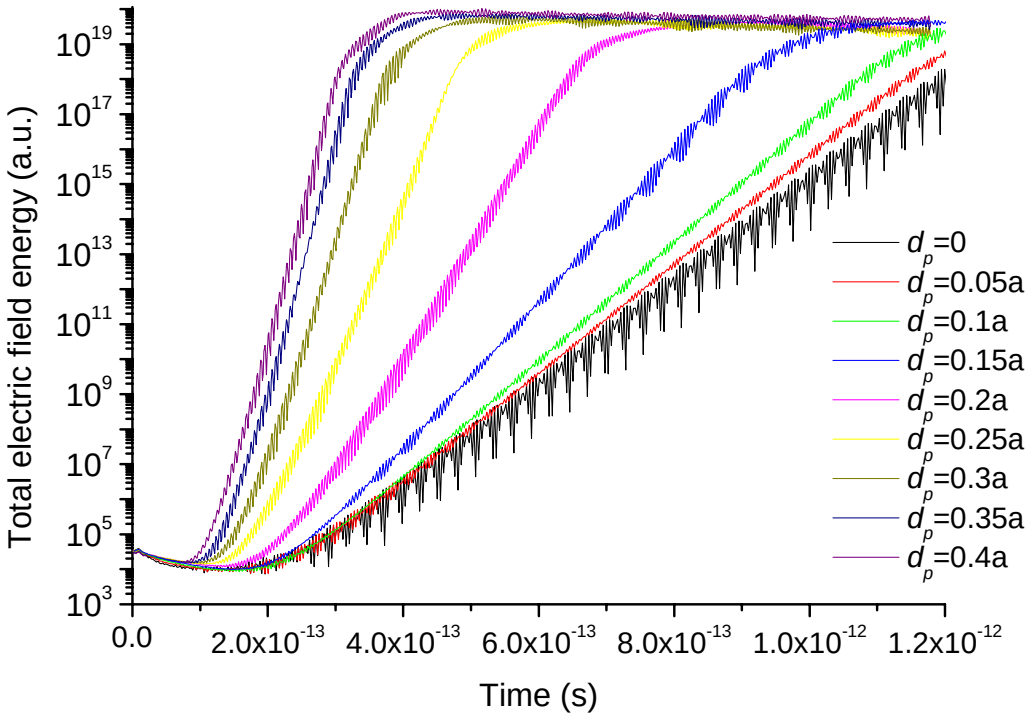

Figure 6.16 Time evolution of the total electric field energy of the disordered systems with various amounts of position disorder. Lattice constant *a* is 200nm.

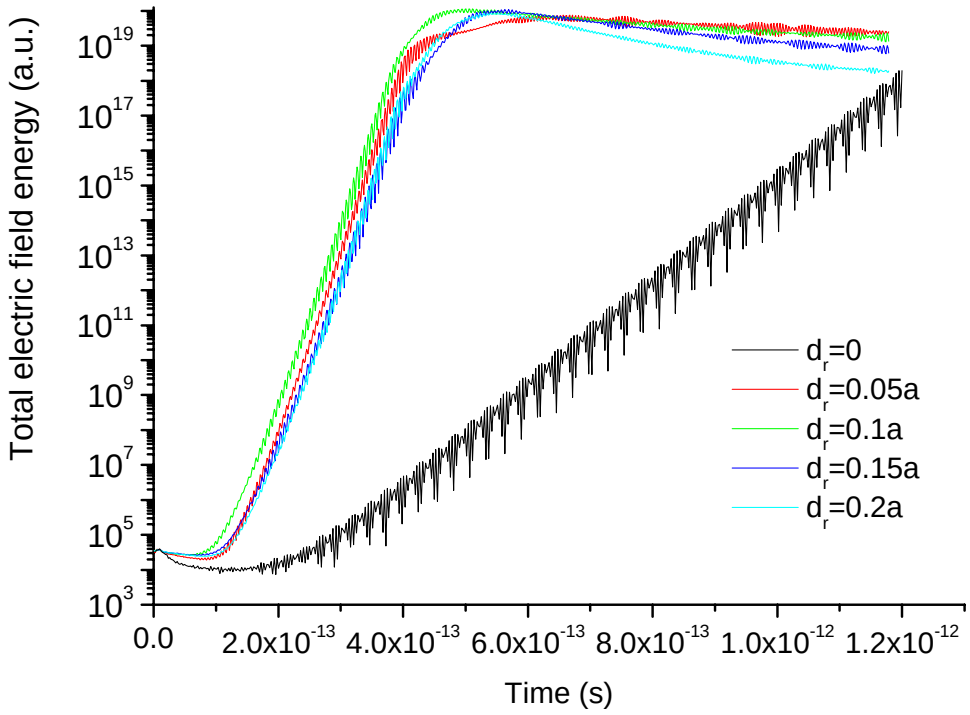

Figure 6.17 Time evolution of the total electric field energy of the disordered systems with various amounts of size disorder. Lattice constant *a* is 200nm.

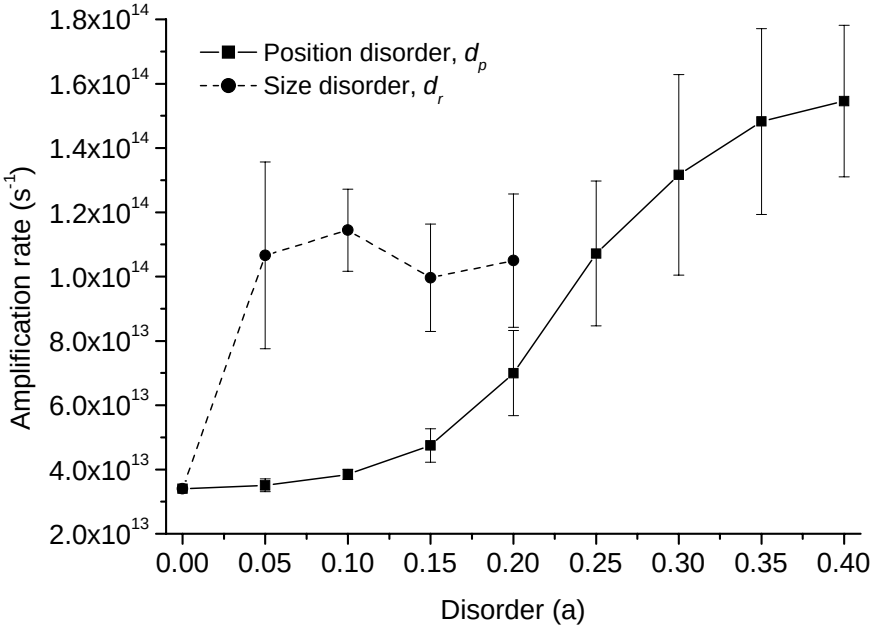

Figure 6.18 Plot of amplification rates of the disordered systems as a function of the amount of the position and size disorder. Lattice constant *a* is 200nm.

Next the dependence of the population difference density is studied as a function of the disorder, as illustrated in Figures 6.19 and 6.20, respectively. In Figure 6.19, it is found that the population inversion build up more quickly as the amount of the position disorder increases. When the amount of the disorder is higher than 0.3a, it is observed that a dip occurs after the drop of population difference density. This dip indicates that a large number of excited electrons transited to the lower energy level simultaneously, which induces a stronger amplification of the EM wave. It is again found that the dip occurs in the active disordered system when the amount of the size disorder is larger than 0.1a. In fact, a stronger amplification of EM wave is demonstrated in highly disordered systems.

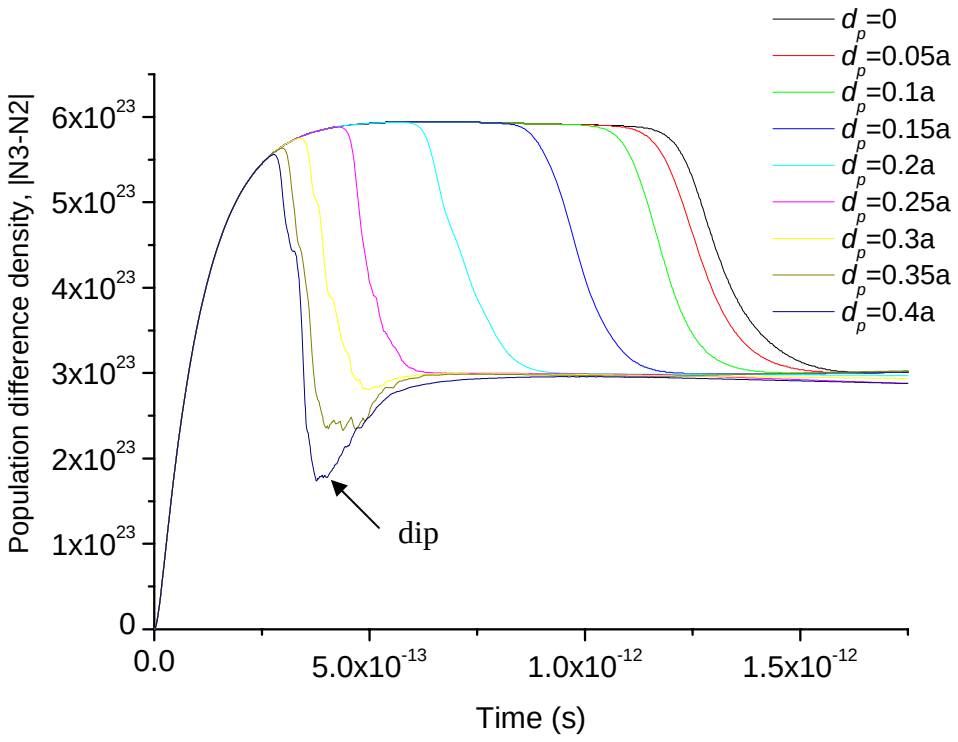

Figure 6.19 Population difference density of the disordered systems with various amounts of the position disorder. Lattice constant *a* is 200nm.

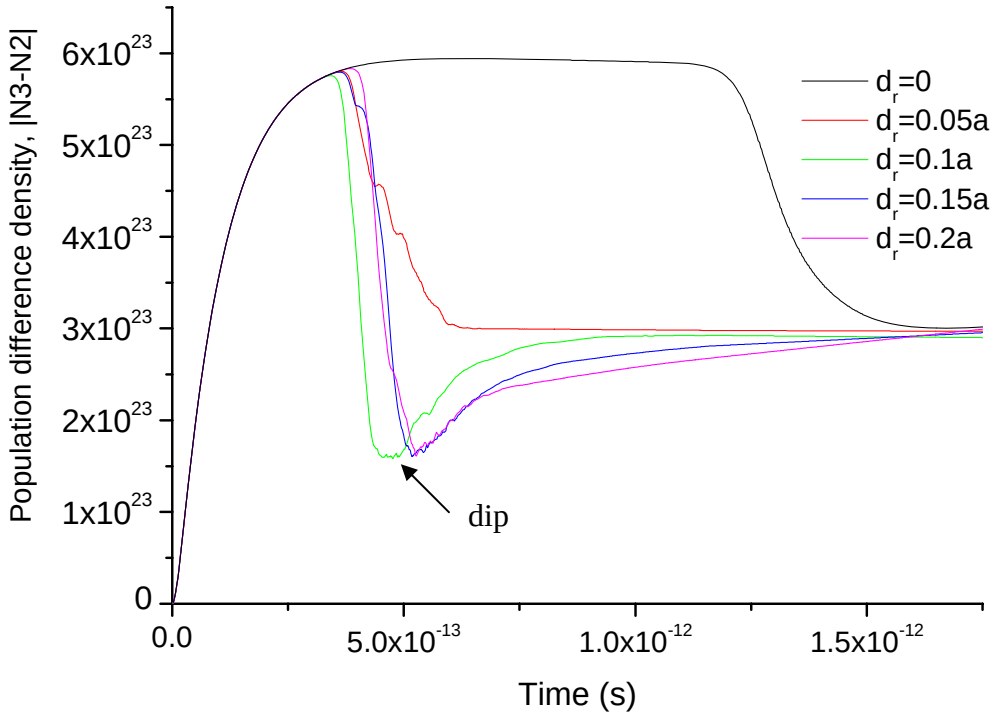

Figure 6.20 Population difference density of the disordered systems with various amounts of the size disorder. Lattice constant *a* is 200nm.

The results can be understood in term of the deformation process of the photonic band gap. In Chapter 4, it is shown that a band gap is found in the frequency range of f = $4.58\text{x}10^{14}$-$5.41\text{x}10^{14}$Hz. The corresponding wavelength range is from 555 to 655nm. In the current study, the wavelength of lasing transition is chosen as 590nm. The gain profile overlaps with the photonic band gap and thereby the amplification is suppressed. Therefore, the amplification rate of the most densely packed disordered system is significantly lower than those do not exhibit photonic band gap, as shown in Table 6.6. Hence, the amplification is enhanced when disorders are assigned in the ordered system.

As mentioned in Chapter 4, the eigen-states emerge in the photonic band gap as the amount of disorder increases. If the eigen-states are created inside the band gap, they

will experience a large amplification because the eigen-states have shorter localization lengths. Thus, the EM field confined in the localized states is significantly reinforced and thereby the amplification rate of the active disordered system increases. When the amount of disorder reaches a high value, more localized states are created deeply inside the band gap and the band gap seems to be destroyed completely. Therefore, the amplification rate reaches the maximum value. Even though the amount of disorder increases, the amplification rate does not further increase because the band gap is fully destroyed. As shown in Figure 6.18, the curve of the amplification rate shows a saturation trend at d_p = 0.35a.

A similar explanation can be applied on the results of the size disorder. Since the band gap is more sensitive to the size disorder, the eigen-states can be created deeply inside the band gap even though the amount of the size disorder is small. It is believed that the band gap is deformed seriously at d_r = 0.05a. Consequently, the saturation of amplification rate is observed at the higher amounts of size disorder.

In the above discussions, it is suggested that the eigen-states would emerge in the band gap and facilitate the random laser emission under certain circumstances. In order to support this suggestion, the lasing mode distribution in the active disordered system is analyzed. The emission spectra of the active disordered systems with various amounts of disorder are calculated and shown in Figures 6.21 and 6.22. To obtain the longest-lived modes, the spectra are recorded after a long time evolution of EM wave in a time window of [487500Δt, 650000Δt]. The duration of the time window is 3.83×10^{-12}s.

Figure 6.21 shows the long-time emission spectra of four disorder systems with position disorder, i.e., d_p = 0.1a, 0.2a, 0.3a and 0.4a. It is evident that the shift of the emission peaks is from the short wavelength to the long wavelength. The emission peaks lie outside the band gap at d_p = 0.1a. At this level of the position disorder, the band gap still keeps in good shape. As the amount of the position disorder rises, the emission peaks slightly shift toward the edge of the band gap. At d_p = 0.3a, it is obvious that several emission peaks emerge inside the band gap and the number of peaks increases significantly.

Figure 6.22 shows the long-time emission spectra of four disorder systems with the size disorder, i.e., d_r = 0.05a, 0.1a, 0.15a and 0.2a. The emission peaks are created inside the band gap even though the amount of the size disorder is small (d_r = 0.05a). When $d_r \geq 0.05$a, there are several emission peaks emerge deep inside the band gap. It is not surprising that the size disorder is more easily to destroy the band gap. The wavelength of the emission peaks with the highest spectral intensity and the number of peaks of the active disordered systems with various amounts of disorder are summarized in Tables 6.7 and 6.8.

For the size disordered system, the effective refractive index of the disordered system is changed as results of the random deviation of the size of the high dielectric scattering particles. For the position disordered system, however, the effective refractive index of the disordered system does not alternate.

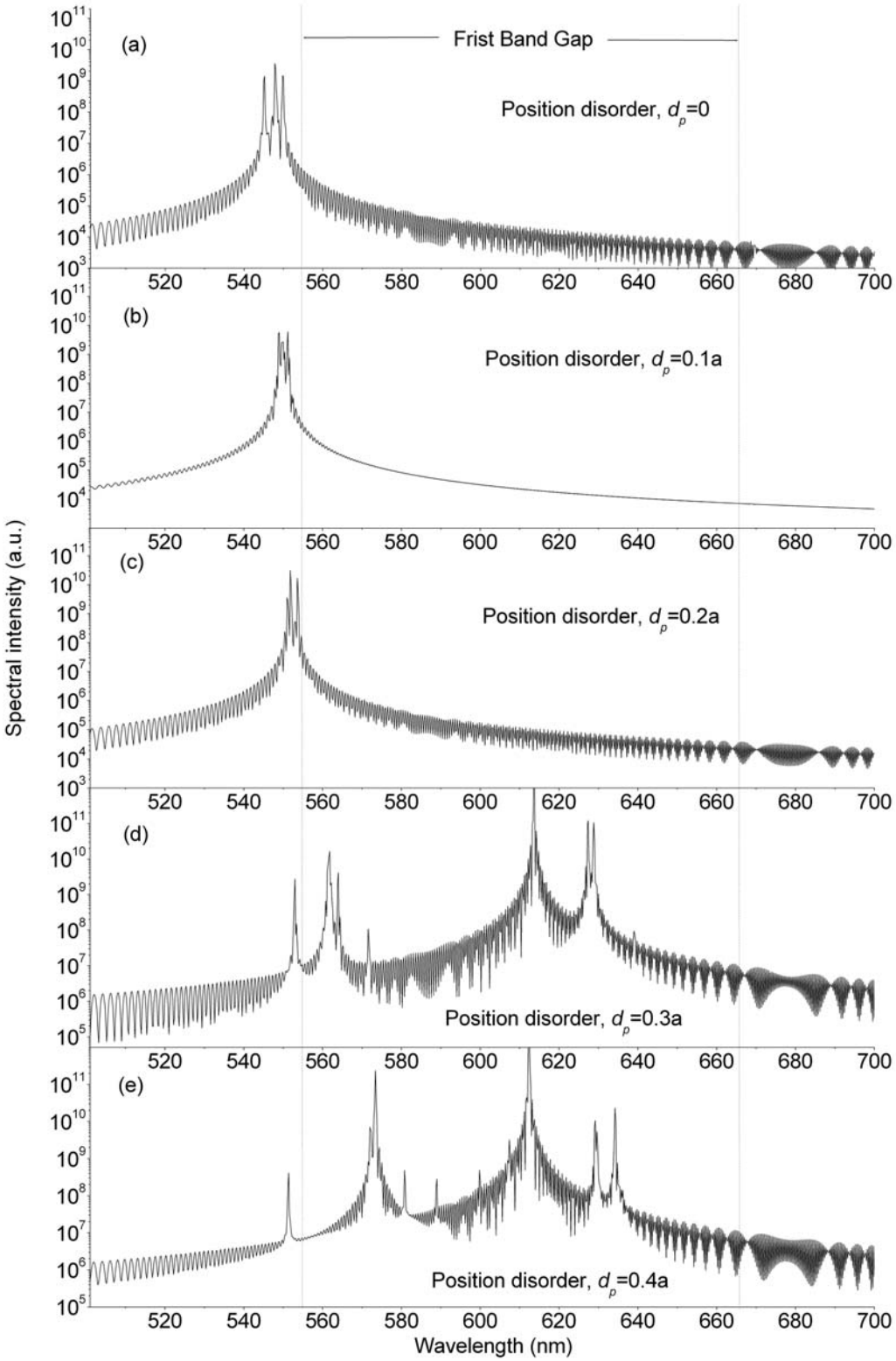

Figure 6.21 Emission spectra of four disorder systems with various amounts of position disorder: (a) d_p= 0, (b) d_p = 0.1a, (c) d_p = 0.2a, (d) d_p = 0.3a and (e) d_p = 0.4a. Lattice constant a is 200nm.Time window is [487500Δt, 650000Δt] (duration =3.83x10^{-12}s)

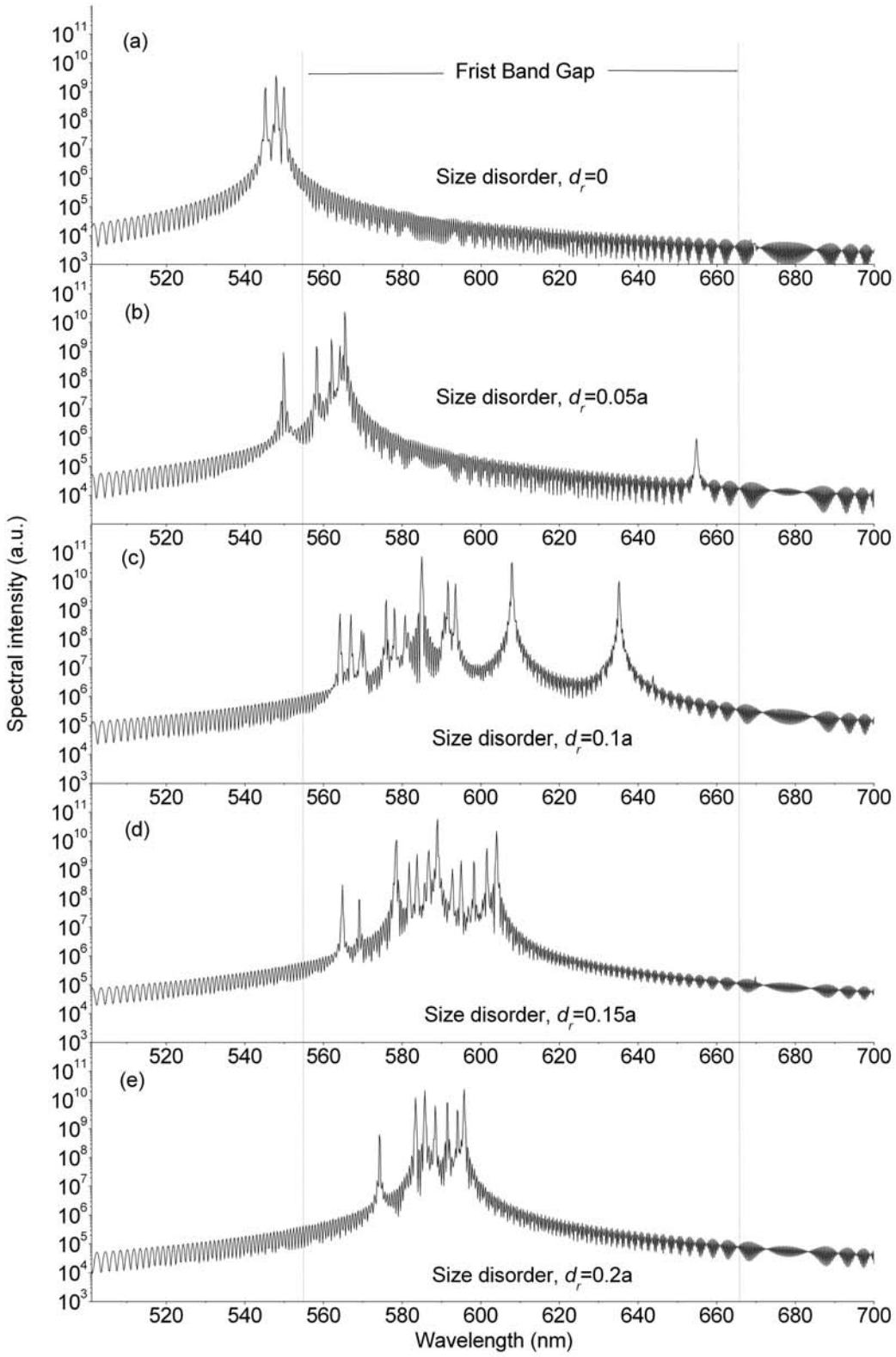

Figure 6.22 Emission spectra of four disorder systems with various amounts of size disorder: (a) d_r = 0, (b) d_r = 0.05a, (c) d_r = 0.1a, (d) d_r = 0.15a and (e) d_r = 0.2a. Lattice constant a is 200nm.Time window is [487500Δt, 650000Δt] (duration =3.83x10^{-12}s)

Table 6.7 Wavelength of the emission peaks and number of peaks of the active disordered systems with position disorder. Time window is [487500Δt, 650000Δt] (duration =3.83x10^{-12}s)

Amount of the position disorder, d_p	Wavelength of the emission peaks with the highest spectral intensity	Number of emission peaks
0	547.8nm	3
0.1a	549nm	4
0.2a	551.8nm	4
0.3a	613.6nm	7
0.4a	612.4nm	10

Table 6.8 Wavelength of the emission peaks and number of peaks of the active disordered systems with size disorder. Time window is [487500Δt, 650000Δt] (duration =3.83x10^{-12}s)

Amount of the size disorder, d_r	Wavelength of the emission peaks with the highest spectral intensity	Number of emission peaks
0	547.8nm	3
0.05a	563.4nm	6
0.1a	585nm	13
0.15a	590nm	12
0.2a	596nm	7

Figures 6.23 and 6.24 illustrate the field distribution patterns of the active systems with position and size disorders, respectively. The field patterns are recorded at t = $1.53x10^{-11}$s. After a long time of mode competition, it is believed that only the longest-lived modes survive in the system. In Figure 6.23, the difference in the field patterns of disordered systems is notable. It may reveal the effect of disorder on the emission mode. At d_p = 0.1a, two regions of high intensity field are observed, which may correspond to the collective behavior of the extended modes in which the field energy extends cross the whole system. As the amount of the disorder increases, the area of high intensity field region reduces. The reduction of the area of high intensity field region is more serious for the systems shown in Figures 6.23c and 6.23d. The field energy is concentrated in few spots. It can be attributed to the confinement of EM wave in localized modes. Similar phenomena can be found in the size disordered systems. The shape of high intensity region for the size disordered systems seems to be rectangular because the scatter particles are arranged in square lattice. When the size of the particle is randomly varied, rectangular cavity is easily created. It is illustrated by comparing the configuration and the field distribution pattern of the size disordered system, as shown in Figure 6.25.

According to the series of the field patterns, the transition between the extended modes and localized modes is confirmed. The transitions are demonstrated in both position and size disordered systems. Obviously, the localized modes are created as a result of the large amount of disorder.

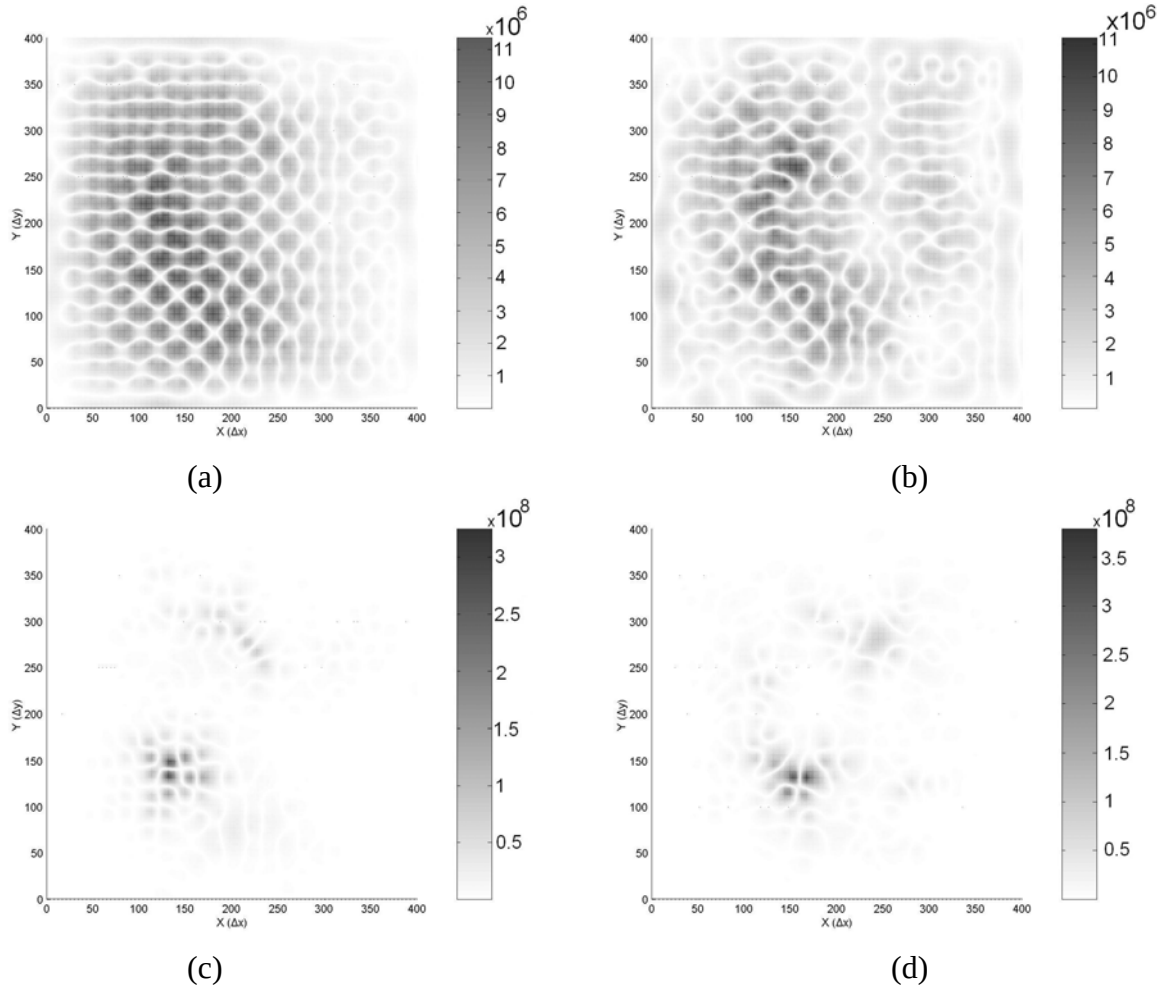

Figure 6.23 Field distribution patterns of the disordered systems with various amounts of position disorder: (a) d_p = 0.1a, (b) d_p = 0.2a, (c) d_p = 0.3a and (d) d_p = 0.4a. Field patterns are recorded at t = 650000Δt = 1.53x10^{-11}s. Lattice constant a is 200nm

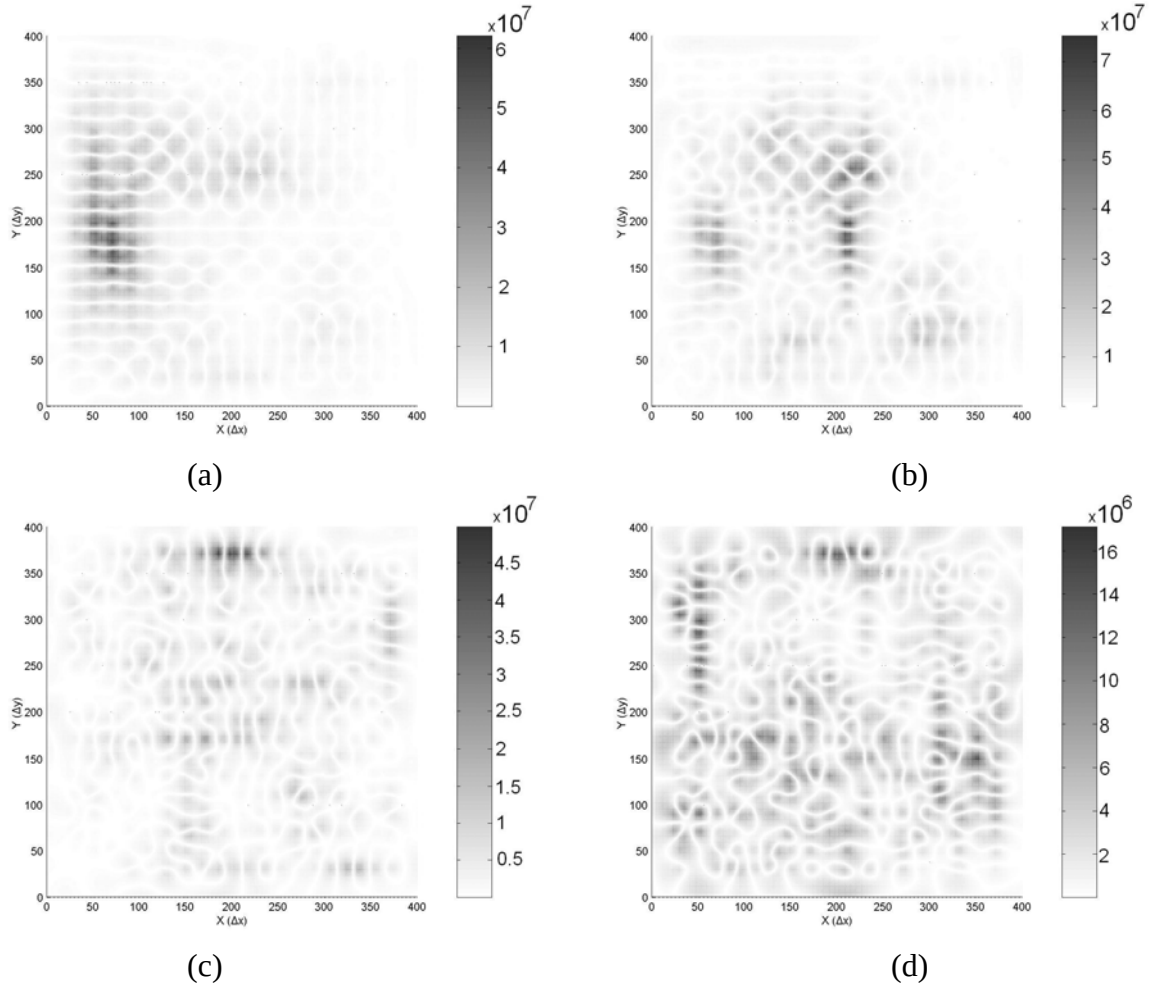

Figure 6.24 Field distribution patterns of the disordered systems with various amounts of size disorder: (a) d_r= 0.05a, (b) d_r= 0.1a, (c) d_r = 0.15a and (d) d_r = 0.2a. Field patterns are recorded at t = 650000Δt = 1.53x10^{-11}s. Lattice constant a is 200nm

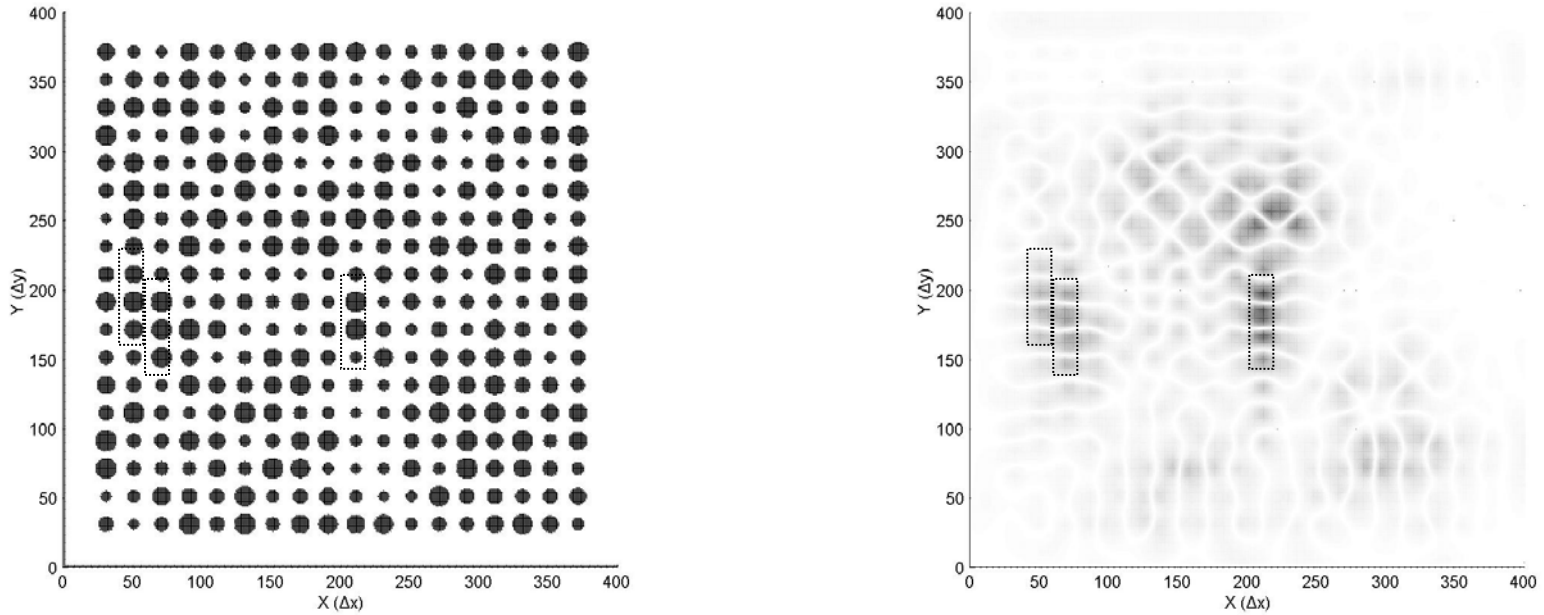

(a) (b)

Figure 6.25 (a) Configuration of the active disordered system with size disorder of d_r = 0.1a. (b) Field distribution pattern of the active disordered system described in (a), which is recorded a t = 1.53×10^{-11}s. Lattice constant *a* is 200nm

6.3.4 Effect of disorder on the laser emission at different lasing transition frequency

In the previous sections, it has been found that the laser emission of the active disorder systems is disturbed due to the spectral overlap of the photonic band gap and the gain profile. The spectral position of the gain profile would alternate the amplification of the EM wave in the active disorder system. In this section, the lasing emission with different gain profiles will be examined. The spectral wavelength of the gain profiles varies, locating at the upper, middle and lower position of the band gap. In the numerical experiments, three lasing transition wavelengths, λ_t = 550, 620 and 650nm are chosen. For each lasing transition wavelength, five levels of the position disorder, i.e., d_p = 0.1a, 0.2a, 0.3a and 0.4a, are considered.

Figures 6.26, 6.27 and 6.28 show the emission spectra of the active disordered systems with λ_t = 550, 620 and 650nm, respectively. Figure 6.29, 6.30 and 6.31 depicts the time evolution of the total electric field energy of the disordered systems with λ_t = 550, 620 and 650nm, respectively.

For λ_t = 550nm, the emission peaks of the systems with various amounts of disorder emerge around the wavelength of 550nm, as shown in Figure 6.26. The shifts of the emission peaks are relatively small. In fact, the distortion on the amplification caused by the band gap is not serious. In Figure 6.29, the rising curves indicate that the amplification rates of the systems with various amounts of disorder are the same. The results are expected because the central wavelength of the gain profile lies just outside the band gap and the band gap does not affect

the laser emission.

For λ_t = 620nm, it is interesting that two emission peaks appear individually in the upper and lower edge of the band gap, as shown in Figures 6.27a and 6.27b. As the amount of the disorder increases, the emission peaks shift toward the central wavelength of the band gap. At a highly disordered system, the emission peaks with longer wavelength dominate the lasing emission while the emission peaks near the upper edge vanish.

For λ_t = 650nm, the results are similar to those of the systems with λ_t = 620nm. However, the emission peak at the lower edge is missing in current results (see Figure 6.28). It is again found that the emission peaks shift from the upper edge to the central wavelength of the band gap as the amount of the disorder increases. In cases of λ_t = 620nm and λ_t = 650nm, the amplification rates of the disordered systems are enhanced in the highly disordered systems, as indicated in Figures 6.30 and 6.31. Accordingly, the disorder can improve the laser emission significantly when the gain profile of the gain material overlaps the photonic band gap. It is concluded that the effect of the band gap is significant when the central wavelength of the gain profile overlaps with the band gap.

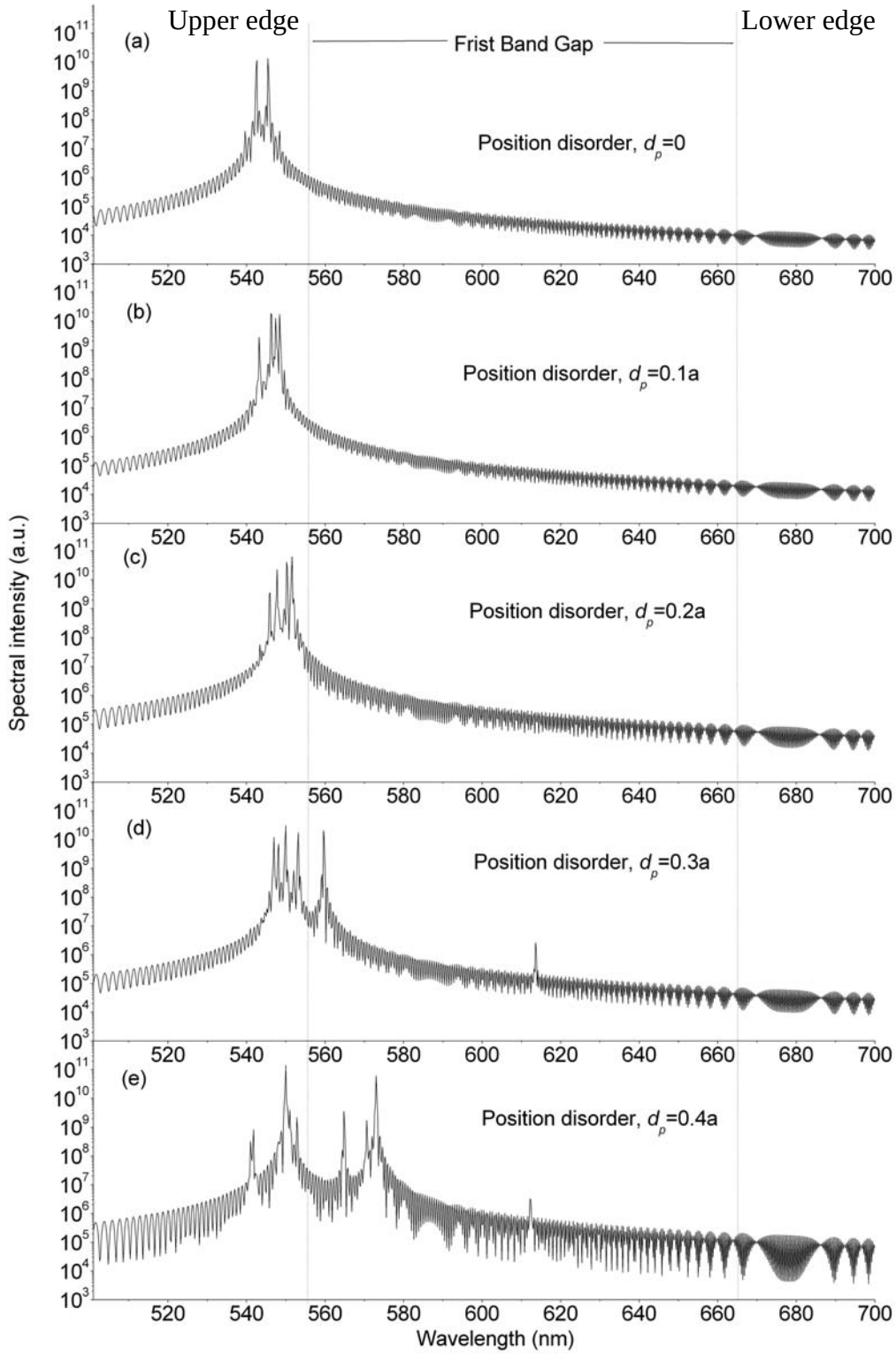

Figure 6.26 Emission spectra of the active disordered systems with λ_t = 550nm. Amount of the position disorder in the systems: (a) d_p= 0, (b) d_p = 0.1a, (c) d_p = 0.2a, (d) d_p = 0.3a and (e) d_p = 0.4a. Lattice constant a is 200nm.Time window is [487500Δt, 650000Δt] (duration =3.83x10^{-12}s)

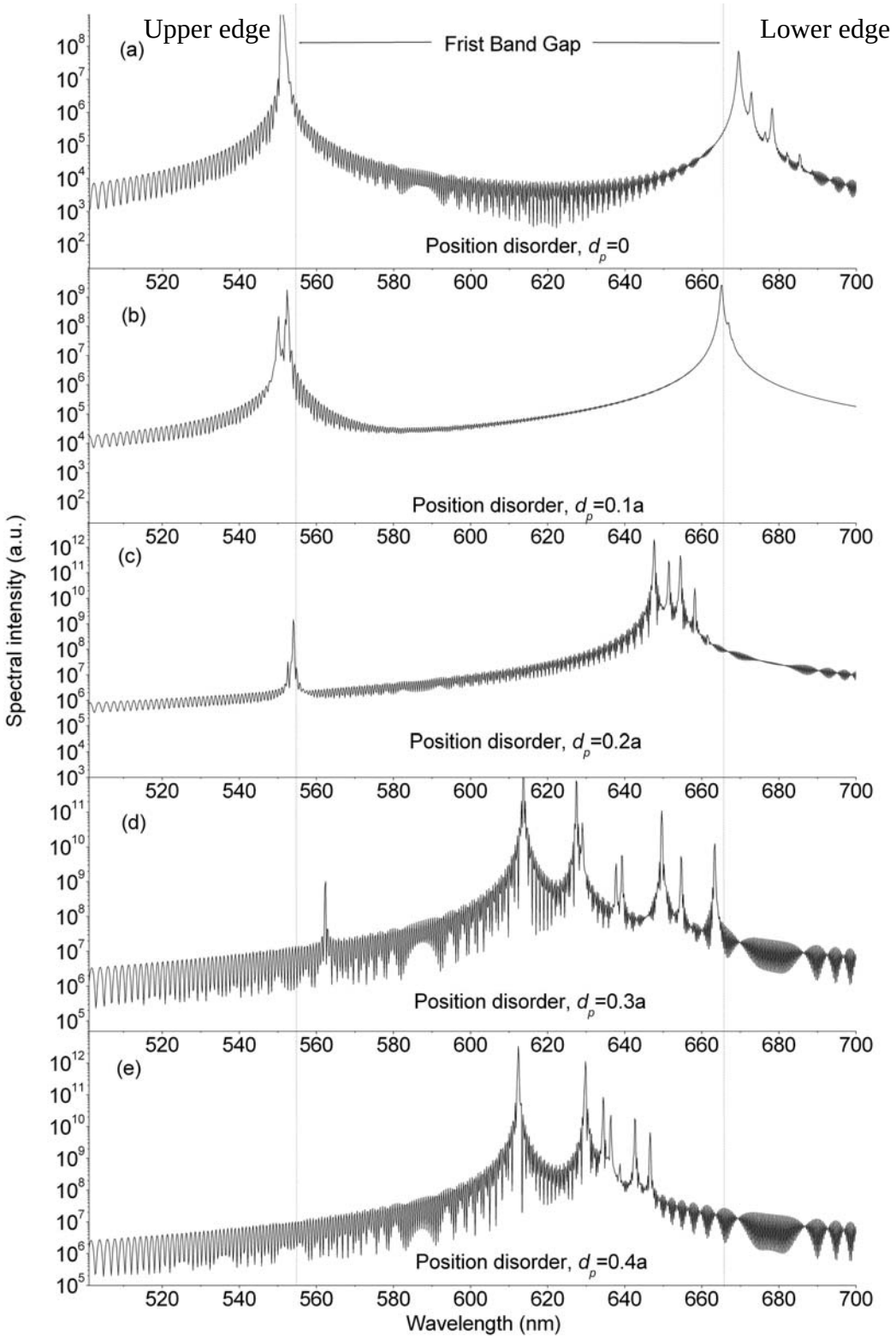

Figure 6.27 Emission spectra of the active disordered systems with λ_t = 620nm. Amount of the position disorder in the systems: (a) d_p= 0, (b) d_p = 0.1a, (c) d_p = 0.2a, (d) d_p = 0.3a and (e) d_p = 0.4a. Lattice constant a is 200nm.Time window is [487500Δt, 650000Δt] (duration =3.83x10^{-12}s)

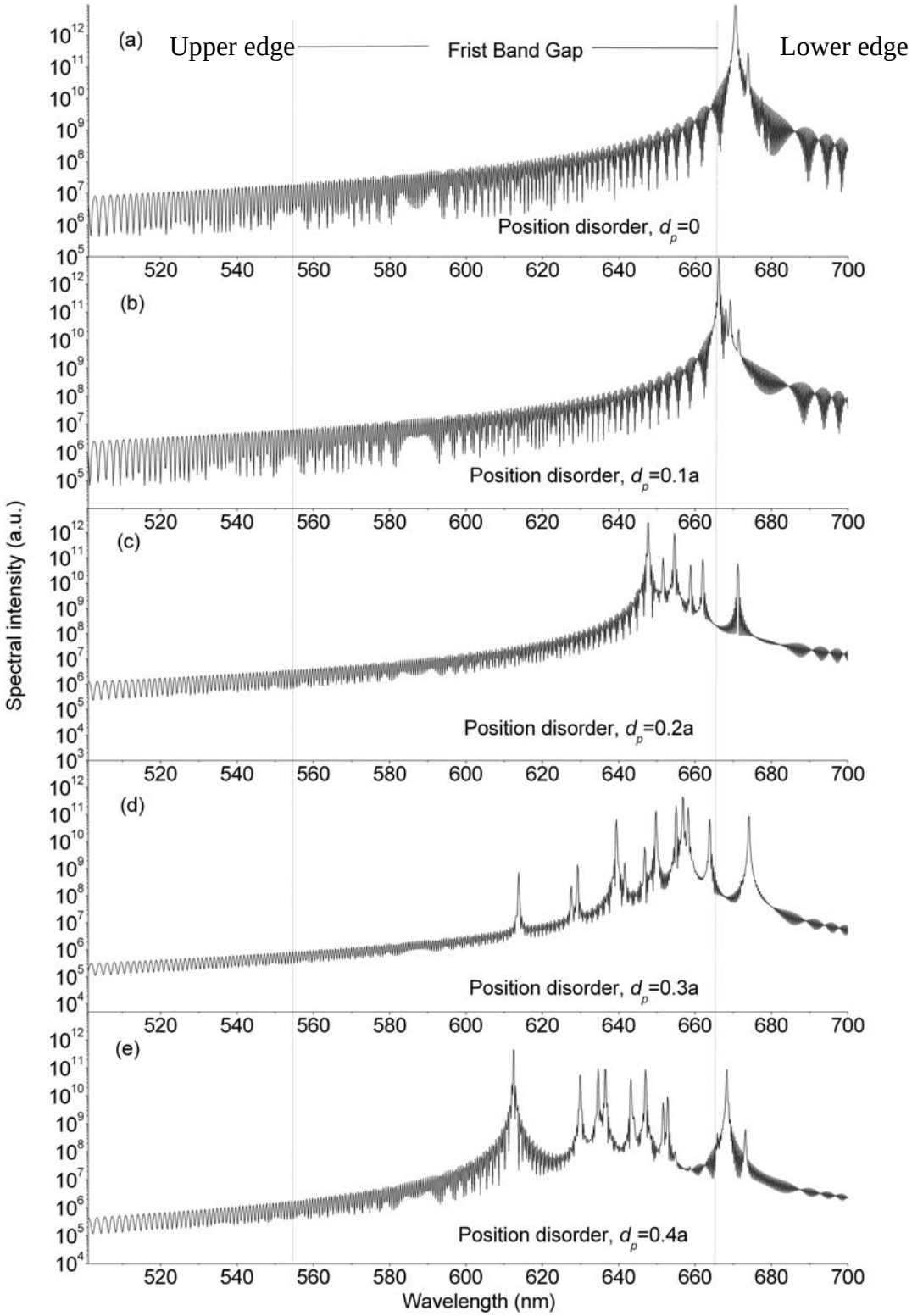

Figure 6.28 Emission spectra of the active disordered systems with λ_t = 650nm. Amount of the position disorder in the systems: (a) d_p= 0, (b) d_p = 0.1a, (c) d_p = 0.2a, (d) d_p = 0.3a and (e) d_p = 0.4a. Lattice constant a is 200nm.Time window is [487500Δt, 650000Δt] (duration =3.83x10^{-12}s)

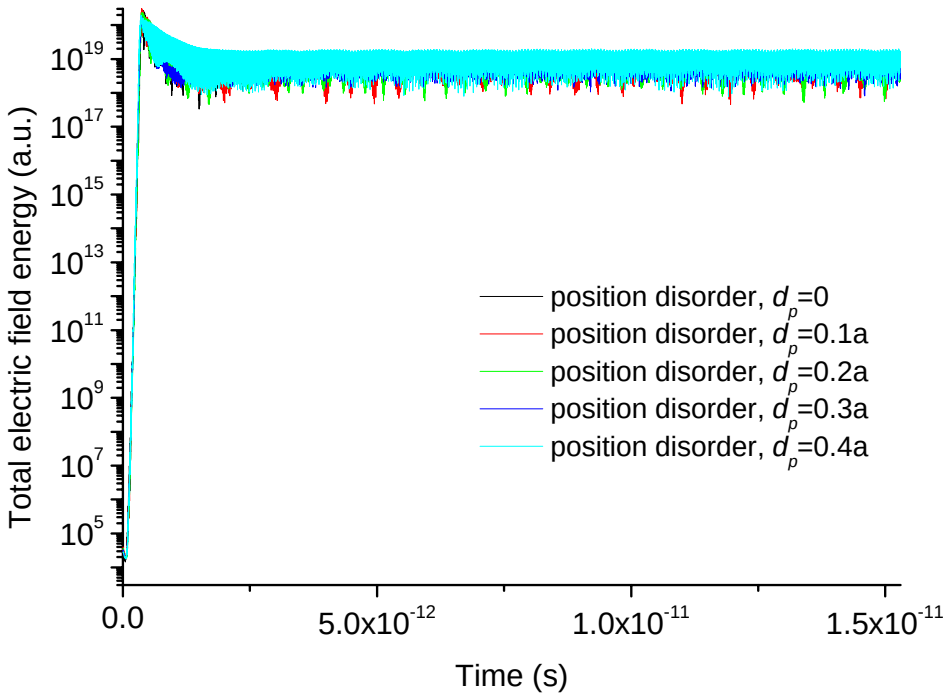

Figure 6.29 Time evolution of the total electric field energy of the active disordered systems with λ_t = 550nm. Lattice constant a is 200nm.

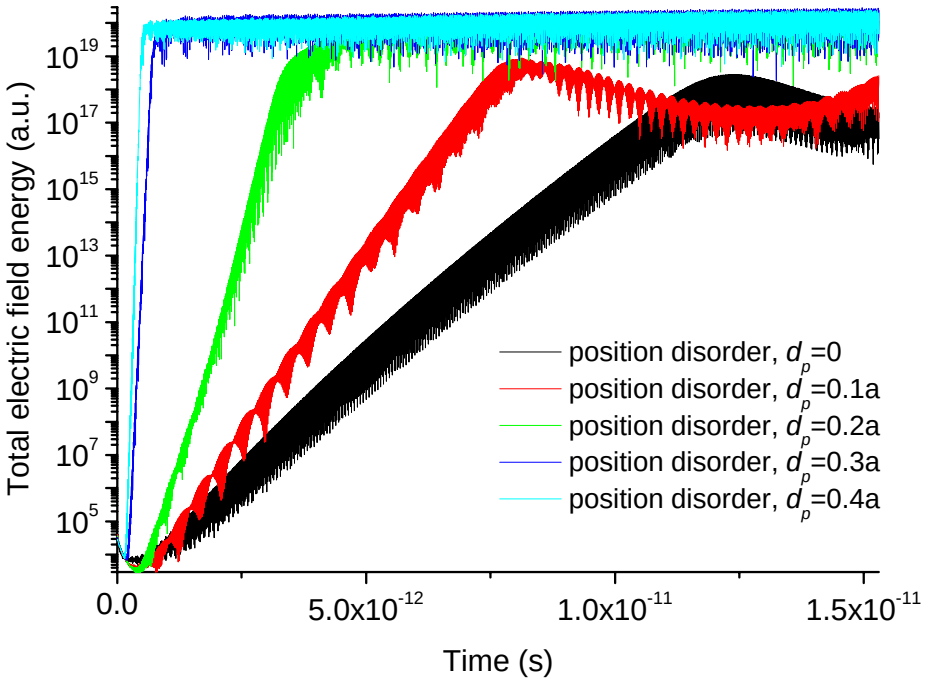

Figure 6.30 Time evolution of the total electric field energy of the active disordered systems with λ_t = 620nm. Lattice constant a is 200nm.

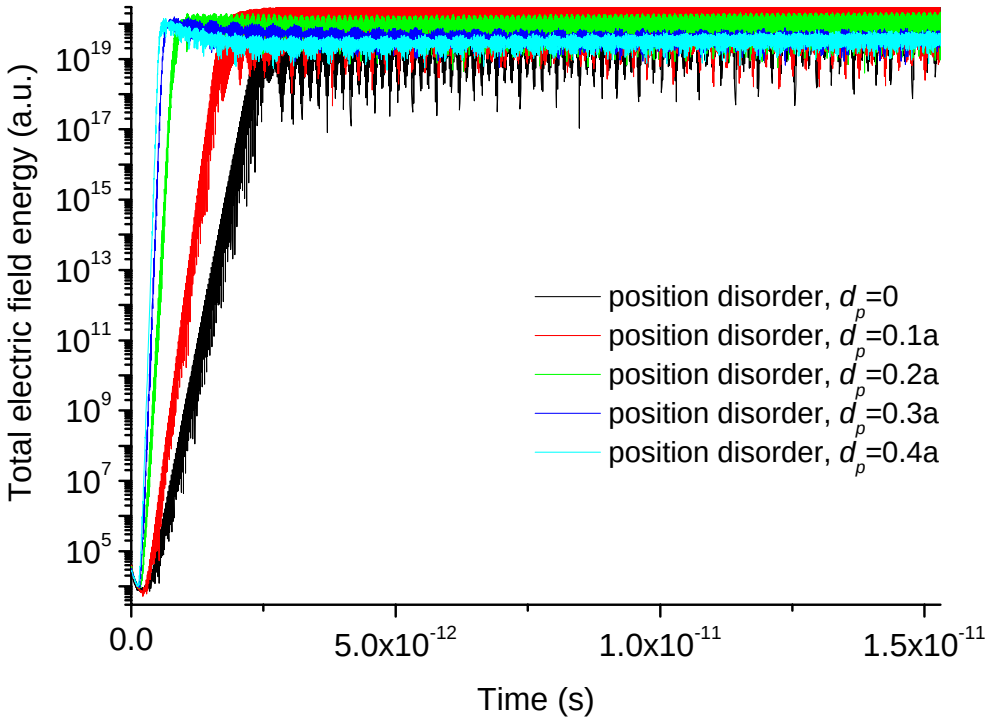

Figure 6.31 Time evolution of the total electric field energy of the active disordered systems with λ_t = 650nm. Lattice constant a is 200nm.

6.4 Summary

In this chapter, the disorder effects on the active disordered media have been investigated in a numerical approach. The numerical experiments were preformed based on a two-dimensional (2D) active disordered dielectric system with circular dielectric scattering particles.

The amplification process of active disordered systems was investigated. It has been found that the amplification curve is following an exponential relation. The exponential growth of total field energy and the dramatic drop of population difference density are the evidences of laser emission. It is observed that laser emissions are suppressed by the photonic band gap. By increasing the amount of

disorder, the strength of amplification of EM wave can be enhanced. The laser emission can also be modified by alternating the relative spectral position of the band gap and the gain profile. The results implicate that the laser emission can be actively controlled by varying the amount of the disorder and the central wavelength of gain profile.

CHAPTER 7

CONCLUSIONS AND RECOMMENDED FUTURE WORK

7.1 Conclusions

A theoretical investigation has been carried out on 2D passive and active disordered dielectric systems with circular inclusions, based on the time-dependent Maxwell's equations combined a semi-classical laser theory. This approach is adequate to analyse the optical properties of passive and active disordered media with arbitrary scattering structures. The Maxwell's equations coupled with the rate equations of electronic population of a four-level electronic system are solved numerically by using with finite-difference time-domain method. The following have been determined: the emission spectra, time evolution of electromagnetic fields and spatial distribution of eigen-modes of passive disordered media, the lasing modes and the electronic population of atomic levels of active disordered media. Numerical simulations have been carried out to compare with the published results of other research groups. The present simulation results are in agreement with the experimental and simulation results of other research groups in both passive and active media.

In addition to the theoretical investigation, experiments were conducted with

polymeric colloid liquid and solid random laser systems, their laser emission were explored. In the course of the research, several significant conclusions have been drawn, which represent original contributions to knowledge in the area of optical material systems. These are summarized as follows:

7.1.1 Disorder effect on photonic band gap deformation

Among various two-dimensional passive periodic dielectric systems with different scattering particle density, photonic band gaps are demonstrated in the most densely packed systems (scattering particle density = $2x10^{13}m^{-2}$). The dependence of the photonic band gap deformation on the position and size disorder is systemically examined. In order to introduce the position and size disorder into the periodic system with circular inclusions, the positions and the radius of each scattering particle are randomized with a moderate degree, respectively. The bandwidth of the photonic band gaps decreases as the amount of position and size disorder increase. When a high amount of disorder is introduced into the periodic system, the photonic band gaps diminish. The phenomenon can be understood in term of defect modes induced by the disorder. The spatial and radial perturbations of scattering particles sitting on the regular lattice points create defects in the periodic systems and thereby extra states may be created in the band gap. Consequently, extra states are induced and the size of

the band gaps becomes smaller when the disorder is intensified. The numerical results also confirm that the effect of the size disorder on the photonic band gap is more serious than that of the position disorder. It is shown that the photonic band gap is very robust against the presence of position disorder and the induced states appear close to the band edge. For the case of size disorder, states can appear well inside the gap with a relatively smaller amount of disorder. This is in agreement with the previously published results by others.

7.1.2 Disorder effect on electromagnetic wave localization

The localization of electromagnetic waves are achieved in both passive and active disordered systems when the periodic structure transits to the highly disorder structure. The regular and symmetrical field distribution patterns are demonstrated in the two-dimensional periodic systems due to coherent feedback from the periodic structure. As the amount of disorder increases, the regular pattern is destroyed and high intensity spots are emerged randomly in the disordered systems. The high intensity spots in the field distribution pattern provide an evidence of the existence of localized modes. It suggests that the effect of disorder can enhance the confinement of EM waves in passive and active disordered dielectric media as the localized modes are more easily to be

created in the highly disordered media. Furthermore, the lasing emission can be facilitated in highly disordered active system due to the short localization length and long residence time of the localized modes.

7.1.3 Disorder effect on lasing emission

The amplification processes in active ordered and disordered systems have been analyzed in term of the total field energy and the population difference density of the electronic systems. The energy-time curve is an exponential function. The exponential growth of the total field energy and the dramatic drop of population difference density unambiguously show the occurrence of the laser emission in active disordered systems.

Light amplification is suppressed by the photonic band gap in a densely packed disordered active system, when the gain profile of the active material overlaps with the photonic band gap. Emission modes emerge close to the edge of the band gap rather than the central frequency of gain profile of active material. By controlling the amounts of disorder, the amplification rate of EM wave can be reinforced in active disordered systems because of the vanished band gap. The emission modes shift to the central frequency of gain profile.

The laser emission can also be modified by alternating the relative spectral position of the band gap and the gain profile. The results imply that the laser emission can be actively controlled by varying the amount of the disorder and the central wavelength of gain profile.

7.1.4 Characterization of lasing emission in random laser system

Liquid and solid random laser systems have been fabricated and studied. Coherent and incoherent laser emission exhibit in the colloid dye solution consisting of Coumarin 480 and TiO_2 nano-particles and PMMA films doped with Rhodamine 590 and TiO2 nano-particles. The structure of the PMMA composite films was investigated by using optic microscopy and scanning probe microscopy. Single particles and clusters with multiple particles are found and distributed randomly on the surface of PMMA films. In the photoluminescence experiments, the lasing threshold and saturation behavior are demonstrated in the PMMA composite films while the saturation effect is absent in the colloid solution within the experimental range. The existent of lasing threshold is corroborated by experimental observations such as the dramatic reduction of line-width and intensification of the intensity of the emission peak. Discrete peaks emerge in the emission spectra of the PMMA composite films when the

pump energy was over the lasing threshold. This is a direct consequence of random laser emission with coherent feedback of the random laser system.

7.2 Project significance

This project is concerned with the behavior of EM waves in the intermediate regime between perfect order and disorder structure, where little have been known previously in the literature It is valuable to investigate the interplay between the disorder effect and the photonic band gap in active random media. In the current study, extensive computational work shows that the degree of disorder is crucial to compensate the detrimental effect of the photonic band gap in photonic crystals with optical gain. The results of numeric simulation unambiguously demonstrate the lasing mode shifting in active disordered media under the influence of the photonic band gap deformation. By modifying the uniformity of the scattering element of the periodic system with optical gain, the gain and lasing frequency can be selectively excited that may open up the possibility of active wavelength tuning in photonic device. It will bring great benefits to the development of new photonic fiber. It will contribute to the development of new technologies of smart textile and highly value-added products such as light emitting fibers and flexible fabric displays.

7.3 Recommended future work

The major objectives of this thesis have been achieved. However, further work should be considered to develop a more comprehensive method for analyzing the mechanism of light amplification in polymeric composite systems. The following aspects are suggestions for future work:

7.3.1 Active disordered metallic system

In the current research, the studies only focus on the disordered dielectric systems because of time limitation. Further investigation of random laser emission should be extended to the active disordered metallic system based on the established theoretical framework and FDTD method. Recently, random lasers have been reported in a dye solution consisting nanometer-sized metallic silver particles (Dice, Mujumdar and Elezzabi, 2005). Compared to dielectric particles with the same size, the scattering cross section of the metallic silver particles is enhanced due to the surface phamsons. The collective scattering strength and the gain volume of the system are also intensified, which facilitates the reduction of lasing threshold. Thus, it is valuable to study the origin of the enhancement of light amplification caused by the surface phamson of metallic

particles. Investigations should address the relationship between the surface phamson and light confinement. The time-dependent theory of random laser and modified FDTD methods should be extended in order to predict the surface phamson effect on the random laser emission of the metallic systems.

7.3.2 Simulation of three-dimensional (3D) active disordered system

The localization of EM wave in 2D active disordered systems has been demonstrated in the current study by using a numerical simulation framework. If the simulation of 3D active disordered system is built up, random laser emission and light confinement in active disordered systems can be manifested and comparable to the real random laser systems. Hence, it is a challenging task to simulate the light localization in 3D active disordered systems by using 3D FDTD technique because of a very high demand on the computer resource and time.

REFERENCES

AHMED, S. A., ZANG, Z.-W., YOO, K. M., ALI, M. A. & ALFANO, R. R. (1994) Effect of multiple light scattering and self-absorption on the fluorescence and excitation spectra of dye in random media. *Applied Optics,* 33**,** 2746.

ANDERSON, P. W. (1958) Absence of diffusion in certain random lattices. *Physical Review,* 109**,** 1492.

ANNI, M., LATTANTE, S., CINGOLANI, R., GIGLI, G., BARBARELLA, G. & FAVARETTO, L. (2003) Far-field emission and feedback origin of random lasing in oligothiophene dioxide neat films. *Applied Physics Letters,* 83**,** 2754.

ANNI, M., LATTANTE, S., CINGOLANI, R., GIGLI, G., BARBARELLA, G. & FAVARETTO, L. (2004) Emission properties of organic random lasers. *Phys. stat. sol. (c),* 1**,** 450.

ANNI, M., LATTANTE, S., STOMEO, T., CINGOLANI, R. & GIGLI, G. (2004) Modes interaction and light transport in bidimensional organic random lasers in the weak scattering limit. *Physical Review B,* 70**,** 195216.

BAHOURA, M., MORRIS, K. J. & NOGINOV, M. A. (2002) Threshold and slope efficiency of $Nd_{0.5}La_{0.5}Al_3(BO_3)_4$ ceramic random laser: effect of the pumped spot size. *Optics Communications,* 201**,** 405.

BAHOURA, M., MORRIS, K. J., ZHU, G. & NOGINOV, M. A. (2005) Dependence of the neodymium random laser threshold on the diameter of the pumped spot. *IEEE Journal of Quantum Electronics,* 41**,** 677.

BALACHANDRAN, R. M. & LAWANDY, N. M. (1995) Interface reflection effects in photonic paint. *Optics Letters,* 20**,** 1271.

BALACHANDRAN, R. M., LAWANDY, N. M. & MOON, J. A. (1997) Theory of laser action in scattering gain media. *Optics Letters,* 22**,** 319.

BALACHANDRAN, R. M., PACHECO, D. P. & LAWANDY, N. M. (1996a) Laser action in polymeric gain media containing scattering particles. *Applied Optics,* 35**,** 640.

BALACHANDRAN, R. M., PACHECO, D. P. & LAWANDY, N. M. (1996b) Photonic textile fibers. *Applied Optics,* 35**,** 1991.

BASS, M. (2002) *Fiber Optics Handbook: fiber, devices, and systems for optical communications,* USA, The McGraw-Hill Companies, Inc.

BERENGER, J. P. (1995) *Journal of Computational Physics,* 115**,** 185.

BERGER, G. A., KEMPE, M. & GENACK, A. Z. (1997) Dynamics of stimulated emission from random media. *Physical Review E,* 56**,** 6118.

BURIN, A. L., CAO, H. & RATNER, M. A. (2003) Two Photon Pumping of a Random Laser. *IEEE Journal of selected topics in quantum electronics,* 9**,** 124.

BURIN, A. L., CAO, H. & RATNER, M. A. (2003) Understanding and control of random lasing. *Physica B,* 338**,** 212.

BURIN, A. L., RATNER, M. A., CAO, H. & CHANG, S. H. (2002) Random laser in one dimension. *Physical Review Letter,* 88**,** 093904.

CAO, H., LING, Y., XU, J. Y., BURIN, A. L. & CHANG, R. P. H. (2003) Lasing with resonant feedback in random media. *Physica B,* 338**,** 215.

CAO, H., XU, J. Y., CHANG, S. H. & HO, S. T. (2000) Transition from Amplified Spontaneous Emission to Laser Action in Strongly Scattering Media. *Physical Review E,* 61**,** 1985.

CAO, H., XU, J. Y., CHANG, S. H., HO, S. T., SEELIG, E. W., LIU, X. & CHANG, R. P. H. (2000) Spatial Confinement of Laser Light in Active Random Media. *Physical Review Letter,* 84**,** 5584.

CAO, H., XU, J. Y., LING, Y., BURIN, A. L., SEELING, E. W., LIU, X. & CHANG, R. P. (2003) Random Laser With Coherent Feedback. *IEEE Journal of selected topics in quantum electronics,* 9**,** 111.

CAO, H., XU, J. Y., SEELIG, E. W. & CHANG, R. P. H. (2000) Microlaser made of disordered media. *Applied Physics Letters,* 76**,** 2997.

CAO, H., ZHAO, Y. G., HO, S. T., SEELIG, E. W., WANG, Q. H. & CHANG, R. P. H. (1999) Random laser action in semiconductor powder. *physical Review Letter,* 82**,** 2278.

CAO, H., ZHAO, Y. G., ONG, H. C. & CHANG, R. P. H. (1999) Far-field Characteristics of Random Lasers. *Physical Review B,* 59**,** 15107.

CAO, H., ZHAO, Y. G., ONG, H. C., HO, S. T., DAI, J. Y., WU, J. Y. & CHANG, R. P. H. (1998) Ultraviolet Lasing in Resonators Formed by Scattering in Semiconductor Polycrystalline Films. *Applied Physics Letters,* 73**,** 3656.

CHANG, S. H., CAO, H. & HO, S. T. (2003) Cavity Formation and Light Propagation in Partially Ordered and Completely Random One-Dimensional Systems. *IEEE Journal of Quantum Electronics,* 39**,** 364.

DIAZ-GARCIA, M. A., HIDE, F., SCHWARTZ, B. J. & ANDERSSON, M. R. (1997) Plastic lasers: Semiconducting polymers as a new class of solid-state laser materials. *Synthetic Metals,* 84**,** 455.

DICE, G. D., MUJUMDAR, S. & ELEZZABI, A. Y. (2005) Plasmonically enhanced diffusive and subdiffusive metal nanoparticle-dye random laser. *Applied Physics Letters,* 86**,** 131105.

DU, W. C., TAO, X. M. & TAM, H. Y. (1999) Fiber Bagg grating cavity sensie for simultaneous measurement of strain and temperature. *IEEE Photonics Technology Letters,* 44**,** 105.

ERADAT, N., SHKUNOV, M. N., FROLOV, S. V., GELLERMANN, W., VARDENY, Z. V., ZAKHIDOV, A. A., BAUGHMA, R. H. & YOSHINO, K. (1999) Laser action of doo-ppv and rhodamine 590; a comparison. *Synthetic Metals,* 101**,** 206.

FAN, S., VILLENEUVE, P. R. & JOANNOPOULOS, J. D. (1995) Theoretical investigation of fabrication-related disorder on the properties of photonic crystals. *Journal of Applied Physics*, 78**,** 1415.

FENG, Y., BISSON, J.-F., LU, J., HUANG, S., TAKAICHI, K., SHIRAKAWA, A., MUSHA, M. & UEDA, K.-I. (2004) Thermal effects in quasi-continuous-wave Nd^{3+}:$Y_3Al_5O_{12}$ nanocrystalline-powder random laser. *Applied Physics Letters,* 84**,** 1040.

FLORESCU, L. & JOHN, S. (2004) Lasing in a random amplifying medium: Spatiotemporal characteristics and nonadiabatic atomic dynamics. *Physical Review E,* 70**,** 036607.

FROLOV, S. V., OZAKI, M., GELLERMANN, W., VARDENY, Z. V. & YOSHINO, K. (1996) Mirrorless lasing conducting polymer poly(2,5-dioctyloxy -pphenylevinylene) films. *Japanese Journal of Applied Physics., Part 2,* 35**,** L1371.

FROLOV, S. V., SHKUNOV, M., FUJII, A., YOSHINO, K. & VARDENY, Z. V. (2000) Lasing and Stimulated Emission in π-Conjugated Polymers. *IEEE Journal of Quantum Electronics,* 36**,** 2.

FROLOV, S. V., VARDENY, Z. V., YOSHINO, K., ZAKHIDOV, A. & BAUGHMAN, R. H. (1999) Stimulated emission in high-gain organic media. *Physical Review B,* 59**,** R5284.

GOUEDARD, C., HUSSON, D., SAUTERET, C., AUZEL, F. & MIGUS, A. (1993) Generation of spatially incoherent short pulses in laser-pumped neodymiun stoichiometric crystals and powders. *Journal of the Optical Society of America B,* 10**,** 2362.

GRADEčAK, S., QIAN, F., LI, Y., PARK, H.-G. & LIEBER, C. M. (2005) GaN nanowire lasers with low lasing thresholds. *Applied Physics Letters,* 87**,** 173111.

GU, Z.-H. & PENG, G. D. (2000) Amplification of enhanced backscattering from a dye-doped polymer bounded by a rough surface. *Optical Letters,* 25**,** 375.

GU, Z.-H. & PENG, G.-D. (2001) Enhanced backscattering from organic laser gain media bounded with rough gold films. *Applied Optics,* 40**,** 24.

GU, Z.-H., LU, J. Q., MARTINEZ, A., MENDEZ, E. R. & MARADUDIN, A. A. (1994) Enhanced backscattering from a one-dimensional rough dielectric film on a glass substrate. *Optical Letters,* 19**,** 604.

GUO, S. & ALBIN, S. (2003) Numerical techniques for excitation and analysis of defect modes in photonic crystals. *Optics Express,* 11**,** 108.

HAN, X., WANG, G., WANG, Q., CAO, L., LIU, R., ZOU, B. & HOU, J. G. (2005) Ultraviolet lasing and time-resolved photoluminescence of well-aligned ZnO nanorod arrays. *Applied Physics Letters,* 86**,** 223106.

HAWKINS, R. J. & KALLMAN, J. S. (1993) Linear electronic dispersion and finite-difference time-domain calculations: a simple approach. *Journal of Lightwave Technology,* 11**,** 1872.

HIDE, F., DIAZ-GARCIA, M. A., SCHWARTZ, B. J. & ANDERSSON, M. R. (1996) Semiconducting polymers: A new class of solid-state laser materials. *Science,* 273**,** 1833.

HIDE, F., DIAZ-GARCIA, M. A., SCHWARTZ, B. J. & HEEGER, A. J. (1997) New Developments in the Photonic Applications of Conjugated Polymers. *Accounts of Chemical Research,* 30**,** 430.

HIDE, F., SCHWARTZ, B. J., DIAZ-GARCIA, M. A. & HEEGER, A. J. (1997) Conjugated polymers as solid-state laser materials. *Synthetic Metals,* 91**,** 35.

HILL, K. O. & FUJII, Y. (1978) Photosensitivity in optical fiber waveguides, application to reflection filter fabrcation. *Applied Physics Letters,* 32**,** 647.

HSU, H.-C., WU, C.-Y. & HSIEH, W.-F. (2005) Stimulated emission and lasing of random-growth oriented ZnO nanowires. *Journal of Applied Physics,* 97**,** 64315.

JéZéQUEL, D., GUENOT, J., JOUINI, N. & FIéVET, F. (1995) Submicrometer zinc oxide particles: Elaboration in polyol medium and morphological characteristics. *Journal of Materials Research,* 10**,** 77.

JIANG, X. Y. & SOUKOULIS, C. M. (2000) Time dependent theory for random lasers. *Physical Review Letter,* 85. 70

JIANG, X. Y. & SOUKOULIS, C. M. (2001) *Photonic Crystals and Light Localization,* Kluwer Publish.

JIANG, X. Y. & SOUKOULIS, C. M. (2002) Localized random lasing modes and a path for observing localization. *Physical Review E,* 65**,** 25601.

JOHN, S. & PANG, G. (1996) Theory of lasing in a multiple-scattering medium. *physical Review A,* 54**,** 3642.

JOHN, S. (1984) Electromagnetic Absorption in a Disordered Medium near a Photon Mobility Edge. *Physical Review Letter,* 53**,** 2169.

JOHN, S. (1987) Strong localization of photons in certain disordered dielectric superlattices. *Physical Review Letter,* 58**,** 2486.

JOHN, S. (1991) Localization of Light. *Physics Today,* 44**,** 32.

KERSEY, A. D. (1996) A review if recent developments in fiber optic sensor technology. *Macromolecular Chemistry and Physics,* 2**,** 291.

KOPP, V. I., GENACK, A. Z. & ZHANG, Z. Q. (2001) Large Coherence Area Thin-Film Photonic Stop-Band Lasers. *Physical Review Letter,* 93**,** 13602.

LAI, C. W., AN, J. & ONG, H. C. (2005) Surface-plasmon-mediated emission from metal-capped ZnO thin films. *Applied Physics Letters,* 86**,** 251105.

LAU, S. P., YANG, H. Y., YU, S. F., LI, H. D., TANEMURA, M., OKITA, T., HATANO, H. & HNG, H. H. (2005) Laser action in ZnO nanoneedles selectively grown on silicon and plastic substrates. *Applied Physics Letters,* 87**,** 13104.

LAU, S. P., YANG, H. Y., YU, S. F., YUEN, C., LEONG, E. S. P., LI, H. & HNG, H. H. (2005) Flexible ultraviolet Random Lasers Based on Nanoparticles. *Nanoparticle Lasers,* 1**,** 956.

LAWANDY, N. M., BELACHANDRAN, R. M., GOMES, A. S. L. & SAUVIN, E. (1994) Laser action in strongly scattering media. *Nature,* 368**,** 436.

LEE, C. W., WONG, K. S., HUANG, J. D., FROLOV, S. V. & VARDENY, Z. V. (1999) Femtosecond time-resolved laser action in poly(p-phenylene vinylene) films: stimulated emission in an inhomogeneously broadened exciton distribution. *Chemical Physics Letters,* 314**,** 564.

LEONG, E. S. P., YU, S. F., ABIYASA, A. P. & LAU, S. P. (2006) Polarization characteristics of ZnO rib waveguide random lasers. *Applied Physics Letters,* 88**,** 91116.

LETOKHOV, V. S. (1967) Stimulated emission of an ensemble of scattering particles with negative absorption. *Sov. Phys. JETP,* 5**,** 212.

LETOKHOV, V. S. (1968) Generation of light by a scattering medium with negative resonance absorption. *Sov. Phys. JETP,* 26**,** 835.

LI, Z.-Y., ZHANG, X. & ZHANG, Z.-Q. (2000) Disordered photonic crystals understood by a perturbation formalism. *Physical Review B,* 61**,** 15738.

LING, Y., CAO, H., BURIN, A. L., RATNER, M. A., LIU, X., SEELIG, E. W. & CHANG, R. P. H. (2001) Investigation of random lasers with resonant feedback. *Physical Review A,* 64**,** 063808.

LIU, B., YAMILOV, A., LING, Y., XU, J. Y. & CAO, H. (2003) Dynamic Nonlinear effect on lasing in a random media. *Physical Review Letter,* 91**,** 063903.

LIU, C., LIU, J., ZHANG, J. & DOU, K. (2005) Random lasing with scatterers of diameters 20 nm in an active medium. *Optics Communications,* 244**,** 299.

LIU, X., YAMILOV, A., WU, X., ZHENG, J.-G., CAO, H. & CHANG, R. P. H. (2004) Effect of ZnO Nanostructures on 2-Dimensional Random Lasing Properties. *Chemistry of Materials,* 16**,** 5414.

LV, Y., LI, C., GUO, L., WANG, Q., WANG, R., XU, H., YANG, S., AI, X. & ZHANG, J. (2005) Nanostructured stars of ZnO microcrystals with intense stimulated emission. *Applied Physics Letters,* 87**,** 163103.

MARKUSHEV, V. M., ZOLIN, V. F. & BRISKINA, C. M. (1986) Luminescence and stimulated emission of neodymium in sodium lanthanum molybdate powders. *Sov. J. Quant. Electron.,* 16**,** 281.

MITRA, A. & THAREJA, R. K. (2001) Photoluminescence and ultraviolet laser emission from nanocrystalline ZnO thin films. *Journal of Applied Physics,* 89**,** 2025.

MOTT, N. F. (1974) *Metal-Insulator Transitions,* London, Taylor and Francis.

MUJUMDAR, S., RICCI, M., TORRE, R. & WIERSMA, D. S. (2004) Amplified Extended Modes in Random Lasers. *Physical Review Letter,* 93**,** 53903.

NAGRA, A. S. & YORK, R. A. (1998) FDTD Analysis of Wave Propagation in Nonlinear Absorbing and Gain Media. *IEEE Transactions on Antennas and Propagation,* 46**,** 334.

NIKITENKO, V. N., TERESCHENKO, A. I., KUZ'MINA, I. P. & LOBACHEV, A. N. (1981) Stimulated emission of ZnO at high level of single photon excitation. *Optika i Specktroskopiya,* 50**,** 605.

NOGINOV, M. A., NOGINOVA, N. E., CAULFIELD, H. J., VENKATESWARLU, P. & MAHDI, M. (1995) Line narrowing in the dye solution with scattering centers. *Optics Communications,* 118**,** 430.

NOGINOV, M. A., NOGINOVA, N. E., CAULFIELD, H. J., VENKATESWARLU, P., THOMPSON, T., MAHDI, M. & OSTROUMOV, V. (1996) Short-pulsed stimulated emission in the powders of $NdAl_3(BO_3)_4$, $NdSc_3(BO_3)_4$, and $Nd:Sr_5(PO_4)_3F$ laser crystals. *Journal of the Optical Society of America B,* 13**,** 2024.

NOGINOV, M. A., ZHU, G., FOWLKES, I. & BAHOURA, M. (2004) GaAs random laser. *Laser Physical Letter,* 1**,** 291.

NOGINOV, M. A., ZHU, G., FRANTZ, A. A., NOVAK, J., WILLIAMS, S. N. & FOWLKES, I. (2004) Dependence of $NdSc_3(BO_3)_4$ random laser parameters on particle size. *Journal of the Optical Society of America B,* 21**,** 191.

NOGINOV, M., NOVAK, J., GRIGSBY, D., ZHU, G. & BAHOURA, M. (2005) Optimization of the transport mean free path and the absorption length in random lasers with non-resonant feedback. *Optics Express,* 13**,** 8829.

ONG, H. C., DAI, J. Y., LI, A. S. K., DU, G. T., CHANG, R. P. H. & HO, S. T. (2001) Effect of a microstructure on the formation of self-assembled laser cavities in polycrystalline ZnO. *Journal of Applied Physics,* 90**,** 1663.

PARK, W. I., KIM, D. H., JUNG, S.-W. & YI, G.-C. (2002) Metalorganic vapor-phase epitaxial growth of vertically well-aligned ZnO nanorods. *Applied Physics Letters,* 80**,** 4232.

PATRA, M. (2003) Influence of spatial correlations on the lasing threshold of random lasers. *Physical Review E,* 67**,** 65603.

PENG, G.-D. & GU, Z.-H. (1999) Amplified backscattering from a rough surface through dye-doped polymer. *Proceedings of SPIE-The International Society for Optical Engineering.* SPIE-The International Society for Optical Engineering.

PENG, G.-D. & GU, Z.-H. (2000) Amplified backscattering from dye-doped polymer bounded with 1D rough metal film. *Proceedings of SPIE-The International Society for Optical Engineering (2000).* Kensington, Australia.

PINHEIRO, F. A. & SAMPAIO, L. C. (2006) Lasing threshold of diffusive random lasers in three dimensions. *Physical Review A,* 73**,** 13826.

POLSON, R. C. & VARDENY, Z. V. (2003) Random lasing in dye-TiO2 solutions and π-conjugated polymer films. *Physica B,* 338**,** 219.

POLSON, R. C. & VARDENY, Z. V. (2004) Random lasing in human tissues. *Applied Physics Letters,* 85**,** 1289.

POLSON, R. C. & VARDENY, Z. V. (2005) Organic random lasers in the weak-scattering regime. *Physical Review B,* 71**,** 45205.

POLSON, R. C., HUANG, J. D. & VARDENY, Z. V. (2001a) Analysis of random lasers in thin films of π-conjugated polymers. *Photonic Crystals and Light Localization in the 21 st Century.* Kluwer: Dordrech, The Netherlans.

POLSON, R. C., HUANG, J. D. & VARDENY, Z. V. (2001b) Random lasers in π-conjugated polymer films. *Synthetic Metals,* 119**,** 7.

POLSON, R. C., RAIKH, M. E. & VARDENY, Z. V. (2002) Random lasing from weakly scattering media; spectrum universality in DOO–PPV polymer films. *Physica E,* 13**,** 1240.

PRASAD, B. R., RAMACHANDRAN, H., SOOD, A. K., SUBRAMANIAN, C. K. & KUMAR, N. (1997) Lasing in active, sub-mean-free path-sized systems with dense, random, weak scatterers. *Applied Optics,* 30**,** 7718.

QIU, M. & HE, S. (2000) Numerical method for computing defect modes in two-dimensional photonic crystals with dielectric or metallic inclusions. *Physical Review B,* 61**,** 12871.

QIU, Z., WONG, K. S., WU, M., LIN, W. & XU, H. (2004) Microcavity lasing behavior of oriented hexagonal ZnO nanowhiskers grown by hydrothermal oxidation. *Applied Physics Letters,* 84**,** 2739.

QUOCHI, F., CORDELLA, F., ORRU`, R., COMMUNAL, J. E., VERZEROLI, P., MURA, A. & BONGIOVANNI, G. (2004) Random laser action in self-organized para-sexiphenyl nanofibers grown by hot-wall epitaxy. *Applied Physics Letters,* 84**,** 4454.

RUSEK, M. & ORŁOWSKI, A. (1995) Analytical approach to localization of electromagnetic waves in two-dimensional random media. *Physical Review E,* 51**,** R2763.

SCHAFER, F. P. (1977) *Dye Lasers,* Berlin, Heidelberg, New York, Springer-Verlag.

SCHMIDTKE, J., STILLE, W. & FINKELMANN, H. (2003) Defect Mode Emission of a Dye Doped Cholesteric Polymer Network. *Physical Review Letter,* 90**,** 83902.

SEBBAH, P. & VANNESTE, C. (2002) Random laser in the localized regime. *Physical Review B,* 66**,** 144202.

SFEZ, B. G. & KOTLER, Z. (1997) Lasing action from random media with gain. *Optical Materials,* 7**,** 1.

SHA, W. L., LIU, C. H. & ALFANO, R. R. (1994) Spectral and temporal measurements of laser action of rhodamine 640 dye in strongly scattering media. *Optics Letters,* 19**,** 1922.

SHA, W. L., LIU, C. H., LIU, F. & ALFANO, R. R. (1996) Competition between two lasing modes of Sulforhodamine 640 in highly scattering media. *Optics Letters,* 21**,** 1277.

SIDDIQUE, M., ALFANO, R. R., BERGER, G. A., KEMPE, M. & GENACK, A. Z. (1996) Time-resolved studies of stimulated emission from colloidal dye solutions. *Optics Letters,* 21**,** 450.

SIEGMAN, A. E. (1986) *Lasers,* California, Mill Valley, CA: Univ. Sci. Books.

SIEGMAN, A. E. (1986) *Lasers,* California, Mill Valley, CA: Univ. Sci. Books.

SIGALAS, M. M., SOUKOULIS, C. M., CHAN, C. T. & TURNER, D. (1996) Localization of electromagnetic waves in two-dimensional disordered systems. *Physical Review B,* 53**,** 8340.

SOBEL, F., GINDRE, D., NUNZI, J.-M., DENIS, C., DUMARCHER, V., FIORINI-DEBUISSCHERT, C., KRETSCH, K. P. & ROCHA, L. (2004) Multimode distributed feedback laser emission in a dye-doped optically pumped polymer thin-film. *Optical Materials*.

SOEST, G. V., POELWIJK, F. J. & LAGENDIJK, A. (2002) Speckle experiments in random lasers. *Physical Review E,* 65**,** 46603.

SOEST, G. V., TOMITA, M. & LAGENDIJK, A. (1999) Amplifying volume in scattering media. *Optics Letters,* 24**,** 306.

SOUKOULIS, C. M., JIANG, X., XU, J. Y. & CAO, H. (2002) Dynamic response and relaxation oscillation in random lasers? *Physical Review B,* 65**,** R41103.

STASSINOPOULOS, A., DAS, R. N., GIANNELIS, E. P., ANASTASIADIS, S. H. & ANGLOS, D. (2005) Random lasing from surface modified films of zinc oxide nanoparticles. *Applied Surface Science,* 247**,** 18.

SUN, B. Q. & JIANG, D. S. (2006) Photon localization and lasing in disordered GaN_xAs_{1-x} optical superlattices. *Physical Review B,* 73**,** 195112.

SUN, B. Q., GAL, M., GAO, Q., TAN, H. H., JAGADISH, C., PUZZER, T., OUYANG, L. & ZOU, J. (2003) Epitaxially grown GaAsN random laser. *Journal of Applied Physics,* 93**,** 5855.

TAFLOVE, A. & BRODWIN, M. E. (1975) Numerical Solution of Steady-State Electromagnetic Scattering Problems Using the Time-Dependent Maxwell's Equations. *IEEE Transactions on Microwave Theory and Techniques,* 23**,** 623.

TAFLOVE, A. & HAGINESS, S. C. (2000) *Computational Electrodynamics: The Finite-Difference Time Domain Method,* London, Attech House Boston.

TAFLOVE, A. (1995) *Computational Electrodynamics: The Finite-Difference Time-Domain Method,* Norwood, Artech House.

TAO, X. M. (2001) *Smart Fibers, Fabrics and Textiles, Fundamental and Application,* Cambridge, UK, Woodhead Publishing Ltd.

THAREJA, R. K. & MITRA, A. (2000) Random laser action in ZnO. *Applied Physics B,* 71**,** 181.

TONG, M., SHENG, C. X., YANG, C., VARDENY, Z. V. & PANG, Y. (2004) Photoexcitation dynamics and laser action in solutions and films of PPE-PPV copolymer. *Physical Review B,* 69**,** 155211.

VANNESTE, C. & SEBBAH, P. (2001) Selective Excitation of Localized Modes in Active Random Media. *Physical Review Letter,* 87**,** 183903.

VILLENEUVE, P. R., FAN, S. & JOANNOPOULOS, J. D. (1996) Microcavities in photonic crystals: Mode symmetry, tunability, and coupling efficiency. *Physical Review B,* 54**,** 7837.

VUTHA, A. C., TIWARI, S. K. & THAREJA, R. K. (2006) Random laser action in ZnO doped polymer. *Journal of Applied Physics,* 99**,** 123509.

WANG, C. & LIU, J. (2006) Polarization dependence of lasing modes in two-dimensional random lasers. *Physics Letters A,* 353**,** 269.

WANG, H., LIU, J. & YUAN, X. (2005) Effect of gain lineshape on amplification of localized modes in active random media. *Journal of Modern Optics,* 52**,** 1309.

WATANABE, H., OKI, Y., MAEDA, M. & OMATSU, T. (2005) Waveguide dye laser including a SiO₂ nanoparticle-dispersed random scattering active layer. *Applied Physics Letters,* 86**,** 151123.

WEICHEL, H. (1991) *Selected paper on laser design,* Washington, SPIE Optical Engineering Press.

WIERSMA, D. S. & LAGENDIJK, A. (1996) Light diffusion with gain in random lasers. *Physical Review E,* 54**,** 4256.

WU, C.-Y., HSU, H.-C., CHENG, H.-M., YANGA, S. & HSIEH, W.-F. (2006) Structural and optical properties of ZnO nanosaws. *Journal of Crystal Growth,* 287**,** 189.

XIA, R., HELIOTIS, G. & BRADLEY, D. D. C. (2003) Fluorene-based polymer gain media for solid-state laser emission across the full visible spectrum. *Applied Physics Letters,* 82**,** 3599.

XU, J. & XIAO, M. (2005) Lasing action in colloidal CdS/CdSe/CdS quantum wells. *Applied Physics Letters,* 87**,** 172117.

YABLONOVITCH, E. (1987) Inhibited Spontaneous Emission in Solid-State Physics and Electronics. *Physical Review Letter,* 58**,** 2059.

YAMILOV, A. & CAO, H. (2004) Highest-quality modes in disordered photonic crystals. *Physical Review A,* 69**,** 031803.

YAMILOV, A. & CAO, H. (2004a) Effects of localization and amplification on intensity distribution of light transmitted through random media. *Physical Review E,* 70**,** 037603.

YAMILOV, A. & CAO, H. (2004b) Highest-quality modes in disordered photonic crystals. *Physical Review A,* 69**,** 031803.

YAMILOV, A., WU, X., CAO, H. & BURIN, A. L. (2005) Absorption-induced confinement of lasing modes in diffusive random medium. *Optics Letters,* 30**,** 2430.

YEE, K. S. (1966a) *IEEE Trans. Antennas Propag.,* 14**,** 302.

YEE, K. S. (1966b) Numerical solution of initial boundary value problems involving Maxwell's equations in isotropic media. *IEEE Transactions on Antennas and Propagation,* 14**,** 302.

YU, S. F. & LEONG, E. S. P. (2004) High-power single-mode ZnO thin-film random lasers. *IEEE Journal of Quantum Electronics,* 40**,** 1186.

YU, S. F., YUEN, C., LAU, S. P. & LEE, H. W. (2004) Zinc oxide thin-film random lasers on silicon substrate. *Applied Physics Letters,* 84**,** 3244.

YU, S. F., YUEN, C., LAU, S. P., PARK, W. I. & YI, G.-C. (2004) Random laser action in ZnO nanorod arrays embedded in ZnO epilayers. *Applied Physics Letters,* 84**,** 3241.

YUEN, C., YU, S. F., LEONG, E. S. P., YANG, H. Y., LAU, S. P. & HNG, H. H. (2005) Formation Conditions of Random Laser Cavities in Annealed ZnO Epilayers. *IEEE Journal of Quantum Electronics,* 41**,** 970.

ZACHARAKIS, G., PAPADOGIANNIS, N. A. & PAPAZOGLOU, T. G. (2002) Random lasing following two-photon excitation of highly scattering gain media. *Applied Physics Letters,* 81**,** 2511.

ZHANG, D., CHENG, B., YANG, J., ZHANG, Y., HUI, W. & LI, Z. (1995) Narrow-bandwidth emission from a suspension of dye and scatterers. *Optics Communications,* 118**,** 462.

ZHANG, W., CUE, N. & YOO, K. M. (1995) Emission linewidth of laser action in random gain media. *Optics Letters,* 20**,** 961.

ZHANG, X. H., CHUA, S. J., YONG, A. M., LI, H. D., YU, S. F. & LAU, S. P. (2006) Exciton related stimulated emission in ZnO polycrystalline thin film deposited by filtered cathodic vacuum arc technique. *Applied Physics Letters,* 88**,** 191112.

ZHANG, Z. Q. (1995) Light amplification and localization in randomly layered media with gain. *Physical Review B,* 52**,** 7960.

APPENDIX

Program of the finite-difference time-domain (FDTD) modeling for active disordered system

The following program is used for calculating the emission spectrum, the time evolution of the electronic population of atomic levels, the electric and magnetic fields of two-dimensional (2D) disordered system with gain. The calculation is performed using FDTD method. A discretization of Maxwell's equations, polarization equation and rate equation in both the space and time domains leads to the finite difference equations (equation 3.39-3.46 in Chapter 3) linking the electric and magnetic fields and the electronic population of atomic levels at one time step to the next time step. After calculating the electric and magnetic fields in the time domain, Fourier transform is performed to obtain the power spectrum of the field signal. In the 2D FDTD simulation, the transverse-magnetic (TM) fields are absorbed in the perfectly matched layer (PML) boundary condition and terminated by prefect conducting boundary. The program is written in FORTRAN 90 and executed in Unix environment.

```
c*****************************************************************
c    This 2D FDTD TM code with PML absorbing boundary conditions calculates
c    the electric field, the magnetic field and electronic population of 2D
c    disordered system in time domain. The 2D system is a square size active
c    medium.
c*****************************************************************

c*****************************************************************
c    Fundamental constant declarations:
c    dx is sspatial increment, dt is time increment, nmax is total time step,
c    ie is the total number of grid point of x-direction, je is the total number of
c    grid point in y-direction, iebc is the number of grid point of the perfectly
c    matched layer in
c*****************************************************************
          MODULE Globals
          real, parameter :: cc=2.99792458e8
          real, parameter :: pi=3.141592653589793d0
          real, parameter :: muz=4*pi*(1.0e-7)
```

```
      real, parameter :: epsz=1.0/(cc*cc*muz)
      real, parameter :: dx=10.0e-9 !dt=2.36e-17
      real, parameter :: dt=dx/(1.414213562*cc)
      real, parameter :: lattice=20
      integer, parameter :: nmax=50002
      integer, parameter :: numx=18; numy=18
      integer, parameter :: rodn=numx*numy
      integer, parameter :: ie=402; je=402
      integer, parameter :: ib=ie+1; jb=je+1
      integer, parameter :: iebc=10; jebc=10
      integer, parameter :: ibbc=iebc+1; jbbc=jebc+1
      integer, parameter :: iefbc=ie+2*iebc; jefbc=je+2*jebc
      integer, parameter :: ibfbc=iefbc+1; jbfbc=jefbc+1
      END MODULE Globals

      Program ftdt
      use globals
      implicit none

c*************************************************************
c     Variables declarations:
c*************************************************************
      integer :: i,j,n,ij,nn,limit,tt,abc,gg
      integer :: is,orderbc,media
      real :: eps(4),sig(4),mur(4),sim(4)
      integer :: diam,halfd,icenter,jcenter
      real :: rmax,rtau,tau,delay
      real :: eaf,haf
      real :: delbc,sigmam,bcfactor
      real :: y1,y2,sigmay,sigmays
      real :: x1,x2,sigmax,sigmaxs
      real :: ca1,cb1,da1,db1
      real :: source(300)
      real :: ca(4),cb(4),da(4),db(4)
      real :: aa,bb
      real :: a(rodn),b(rodn)

c*************************************************************
```

```
c     Variables declarations and initializations for the coefficient of PML layer:
c*****************************************************************

      real :: dahy(1:ie,1:jb)=0.0; dbhy(1:ie,1:jb)=0.0
      real :: dahx(1:ib,1:je)=0.0; dbhx(1:ib,1:je)=0.0
      real :: caez(1:ib,1:jb)=0.0; cbez(1:ib,1:jb)=0.0
      real :: dahybcf(1:iefbc,1:jebc)=0.0; dbhybcf(1:iefbc,1:jebc)=0.0
      real :: dahybcl(1:iebc,1:jb)=0.0; dbhybcl(1:iebc,1:jb)=0.0
      real :: dahybcr(1:iebc,1:jb)=0.0; dbhybcr(1:iebc,1:jb)=0.0
      real :: dahybcb(1:iefbc,1:jbbc)=0.0; dbhybcb(1:iefbc,1:jbbc)=0.0
      real :: dahxbcf(1:ibfbc,1:jebc)=0.0; dbhxbcf(1:ibfbc,1:jebc)=0.0
      real :: dahxbcl(1:iebc,1:je)=0.0; dbhxbcl(1:iebc,1:je)=0.0
      real :: dahxbcr(1:ibbc,1:je)=0.0; dbhxbcr(1:ibbc,1:je)=0.0
      real :: dahxbcb(1:ibfbc,1:jebc)=0.0; dbhxbcb(1:ibfbc,1:jebc)=0.0
      real :: caezxbcf(1:ibfbc,1:jebc)=0.0; cbezxbcf(1:ibfbc,1:jebc)=0.0
      real :: caezxbcl(1:iebc,1:jb)=0.0; cbezxbcl(1:iebc,1:jb)=0.0
      real :: caezxbcr(1:ibbc,1:jb)=0.0; cbezxbcr(1:ibbc,1:jb)=0.0
      real :: caezxbcb(1:ibfbc,1:jbbc)=0.0; cbezxbcb(1:ibfbc,1:jbbc)=0.0
      real :: caezybcf(1:ibfbc,1:jebc)=0.0; cbezybcf(1:ibfbc,1:jebc)=0.0
      real :: caezybcl(1:iebc,1:jb)=0.0; cbezybcl(1:iebc,1:jb)=0.0
      real :: caezybcr(1:ibbc,1:jb)=0.0; cbezybcr(1:ibbc,1:jb)=0.0
      real :: caezybcb(1:ibfbc,1:jbbc)=0.0; cbezybcb(1:ibfbc,1:jbbc)=0.0
      real :: hy(1:ie,1:jb)=0.0,hx(1:ib,1:je)=0.0; ez(1:ib,1:jb)=0.0
      real :: nhy(1:ie,1:jb)=0.0,nhx(1:ib,1:je)=0.0; nez(1:ib,1:jb)=0.0
      real :: hybcf(1:iefbc,1:jebc)=0.0; hxbcf(1:ibfbc,1:jebc)=0.0
      real :: nhybcf(1:iefbc,1:jebc)=0.0; nhxbcf(1:ibfbc,1:jebc)=0.0
      real :: hybcb(1:iefbc,1:jbbc)=0.0; nhybcb(1:iefbc,1:jbbc)=0.0
      real :: hxbcb(1:ibfbc,1:jebc)=0.0; nhxbcb(1:ibfbc,1:jebc)=0.0
      real :: hybcl(1:iebc,1:jb)=0.0; nhybcl(1:iebc,1:jb)=0.0
      real :: hxbcl(1:iebc,1:je)=0.0; nhxbcl(1:iebc,1:je)=0.0
      real :: hybcr(1:iebc,1:jb)=0.0; nhybcr(1:iebc,1:jb)=0.0
      real :: hxbcr(1:ibbc,1:je)=0.0; nhxbcr(1:ibbc,1:je)=0.0
      real :: ezxbcf(1:ibfbc,1:jebc)=0.0; ezybcf(1:ibfbc,1:jebc)=0.0
      real :: nezxbcf(1:ibfbc,1:jebc)=0.0; nezybcf(1:ibfbc,1:jebc)=0.0
      real :: ezxbcb(1:ibfbc,1:jebc)=0.0; ezybcb(1:ibfbc,1:jebc)=0.0
      real :: nezxbcb(1:ibfbc,1:jebc)=0.0; nezybcb(1:ibfbc,1:jebc)=0.0
      real :: ezxbcl(1:iebc,1:jb)=0.0; ezybcl(1:iebc,1:jb)=0.0
      real :: nezxbcl(1:iebc,1:jb)=0.0; nezybcl(1:iebc,1:jb)=0.0
```

```
      real :: ezxbcr(1:ibbc,1:jb)=0.0; ezybcr(1:ibbc,1:jb)=0.0
      real :: nezxbcr(1:ibbc,1:jb)=0.0; nezybcr(1:ibbc,1:jb)=0.0

c*****************************************************************
c     Variables declarations and initializations for discrete fourier transformation
c*****************************************************************
      integer :: im,jm,m
      real :: ow oww
      complex :: ft3ez(1:10,1:10,1:600)=0.0
      complex :: ft3ezb(1:10,1:10,1:600)=0.0
      complex :: ft4ez(1:10,1:10,1:600)=0.0
      complex :: ft4ezb(1:10,1:10,1:600)=0.0
      complex :: ft3ezw(1:10,1:10,1:600)=0.0
      complex :: ft3ezbw(1:10,1:10,1:600)=0.0
      complex :: ft4ezw(1:10,1:10,1:600)=0.0
      complex :: ft4ezbw(1:10,1:10,1:600)=0.0
      complex,parameter :: ci=(0.0,1.0)
      real :: ftezi(1:600)=0.0; ftezib(1:600)=0.0
      real :: fteziw(1:600)=0.0; ftezibw(1:600)=0.0
      real :: fffi(1:600)=0.0; fffw(1:600)=0.0

c*****************************************************************
c     Variables declarations and initializations for random number generator
c*****************************************************************
      integer :: seed=2,ssd(1:2)=2
      real :: randx,randy
      intrinsic :: random_seed
      intrinsic :: random_number
      real :: distxs
      real :: gatez(1:ib,1:jb)=0.0; gz(1:ib,1:jb)=1.0
      real :: gsum(1:1001)=0.0; gtemp=0.0

c*****************************************************************
c    Variables declarations and initializations for atomic system
c*****************************************************************
      real :: t21,t32,t43
      real :: pcon,time2,wtran
      real :: u1(1:ib,1:jb)=0.0; u2(1:ib,1:jb)=0.0
```

```
      real :: u3(1:ib,1:jb)=0.0; u4(1:ib,1:jb)=0.0
      real :: nu1(1:ib,1:jb)=0.0; nu2(1:ib,1:jb)=0.0
      real :: nu3(1:ib,1:jb)=0.0; nu4(1:ib,1:jb)=0.0
      real :: pold(1:ib,1:jb)=0.0; p(1:ib,1:jb)=0.0; newp(1:ib,1:jb)=0.0
      real :: kcon,wrate,density
      real :: pump=0.0
      real :: a1z,a2z,a3z,a4z,a5z,a6z
      real :: a7z,a8z,a9z,a10z,a11z
      real :: a12z,a13z
      real :: te(1:1001)=0.0; temax(1:1001)=0.0

c*****************************************************************
c     Variables definition:
c     density is the total number of atomic system, wtran is the lasing transition
c     frequency, t43, t32, t21 are the lifetime of the energy state L4 L3 L2,
c     respectively, time2 is the collision time, pump is the pumping rate
c*****************************************************************
      pcon=1.05459e-34
      kcon=6.0*pi*epsz*(cc**3)/((wtran**2)*t32)
      wrate=(1.0/t32)+(2/time2)
      pump=1.0e+14

      tt=1; gg=1
      density=6.02217e+23
      wtran=2.0*pi*5.0847e+14
      t43=1.0e-13; t32=1.0e-10; t21=5.0e-12; time2=2.0e-14
      pcon=1.05459e-34
      kcon=6.0*pi*epsz*(cc**3)/((wtran**2)*t32)
      wrate=(1.0/t32)+(2/time2)
      pump=1.0e+14
      u1(1:ib,1:jb)=density

      a1z=(2.0-(wtran*dt)**2)/(1.0+wrate*dt/2.0)
      a2z=((wrate*dt/2.0)-1.0)/(1.0+wrate*dt/2.0)
      a3z=((dt**2)*kcon)/(1.0+wrate*dt/2.0)
      a4z=(2.0*t21-dt)/(2.0*t21+dt); a5z=t21*dt/(t32*(2.0*t21+dt))
      a6z=t21/(pcon*wtran*(2.0*t21+dt))
      a7z=(2.0*t32-dt)/(2.0*t32+dt); a8z=t32*dt/(t43*(2.0*t32+dt))
```

```
          a9z=t32/(pcon*wtran*(2.0*t32+dt))
          a10z=(2.0*dt*t43*pump)/(2.0*t43+dt) !remark
          a11z=(2.0*t43-dt)/(2.0*t43+dt)
          a12z=(1.0-dt*pump); a13z=dt/(2.0*t21)

c*************************************************************
c    Assignation of the material parameters:
c    eqs(1) represents the dielectric constant of air
c    eqs(2) represents the dielectric constant of titanium dioxide
c*************************************************************
          eps(1)=1.0; sig(1)=0.0; mur(1)=1.0; sim(1)=0.0
          eps(2)=7.0; sig(2)=0.0; mur(2)=1.0; sim(2)=0.0

c*************************************************************
c       Gaussian pulse function
c*************************************************************
          tau=5.0; delay=20.0; source=0.0
          do n=1,299
             source(n)=10*exp(-((n-delay)/tau)**2)
          enddo

c*************************************************************
c        Update the coefficients of the discretized Maxwell's equations
c*************************************************************

          do i=1,media
               eaf=dt*sig(i)/(2.0*epsz*eps(i))
             ca(i)=(1.0-eaf)/(1.0+eaf)
             cb(i)=dt/(epsz*eps(i)*dx*(1.0+eaf))
               haf=dt*sim(i)/(2.0*muz*mur(i))
             da(i)=(1.0-haf)/(1.0+haf)
             db(i)=dt/(muz*mur(i)*dx*(1.0+haf))
          enddo

c*************************************************************
c    Assign the material parameters to the system grid
c*************************************************************
```

```
            caez=ca(1); cbez=cb(1); dahx=da(1); dbhx=db(1)
            dahy=da(1); dbhy=db(1)

            do i=2,401
              do j=2,401
            caez(i,j)=ca(1); cbez(i,j)=cb(1)
            gatez(i,j)=1.0; gz(i,j)=eps(1)
              enddo
            enddo

c*****************************************************************
c       Generateg the array of the cylinder with square lattice
c       halfd is the radius of the cylinder
c*****************************************************************
            halfd=6; icenter=ie/2; jcenter=je/2; limit=2
            ij=1

            do i=-numx/2,(numx/2)-1
              do j=-numy/2,(numy/2)-1
            a(ij)=(i+0.5)*lattice+icenter; b(ij)=(j+0.5)*lattice+jcenter
            ij=ij+1
              enddo
            enddo

            call random_seed(size=seed)
            call random_seed(put=ssd(1:2))

c*****************************************************************
c       Randomize the position of the cylinder using random number generator
c*****************************************************************

            do i=1,ij-1
            call random_number(randx)
            a(i)=a(i)-limit/2+nint(randx*limit)
            call random_number(randy)
            b(i)=b(i)-limit/2+nint(randy*limit)
            enddo
```

```
              do nn=1,rodn
              do i=1,ib
              do j=1,jb
                 distxs=sqrt((a(nn)-i)**2+(b(nn)-j)**2)
                  if(distxs.le.halfd)then
                  caez(i,j)=ca(2); cbez(i,j)=cb(2)
                  gatez(i,j)=0.0; gz(i,j)=eps(2)
                  endif
             enddo
             enddo
            enddo

c*****************************************************************
c         Assign the coefficient of PML
c*****************************************************************
              delbc=iebc*dx
              sigmam=-log(rmax/100.0)*epsz*cc*(orderbc+1)/(2*delbc)
              bcfactor=eps(1)*sigmam/(dx*(delbc**orderbc)*(orderbc+1))

c******For the front region of PML*********************************
              do j=2,jebc
                  y1=(jebc-j+1.5)*dx ; y2=(jebc-j+0.5)*dx
                  sigmay=bcfactor*(y1**(orderbc+1)-y2**(orderbc+1))
                  ca1=exp(-sigmay*dt/(epsz*eps(1)))
                  cb1=(1.0-ca1)/(sigmay*dx)
                  caezybcf(1:ibfbc,j)=ca1 ; cbezybcf(1:ibfbc,j)=cb1
              enddo

              sigmay=bcfactor*((0.5*dx)**(orderbc+1))
              ca1=exp(-sigmay*dt/(epsz*eps(1)))
              cb1=(1-ca1)/(sigmay*dx)
              caezybcl(1:iebc,1)=ca1; cbezybcl(1:iebc,1)=cb1
              caez(1:ib,1)=ca1; cbez(1:ib,1)=cb1
              caezybcr(1:iebc,1)=ca1; cbezybcr(1:iebc,1)=cb1

              do j=1,jebc
                  y1=(jebc-j+1)*dx; y2=(jebc-j)*dx
                  sigmay=bcfactor*(y1**(orderbc+1)-y2**(orderbc+1))
```

```
                sigmays=sigmay*(muz/(epsz*eps(1)))
                da1=exp(-sigmays*dt/muz)
                db1=(1-da1)/(sigmays*dx)
                dahxbcf(1:ibfbc,j)=da1; dbhxbcf(1:ibfbc,j)=db1
                caezxbcf(1:ibfbc,j)=ca(1); cbezxbcf(1:ibfbc,j)=cb(1)
                dahybcf(1:iefbc,j)=da(1); dbhybcf(1:iefbc,j)=db(1)
            enddo

c******For the back region of PML**********************************
            do j=2,jebc
                y1=(j-0.5)*dx; y2=(j-1.5)*dx
                sigmay=bcfactor*(y1**(orderbc+1)-y2**(orderbc+1))
                ca1=exp(-sigmay*dt/(epsz*eps(1)))
                cb1=(1-ca1)/(sigmay*dx)
                caezybcb(1:ibfbc,j)=ca1; cbezybcb(1:ibfbc,j)=cb1
            enddo

            sigmay=bcfactor*((0.5*dx)**(orderbc+1))
            ca1=exp(-sigmay*dt/(epsz*eps(1)))
            cb1=(1-ca1)/(sigmay*dx)
            caezybcl(1:iebc,jb)=ca1; cbezybcl(1:iebc,jb)=cb1
            caez(1:ib,jb)=ca1; cbez(1:ib,jb)=cb1
            caezybcr(1:iebc,jb)=ca1; cbezybcr(1:iebc,jb)=cb1

           do j=1,jebc
               y1=j*dx; y2=(j-1)*dx
               sigmay=bcfactor*(y1**(orderbc+1)-y2**(orderbc+1))
               sigmays=sigmay*(muz/(epsz*eps(1)))
               da1=exp(-sigmays*dt/muz)
               db1=(1-da1)/(sigmays*dx)
               dahxbcb(1:ibfbc,j)=da1; dbhxbcb(1:ibfbc,j)=db1
               caezxbcb(1:ibfbc,j)=ca(1); cbezxbcb(1:ibfbc,j)=cb(1)
               dahybcb(1:iefbc,j)=da(1); dbhybcb(1:iefbc,j)=db(1)
           enddo
               dahybcb(1:iefbc,jbbc)=da(1); dbhybcb(1:iefbc,jbbc)=db(1)

c******For the left region of PML**********************************
           do i=2,iebc
```

```
            x1=(iebc-i+1.5)*dx; x2=(iebc-i+0.5)*dx
            sigmax=bcfactor*(x1**(orderbc+1)-x2**(orderbc+1))
            ca1=exp(-sigmax*dt/(epsz*eps(1)))
            cb1=(1-ca1)/(sigmax*dx)
            caezxbcb(i,1:jbbc)=ca11; cbezxbcb(i,1:jbbc)=cb1
            caezxbcl(i,1:jb)=ca1; cbezxbcl(i,1:jb)=cb1
            caezxbcf(i,1:jebc)=ca1; cbezxbcf(i,1:jebc)=cb1
          enddo

          sigmax=bcfactor*((0.5*dx)**(orderbc+1))
          ca1=exp(-sigmax*dt/(epsz*eps(1)))
          cb1=(1-ca1)/(sigmax*dx)
          caezxbcb(iebc+1,1:jbbc)=ca1; cbezxbcb(iebc+1,1:jbbc)=cb1
          caez(1,1:jb)=ca1; cbez(1,1:jb)=cb1
          caezxbcf(iebc+1,1:jebc)=ca1; cbezxbcf(iebc+1,1:jebc)=cb1

          do i=1,iebc
            x1=(iebc-i+1)*dx; x2=(iebc-i)*dx
            sigmax=bcfactor*(x1**(orderbc+1)-x2**(orderbc+1))
            sigmaxs=sigmax*(muz/(epsz*eps(1)))
            da1=exp(-sigmaxs*dt/muz)
            db1=(1-da1)/(sigmaxs*dx)
            dahybcb(i,1:jbbc)=da1; dbhybcb(i,1:jbbc)=db1
            dahybcl(i,1:jb)=da1; dbhybcl(i,1:jb)=db1
            dahybcf(i,1:jebc)=da1; dbhybcf(i,1:jebc)=db1
            caezybcl(i,2:je)=ca(1) ; cbezybcl(i,2:je)=cb(1)
            dahxbcl(i,1:je)=da(1); dbhxbcl(i,1:je)=db(1)
           enddo

c******For the right region of PML**********************************
           do i=2,iebc
             x1=(i-0.5)*dx; x2=(i-1.5)*dx
             sigmax=bcfactor*(x1**(orderbc+1)-x2**(orderbc+1))
             ca1=exp(-sigmax*dt/(epsz*eps(1)))
             cb1=(1-ca1)/(sigmax*dx)
             caezxbcb(i+iebc+ie,1:jbbc)=ca1
             cbezxbcb(i+iebc+ie,1:jbbc)=cb1
             caezxbcr(i,1:jb)=ca1; cbezxbcr(i,1:jb)=cb1
```

```
        caezxbcf(i+iebc+ie,1:jebc)=ca1; cbezxbcf(i+iebc+ie,1:jebc)=cb1
      enddo

      sigmax=bcfactor*((0.5*dx)**(orderbc+1))
      ca1=exp(-sigmax*dt/(epsz*eps(1)))
      cb1=(1-ca1)/(sigmax*dx)
      caezxbcb(iebc+ib,1:jbbc)=ca1; cbezxbcb(iebc+ib,1:jbbc)=cb1
      caez(ib,1:jb)=ca1; cbez(ib,1:jb)=cb1
      caezxbcf(iebc+ib,1:jebc)=ca1; cbezxbcf(iebc+ib,1:jebc)=cb1

      do i=1,iebc
        x1=i*dx; x2=(i-1)*dx
        sigmax=bcfactor*(x1**(orderbc+1)-x2**(orderbc+1))
        sigmaxs=sigmax*(muz/(epsz*eps(1)))
        da1=exp(-sigmaxs*dt/muz)
        db1=(1-da1)/(sigmaxs*dx)
        dahybcb(i+ie+iebc,1:jbbc)=da1; dbhybcb(i+ie+iebc,1:jbbc)=db1
        dahybcr(i,1:jb)=da1; dbhybcr(i,1:jb)=db1
        dahybcf(i+ie+iebc,1:jebc)=da1; dbhybcf(i+ie+iebc,1:jebc)=db1
        caezybcr(i,2:je)=ca(1); cbezybcr(i,2:je)=cb(1)
        dahxbcr(i,1:je)=da(1); dbhxbcr(i,1:je)=db(1)
      enddo
        dahxbcr(ibbc,1:je)=da(1); dbhxbcr(ibbc,1:je)=db(1)

c**********************************************************************
c       Terminate the 2D system at perfect conducting boundary
c**********************************************************************
        caezxbcf(1:ibfbc,1)=1.0; cbezxbcf(1:ibfbc,1)=0.0
        caezybcf(1:ibfbc,1)=1.0; cbezybcf(1:ibfbc,1)=0.0
        caezxbcb(1:ibfbc,jbbc)=1.0; cbezxbcb(1:ibfbc,jbbc)=0.0
        caezybcb(1:ibfbc,jbbc)=1.0; cbezybcb(1:ibfbc,jbbc)=0.0
        caezxbcf(1,1:jebc)=1.0; cbezxbcf(1,1:jebc)=0.0
        caezybcf(1,1:jebc)=1.0; cbezybcf(1,1:jebc)=0.0
        caezxbcf(ibfbc,1:jebc)=1.0; cbezxbcf(ibfbc,1:jebc)=0.0
        caezybcf(ibfbc,1:jebc)=1.0; cbezybcf(ibfbc,1:jebc)=0.0
        caezxbcb(1,1:jbbc)=1.0; cbezxbcb(1,1:jbbc)=0.0
        caezybcb(1,1:jbbc)=1.0; cbezybcb(1,1:jbbc)=0.0
        caezxbcb(ibfbc,1:jbbc)=1.0; cbezxbcb(ibfbc,1:jbbc)=0.0
```

```
            caezybcb(ibfbc,1:jbbc)=1.0; cbezybcb(ibfbc,1:jbbc)=0.0
            caezxbcl(1,1:jb)=1.0; cbezxbcl(1,1:jb)=0.0
            caezybcl(1,1:jb)=1.0; cbezybcl(1,1:jb)=0.0
            caezxbcr(ibbc,1:jb)=1.0; cbezxbcr(ibbc,1:jb)=0.0
            caezybcr(ibbc,1:jb)=1.0; cbezybcr(ibbc,1:jb)=0.0

c*****************************************************************
c       Start the time–stepping loop
c*****************************************************************
          do n=1,nmax

c*****************************************************************
c       Calculate the value of electric fields (Ez) in main grid
c       in n+1 time step
c*****************************************************************
            newp(2:ie,2:je)=(a1z*p(2:ie,2:je)+a2z*pold(2:ie,2:je)+
     &                  a3z*(u2(2:ie,2:je)-u3(2:ie,2:je))*ez(2:ie,2:je))*
     &                  gatez(2:ie,2:je)

             nez(2:ie,2:je)=ez(2:ie,2:je)+cbez(2:ie,2:je)*
     &       (hy(2:ie,2:je)-hy(1:ie-1,2:je)-(hx(2:ie,2:je)-hx(2:ie,1:je-1)))-
     &       (1/(epsz*eps(3)))*(newp(2:ie,2:je)-p(2:ie,2:je))*
     &         gatez(2:ie,2:je)

            nez(2:ie,1)=caez(2:ie,1)*ez(2:ie,1)+cbez(2:ie,1)*
     &                  (hy(2:ie,1)-hy(1:ie-1,1)-
     &                  (hx(2:ie,1)-hxbcf(2+iebc:ie+iebc,jebc)))

            nez(2:ie,jb)=caez(2:ie,jb)*ez(2:ie,jb)+cbez(2:ie,jb)*
     &                    (hy(2:ie,jb)-hy(1:ie-1,jb)-
     &                    (hxbcb(2+iebc:ie+iebc,1)-hx(2:ie,je)))

            nez(1,2:je)=caez(1,2:je)*ez(1,2:je)+cbez(1,2:je)*
     &                  (hy(1,2:je)-hybcl(iebc,2:je)-(hx(1,2:je)-hx(1,1:je-1)))

            nez(ib,2:je)=caez(ib,2:je)*ez(ib,2:je)+cbez(ib,2:je)*
     &                 (hybcr(1,2:je)-hy(ie,2:je)- (hx(ib,2:je)-hx(ib,1:je-1)))
```

```
            nez(1,1)=caez(1,1)*ez(1,1)+cbez(1,1)*
     &                (hy(1,1)-hybcl(iebc,1)- (hx(1,1)-hxbcf(iebc+1,jebc)))

            nez(1,jb)=caez(1,jb)*ez(1,jb)+cbez(1,jb)*
     &                 (hy(1,jb)-hybcl(iebc,jb)-(hxbcb(iebc+1,1)-hx(1,je)))

            nez(ib,jb)=caez(ib,jb)*ez(ib,jb)+cbez(ib,jb)*
     &                 (hybcr(1,jb)-hy(ie,jb)-(hxbcb(iebc+ie+1,1)-hx(ib,je)))

            nez(ib,1)=caez(ib,1)*ez(ib,1)+cbez(ib,1)*
     &                 (hybcr(1,1)-hy(ie,1)-(hx(ib,1)-hxbcf(iebc+ie+1,jebc)))

c*************************************************************
c       Gaussian pulse is injected at the center part of the computation
c       domains
c*************************************************************
          if(n.le.250)then
            do i=1,ib
            do j=1,jb
             distxs=(200-i)**2+(200-j)**2
             if(distxs.le.180)then
             nez(i,j)=source(n)
             endif
           enddo
          enddo
          endif

c*************************************************************
c       Calculate the value of electronic populations (N1, N2, N3 and
c       N4) in active part in n+1 time step
c*************************************************************
          nu4(2:ie,2:je)=(a10z*u1(2:ie,2:je)+a11z*u4(2:ie,2:je))*
     &                    gatez(2:ie,2:je)
          nu3(2:ie,2:je)=(a7z*u3(2:ie,2:je)+
     &              a8z*(nu4(2:ie,2:je)+u4(2:ie,2:je))+
     &              a9z*(nez(2:ie,2:je)+ez(2:ie,2:je))*
     &              (newp(2:ie,2:je)-p(2:ie,2:je)))*gatez(2:ie,2:je)
          nu2(2:ie,2:je)=(a4z*u2(2:ie,2:je)+a5z*
```

```
     &              (nu3(2:ie,2:je)+u3(2:ie,2:je))-
     &              a6z*(nez(2:ie,2:je)+ez(2:ie,2:je))*
     &              (newp(2:ie,2:je)-p(2:ie,2:je)))*gatez(2:ie,2:je)
        nu1(2:ie,2:je)=(a12z*u1(2:ie,2:je)+a13z*
     &               (nu2(2:ie,2:je)+u2(2:ie,2:je)))*gatez(2:ie,2:je)


c*************************************************************
c       Update the value of electric fields in PML grids in n+1 time step
c*************************************************************

c******For the front region of PML*********************************
            nezxbcf(2:iefbc,2:jebc)=caezxbcf(2:iefbc,2:jebc)*
     &                      ezxbcf(2:iefbc,2:jebc)+cbezxbcf(2:iefbc,2:jebc)*
     &                      (hybcf(2:iefbc,2:jebc)-hybcf(1:iefbc-1,2:jebc))
            nezybcf(2:iefbc,2:jebc)=caezybcf(2:iefbc,2:jebc)*
     &                     ezybcf(2:iefbc,2:jebc)-cbezybcf(2:iefbc,2:jebc)*
     &                      (hxbcf(2:iefbc,2:jebc)-hxbcf(2:iefbc,1:jebc-1))
c******For the back region of PML*********************************
            nezxbcb(2:iefbc,2:jebc)=caezxbcb(2:iefbc,2:jebc)*
     &                      ezxbcb(2:iefbc,2:jebc)+cbezxbcb(2:iefbc,2:jebc)*
     &                      (hybcb(2:iefbc,2:jebc)-hybcb(1:iefbc-1,2:jebc))
            nezybcb(2:iefbc,2:jebc)=caezybcb(2:iefbc,2:jebc)*
     &                      ezybcb(2:iefbc,2:jebc)-cbezybcb(2:iefbc,2:jebc)*
     &                      (hxbcb(2:iefbc,2:jebc)-hxbcb(2:iefbc,1:jebc-1))
c******For the left region of PML*********************************
            nezxbcl(2:iebc,1:jb)=caezxbcl(2:iebc,1:jb)*
     &                     ezxbcl(2:iebc,1:jb)+cbezxbcl(2:iebc,1:jb)*
     &                      (hybcl(2:iebc,1:jb)-hybcl(1:iebc-1,1:jb))
            nezybcl(2:iebc,2:je)=caezybcl(2:iebc,2:je)*
     &                ezybcl(2:iebc,2:je)-cbezybcl(2:iebc,2:je)*
     &                      (hxbcl(2:iebc,2:je)-hxbcl(2:iebc,1:je-1))
            nezybcl(2:iebc,1)=caezybcl(2:iebc,1)*
     &                      ezybcl(2:iebc,1)-cbezybcl(2:iebc,1)*
     &                      (hxbcl(2:iebc,1)-hxbcf(2:iebc,jebc))
            nezybcl(2:iebc,jb)=caezybcl(2:iebc,jb)*
     &                       ezybcl(2:iebc,jb)-cbezybcl(2:iebc,jb)*
     &                       (hxbcb(2:iebc,1)-hxbcl(2:iebc,je))
```

```
c******For the right region of PML**********************************
              nezxbcr(2:iebc,1:jb)=caezxbcr(2:iebc,1:jb)*
     &                        ezxbcr(2:iebc,1:jb)+cbezxbcr(2:iebc,1:jb)*
     &                        (hybcr(2:iebc,1:jb)-hybcr(1:iebc-1,1:jb))
              nezybcr(2:iebc,2:je)=caezybcr(2:iebc,2:je)*
     &                        ezybcr(2:iebc,2:je)-cbezybcr(2:iebc,2:je)*
     &                        (hxbcr(2:iebc,2:je)-hxbcr(2:iebc,1:je-1))
              nezybcr(2:iebc,1)=caezybcr(2:iebc,1)*
     &                  ezybcr(2:iebc,1)-cbezybcr(2:iebc,1)*
     &                 (hxbcr(2:iebc,1)-hxbcf(2+iebc+ie:iebc+iebc+ie,jebc))
              nezybcr(2:iebc,jb)=caezybcr(2:iebc,jb)*ezybcr(2:iebc,jb)-
     &                           cbezybcr(2:iebc,jb)*
     &                 (hxbcb(2+iebc+ie:iebc+iebc+ie,1)-hxbcr(2:iebc,je))

c*********************************************************************
c       Substitute the value of electric field in n time step by those in n+1 time
c       step
c*********************************************************************
            ez=nez; ezxbcf=nezxbcf; ezybcf=nezybcf; ezxbcb=nezxbcb
            ezybcb=nezybcb; ezxbcl=nezxbcl; ezybcl=nezybcl;
            ezxbcr=nezxbcr; ezybcr=nezybcr

c*********************************************************************
c       Calculate the value of magnetic fields (Hx,Hz) in main grid
c       in n+1 time step
c*********************************************************************
              nhx(1:ib,1:je)=hx(1:ib,1:je)-
     &                    dbhx(1:ib,1:je)*(ez(1:ib,2:je+1)-ez(1:ib,1:je))
              nhy(1:ie,1:jb)=hy(1:ie,1:jb)+
     &                    dbhy(1:ie,1:jb)*(ez(2:ie+1,1:jb)-ez(1:ie,1:jb))

c*********************************************************************
c       Calculate the value of magnetic fields in PML grids in n+1
c       time step
c*********************************************************************

c******For the front region of PML**********************************
              nhybcf(1:iefbc,2:jebc)=dahybcf(1:iefbc,2:jebc)*
```

```
     &              hybcf(1:iefbc,2:jebc)+dbhybcf(1:iefbc,2:jebc)*
     &                    (ezxbcf(2:iefbc+1,2:jebc)-
     &              ezxbcf(1:iefbc,2:jebc)+ezybcf(2:iefbc+1,2:jebc)-
     &                    ezybcf(1:iefbc,2:jebc))
          nhxbcf(2:iefbc,1:jebc-1)=dahxbcf(2:iefbc,1:jebc-1)*
     &         hxbcf(2:iefbc,1:jebc-1)-dbhxbcf(2:iefbc,1:jebc-1)*
     &         (ezxbcf(2:iefbc,2:jebc)-ezxbcf(2:iefbc,1:jebc-1)+
     &         ezybcf(2:iefbc,2:jebc)-ezybcf(2:iefbc,1:jebc-1))
        nhxbcf(2:iebc,jebc)=dahxbcf(2:iebc,jebc)*hxbcf(2:iebc,jebc)-
     &         dbhxbcf(2:iebc,jebc)*(ezxbcl(2:iebc,1)-ezxbcf(2:iebc,jebc)+
     &         ezybcl(2:iebc,1)-ezybcf(2:iebc,jebc))
          nhxbcf(iebc+1:iebc+ib,jebc)=dahxbcf(iebc+1:iebc+ib,jebc)*
     &         hxbcf(iebc+1:iebc+ib,jebc)-dbhxbcf(iebc+1:iebc+ib,jebc)*
     &         (ez(1:ib,1)-ezxbcf(iebc+1:iebc+ib,jebc)-
     &         ezybcf(iebc+1:iebc+ib,jebc))
        nhxbcf(iebc+ib+1:iefbc,jebc)=dahxbcf(iebc+ib+1:iefbc,jebc)*
     &        hxbcf(iebc+ib+1:iefbc,jebc)- dbhxbcf(iebc+ib+1:iefbc,jebc)*
     &        (ezxbcr(2:iefbc-(iebc+ib)+1,1)-ezxbcf(iebc+ib+1:iefbc,jebc)+
     &        (ezybcr(2:iefbc-(iebc+ib)+1,1)-ezybcf(iebc+ib+1:iefbc,jebc)))

c******For the back region of PML**********************************
          nhybcb(1:iefbc,2:jebc)=dahybcb(1:iefbc,2:jebc)*
     &              hybcb(1:iefbc,2:jebc)+dbhybcb(1:iefbc,2:jebc)*
     &                    (ezxbcb(2:iefbc+1,2:jebc)-
     &              ezxbcb(1:iefbc,2:jebc)+ezybcb(2:iefbc+1,2:jebc)-
     &                    ezybcb(1:iefbc,2:jebc))
          nhxbcb(2:iefbc,2:jebc)=dahxbcb(2:iefbc,2:jebc)*
     &        hxbcb(2:iefbc,2:jebc)-dbhxbcb(2:iefbc,2:jebc)*
     &        (ezxbcb(2:iefbc,3:jebc+1)-ezxbcb(2:iefbc,2:jebc)+
     &        ezybcb(2:iefbc,3:jebc+1)-ezybcb(2:iefbc,2:jebc))
          nhxbcb(2:iebc,1)=dahxbcb(2:iebc,1)*hxbcb(2:iebc,1)-
     &         dbhxbcb(2:iebc,1)*(ezxbcb(2:iebc,2)-ezxbcl(2:iebc,jb)+
     &         ezybcb(2:iebc,2)-ezybcl(2:iebc,jb))
          nhxbcb(iebc+1:iebc+ib,1)=dahxbcb(iebc+1:iebc+ib,1)*
     &         hxbcb(iebc+1:iebc+ib,1)-dbhxbcb(iebc+1:iebc+ib,1)*
     &       (ezxbcb(iebc+1:iebc+ib,2)+ezybcb(iebc+1:iebc+ib,2)-
     &         ez(1:ib,jb))
          nhxbcb(iebc+ib+1:iefbc,1)=dahxbcb(iebc+ib+1:iefbc,1)*
```

```
      &          hxbcb(iebc+ib+1:iefbc,1)-dbhxbcb(iebc+ib+1:iefbc,1)*
      &          (ezxbcb(iebc+ib+1:iefbc,2)-ezxbcr(2:iefbc-(iebc+ib)+1,jb)+
      &          ezybcb(iebc+ib+1:iefbc,2)-ezybcr(2:iefbc-(iebc+ib)+1,jb))

c******For the left region of PML**********************************
          nhybcl(1:iebc-1,1:jb)=dahybcl(1:iebc-1,1:jb)*
      &                  hybcl(1:iebc-1,1:jb)+dbhybcl(1:iebc-1,1:jb)*
      &                   (ezxbcl(2:iebc,1:jb)-ezxbcl(1:iebc-1,1:jb)+
      &                   ezybcl(2:iebc,1:jb)-ezybcl(1:iebc-1,1:jb))
          nhybcl(iebc,1:jb)=dahybcl(iebc,1:jb)*hybcl(iebc,1:jb)+
      &                       dbhybcl(iebc,1:jb)*
      &                       (ez(1,1:jb)-ezxbcl(iebc,1:jb)-ezybcl(iebc,1:jb))
          nhxbcl(2:iebc,1:je)=dahxbcl(2:iebc,1:je)*
      &         hxbcl(2:iebc,1:je)-dbhxbcl(2:iebc,1:je)* (ezxbcl(2:iebc,2:je+1)-
      &         ezxbcl(2:iebc,1:je)+ezybcl(2:iebc,2:je+1)-ezybcl(2:iebc,1:je))

c******For the right region of PML**********************************
         nhybcr(2:iebc,1:jb)=dahybcr(2:iebc,1:jb)*hybcr(2:iebc,1:jb)+
      &                    dbhybcr(2:iebc,1:jb)*
      &                 (ezxbcr(3:iebc+1,1:jb)-ezxbcr(2:iebc,1:jb)+
      &                 ezybcr(3:iebc+1,1:jb)-ezybcr(2:iebc,1:jb))
         nhybcr(1,1:jb)=dahybcr(1,1:jb)*hybcr(1,1:jb)+dbhybcr(1,1:jb)*
      &                     (ezxbcr(2,1:jb)+ezybcr(2,1:jb)-ez(ib,1:jb))
           nhxbcr(2:iebc,1:je)=dahxbcr(2:iebc,1:je)*
      &               hxbcr(2:iebc,1:je)-dbhxbcr(2:iebc,1:je)*
      &               (ezxbcr(2:iebc,2:je+1)- ezxbcr(2:iebc,1:je)+
      &                ezybcr(2:iebc,2:je+1)-ezybcr(2:iebc,1:je))


c*****************************************************************
c       Substitute the value of magnetic field in n time step by those in n+1 time
c       step
c*****************************************************************
          pold=p; p=newp; hx=nhx; hy=nhy
          hxbcf=nhxbcf; hybcf=nhybcf; hxbcb=nhxbcb; hybcb=nhybcb
          hxbcl=nhxbcl; hybcl=nhybcl; hxbcr=nhxbcr; hybcr=nhybcr
          u1=nu1; u2=nu2; u3=nu3; u4=nu4;
c*****************************************************************
```

```
c*****************************************************************
c       Perform the Discrete Fourier Transformation
c       The electric field signal is transformed from time domain to spectral
c       domain
c*****************************************************************

          do i=1,10
           do j=1,10

            im=(i-1)*40+10
            jm=(j-1)*40+10

           do m=1,600
            oww=2*pi*cc/(m*0.5e-9+450.0e-9)
            ow=2*pi*(m*1e12+3.5e14)
            ft3ezw(i,j,m)=ez(im,jm)*(cexp(ci*oww*n*dt))/(100*nmax)
            ft4ezw(i,j,m)=ft4ezw(i,j,m)+ft3ezw(i,j,m)
            ft3ez(i,j,m)=ez(im,jm)*(cexp(ci*ow*n*dt))/(100*nmax)
            ft4ez(i,j,m)=ft4ez(i,j,m)+ft3ez(i,j,m)
           enddo
           enddo
          enddo

c*****************************************************************
c      Record the total electric field energy of the system
c*****************************************************************
          if(mod(n,50).eq.0)then
            do i=1,ib
            do j=1,jb
              gtemp=0.5*gz(i,j)*ez(i,j)*ez(i,j)
              gsum(gg)=gsum(gg)+gtemp
           enddo
           enddo
             gg=gg+1
             te(tt)=ez(200,200)
             temax(tt)=maxval(ez)
             tt=tt+1
```

```
          endif

c*************************************************************
c         End the time loop
c*************************************************************
          enddo

c*************************************************************
c         Output data of the powder spectrum and the time evolution of field
c*************************************************************

c*************************************************************
c         Generate the data file of the powder spectrum
c*************************************************************
          open(unit=21,file="spe_ez_full",status="unknown")
          open(unit=22,file="spe_ez_half",status="unknown")
          open(unit=221,file="spe_wave_full",status="unknown")
          open(unit=222,file="spe_wave_half",status="unknown")

            do m=1,600
              do i=1,10
                do j=1,10
                ftezi(m)=ftezi(m)+abs(ft4ez(i,j,m)*conjg(ft4ez(i,j,m)))
                ftezib(m)=ftezib(m)+abs(ft4ezb(i,j,m)*conjg(ft4ezb(i,j,m)))
                fteziw(m)=fteziw(m)+abs(ft4ezw(i,j,m)*conjg(ft4ezw(i,j,m)))
                ftezibw(m)=ftezibw(m)+abs(ft4ezbw(i,j,m)*
     &           conjg(ft4ezbw(i,j,m)))
                enddo
              enddo

            write(21,888)
     &     m*0.01+3.5,ftezi(m)
            write(22,888)
     &     m*0.01+3.5,ftezib(m)
            write(221,888)
     &     (m*0.5+450),fteziw(m)
            write(222,888)
     &     (m*0.5+450),ftezibw(m)
```

```
            enddo

c*****************************************************************
c       Generate the data file of the electric field distribution pattern
c*****************************************************************
            open(unit=24,file="ez_final",status="unknown")
            write(24,'(403e15.6)') ez
            close(24)

 666     format(i10,e25.15)
 777     format(i8,e16.7)
 888     format(e16.7,e16.7)
         stop
         end

c*****************************************************************
c       End of program
c*****************************************************************
```